New Access Hatches in Existing Curved Box Girder Bridges

A Study Based on Practical and Structural Considerations

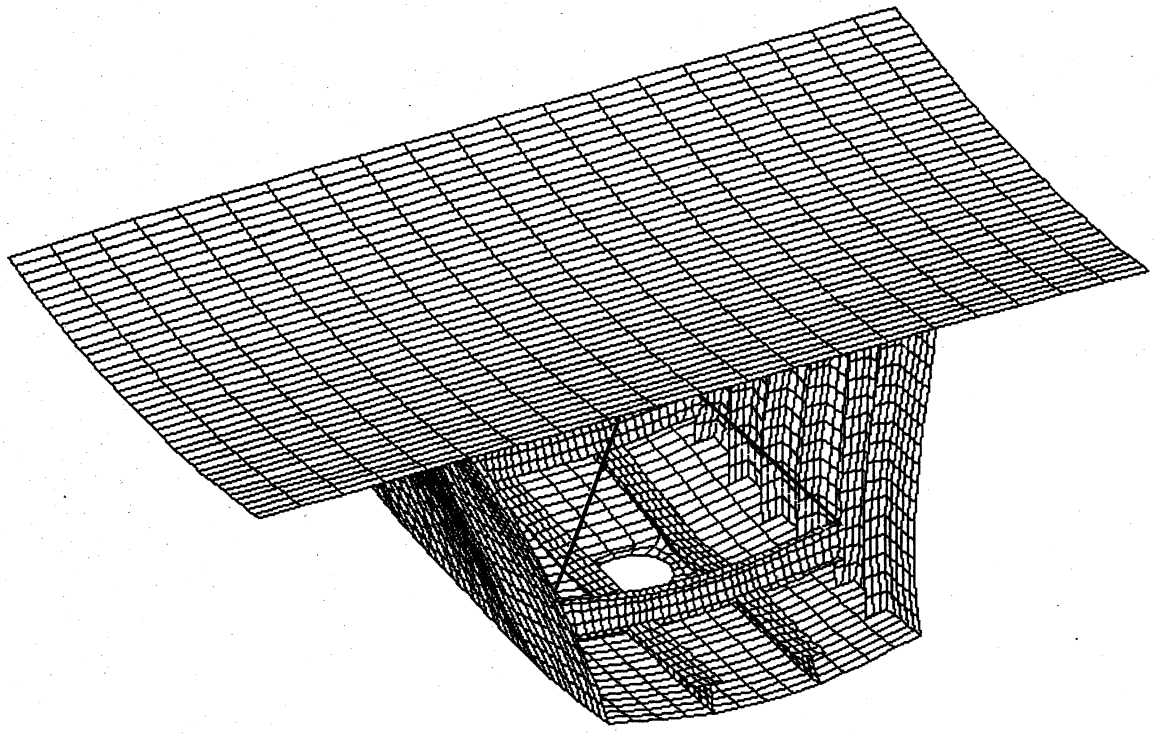

University of Central Florida

Contract WPI 0510839

NEW ACCESS HATCHES IN EXISTING CURVED BOX GIRDER BRIDGES

A STUDY BASED ON PRACTICAL AND STRUCTURAL CONSIDERATIONS

FINAL REPORT
(JANUARY 2000)

Ayman M. Okeil, Sherif El-Tawil, and Mandar Chaphalkhar

Department of Civil and Environmental Engineering
University of Central Florida, Orlando, FL 32816-2450

This report was prepared in cooperation with the State of Florida Department of Transportation and the U.S. Department of Transportation. The report does not constitute a design standard, specification, or regulation. The opinions, findings, and conclusions expressed in this publication are those of the authors in the course and scope of employment by the University of Central Florida and not necessarily those of the Florida Department of Transportation or the U.S. Department of Transportation.

ACKNOWLEDGMENTS

This research was funded in part by the Florida Department of Transportation and the Department of Civil and Environmental Engineering at the University of Central Florida. The authors would like to express their appreciation to the Offices of Bridge Safety, Inspection, and Structures at the Florida Department of Transportation for support of this research. Special thanks are due the following individuals for their substantial contributions to this project:

Office of Bridge Safety:	Earl Jacobs
Office of Bridge Inspection:	Joe Quintana
	Brian O'Donoghue

TABLE OF CONTENTS

Acknowledgments **3**
Table of Contents **4**
Abstract **6**
Introduction **8**
Literature Review **10**
Analysis Tool **18**
Verification of ABAQUS 18
Shell Model Verification 18
Beam Model Verification 20
Analysis Models **21**
Beam (Simplified) Element Model 21
Shell (Detailed) Finite Element Models 22
Bridge 538 ..... **24**
Shell Model I for Br538 25
Material Modeling for Shell Model I 25
Modeling of Stiffeners 26
Loading of Shell Model I 27
Shell Model II for Br538 28
Material Modeling for Shell Model II 28
Loading of Shell Model II 28
Beam Model for Br538 30
Geometric properties for Bridge 538 31
Loading of Beam Model 32
Results for Br538 33
Comparison between Models 33
Nonlinear Analysis of Bridge 538 34
Fatigue Investigation of Hole Locations 34
Effects of Access Holes on Flexural Strength 38
Access Hole Locations **41**
Strategy 41
Location of Current Access Holes 42
Alternative Access Hole Locations 42
Minimally Stressed Locations 46
Case Study of DOT Bridges 53
Bridge 390 53
Bridge 521 53
Bridge 525 54
Bridge 598 54
Bridge 601 54
Bridge 606 55

Bridge 607 55
Bridge 528 55
Bridge 537 56
Bridge 538a 56
Bridge 538b 56
Bridge 538c 56
Bridge 538d 57
Bridge 539 57
Bridge 540 57
Bridge 541a 58
Bridge 541b 58
Bridge 542a 58
Bridge 542b 59
Summary and Findings 61
Summary 61
Need for Access Holes in Box Girder Bridges 61
Strengthening Considerations 61
Special Considerations for Fatigue 62
Access Hole Location Alternatives in a Cross-Section 62
Findings 63
Longitudinal Access Hole Location Alternatives 64
References 66
Appendix A 120
Appendix B 128
Appendix C 168

ABSTRACT

Steel box girders are inspected periodically by maintenance crews who walk or crawl through the inside of the girders searching for signs of corrosion or damage. The interior of the box, which can be dangerous because of unusual temperatures and poor ventilation, is reached through access hatches that are usually provided in the bottom flange immediately before or after an expansion joint. These locations are chosen because 1) bending moments are small close to the expansion joint and 2) the pier over which the expansion joint is located facilitates access; inspection crews need only a ladder to reach the access hole. Nevertheless, the spans covered by box girders are often long, and the girders are constructed as continuous segments over three or more supports. Hence the distance between access hatches frequently exceeds the limit that rescue crews can reach in the event of an emergency. This situation has concerned safety officials and has prompted the Florida Department of Transportation safety office to request the construction of additional access holes in all existing box girder bridges.

This study looks into finding locations where additional access holes can be placed in order to decrease the distance between access hatches in existing bridges. Since new access holes should not adversely affect the structural behavior of the bridge, local strengthening may be necessary. With the strengthening option available, designers may freely choose the location of access holes, generally to satisfy other criteria such as practicality or accessibility. However, strengthening may be costly if the access hole is placed at a heavily stressed location. To eliminate or reduce the amount of strengthening work needed for adding a new access hole, minimally stressed locations are suggested.

Minimally stressed regions are identified through detailed elastic and inelastic finite element analyses of 19 box girder bridges from the State of Florida inventory that are being considered for rehabilitation. Many of the bridges under consideration are horizontally curved and are comprised of steel U-shapes acting compositely with a reinforced concrete deck. Finding appropriate locations for the placement of access hatches in such bridges is complicated by the horizontal curvature and requires a thorough understanding of both elastic and inelastic

behavior of the structural system. A detailed finite element model is created from four node shell elements and is used in a case study of one of the existing bridges. Material and geometric nonlieanities are included in the analyses which focus on the behavior and strength (both static and fatigue) of the bridge. A smaller but more detailed shell element model is also used to investigate flexural strength of a segment of the same bridge. In addition to the shell models, a beam-column finite element model that accounts for warping is created. This model is computationally more efficient than the shell models and is used in case studies of all nineteen existing bridges. The force and moment envelopes due to dead and live load combinations following AASHTO's LRFD specifications are calculated and are presented in an appendix.

Based on the results of the finite element analyses, five different schemes are devised for locating regions where additional access holes could be added without strengthening. The construction sequence is considered in the analyses by adopting quasi-open section properties for dead loads and closed section properties for live loads. The five schemes incorporate different levels of interaction between normal and shear stresses and account for fatigue considerations. Analysis results show that fatigue is an important factor in determining these locations and should be carefully considered in any evaluation, especially if welding in the vicinity of the holes will be used. Based on the proposed schemes, suitable regions where access hole can be placed without additional strengthening are identified for each bridge. In addition to bottom flange access holes, locations are also identified for placing openings in the webs. Strengthening should be considered for access holes located outside the proposed regions.

INTRODUCTION

Motivation

On a regular basis, DOT personnel have to crawl inside box girders for inspection purposes. Access hatches are usually provided before and after an expansion joint where bending moments are at their minimums. The spans covered by box girders are often long spans, and the girders are constructed as continuous girders over two or more supports. In many cases, the distance between access hatches is likely to violate the recommended distance of 600 ft, which is the limit that rescue crews can reach in the eventuality of an emergency (NIOSH safety standard).

A number of existing box girder bridges in District IV of the Florida Department of Transportation do not satisfy the NIOSH recommendations for distance between access points, which places workers inspecting the inside of the bridges at risk. This situation has concerned the FDOT Safety Office and resulted in the Safety Office requesting the construction of additional access holes in box girder bridges that do not satisfy safety standards. The additional access holes must be constructed without compromising the structural integrity and safety of the bridges. Due to lack of information about this topic, a research proposal from the University of Central Florida (UCF) was approved for funding by FDOT to investigate the problem and provide recommendations that would help in identifying suitable locations for adding access holes to existing box girder bridges.

Approach

It was evident from a review of the literature that not much information is available about the behavior of curved box girder bridges. The effect of holes on the behavior of this type of bridges could not be found in any published work. To overcome the lack of information in depth studies were needed.

The problem was approached from an analytical point of view. Several models were developed to understand the behavior of horizontally curved box girder bridges and the impact

of adding access holes on this behavior. Both elastic and inelastic analyses were performed. The AASHTO-LRFD code was followed in determining some of the guidelines needed to conduct the analyses. The goal of the study was, first to investigate the feasibility of adding access holes to existing bridges, and second to reach an understanding of where these holes may be added. To achieve the second goal, several schemes for determining hole locations were tested and applied to existing bridges.

Organization of the Report

This draft final report presents the work done through the project titled "Strategies for Placing Openings in Curved Box Girders". During the period of the project several progress reports were presented to FDOT. The report integrates the work reported in the previous progress reports and summarizes the findings from this study.

The report is organized in six sections and three appendices. After the introduction section, the literature related to the topic is reviewed. The following section describes the finite element package chosen for the study. In this section, the verification study of the commercially available package is reported. A separate section is devoted to describing the finite element models used to conduct the analyses in this project. Two sections report the results of the analyses performed using these models. The first describes detailed finite element analyses on an existing bridge. This bridge was investigated using linear elastic and nonlinear inelastic models. Effects of holes on the strength and fatigue aspects of design are presented in this section. The other analysis section reports a study on nineteen bridges. The study was performed using a beam element model. These linear elastic analyses followed the AASHTO-LRFD code in terms of loading and load factors. Finally, the section summarizing the findings is given followed by a list of references. At the end of the report 3 appendices can be found. The first of the appendices gives a theoretical background about the warping theory of closed sections. The other two appendices provide the results of the beam element study on the nineteen existing bridges.

LITERATURE REVIEW

The literature review has yielded more than 25 references (journal articles, reports, books, ...etc.) that deal with the behavior, strength, and design of curved steel box girders. Articles of direct interest were reviewed thoroughly leading to a categorization of available literature into two main groups. The first of these two groups deals with methods of analysis and design, while the second addresses experimental studies and the behavior of curved steel box girder. A summary of the contents of these articles is given in the next sections. A list of these references can be found at the end of this report.

1) METHODS OF ANALYSIS AND DESIGN:

DESIGN OF HORIZONTALLY CURVED COMPOSITE BOX-GIRDER BRIDGES: A SIMPLIFIED APPROACH. (*Cheung, M. S., Foo, S. H. C.*)

This paper presents results of a parametric study on the relative behavior of curved and straight box-girder bridges. The authors also developed a simplified design method for the combined longitudinal moment of curved bridges. The parameters considered were cross-section, span length, radius of curvature, and finally, types, location and magnitude of loads.

In order to establish a simple design aid for combined longitudinal moment of horizontally curved bridges, a series of curved and straight bridges with different configurations were analyzed using the finite strip method. Stress distributions were plotted with respect to the span-to-radius ratio (L/R), as the results of the study have shown that the structural behavior of curved bridges is essentially governed by this dimensionless parameter (L/R).

Results were presented in the form of L/R vs. moment ratio plots for different variables. Based on these results, the simplified method for the design of horizontally curved bridges with simple supports was proposed, and a maximum subtended angle of less than 60°. Tables were provided to determine the combined longitudinal moments of a simply supported curved composite box girder bridge by means of multiplying the longitudinal moments of an equivalent

straight bridge by the appropriate factors. It was also found that interior girders as well as deep box-girders are more sensitive to the degree of curvature.

REFINED ANALYSIS OF CURVED THIN-WALLED MULTI-CELL BOX GIRDERS. *(Razaqpur, A. G., Li, H. G.)*

The main objective of this paper was to develop a curved thin-walled multicell box beam finite element which can model extension, flexure, torsion, torsional warping, distortion, distortional warping, and shear lag effects. The theory is based on the generalized Vlasov's thin-walled beam theory and finite element technique. In this paper the interaction between the longitudinal and transverse deformations of the box girder was also studied.

Since the proposed element is essentially a one-dimensional beam model, the required computer resource will be small compared to the standard finite element technique, and thus it can be easily implemented on practically any microcomputer. The element stiffness matrix and nodal load vector will be derived first based on the degrees of freedom (DOFs) of three nodes. A static condensation technique is subsequently used to eliminate the internal DOFs. To demonstrate the accuracy and versatility of this theory, various examples for different types of box girder bridges were presented, and the results were compared to the experimental model studies or to the alternative numerical method by other researchers. Numerical examples show that the stresses and displacements are in good agreement with results of shell finite element and finite strip analyses.

AN IMPROVED HORIZONTALLY CURVED BEAM ELEMENT. *(Hsu, Y. T., Fu, C. C., Shelling, D. R.)*

The authors of this paper proposed the use of an improved horizontally curved beam finite element to include a true warping degree of freedom.

The capability of the stiffness matrix of a horizontally curved beam element has been demonstrated. It was shown that the developed stiffness matrix is especially effective and fairly accurate for analyzing a horizontally curved bridge. The variational method was used to formulate the stiffness matrix in an explicit form.

In order to verify the validity and accuracy of the suggested curved beam element, a computer program was developed. An example girder, analyzed by Brookhart using a closed form solution, was analyzed using the program. The results from this theory show excellent agreement with those obtained by Brookhart. Also, the proposed stiffness matrix for the curved beam is valid for both open and closed sections as long as the curved girders are modeled as curved beam structures.

METHODOLOGY FOR IMPACT FACTOR OF HORIZONTALLY CURVED BOX BRIDGES. *(Galdos, N. H., Shelling, D. R., Sahin, M.A.)*

In this paper, a method to determine the dynamic impact factor of horizontally curved steel box girder bridges is proposed. The two-dimensional planar grid method was used for modeling curved box girder bridges to investigate the dynamic behavior, under truck loading. The authors used the DESCUS II computer program for the modeling of curved box bridges.

The bridge samples used here comprise four idealized composite curved box girders. Comparison of typical solution responses of different girders for maximum absolute moment and maximum absolute torque were studied. The mode superposition method, the direct integration method, and a static solution were utilized. The bridge behavior under moving vehicles was observed by calculating the dynamic increment factor (DIF).

AASHTO recommends that curved bridges be analyzed as a system such that maximum forces or stresses are searched to predict critical loading cases. As a result, DIFs are to be calculated for each loading case and truck loading path. So there will be several sets of DIFs for different circumferential paths for each loading case.

Alternate impact factor criteria are proposed. The criteria are correlated with the maximum static effects as opposed to the classical criterion of selecting the maximum absolute impact-factor values.

EVALUATION OF IMPACT FACTORS FOR HORIZONTALLY CURVED STEEL BOX GIRDERS. *(Shelling, D. R., Galdos, N. H., Sahin, M. A.)*

The impact factors specified within the AASHTO "Guide Specifications for Horizontally Curved Highway Bridges"(1980) for steel box girder bridges are restrictive. They require a rational dynamic analysis when the bridge under consideration falls outside the specification criteria. So a comprehensive multivariant dynamic analysis was conducted for a data set of 288 horizontally curved steel box-girder bridges with radii, span lengths, and box configurations that represent those on the national inventory.

The planar grid method was selected as the model to generate the results reported herein. The stiffness method is applied to the analysis of the grid system with straight and curved elements. The results from the grid model were compared to those given by finite element models including SAP-IV and those developed by others.

The impact factors were obtained from the results of dynamic analyses of the contained in the data set. These results are given as a function of the radii of curvature, the fundamental natural frequencies, and the span length. The first fundamental frequency was found to be the governing frequency for all bridges studied herein. The results of the impact analysis for moment, torque, shear, reactions, and deflection are given as functions of the fundamental natural frequency.

FREE VIBRATION ANALYSIS OF CURVED THIN-WALLED GIRDER BRIDGES. *(Huan, C., Bezley, S. E., Huang, J.)*

This paper includes a theory that incorporates a special treatment of warping in the free vibration analysis of continuous curved thin-walled girder bridges. An additional degree of freedom, which represents the effect of warping for curved beam element with thin-walled sections, was used.

The theory is based on the development of the flexibility matrix using the theory of strain energy. Stiffness matrix is also formulated for a straight thin-walled element. Free vibration analysis is described, and natural frequencies are examined to confirm that the derived theory is accurate.

The effects of various factors including warping, the noncoincidence of the shear center and the centroid of the section, the flexibility of piers, and the radius of curvature are also discussed. To compare the results of the theory, the free vibration analysis of two different curved bridges was performed. Finite element program SAP-IV was used for comparison. The calculated results of the free vibration analysis compares favorably to results from other methods.

VIBRATION OF THIH-WALLED BOX-GIRDER BRIDGES EXCITED BY VEHICLES. *(Huang, D., Wang, T., Shahawy, M.)*

The purpose of this study is to develop a procedure for evaluating the dynamic load of box-girder bridges with one or more vehicles passing over the rough bridge decks. The paper also studies the dynamic characteristics of different types of responses of bridge with different diaphragm arrangements due to vehicle movement over different classes of road surface roughness with various speeds. Both warping torsion and distortion are considered in the study.

To predict the dynamic response of bridges to moving vehicles, the authors treat both vehicle and bridge as mathematical space models. The finite element method of thin-walled beams is used to determine the response of the box-girder bridges with variable depth, deformable cross sections over supports, and intermediate diaphragms,.

The results obtained by the presented method are in good agreement with those calculated using a folded-plate model as proposed by other authors. It is easy to obtain impact factors of different types of stresses as well as different types of inner forces, such as bending moments, torques, and bimoments. The meaningful impact factors used in bridge design are related to the loading model, which can induce maximum static responses.

Further field tests are recommended. Also, there is no attempt to give the impact factors for practical design in this paper.

STRENGTH OF THIN-WALLED BOX GIRDERS CURVED IN PLAN. *(Yabuki, T., Arizumi, Y., Vinnakota, S.)*

A numerical method for predicting the influence of local buckling in component plates and distortion phenomenon on the ultimate strength of the thin-walled, welded steel box girders curved in plan is proposed.

Loads causing torsional deformation in curved box girders lead to distortion of the girder's cross-section. These distortions reduce cross sectional stiffness, which causes a reduction in the ultimate strength of the girder.

A nonlinear finite element analysis is used to study the nonlinear flexural behavior of curved girders. The effects of finite deformation, yielding of material under combined bending and St. Venannt's torsion, unloading caused by stress reduction, spread of yielding, and residual stresses due to welding are all taken into account in flexural analysis by a finite element method. Local buckling of component plates and distortional warping is also considered. The effect of local buckling can be evaluated by using either the effective width method or by adopting a modified stress-stain curve allowing for local buckling.

Experimentally, a model segment of the girder is loaded gradually. The strains and displacements were measured during the experiment.

The analytical and experimental results show good agreement. The authors thus suggest that the local buckling of component plates can be evaluated using the proposed stress-strain relationship. This constitutive relationship can be incorporated into nonlinear analyses. Finally, the authors suggest that use of transverse diaphragms considerably increase the ultimate strength of the girder.

2) EXPERIMENTAL STUDIES AND BEHAVIOR OF STEEL BOX GIRDERS:

BEHAVIOR STUDY OF CURVED COMPOSITE BOX GIRDERS. *(Arizumi, Y., Hamada, S., Oshiro, T.)*

This paper investigates the distortional and slip behavior of simply-supported curved composite box girders on the basis of elastic analyses and static tests.

Three test specimens were prepared for this study. Variable parameters included intermediate diaphragm spacing, the central angle, placement of shear connectors, and the width of the extended concrete slab. The cross-sectional deformations have been calculated using three different methods, namely the curved beam theory, the distortional theory proposed by Dabrowski, and the finite strip method, including the effect slippage between the concrete slab and steel girder.

The present analytical results of normal stresses based on the curved beam theory and the distortional theory proposed by Dabrowski were found to be in good agreement with experimental results for all test girders.

STUDY OF A CURVED CONTINUOUS COMPOSITE BOX GIRDER BRIDGE. *(Ng S. F., Cheung M. S., Hachem, H. M.)*

The objective of this study is to establish accurate experimental bridge response, which is later used for checking the predictions by computer analyses for structures of this type. Also obtaining sufficient data related to eccentrically loaded box girder bridges helps in establishing a general trend of behavior.

For the experimental purpose a 1/24 linear scale model was studied. The experimental strain data at a given load were the basis from which normal stresses were computed by using the classical Hooke's law relation. In the analytical method, the ADINA program was used to study the response of the bridge. Analytical predictions of both vertical displacement and normal stresses at critical sections compared fairly well with those evaluated experimentally. The authors finally conclude that the ADINA finite element program can be successfully utilized to predict accurate elastic response of composite curved box girder bridges.

SHEAR DISTRIBUTION IN SIMPLY-SUPPORTED CURVED COMPOSITE CELLULAR BRIDGES. *(Sennah, K., Kennedy, J. B.)*

In this paper, a parametric study on simply-supported curved composite cellular bridges is conducted. The effect of key parameters (e.g. the cross-bracing system, aspect ratio, number of lanes, number of cells, and degree of curvature) on the shear distribution of this type of bridge is examined. The main goals of the parametric study was to: (1) investigate the influence of all

major parameters affecting the shear distribution between the webs; (2) generate a database for shear distribution factors; and (3) develop empirical expressions for shear distribution factors for AASHTO truck loading as well as for dead load.

Results from testing four simply-supported curved composites three-cell bridge models are used to verify and substantiate the analytical model. The data generated from the parametric study is used to deduce expressions for the shear distribution factors for different loading conditions.

The experimental program involved the construction, instrumentation, and testing of four 1/12 linear scale three-cell bridge models. Each bridge model was tested elastically using a simulated truckload. In the theoretical study, the finite element modeling was carried out using the ABAQUS software. Shear forces in the webs were derived for truck loading as well as for dead load. Theoretical and experimental results agreed favorably.

Through this extensive study the authors have suggested an empirical formula for Shear Distribution Factor, D_f.

3) OPENINGS IN GIRDERS:

The literature search did not yield any published work on the effects of openings on the strength or behavior of box girder bridges. A guideline for the design of steel and composite beams with web openings (AISC-1990) could be found. However, it is limited to the design of beams in buildings only, and hence cannot be applied to bridges, specially curved bridges.

ANALYSIS TOOL

The finite element analyses were conducted using the commercially available software package ABAQUS (1996). ABAQUS is available at UCF on a SUN UltraSpark workstation. This hardware/software combination allowed for the analysis of relatively large models. Even though ABAQUS is a reputable software package, it is still necessary to verify the quality of the results that are obtained from the analyses versus experimental or other analytical methods. The following section reports the verification work done at the beginning of the project.

VERIFICATION OF ABAQUS

In order to make sure that ABAQUS is the right tool for this study, which involves many analyses of box girder bridges, several verification cases were considered. As will be seen later in the report, two types of models were used in this study. Therefore, verification studies were needed for each model type. The results of these studies are reported next.

SHELL MODEL VERIFICATION

The first verification girders are approximately one-quarter scale of box girder projected in the construction of a monorail bridge in Naha City, Japan (Yabuki et al. – 1995). The steel box has a height of 800mm and a width of 200 mm. The top and bottom flanges extend 30mm beyond the webs on each side (i.e. flange width=260 mm). The high depth-to-width ratio of the girder is strengthened by 5 diaphragms (3 intermediate diaphragms for M-3) in addition to the end diaphragms. Plate thicknesses are 9 mm and 6 mm for flanges and webs, respectively. The radius of curvature is 12 m and the central angle is 30°

The girder was modeled using the four-node shell element (S4R5), which uses a reduced integration scheme. Steel was modeled with a bilinear stress strain relationship. The first

segment was defined based on the modulus of elasticity reported by the authors. Beyond yield a slope of $1\%E_{initial}$ was assumed for the second segment of the stress-strain relationship. One concentrated load was applied to the girder at mid span. A thick loading plate was used to apply the load during the experiment and was modeled as a beam element over the top flange (in the radial direction) with thick dimensions in the finite element model. This was necessary to avoid stress concentrations under point loads. Boundary conditions were imposed on the girder as those reported for the experiment. In addition to the classical simple beam boundary constraints, the beam was fixed against rotation at supports. However, it was allowed to warp freely.

Several runs were conducted to investigate the behavior of the girder. The variable parameter was the magnitude of imperfection incorporated in the model. A buckling analysis was carried out to obtain the buckled shapes of the girder. Two modes (1st and 2nd) were used for the subsequent nonlinear analyses. Four different levels of initial imperfection were considered, namely 0mm (no imperfection), 2mm, 4mm, and 8mm. It was observed that the level of imperfection greatly affected the maximum achievable deflection of the girder at mid-span. This implies that failure is controlled by buckling; an observation that matches the reported experimental failure. When comparing the ultimate load capacity obtained from analyses to that from the test, the difference was found to range from 7.5% to 10.2% depending on the magnitude of initial imperfection added to the model. The difference can be attributed to the analytical boundary conditions, and how they were modeled. As reported by the authors, it is possible that the test apparatus has offered some flexibility to the tested girder.

Another comparison looks at the distribution of normal stresses obtained from the analysis and from the experiment as reported by the authors. Figures 1 and 2 show the plots for the inner and outer webs at mid-span of girder M-5 (5 intermediate diaphragms). It is obvious that the distributions match very well, and that the analytical distribution of the normal stress follows the experimental trend closely.

Figure 3 shows the deformed shape of Girder M-3 at failure. It is obvious that buckling is the controlling factor in the behavior. The main buckled members are the webs between adjacent stiffeners. The final load-deflection curves are given in Figs. 4 and 5. The ABAQUS results were obtained from nonlinear analyses that took into account material nonlinearities as well as geometric nonlinearities. Also residual stresses were included as reported by the authors.

For both models (M-3 and M-5) buckling was a major factor and affected the behavior greatly. This conclusion was also observed experimentally.

BEAM MODEL VERIFICATION

To verify the beam element model, two simply supported box beams were analyzed. The cross sectional properties of the beams were chosen from an actual bridge. In warping, the parameter $\kappa = L\sqrt{\frac{GK}{EI_\omega}}$ is the controlling factor in the response of a beam; where L is the span length, E and G are respectively the material modulus of elasticity and shear modulus, I_ω is the warping constant, and K is the torsion constant. The verification beams were given a value for κ equal to 30. The first beam was loaded with a concentrated unit torque acting at midspan, while a uniformly distributed torsional moment was used for the second beam. These cases were chosen as their closed form solution is reported in the literature. Each of the beams was analyzed using two models. The first model used 100 elements for the entire span. The other model was built using 1000 elements. Figures 6 and 7 show the results obtained from ABAQUS for both beams. The results obtained were in good agreement with the closed form solutions. It was obvious that more elements were needed to capture spikes that take place under concentrated torsional moments. The 1000-element model resulted in values for the bimoment and the warping torsional moment that are much closer to the closed form solution results than those of the 100-element model are. Under uniform torque, the bimoment results were exactly equal to what is obtained from closed form solution.

ANALYSIS MODELS

Two modeling approaches were utilized in the analytical study. The first is a simplified elastic model based on special beam elements that have a warping degree of freedom. The second model was created using shell finite elements and was designed to capture as much detail as possible. The first model was used only for elastic analyses, while the second was used to perform both elastic and nonlinear studies. The following sections describe these approaches in detail.

BEAM (SIMPLIFIED) ELEMENT MODEL

The goal from developing this model is to study the global behavior of curved girders. This model provides information on the distribution of internal forces associated with curved girders (bending moments, shear forces, torsional moments, warping torsional moments, and bimoments). Stresses can then be calculated at various locations in the structure from these internal forces. All analysis performed using this model were conducted using elastic material properties even though factored loads as adopted by design codes were considered.

This simplified model is based on a special beam element from the ABAQUS element library. The element accounts for the effect of warping and requires cross-sectional geometric properties (area, moments of inertia, warping constant, ...etc.) as input. These properties have to be calculated separately. While calculations of areas and moments of inertia are fairly easy and straightforward, this is not the case for the warping constant. A computer program was developed for this purpose using the MATLAB software package.

MATLAB is a software package capable of performing many mathematical operations symbolically. Utilizing its programming language it was possible to implement the complex

formulas involved in determining the warping constant. Appendix A describes the derivation of the expression of the warping constant, $I_{\omega\omega}$. The program can handle single-cell cross-sections with overhanging decks. It was developed in a general way so that nonsymmetric cross-sections can be treated. By breaking the cross-section into several segments, different properties (thicknesses, materials) can be given to each part (webs and flanges). The developed program was verified by comparing the obtained results to those reported in the literature for two problems. In order to visually inspect the results, a function was added to the program to plot the geometrical properties of the cross section. Figure 61 in Appendix A shows the plot of the warping function, ω, for one of the verification problems.

SHELL (DETAILED) FINITE ELEMENT MODELS

To study the behavior of box girders in more detail, more detailed finite element models are needed. The detailed models are based on shell elements, S4R5 from ABAQUS element library. Other element types, such as 3-D beam elements, were used where necessary to model structural parts that do not need the sophistication of shell elements. The shell elements were used to model the plates forming the cross section of the girders. Details such as stiffeners, cross frames, end diaphragms, were taken into account. Steel and concrete material properties were accurately modeled. Steel rebars were also included in the concrete deck part. Each shell element was assigned a thickness based on which plate it is a part of. It is believed that these models are capable of capturing all the aspects of the behavior of composite box girder bridges. Linear elastic runs and nonlinear inelastic runs were conducted using these models.

Two types of shell element models were used. The first is a model of several spans of a bridge. This model was used to investigate the actual behavior of an existing bridge beyond the elastic range. It modeled 3 spans of the bridge. A finer mesh was used at the locations of interest. To study fatigue, elastic runs were executed on this model. This model will be referred to as "Shell Model I" in this report. Details of this model can be found in a separate section.

The other shell model, referred to as "Shell Model II", was developed to study a small segment of box girder bridges. The length of the straight segment considered is equal to four times the depth of the girder. Nonlinear material properties were modeled for the middle part of the model only. This was done to avoid any stress disturbances that occur due to boundary conditions. The elastic parts at the ends worked as a distribution region to keep the condition at the study region as desired. In addition to the elastic regions at the ends, a rigid diaphragm was provided to distribute loading to all nodes at the ends avoiding any stress concentrations. It was possible to use more elements and include more details in this model since its length is very limited as compared to the other shell element model (28 feet vs. 572 feet). Details of the model are given in a later section.

BRIDGE 538

Based on the plans provided to the project team by FDOT detailed finite element models were built for Bridge 538. The bridge serves as the interchange between I-95 and I-595. It consists of 2 trapezoidally shaped cells. The layout of the bridge shows that the desired curvature is achieved through 2 spiral segments and 5 circular curves. The degree of curvature varies depending on the location. A total of 21 spans varied in length from 121 to 210 feet.

Modeling the bridge in its entirety is not believed to be necessary. Studying the local behavior around openings is not greatly affected by loading cases specially designed for developing extreme internal forces in far away locations. Furthermore, modeling of the entire bridge would have required great computer resources for no additional gain. It was therefore decided that modeling three spans of the bridge is adequate for the purpose of this study. The three spans were picked such that the maximum curvature (D=4°) and the maximum span (L=210ft) are included. Only one cell is considered. The modeled bridge is assumed to be horizontal neglecting small vertical curvature. This configuration would include the major factors affecting the design of curved bridges. Its continuity would include the effects of negative moments in addition to positive moments and shear forces. The included curvature allows for torsion to develop which is a major player in the design of curved girder bridges due to the additional normal (due to warping) and shear stresses it creates.

The three models were developed for the bridge are described in the following section.

SHELL MODEL I FOR BR538

The developed model incorporates most of the important details found in the actual bridge. Changes in plates' thicknesses for webs and flanges are included. Web stiffeners are modeled using beam elements, while the concrete deck is modeled using shell elements. The plane of shell elements modeling the deck is higher than the top flange by half the thickness of the concrete deck (4 inches). Constraint equations will be added to connect both parts (steel box and concrete deck). Steel reinforcement in the concrete deck was modeled according to the information provided in the bridge plans. The top steel flange is modeled using beam elements that have the same area as that of the top flange. Cross frames are included in the model using beam elements. Meshing of the bridge is done in such a way that focuses on locations of interest. This is achieved by increasing the number of elements around locations where openings are expected to be located. Transition from a coarse mesh arrangement to a fine mesh arrangement is achieved using appropriate constraint equations. This mesh arrangement reduces computer resource requirements. Figures 8 through 10 show general views of the developed model. The cross-section of Bridge 538 can be seen in Fig.11.

The model has about 7000 elements. The number of elements varies slightly based on whether an access hole is added to the bridge or not.

MATERIAL MODELING FOR SHELL MODEL I

The provided plans were used to extract the material properties used in the analyses. Steel was assumed to have a bilinear stress-strain relationship in both tension and compression. A yield stress, F_y, of 248 N/mm^2 was used for steel. The modulus of elasticity, E_s, was assumed to be 200,000 N/mm^2. Beyond yield, the slope of the stress-strain relations ship was taken as 2% of the initial modulus of elasticity, E_s. It is believed that this slope does not affect strength predictions, however, it enhances the numerical stability of the model. Rebars were assumed to have the same properties.

The maximum stress used for concrete, f_c', was 23.44 N/mm^2 in compression. The tensile strength of concrete was taken as 10% of f_c'. The modulus of elasticity, E_c, was determined

based on the equation proposed by ACI. E_c was taken to be equal to 22,915 N/mm^2. After reaching f_c', it was assumed the slope of the second linear segment of the stress strain curve for concrete to be 2% of the initial modulus of elasticity, E_c. Tension stiffening for concrete was assumed to fade away from the maximum tensile strength to zero over a strain value equal to 0.005. Steel reinforcement was assumed to have the same material properties described before.

MODELING OF STIFFENERS

Stiffeners are provided to strengthen steel webs and flanges. They are welded to one side of the parent plate. This arrangement shifts the centroid of the stiffener from the middle surface of the parent plate. Stiffeners are modeled as 2-node beam elements (BEAM GENERAL SECTION in ABAQUS). While it is possible to provide a shift of the centroid and the shear center for this element, this is only limited to elastic analyses. Since the detailed shell element model will be used to study the behavior beyond the elastic limit, it was necessary to find a way to overcome this problem. Any model should be able to simulate the original configuration both in the elastic range and the plastic range.

In the elastic range, the parallel axis theorem is used to find a moment of inertia which takes the shift of centroids into account.

A more detailed scheme is needed to get the shift effect beyond the elastic limit. For this purpose a problem similar to the bridge conditions was analyzed. The model is based on an arrangement that is repeated in Bridge 538. This part is a web plate (12.7 mm) that is strengthened by a stiffener which is 152.4 mm x 12.7 mm. This stiffener is provided every 2438mm. This part was isolated and studied using two models. The first is an all shell element model. The second model uses shell elements to model the web plate and beam elements to model the stiffener. Geometric properties were calculated for the stiffener taking into account the shift between centroids. Initially the M-ϕ relationship was provided for a concentric arrangement. Figure 12 shows the load-deflection curves obtained from both models. It can be seen that a constant difference appears between both results because of ignoring the shift effect beyond the elastic limit. This difference was determined to require a modification factor of 1.6 for the M-ϕ relationship of the eccentric beam element. Rerunning the problem with the

modified properties yields in the results shown in Fig. 13. Load-deflection relationships from both models are found to be in good agreement after using the M-ϕ modification factor. This modification factor will be used for all web stiffeners in the detailed model.

LOADING OF SHELL MODEL I

Several load cases are considered to study Bridge 538. For dead loads, one load case is analyzed. In accordance with AASHTO (1994), a combination of a tandem load and a lane load were considered to study the live load effects.

The tandem load was applied in positions that would cause maximum stress at the section being studied. A tandem load is a group of 4 concentrated forces representing 2 axles. Each axle exerts a 110 kN force on the bridge. The distance between the axles is 1200 mm while the distance between the wheels in one axle is 1800 mm. In addition to the gravitational vertical forces, a centrifugal force was included according to AASHTO. The level at which the centrifugal force acted was 1800 mm higher than the surface of the deck. For the fatigue study, a standard AASHTO truck replaced the tandem load. The standard truck consists of 3 axles, two of which are equal in weight (145 kN), and a lighter axle (35 kN) totaling 225 kN. The distance between the main axles can vary between 4500 mm and 9000 mm, which is much larger than that between the tandem axles.

Uninterrupted lane load was considered to act on entire span(s), but only applied to the span(s) that make the loading condition more sever. The width of the lane load is taken as 3000 mm. The intensity of the lane load is 9.3 N/mm. Positioning of loads on the cross-section is illustrated in Fig. 14.

SHELL MODEL II FOR BR538

This is the second shell model for Bridge 538. With this model an accurate strength assessment of the cross sections of box girder bridges can be reached. Effects of adding access hole on the strength of the cross sections were investigated for several loading conditions. Because of the limited length of the model, it was possible to model details more accurately. The stiffeners were modeled using shell elements. The main part of the cross frames (horizontal bottom member) was also modeled using shell elements.

The same dimensions reported earlier in the discussion of Shell Model I for Bridge 538 were used for this study.

MATERIAL MODELING FOR SHELL MODEL II

The same material properties used for Shell Model I were also used for Shell Model II. A minor change was introduced the to the slopes of the second segment of the stress-strain relationships of both concrete and steel. Beyond the peak stress a 1% $E_{initial}$ slope was used for the second segment. Shell Model I used a 2% $E_{initial}$ slope. This measure was taken to avoid excessive strain hardening that takes place at high strain levels and result in unrealistic strength values. The tension stiffening model for Shell Model II was the same as for Shell Model I.

In order to minimize any disturbance in the stress distribution, the elastic parts at both ends of the model were given the same material moduli but were not allowed to yield or crack as for the intermediate zone.

LOADING OF SHELL MODEL II

The loading for this study was designed to create a case of pure moment on the cross section. The rigid end diaphragms reduced any stress concentrations due to loading at the ends. Elastic regions dissipated stress disturbance that may develop near boundary conditions. These facts left the region of interest in a pure state of flexure. Both positive moments (concrete in compression) and negative moments (concrete in tension) were studied. Each case was run

twice, once with a hole in the bottom flange and the other without the hole (original configuration).

In summary the following load cases were considered:

- Positive moments and without a hole in the girder.
- Positive moments and with a hole in the girder.
- Negative moments and without a hole in the girder.
- Negative moments and with a hole in the girder.

Figure 15 shows the positive moment case for Shell Model II.

BEAM MODEL FOR BR538

A simplified model was created for bridge 538. The model is based on a 2-node 7-DOF beam element. A seventh DOF allows for capturing the warping of the bridge cross-section. All together the model provides information on the distribution of internal forces associated with curved girders (bending moments, shear forces, torsional moments, warping torsional moments, and bimoments). Details of the derivations of formulas for warping cross-sectional properties can be in Appendix A.

The cross-sectional properties of the bridge were determined using the MATLAB program which was specifically developed for this purpose. The cross-sectional properties are calculated taking into consideration the different material properties of concrete and steel. The geometric properties of each cross section were calculated twice. The first set of geometric properties is for a quasi-open cross section, and was used for dead load calculations. The member connecting the top flanges was determined according to the Equivalent Plate Method (EPM) based on the formula developed by Kohlbrunner and Basler (1969), that provides the thickness of the equivalent member. This method accounts for the bracings that are usually provided during construction before placing the concrete deck. After casting the concrete deck a steel/concrete composite closed cross section is created. The second set was based on this type of section and was used for live load calculations. A perfect bond between steel and concrete is assumed.

The cross-sectional properties of the open noncomposite cross-section as well as the closed composite cross-section of Br538 at one of its sections can be found in the following tables. Plots of these properties can be seen in Figs. 16 through 18. For comparison purposes, the geometric properties of a true open cross section are also provided.

GEOMETRIC PROPERTIES FOR BRIDGE 538

Open cross section – noncomposite

Shear Center Location: (from Centroid +=down,right)

x_s = 0.0000 mm y_s = 1707.3388 mm

I_x = 9.8395e+010 mm^4 I_y = 1.9921e+011 mm^4

K = 1.9869e+007 mm^4 I_ω = 5.7075e+016 mm^6

Elem	S_x		S_y		ω		S_ω	
1	0.000e+000	-6.941e+006	0.000e+000	-8.137e+006	1.454e+006	8.388e+005	0.000e+000	-5.823e+009
2	6.941e+006	0.000e+000	9.153e+006	0.000e+000	8.388e+005	2.241e+005	2.700e+009	0.000e+000
3	-1.388e+007	-2.227e+007	-1.729e+007	-5.713e+007	8.388e+005	-1.075e+006	-8.522e+009	-5.220e+009
4	-2.227e+007	2.227e+007	-5.713e+007	-5.713e+007	-1.075e+006	1.075e+006	-5.220e+009	-5.220e+009
5	2.227e+007	1.388e+007	-5.713e+007	-1.729e+007	1.075e+006	-8.388e+005	-5.220e+009	-8.522e+009
6	-6.941e+006	0.000e+000	9.153e+006	0.000e+000	-8.388e+005	-2.241e+005	2.700e+009	0.000e+000
7	6.941e+006	-2.476e-008	-8.137e+006	1.118e-008	-8.388e+005	-1.454e+006	-5.823e+009	-6.939e-006

Closed cross section (only bracing) – noncomposite

Shear Center Location: (from Centroid +=down,right)

x_s = 0.0000 mm y_s = 1277.6218 mm

I_x = 1.0653e+011 mm^4 I_y = 2.0259e+011 mm^4

K = 6.0014e+010 mm^4 I_ω = 2.9271e+016 mm^6

Elem	S_x		S_y		ω		S_ω	
1	-2.978e+006	-9.694e+006	7.054e+006	-1.084e+006	1.045e+006	5.645e+005	2.591e+008	-3.830e+009
2	6.716e+006	0.000e+000	9.153e+006	0.000e+000	5.645e+005	4.454e+004	1.547e+009	0.000e+000
3	-1.641e+007	-2.746e+007	-1.024e+007	-3.211e+007	5.645e+005	-9.536e+004	-5.377e+009	-8.662e+009
4	-2.746e+007	-2.356e+007	-3.211e+007	-5.008e+007	-9.536e+004	-7.552e+005	-8.662e+009	-2.706e+009
5	-2.356e+007	-2.421e-008	-5.008e+007	-6.667e+007	-7.552e+005	-4.987e-010	-2.706e+009	8.257e+009
6	-2.421e-008	2.356e+007	-6.667e+007	-5.008e+007	-4.987e-010	7.552e+005	8.257e+009	-2.706e+009
7	2.356e+007	2.746e+007	-5.008e+007	-3.211e+007	7.552e+005	9.536e+004	-2.706e+009	-8.662e+009
8	2.746e+007	1.641e+007	-3.211e+007	-1.024e+007	9.536e+004	-5.645e+005	-8.662e+009	-5.377e+009
9	-6.716e+006	0.000e+000	9.153e+006	0.000e+000	-5.645e+005	-4.454e+004	1.547e+009	0.000e+000
10	9.694e+006	2.978e+006	-1.084e+006	7.054e+006	-5.645e+005	-1.045e+006	-3.830e+009	2.591e+008
11	2.978e+006	6.054e-009	7.054e+006	8.745e+006	-1.045e+006	-1.171e-010	2.591e+008	1.437e+009
12	6.054e-009	-2.978e+006	8.745e+006	7.054e+006	-1.171e-010	1.045e+006	1.437e+009	2.591e+008

Closed cross section – composite

Shear Center Location: (from Centroid +=down,right)

x_s = 0.0000 mm y_s = 22.9733 mm

I_x = 2.4814e+011 mm^4 I_y = 6.9727e+011 mm^4

K = 2.7224e+011 mm^4 I_ω = 4.4128e+016 mm^6

Elem	S_x		S_y		ω		S_ω	
1	-8.026e-009	-2.929e+007	1.214e+008	8.647e+007	-1.155e-009	2.572e+005	2.594e+009	-2.680e+009
2	2.667e+007	0.000e+000	9.246e+007	0.000e+000	2.572e+005	-8.851e+005	-1.172e+010	0.000e+000
3	-5.596e+007	-4.416e+007	-5.991e+006	-4.761e+007	2.572e+005	7.489e+005	9.041e+009	-5.678e+009
4	-4.416e+007	2.293e-009	-4.761e+007	-6.420e+007	7.489e+005	1.426e-009	-5.678e+009	-1.655e+010
5	2.293e-009	4.416e+007	-6.420e+007	-4.761e+007	1.426e-009	-7.489e+005	-1.655e+010	-5.678e+009
6	4.416e+007	5.596e+007	-4.761e+007	-5.991e+006	-7.489e+005	-2.572e+005	-5.678e+009	9.041e+009
7	-2.667e+007	0.000e+000	9.246e+007	0.000e+000	-2.572e+005	8.851e+005	-1.172e+010	0.000e+000
8	2.929e+007	3.078e-008	8.647e+007	1.214e+008	-2.572e+005	-1.566e-010	-2.680e+009	2.594e+009

LOADING OF BEAM MODEL

Several load cases are considered to study Bridge 538 using the beam element model. For dead loads, one load case is analyzed. As described before for the shell element model, a combination of a tandem load and a Lane load were considered to study the live load effects. Three load cases were considered for the lane load. Each case with one span entirely covered by the lane load. The tandem load, which consists of a pair of axles, was positioned at twenty-two different positions along the bridge span. Tandem load cases also included the centrifugal force effects. Overall, twenty-six load cases were considered for the study. Load cases were then combined to obtain envelopes of maximum and minimum straining actions. Following AASHTO, only one tandem load pair was considered for positive straining actions values. Two tandem load pairs (having a distance of 8000 mm to 12000 mm in between) were considered for negative straining actions values and inner support reactions.

RESULTS FOR BR538

COMPARISON BETWEEN MODELS

Since only elastic analyses can be performed using the beam element model, a linear elastic analysis was executed using Shell Model I. The run is that of the dead load case. Table 1 shows a comparison between reactions at each of the bridge supports. It can be seen that the maximum difference between both results has dropped to less than 1.3%.

Figure 19 shows a comparison between the deflection curves of Bridge 538 that were obtained from the beam element model and the shell element model. It is obvious that both models are in good agreement. Differences in results can be attributed to the dead loads applied to each model which are obvious from the total reaction given in Table 1. Table 2 lists maximum deflection values for all three span of Bridge 538.

It was concluded that the simplified beam element model is a valid tool for conducting research on the general behavior of curved box girder bridges.

Table 1: Comparison of Support Reactions (kN)

	Beam Model	Shell Model I
1st Support	979.52	995.66
2nd Support	2903.5	2957.15
3rd Support	2294.3	2310.35
4th Support	644.1	646.14
Total Reaction	6821.42	6909.30

Table 2: Comparison of Bridge Deflections (mm)

	Beam Model	Shell Model I
1st Span	105	103.6
2nd Span	33.52	39.42
3rd Span	22.92	23.92

NONLINEAR ANALYSIS OF BRIDGE 538

A nonlinear analysis was performed on the shell model of the bridge. The bridge was loaded with factored dead loads and live loads (lane load and design tandem load). The live loads were positioned to cause the most severe condition at the middle of the second span. Using Shell Model I, the bridge was analyzed using ABAQUS to include the material and geometric nonlinearities.

Figure 20 shows that parts of the steel box have yielded. The yield is around the maximum positive moment regions where the bottom flange yields in tension. Over the supports, the bottom flange yields in compression due to the large negative moments that develop due to continuity. In Fig. 21 the cracking of concrete is obvious over the supports where negative moments cause tension in the concrete deck. Figure 22 shows the load deflection relationship for this run.

FATIGUE INVESTIGATION OF HOLE LOCATIONS

To study the effect of opening an access hole in the bridge, a finite element analysis of Shell Model I for Bridge 538 was carried out in the elastic range. The objective of this study was to compare the response of the bridge with respect to the locations of the hole. For this comparison, two cases were studied in detail. In the first model, a hole was punched in the bottom flange at the center of the second span (longest L=210ft), where the maximum positive bending moment occurs. In the second case, a hole was positioned in the bottom flange at about one quarter of the same span, which is close to the point of contraflexure. A location closer to the pier (support) was not possible because of the existence of longitudinal bottom flange stiffeners that extend from the supports to about 25% of the span length. This location is not exactly at the contraflexure point which shifts due to the moving nature of the live loads, however, very close to it. The studied access holes were given a diameter of 2ft. The following load cases were considered in the comparison:

- Dead load.
- Dead load + Live load (lane load and design tandem load positioned to cause maximum internal forces at the location of the hole).

- Standard truck load (Including effect of centrifugal force and an impact factor of 1.15 for fatigue (AASHTO-LRFD 3.6.2.1-1))

The geometry of a bottom flange plate with a hole is as shown in figure.

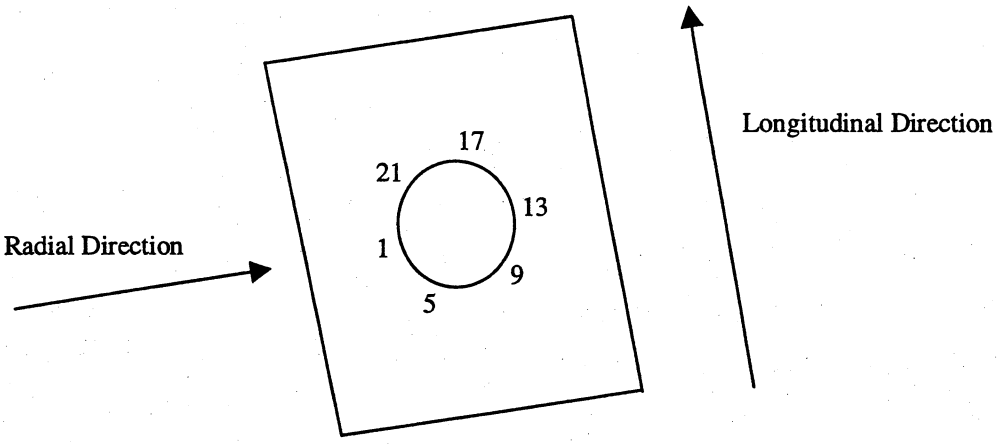

For the finite element model, a finer mesh was used around the hole. The following figure shows the details of the mesh in a panel in which a hole has been punched.

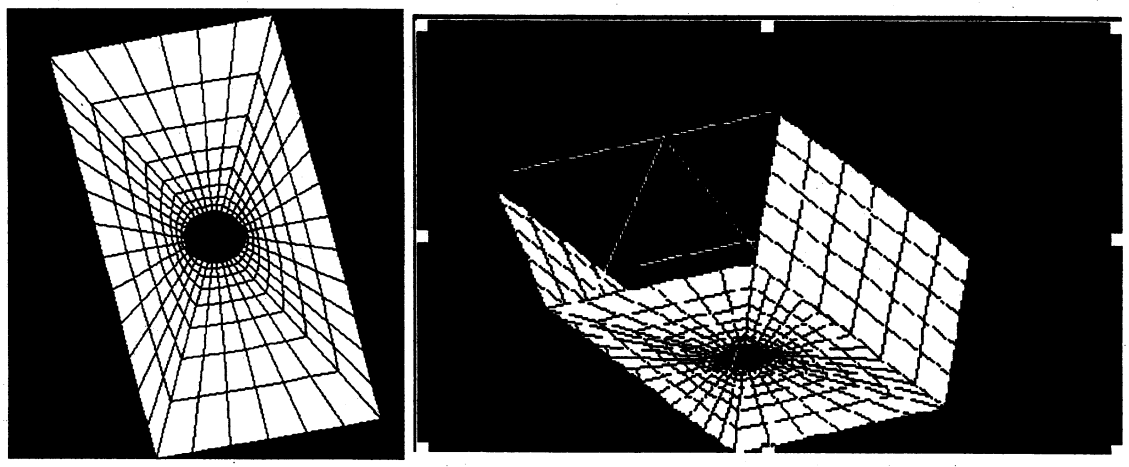

Mesh around the hole. Distribution of stresses in the vicinity of the hole.

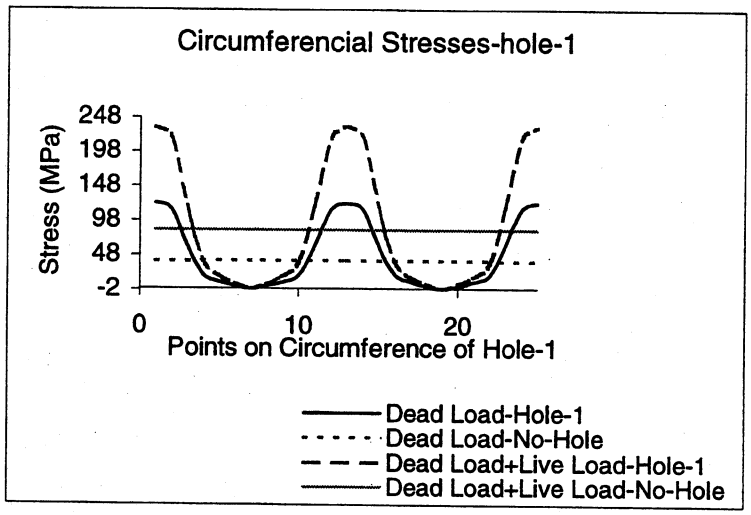

To find out the effect of fatigue, major principal stresses along the circumference of the hole were plotted as shown in figure. Hole-1 is located at the center of the span.

The stress distribution along the circumference of Hole-2, which is located close to the point of contraflexure, is as shown in figure.

The bridge was also checked for the fatigue according to AASHTO. It was assumed that Bridge 538 falls under Category B. (Built-up members with continuous fillet welds parallel to the direction of applied stress)

For load induced fatigue, the following design equation was used:

$$\gamma(\Delta f) \leq (\Delta F)_n$$

where, γ = Load factor specified in Table 3.4.1-1 =0.75

Δf = (Live load stress range due to standard design truck) x (Impact factor)

$$(\Delta F)_n = (\frac{A}{N})^{1/3} \geq 1/2(\Delta F)_{TH}$$

$(\Delta F)_{TH}$ = Constant amplitude fatigue threshold = 110 MPa

$A = 39.3 \times 10^{11}\ MPa^3$

N = (75) (365) n $(ADTT)_{SL}$

n = Number of stress range cycle per truck =1.0 for the given case.

$(ADTT)_{SL}$ = Average daily truck traffic =20,000 x 0.15 = 3000

N = $8.2x10^7$

$\therefore$ $(\Delta F)_n$ =36.3 MPa

But $(\Delta F)_n \geq 1/2(\Delta F)_{TH}$

$\therefore$ $(\Delta F)_n$ = 55 MPa

The following two figures show the maximum principal stresses along the circumference of the holes due to the presence of the fatigue inducing loads, as suggested by AASHTO. AASHTO specifies a single truck placed in the worst location for use in fatigue calculations. A load factor of 0.75 is used. The vertical component of the truck load was increased by 15% to include the impact effect. The horizontal component (centrifugal force) was not increased by any impact factors following AASHTO recommendations.

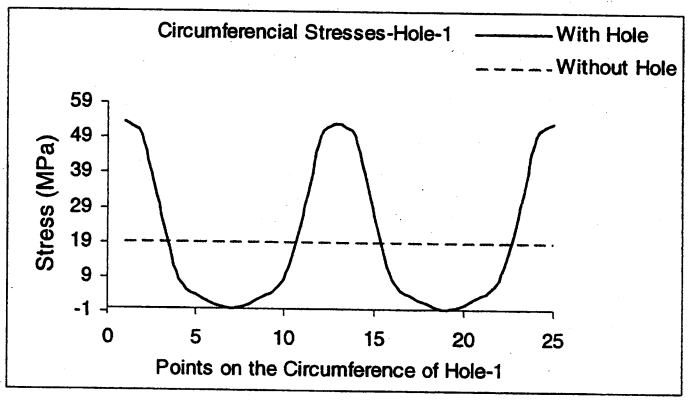

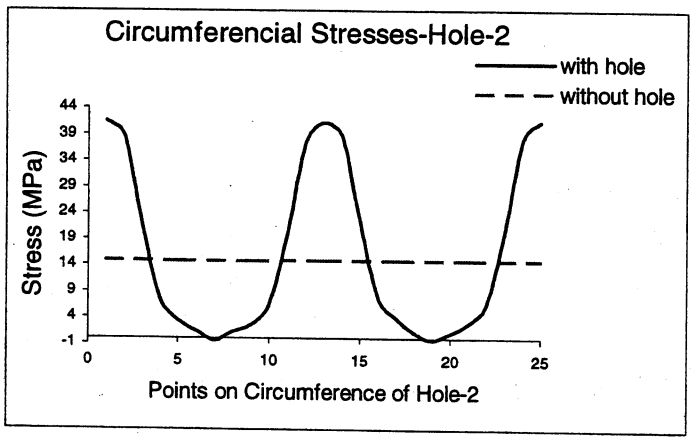

It was observed that both locations have stress ranges less than the AASHTO fatigue limit. However the center location will probably not have enough strength. Stress concentration, in case of the hole in center of the span, approaches yield (F_y=248 MPa) under working conditions. This does not happen in case of a hole in quarter span. This case was only considered for comparison purposes.

It should be noted that the due to stress concentrations, stresses are almost tripled in the vicinity of the hole. This fact is true for dead load stresses and live load stresses. The stress range which is limited by fatigue is caused by the truck portion of the load. The studied case showed that this range has also tripled to a value that is very close to the AASHTO allowable limit of 55 MPa. As will be seen later, fatigue is a limiting factor in determining regions where access holes can be added.

EFFECTS OF ACCESS HOLES ON FLEXURAL STRENGTH

Shell Model II was used to the study the effect of adding a hole to the bottom flange of Bridge 538. Two loading cases were considered. The first is a pure bending case causing the concrete deck to be in compression (positive moment). The other case represents the effects of negative moments which develop in the vicinity of supports and cause the concrete deck to be in tension. For each loading case, two analyzes were performed; the first is that of the original

cross-section and the second is for the cross-section after adding the hole. In all, 4 cases were run for this model.

Nonlinearities due to inelastic material properties and large deformations are included in these analyses. The description of the material properties can be found in the section about Shell Model I.

The following section present the results obtained from these analyses.

Concrete in Compression

The model without a hole showed a lot of yielding at high load levels. Yielding happened in the bottom flange and extended to parts of the web pointing to the formation of a plastic hinge. The moment-curvature relationship can be seen in Fig. 23. On the same figure the plastic moment capacity (from basic principles) and the first yield moments are also given.

The other positive moment run included a hole in the bottom flange of the model. As expected, due to stress concentrations yielding started at the edges of the hole. The capacity of the cross section was reduced by about 10 %. Figure 24 shows the moment-curvature relationship for this case.

A capture of the deformed shapes showing contours of longitudinal normal stresses is given in Figs. 25 and 26.

Concrete in Tension

The behavior for this loading was different than the previous case. The negative moments applied to the model caused the bottom flange to be stressed in compression. Buckling of the bottom flange was prevented by the existence of the bottom flange stiffeners which are connected to the cross frames. Webs are also strengthened by stiffeners, but these are much more flexible than bottom flange stiffeners and are not connected to any cross frames where buckling is likely. The thickness of webs is always much less than the thickness of bottom flange

plates. For the analyzed model it was obvious that buckling was the limiting factor for the strength of the cross section.

Figures 27 and 28 give the moment curvature relationships for both cases (with and without a hole). Also the plastic moment and the first yield moment values are plotted on the figures for comparison purposes. Contours of longitudinal normal stresses can be seen in Figs. 29 and 30.

Figure 31 is a plot of the moment curvature relationships for all cases. The figure shows the amount of loss of flexural capacity due to adding an access hole in the bottom flange. It can be seen that the stiffness of the cross section (initial slope of the relationship) is also affected by adding the hole. However the reduction in stiffness is considered substantial.

Hand calculations of the plastic moment capacity for the four cases showed good agreement with finite element analyses for the case of concrete in compression. An obvious difference existed for the case of concrete in tension. This difference can be attributed to the fact that buckling limited the strength, a phenomenon that hand calculations did not capture. The comparison can be seen in Table 3.

Table 3: Plastic moment capacity (M_p) of Bridge 538 (N.mm)

	Hand Calculations	**ABAQUS**
Nohole-cc	5.46E+10	5.59E+10
Hole-cc	4.46E+11	4.97E+10
Nohole-ct	4.95E+10	3.89E+10
Hole-ct	4.30E+10	3.65E+10

ACCESS HOLE LOCATIONS

The previous sections were concerned with different aspects of the behavior of box girder bridges. In this section, an attempt will be made to investigate the best locations where access holes can be added without severely affecting the strength and integrity of the bridges. This information will assist engineers in determining locations where access holes may be added without the need for major strengthening operations.

The locations discussed in this section are derived from structural analyses and satisfy structural requirements. Practicality of the locations should be investigated elsewhere.

STRATEGY

Several precautions shall be taken when changing the configuration of an existing structure. The most important are precautions regarding the strength of the structure. Durability and serviceability should also be considered.

This part of the study looks into the strength aspect of the behavior of box girder bridges and how it affects the choice of access hole locations. Two approaches can be adopted. In the first approach, the access hole is to be located in regions that are minimally stressed taking advantage of the fact that not all cross sections are stressed equally. Although designers try to optimize their design by varying the cross sectional dimensions (plate thicknesses in steel/concrete composite box girder bridges), still cross sections cannot be stressed equally. This is due to the large variations in straining actions in the longitudinal direction, and also due to the cost limitations on variations engineers can design. The second approach allows designers to freely choose the location of access holes, generally to satisfy other criteria such as practicality

of accessibility. However, as expected, such an approach may require major strengthening of the bridge if the location is one that is acted upon by large straining actions.

The first approach was adopted for this study. It is believed that minimal strengthening will be needed if this approach is followed.

LOCATION OF CURRENT ACCESS HOLES

Existing bridges are provided with access holes at the ends of each segment close to expansion joints. The holes are drilled in the bottom flange providing easy access, in most cases, from beneath the bridge where the pier serves as an access tool. In addition to easy access, this part of the flange is hardly stressed because of its existence in a region where bending moments are close to zero, thus having a minimal effect on the strength of the cross section. Shear stresses, which are high around supports, are mainly resisted by webs. The same cannot be said about intermediate supports where high negative moments make the bottom flange highly stressed.

Another type of access holes is provided in diaphragms. Diaphragms are provided at supports, and the access holes are essential to allow movement from one compartment (span) to another.

ALTERNATIVE ACCESS HOLE LOCATIONS

In addition to the bottom flange alternative, two other alternative locations are possible for providing access holes at any cross-section. Thus, the alternatives available for study are the following three :

- Bottom Flange
- Web
- Concrete Deck

Each of these alternatives has its advantages and disadvantages. The advantages and disadvantages are discussed with respect to their impact of the access hole on the following categories :

- *Strength:* The most important of all since it affects the structural integrity of the bridge. Holes in the bottom flange would have a great impact on the flexural strength of the cross section, and hence the entire structure. This is especially true in the vicinity of the supports where high negative moments develop. To avoid such reduction in strength, major strengthening will be required at such locations. Away from high negative and positive moments, flexural stresses are at their minimum and adding a hole in the bottom flange may be possible without strengthening. Adding access holes to webs has a bigger impact on the strength of the cross section in shear. Webs are usually formed from thin plates. Additional holes in the webs will drastically reduce its shear resistance. Therefore, this should only be considered around midspans where low shear forces and torsional moments exist. The effect of opening an access hole in the concrete deck has the least impact on strength of all three alternatives. This is due to that fact that the dimensions of the concrete are predetermined by traffic considerations (road width) rather than by structural need. The provided concrete is, therefore, more than what a structural design would require. This fact makes it more tolerant for size reductions.

- *Feasibility:* To minimize the amount of work involved in providing an additional access hole, other elements should be left untouched. These elements are the stiffeners and cross frames that enhance the structural qualities of the bridge. Bottom flange stiffeners are generally provided to stiffen the plate and prevent buckling where it is under high compressive stresses (negative moment regions). These stiffeners extend for a portion of the span. Beyond the negative moment regions (positive moment regions) no stiffeners are usually provided. Wide boxes have two bottom flange stiffeners, while narrow boxes are stiffened in the middle of the plate. The one stiffener type creates an obstacle to access holes. In the case of two bottom flange stiffeners, an access hole can be added between the stiffeners if the distance in between is sufficient. Stiffeners for webs are provided in the transverse (direction) inclined, and not longitudinally. Web stiffeners increase the shear resistance of webs. In order to minimize the reduction in

shear strength, the access hole should be added in the space between the stiffeners. The concrete deck alternative has the least limitations from other elements since no longitudinal or transverse stiffeners are attached to it. Top flange bracings, which provide needed strength for the steel plates during construction and before casting the concrete deck, may work as an obstacle for this alternative. However, these elements are not essential for the behavior of the steel/concrete composite closed cross section and can be taken out if needed. For all three alternatives, the locations where cross frames exist should be avoided, since these cross frames enhance the global behavior of the bridge.

- *Accessibility:* For any of the alternatives to be useful, it should be accessible. Easy accessibility of the access hole is an important issue since they are added for use in the eventuality of an emergency. Holes in the concrete deck are accessible easily from the top with no need for special equipment. The other two alternatives will require special equipment (snooper or bucket) to reach the access hole, especially away from the supports. In the vicinity of the supports, piers and abutments facilitate reaching the hole unless the bridge overpasses other roads and bridges at an unreachable level. In the case of multi cell bridges, web openings will be hard to reach if they are located away from the piers due to equipment limitations.

- *Water Leakage:* Corrosion of steel is always accelerated in humid environments. Any modifications in the bridge that would increase the potential for corrosion should be avoided, since it reduces the durability of the structure. Access holes in bottom flanges do not change the possibility of getting water inside the box. The same applies to webs, except for outer webs where some water running on these sides may find its way in. The most critical of all three alternatives is the concrete deck one. The access hole will be under sever weather attacks and in the case of heavy rain may leak some water to the inside of the box. In order to avoid such leaks, water tight doors must be provided.

- *Impact on Traffic:* The use of the access hole should be possible at all times. Access holes that are accessed from the top (concrete deck, or web and bottom flange at midspan with the help of a snooper) will impact the traffic flow and need special arrangement to

use the hole. No such arrangements are needed if for bottom flanges and webs that will be accessed from beneath the bridge using a bucket or simply the piers.

- *Unlawful Access:* Unauthorized people can easily reach access holes in the vicinity of the supports and in the concrete deck. Away from the supports, access is not possible without the use of special equipment except for the concrete deck alternative. In all cases, to avoid unauthorized people from getting into the cells, certain precautions should be followed.

Table 4 summarizes the previous discussion.

Table 4: Summary of advantages and disadvantages of access hole alternatives

Alternative	**Bottom Flange**	**Web**	**Concrete Deck**
Strength	Reduces flexural strength.	Reduces shear, torsional strength.	Less effect on strength than other two alternatives.
Feasibility	Stiffeners should be avoided. May be an obstacle if one stiffener is used.	Stiffeners must be avoided.	No stiffener limitations, but construction bracing may be an obstacle.
	Cross frames must be avoided.		
Access at supports	Easy	Easy	Easier access at any location.
Access between supports	Possible with the help of a snooper or a bucket.	Possible with the help of a snooper or a bucket, except for intermediate cells in multicell bridges.	
Water leakage	Not a concern.	Concern for outer cells.	Watertight doors will be needed.
Impact on traffic	No effect.	No effect.	Special arrangements will be needed for access.
Unlawful Access	Possible at supports.	Possible at supports.	Possible at any location.

MINIMALLY STRESSED LOCATIONS

In this part of the study, locations where stresses are at their minimum will be identified. Taking advantage of the existence of such locations in any bridge girder will result in minimal strengthening requirements, if any at all. The approach differs depending on which of the three alternative locations is targeted. In the case of access holes in the web, shear stresses will be considered. Normal stresses will be considered in the case of the bottom flange or concrete deck alternatives.

Straining Actions

The first step in this study was to find the straining action distributions in the longitudinal direction due to the applied loads. The AASHTO-LRFD code is followed in determining the loads. The philosophy behind most LRFD codes can be summarized in the following:

A bridge design is considered an acceptable design if limit states are satisfied. These limit states are: *Service* limit states, *Fatigue and fracture* limit states, *Strength* limit states, and *Extreme-event* limit states. It is believed that satisfying the specified limit states will result in a structure that will perform satisfactorily within acceptable deformations, and will have an adequate factor of safety against collapse.

Determining low stress regions fall under *Strength I* limit state. According to AASHTO, strength evaluations are conducted by:

- First performing a linear elastic analysis of the structure to obtain the internal forces due to factored loads even though the materials used may behave beyond the linear range.
- Then, study section behavior taking into consideration material nonlinearities.

This procedure was followed. The details of the procedure are given next.

Factored loads are determined according to the following equation:

$$U = \gamma_D D + \gamma_L L$$

where D is the dead load, and L is the live load acting on the bridge. γ_D and γ_L are the load factors that, for *Strength I* limit state, were taken equal to 1.25 and 1.75, respectively. Following AASHTO's provisions for load factors and capacity calculations should result in a structural system with a reliability index around 3.5.

The dead loads were first applied on the noncomposite cross-section (steel only). The geometric properties of the quasi-closed noncomposite girder were determined after adopting the Equivalent Plate Method (EPM) by Kohlbrunner and Basler to account for construction bracing. In this method an additional plate is assumed to connect the top flanges of the box girder. The additional member is given a equivalent thickness, t_{eq}, that has the same effect on the girder as that of the construction bracing connecting the top flanges. The formula used to determine t_{eq} is:

$$t_{eq} = \frac{E}{G}\frac{ab}{\frac{d^3}{F_d} + \frac{2}{3}\frac{a^3}{F_o}}$$

where

E	Modulus of Elasticity
G	Shear Modulus
a	Spacing between cross frames
b	Distance between flanges
d	Length of bracing member
F_o	Area of top flange
F_d	Area of bracing member

The superimposed live load is then applied to the structure by considering the permanent condition after casting the concrete deck. The new geometric properties of the cross-section were determined based on a closed composite girder (steel and concrete).

For illustration purposes, an idealized bridge is analyzed following the previous procedure. The bridge consists of three straight equal-spans with constant cross-sectional dimensions. The length of each span is 75 ft, and cross-sectional properties are those of Bridge 538 which are illustrated in a previous section. This case was studied for 34 load cases; 1 dead load case, 3 lane load cases, and 30 tandem load cases. Straining actions from these load cases were determined based on a linear elastic analysis. Two sets of straining actions were obtained using ABAQUS. In Fig. 35, the first set shows the internal forces due to dead loads. As expected, for the dead load case, only bending moments about the horizontal axis (M_x) and shear forces in the vertical direction (V_y) develop due to the lack of curvature. Envelopes of straining actions due to live loads form the second set, which can be seen in Fig. 36. The live load envelopes show internal forces in other directions (M_y, M_ω, T_s, T_ω). This is due to the eccentricity by which live loads are positioned which applies torsional loads on the bridge resulting in the other straining actions. Figures 32 and 33 show the positioning of live loads for a one-lane deck and a two-lane deck.

Calculation of stresses

Stresses are then calculated based on these internal forces. The normal stress, σ, which develop due to the bending moments (M_x, M_y) and bimoment (M_ω), is evaluated at key points in the cross section according to the following equation:

$$\sigma = \frac{M_x}{I_x} y + \frac{M_y}{I_y} x + \frac{M_\omega}{I_{\omega\omega}} \omega$$

The next equation was used to calculate shear stress, τ, due to shear forces (V_x, V_y) and torsional moments (T, T_ω), at various points in the cross section:

$$\tau = \frac{V_y}{tI_x} S_x(s) + \frac{V_x}{tI_y} S_y(s) + \frac{T_s}{2tA_c} + \frac{T_\omega}{tI_{\omega\omega}} S_\omega(s)$$

where,

V_y is the shear force in the y-direction (vertical shear)

V_x is the shear force in the x-direction (horizontal shear)

M_x is the bending moment (about the x-axis)

M_y is the bending moment (about the y-axis)

M_ω is the bimoment

T_s is the pure torsional moment component of the total torsion

T_ω is the warping torsional moment component of the total torsion

$I_{\omega\omega}$ is the warping constant

ω is the warping function

A_c is the area enclosed by the box

I_x is the moment of inertia (about the x-axis)

I_y is the moment of inertia (about the y-axis)

x is the distance from the point under consideration to the centroid in the x-direction

y is the distance from the point under consideration to the centroid in the y-direction

t is the thickness of the plate where the point under consideration lies

$S_{\omega(s)}$ is the sectoral moment

$S_{x(s)}$ is the first moment of area (about the x-axis)

$S_{y(s)}$ is the first moment of area (about the y-axis)

Stress computations were done based on the following sets of geometric properties. These are:

- *Quasi-closed all steel noncomposite* cross-section for dead load stress calculations

- *Closed concrete/steel composite cross-section* for live load stress calculations.

The total stresses at the key points were obtained by adding both the dead load and live load stresses. This procedure assumes that the construction method does not shore the girders before casting the concrete deck.

The point where the maximum normal stress in the cross section, $\sigma_{max,p}$, was identified for each of the elements forming the model. Also, the point where the maximum shear stress in the cross section, $\tau_{max,p}$, takes place was determined for each element. After obtaining these values for all elements, the elements that have the maximum values, σ_{max} and τ_{max}, were located.

Identifying low stress regions

The information obtained from stress calculations can be manipulated in various ways. Five different approaches were used in this study. In the first approach, regions where normal stresses are at their minimum were located. Regions where σ is less than 20%, 33%, and 45% of σ_{max} were located. The 33% limit is especially important since the stress concentration factor around circular holes is always close to 3. Holes in this special region will cause the stress to be around the maximum stress value, σ_{max}, after being multiplied by the stress concentration factor. These regions have a good potential to be considered for flange openings. For openings in webs, the second approach was devised, where regions of low shear stresses are identified. Three stress levels were considered; τ is less than 20%, 33%, and 45% of τ_{max}. These two approaches consider one type of stress only, either the normal stress or the shear stress. Since interaction between both stress types usually exist, another approach was needed. The third approach locates regions where both normal stresses and shear stresses are below certain limits. It was clear from the third approach that regions determined based on a scheme which targets low normal and shear stresses are very limited. This led to the last two approaches. The scheme adopted in the fourth approach gives more weight to the shear stress over normal stresses; τ is less than 33% of τ_{max} and σ is less than 75% of σ_{max}. Finally, the fifth approach considers normal stresses mainly with some weight given to shear stresses; σ is less than 33% of σ_{max} and τ is less than 75% of τ_{max}. Since the flange alternatives are more likely to be adopted, fatigue limitations

were also incorporated in this final approach; Δf is less than 55 MPa in regions where fatigue should be considered. Since the fatigue stress range obtained from the analysis is that of the original cross section, this range was increased by a stress concentration factor. For uniform plates under uniform in plane normal stress a stress concentration factor of 3 is expected. However, a stress concentration factor of 3 was deemed conservative, and instead a factor of 2.5 was used. This decision was reached after recognizing that point of σ_{max} always took place in the bottom corner of the cell. Access holes will always be located in the middle of the bottom flange plate where the normal stress is lower. This is due to the fact that it is closer to the vertical axis and normal stresses due to the bending moment about the y-axis, M_y, and the bimoment, M_ω, will be less than at the corner. Figure 34 shows a normal stress distribution at a inner support to illustrate the justification of the use of a lower stress concentration factor.

A summary of all approaches can be found in Table 5.

The previous approaches were applied to the results obtained from the idealized bridge model. Each of the approaches yielded regions of low stresses in accordance with the scheme involved in the approach. Figure 37-a shows the regions obtained using Approach I. The regions were around point of contraflexure and close to exterior supports. Approach II resulted in the regions seen in Fig. 37-b. These were around midspans where low shear forces and torsional moments exist. When Approach III was adopted, the regions came out to be as shown in Fig. 38-a. In Fig. 38-b the results are those of Approach IV. The regions shown in Fig. 39-b are those obtained from Approach V, which incorporates the fatigue stress range in determining the regions in addition to the normal and shear stresses. In this plot, all the shown regions satisfy the criteria set previously for Approach V, which means that fatigue is not an issue in these regions. The darkened regions represent the live load stress range in the regions that passed all criteria. The parts of the region that are not darkened correspond to regions where fatigue can be ignored according to AASHTO. This can be seen in Fig. 39-a which shows the fatigue stress range due to live loads. By comparing both figures, the stress concentration factor of 2.5 used with Δf is obvious. It should be noted that, unlike the fatigue study for Bridge 538, fatigue calculations in this study considered one tandem pair instead of the design truck. Only one tandem pair was used in determining the straining action envelope for fatigue calculations; i.e. no double tandems for negative moments and inner support reactions. The live load stress

range was determined by finding the difference between the maximum stress and minimum stress from the fatigue straining action envelopes. This technique implies that each tandem pair induces one fatigue load cycle during its trip on the bridge. The other alternative is to find the maximum live load stress range from one case of loading, which implies that this case is a single fatigue load cycle with a lower live load stress range. Since the adopted technique uses a higher live load stress range for the same number of cycles, it is obviously more conservative.

Table 5: Summary of approaches for determining low stress region locations

	Normal Stress σ	Shear Stress τ	Fatigue Stress Range Δf
Approach I	$< 20\% \sigma_{max}$ $< 33\% \sigma_{max}$ $< 45\% \sigma_{max}$	Not considered	Not considered
Approach II	Not considered	$< 20\% \tau_{max}$ $< 33\% \tau_{max}$ $< 45\% \tau_{max}$	Not considered
Approach III	$< 20\% \sigma_{max}$ $< 33\% \sigma_{max}$ $< 45\% \sigma_{max}$	$< 20\% \tau_{max}$ $< 33\% \tau_{max}$ $< 45\% \tau_{max}$	Not considered
Approach IV	$< 75\% \sigma_{max}$	$< 33\% \tau_{max}$	Not considered
Approach V	$< 33\% \sigma_{max}$	$< 75\% \tau_{max}$	$\Delta f < 55$ MPa (where applicable)

CASE STUDY OF DOT BRIDGES

The previous section describes the strategy that will be followed in determining regions of low stresses. These regions are the recommended regions for adding access holes to the bridges. Nineteen bridges were studied to investigate the generality of the findings of these results. These bridges exist in District IV of the Florida Department of Transportation FDOT. The plans of the bridges were studied and one segment from each bridge was studied. The bridges varied in dimensions covering a scope of curvatures and cross sections. The properties of each of the bridges are summarized next.

BRIDGE 390

The segment considered is a five-span girder with a constant curvature of 620 feet. Span lengths varied from 180 feet to 233.5 feet. The total number of elements used to build the model was 1923 each with a length of 6 inches (152.4 mm). Four different sets of geometric cross sectional properties were used according to the changes in plate thicknesses. The concrete deck width allowed the use of one-lane live load loading only.

BRIDGE 521

A segment of three spans was analyzed for this bridge. The curvature is constant for this segment with a radius of 5770.578 feet. The exterior spans had a length of 76 feet and the middle span was 120 feet long. Using an element length of 4 inches (101.6 mm), 816 elements were needed to build the model. The plans showed that two different sets of geometric cross sectional properties were adequate to model the bridge. The concrete deck width allowed the use of one-lane live load loading only.

BRIDGE 525

This is the bridge with the least number of spans in the study. It has two spans, the first is 162.67 feet, and the second is 136.33 feet. Eight hundred and ninety seven elements of a 4-inch length (101.6 mm) formed the model. No curvature was included in this study since it represents a straight segment. The plans showed that two different sets of geometric cross sectional properties were adequate to model the bridge. The concrete deck width allowed the use of one-lane live load loading only.

BRIDGE 598

For this bridge a segment of four spans was studied. Span lengths varied from 171.5 feet to 145.5 feet. The total number of elements for this model was 1895, each with a length equal to 6 inches (152.4 mm). The curvature varied for the bridge. Two radii were used to define the geometry of the model according to the plans. The first radius was 352.95 feet, and the second was 694.49 feet. Five different sets of geometric cross sectional properties were needed to model the bridge. The concrete deck width showed that only one-lane live load loading should be considered.

BRIDGE 601

This model represented a four-span segment. The first two spans had a curvature of 304.458 feet, the rest of the bridge was straight. Span lengths varied from 133 feet to 238 feet. An element length of 6 inches (152.4 mm) was used. The total number of elements in the model was 1382. The plans showed that six different sets of geometric cross sectional properties were adequate to model the bridge. The concrete deck width allowed the use of one-lane live load loading only.

BRIDGE 606

Three spans were considered. The exterior spans had a length of 184 feet and the middle span was 263.67 feet long. The total number of elements for this model was 1310, each with a length equal to 4 inches (101.6 mm). The curvature varied for the bridge. The outer parts were curved, however, in opposite directions. In between a straight segment linked the two curvatures. The radii of the curved parts were 2872.289 feet and 1439.894 feet. Three different sets of geometric cross sectional properties were needed to model the bridge. The concrete deck width showed that two-lane live load cases should be considered.

BRIDGE 607

This bridge consisted of three spans that varied in length. The exterior spans had a length 154 feet, and the middle span was 219.33 feet long. The total number of elements for this model was 1582, each with a length equal to 4 inches (101.6 mm). The curvature varied for the bridge. The first part of the bridge is a straight segment. Following the straight segment a curvature of 2857.289 feet was used. Five different sets of geometric cross sectional properties were needed to model the bridge. The concrete deck width was enough to allow for two-lane loading for live load cases.

BRIDGE 528

The segment considered is a five-span girder with a constant curvature of 5729.578 feet. Span lengths varied from 158 feet to 192 feet. The total number of elements used to build the model was 1658 each with a length of 6 inches (152.4 mm). Five different sets of geometric cross sectional properties were used according to changes in plate thickness. The concrete deck width allowed the use of two-lane live loading.

BRIDGE 537

For this bridge a segment of five-span was studied. Span lengths varied from 100 feet to 213 feet. The total number of elements for this model was 1390; each having a length of 6 inches (152.4 mm). The curvature of 716.197 feet was constant for all the spans. Eight different sets of geometric cross sectional properties were needed to model the bridge. The concrete deck width showed that two-lane live load loading should be considered.

BRIDGE 538A

This model represented a five-span segment. This was a double curvature bridge having radii of 9951.3558 feet and 1432.3945 feet. The span range was 122.5 feet to 172 feet. The curvature changed in the third span of the bridge. 1585 elements, each of six inches (152.4 mm) in length were used to model this bridge. The plans showed that five different sets of geometric cross sectional properties are adequate to model the bridge. It was seen that two-lane live load loading is possible for the given concrete deck width.

BRIDGE 538B

This was a five-span segment of bridge 538. The spans varied from145.5 feet to 211 feet. The radius was 1432.3945 feet for first two and half spans and 2864.789 feet for rest of the segment. The total number of elements for this model was 1762; each with a length equal to 6 inches (152.4 mm). Seven different sets of geometrical cross sectional properties were needed to model the bridge. The concrete deck width allowed the use of two-lane live loading.

BRIDGE 538C

This was a symmetric bridge having four spans. The exterior spans had a length of 167 feet and the interior spans had a length of 210 feet. A radius of 2864.789 feet was constant throughout the segment. 1508 Elements, having a length of 6 inches (152.4 mm) each, were

needed to model this bridge. The plans showed that only four different sets of geometrical cross sectional properties are enough to model the bridge. It was seen that two-lane live load loading is possible for the given concrete deck width.

BRIDGE 538D

This was the longest segment in all of the bridge data. The segment consists of seven spans ranging from 121 feet to 210 feet. The radius of curvature changed from 2864.789 feet to 1432.3945 feet in the third span of the bridge. A total of 2486 elements, each of 6 inches (152.4 mm) length, were needed to model the bridge. Eight different sets of geometrical cross sectional properties were needed to model this segment. The concrete deck width allowed the use of two-lane live loading.

BRIDGE 539

This was also a symmetric bridge having five spans. The exterior spans were 130 feet, the penultimate spans were 163 feet and the central span was 183.5 feet. This was a single curvature bridge with a radius of 717.1972 feet. A total of 1539 elements, each of 6 inches (152.4 mm) in length, were needed to model the bridge. Four different sets of geometrical cross sectional properties were adequate to model the segment. A two-lane live load loading was considered for the given concrete deck width.

BRIDGE 540

For this bridge, a six span segment was studied. The spans ranged from 78 feet to 178 feet. A radius of 953.9297 feet was constant throughout the segment. An element length of 6 inches (152.4 mm) was used to create the mesh. The total number of elements in the model was 1661. The plans showed that six different sets of geometrical cross sectional properties are required to model the bridge. The concrete deck width allowed the use of two-lane live loading.

BRIDGE 541A

Five spans were considered. The span length varied from 125.5 feet to 207 feet. The total number of elements for this model was 1686 each with a length equal to 6 inches (152.4 mm). According to the plans, two radii were used to define the geometry of the model. The first radius was 1415.7157 feet and the second was 821.511 feet. Seven different sets of geometrical cross sectional properties were needed to model the segment. The concrete deck width showed that two-lane live load loading should be considered.

BRIDGE 541B

This model represented a five-span segment. This was a double curvature bridge having radii of 821.511 feet and 2117.8520 feet. The span range was 105.5 feet to 201 feet. The curvature changed in the fourth span of the bridge. A total of 1604 elements, each of six inches (152.4 mm) in length were used to model this bridge. Eight different sets of geometric cross sectional properties were needed to model the bridge. It was seen that two-lane live load loading is possible for the given concrete deck width.

BRIDGE 542A

This was a single curvature bridge with six spans. The spans ranged from 144 feet to 204 feet and the radius was 1146.9156 feet. An element length of 6 inches (152.4 mm) was used to create the model. The total number of elements in the model was 2096. Five different sets of geometric cross sectional properties were used to model the bridge. The concrete deck width allowed the use of two-lane live loading.

BRIDGE 542B

There were six spans in this bridge and the span length varied from 114 feet to 194 feet. The total number of elements for this model was 1834 each with a length equal to 6 inches (152.4 mm). The plans showed two radii of curvature for the bridge. The first radius was 1146.9156 feet and the second was 28648.8898 feet. Seven different sets of geometrical cross sectional properties were needed to model the segment. The concrete deck width showed that two-lane live load loading should be considered.

Figures 40 through 58 show the geometry of the nineteen bridges. Each of the figures has a plan view and an elevation view if the bridges. Table 6 summarizes the data of the analyzed bridges.

The results obtained from the analysis of the nineteen bridges were divided into two groups. Two sets of straining actions are reported for each bridge. The first set is due to the dead load case, while the second is the results of enveloping live load cases. Each set is an assembly of all involved straining actions as discussed before. The figures can be seen in Appendix B.

The different approaches for determining low stress regions resulted in the figures given in Appendix C. For each bridge five groups of stress regions are given in addition to the fatigue stress range which is used in identifying the regions according to Approach V. The study of these results led to the findings listed at the end of the report. The results are also summarized in Table 7 for the newly analyzed bridges.

Table 6: Summary of bridge data

Bridge	Spans	Lanes	Span lengths		Radius of Curvature		Element length (inches)	Number of elements
			Min (feet)	Max (feet)	Min (feet)	Max (feet)		
390	5	1	180	233.5	620	620	6	1923
521	3	1	76	120	5770.6	5770.6	4	816
525	2	1	136.3	162.7	Straight	Straight	4	897
598	4	1	145.5	171.5	392.9	694.5	6	1895
601	4	1	133	238	304.5	Straight	6	1382
606	3	2	184	263.7	1439.9	2772.3	4	1310
607	3	2	154	219.3	2857.3	Straight	4	1582
528	5	2	158	192	5729.3	5729.3	6	1658
537	5	2	100	213	716.2	716.2	6	1390
538a	5	2	122.5	172	1432.4	9951.3	6	1585
538b	5	2	145.5	211	1432.4	2864.8	6	1762
538c	4	2	167	210	2864.8	2864.8	6	1508
538d	7	2	121	210	1432.4	2864.8	6	2486
539	5	2	130	183.5	717.2	717.2	6	1539
540	6	2	78	178	953.9	953.9	6	1661
541a	5	2	125.5	207	821.5	1415.7	6	1686
541b	5	2	105.5	201	821.5	2117.8	6	1604
542a	6	2	144	204	1146.9	1146.9	6	2096
542b	6	2	114	194	1146.9	28649	6	1834

SUMMARY AND FINDINGS

Based on the analysis of a limited number of box girders, a set of findings specific to the bridges studied can be reported. This section is divided into two parts. In the first part a summary of the problem is given. The conclusions from this research project are reported in the second part.

SUMMARY

NEED FOR ACCESS HOLES IN BOX GIRDER BRIDGES

A number of existing box girder bridges in District IV of the Florida Department of Transportation do not satisfy the NIOSH recommendations for distance between access points. This places workers inspecting the inside of the bridges at risk and has concerned the FDOT Safety Office. The objective of this project is to find appropriate locations for additional access points that satisfy specific practical and structural considerations.

STRENGTHENING CONSIDERATIONS

Although some of the analyses reported have shown that strength capacity could be reduced by as much as 15% due to the addition of an access hole, strengthening in the vicinity of the hole is unnecessary because the locations targeted are not expected to reach their full strength. These locations are shielded from large strength demands when other critical regions in the bridge, namely over the support and at mid span, reach their strength capacity. On the other

hand, the first yield moment, which is another measure of strength, can be greatly affected by the addition of an access hole because of stress concentrations. This fact is important when considering the fatigue strength as discussed in the next section.

SPECIAL CONSIDERATIONS FOR FATIGUE

It is evident from this study that the live load stress range as specified by the AASHTO fatigue provisions has placed restrictions on the length and location of regions that are otherwise possible alternatives for adding access points. The analyses reported herein were based on the assumption that the rehabilitated bridges fall under AASHTO fatigue category B. Care must be exercised when welding or bolting attachments around new access holes since this could change the category under which the bridge falls. A thorough fatigue investigation is needed for each access hole location.

ACCESS HOLE LOCATION ALTERNATIVES IN A CROSS-SECTION

Three alternative locations are possible for providing access holes at any cross-section: concrete deck, bottom flange, and web plates. The concrete deck alternative provides access from the top to the inside of the bridge, and will require certain measures regarding traffic while using the access hole. Only the portion of the deck than is not overhanging can be used to provide access holes to the inside of the box girder and the locations of cross frames have to be avoided for this alternative. Special consideration must be given to the possibility of water leaking through top openings. Since the width of the flange is generally based on traffic requirements rather than structural requirements, the concrete deck is usually minimally stressed and is an ideal alternative from the structural point of view.

The bottom flange is where existing access holes are located. This alternative provides easy access from beneath the bridge at the piers or abutments. Between supports, a snooper or a bucket will be needed to reach access holes of this type. Access holes in the bottom flange are

not practically feasible if they interfere with flange stiffeners or cross-frames. From the structural point of view, this alternative is generally not feasible at mid span and at supports since these locations are heavily stressed.

The web alternative provides easy access when using a snooper for single cell bridges or edge cells in multi-cell bridges. Access holes in intermediate cells will be hard to reach even with the help of a snooper. In addition to cross frames, web stiffeners also have to be avoided when placing holes in web plates. Extreme care must be exercised in locating holes in the web plates since they are usually thin and hence susceptible to buckling.

Although the concrete deck is ideal from the structural point of view and provides for easy access, the possibility of water leakage prohibits consideration of this alternative. The web alternative provides no special structural or practical advantages. Based on these considerations, it is recommended that additional access holes be placed in the bottom flanges. The section below provides information on how to determine the most appropriate locations in all three alternatives.

FINDINGS

For the bridges analyzed in this study, it is possible to locate areas that are stressed minimally. From a structural point of view, these areas are considered to be the most feasible locations for adding extra access holes with minimal effect on the structural integrity of the bridges, and with minimum amount of work, and hence cost, needed for strengthening.

Based on the results of the finite element analyses, five different schemes are devised for locating minimally stressed regions where additional access holes could be added without strengthening. The construction sequence is considered in the analyses by adopting quasi-open section properties for dead loads and closed section properties for live loads. The five schemes incorporate different levels of interaction between normal and shear stresses and account for fatigue considerations. Based on the proposed schemes, suitable regions where access hole can

be placed without additional strengthening are identified for each bridge and the results are summarized for all bridges considered in the investigation. In addition to bottom flange access holes, locations are also identified for placing openings in the webs. Strengthening should be considered for access holes located outside the proposed regions.

LONGITUDINAL ACCESS HOLE LOCATION ALTERNATIVES

The alternatives discussed in the previous section can be categorized into two types. The first category includes alternatives that are affected by normal stresses; namely the *Concrete Deck* alternative and the *Bottom Flange* alternative. The *Web* alternative is affected by shear stresses. It was found that the longitudinal location of the access holes varies greatly based on which category is desired. The following information lists the *extreme* limits found for all 19 bridges considered in the investigation. These limits should *not* be interpreted as general criteria for the locating minimally stressed locations in any bridge. Specific data for all 19 bridges are listed in Table 7 on page 117.

- *Normal Stress Priority*: This is the more appealing choice since it targets feasible alternatives. For the nineteen bridges considered it was found that the location of the minimally stressed regions is not closer than $0.18L$, where L is the span length. For spans that are continuous on both sides, the location of the minimally stressed point is at a distance that ranged from $0.18L$ to $0.42L$ measured from the continuous support. First spans showed that the location ranged from $0.20L$ to $0.54L$ measured from the continuous support. The length of the minimally stressed region varied substantially. On average the length of the region was found to be around $0.044L$. Spans that are continuous on both sides had a length of $0.046L$, and spans that are continuous from one side had an average region length equal to $0.040L$.

- *Shear Stress Priority*: Even though considered an impractical alternative, the minimal shear stress locations are reported. These are mainly around the middle of each span where low shear forces and torsional moments act on the girder. Some of the analyzed bridges showed one region that satisfies all criteria in Approach IV, others had two distinct regions due to the existence of high normal stresses around midspans. In the case of one-region spans, it

was observed that for first spans the regions were at a distance equal to 0.37L measured from the end support, and for spans continuous on both ends 0.50L. The average region length for first spans and spans continuous on both sides was found to be 0.40L and 0.28L, respectively. Spans showing two regions, had an average length of 0.04L for first spans as well as spans continuous on both ends. The location of the minimally stressed region measured from the continuous support was found to be at 0.44L for first spans and 0.37L for spans continuous on both ends.

REFERENCES

1) AASHTO. (1998). *LRFD Bridge Design Specifications*, American Association of State Highway and Transportation Officials, Washington, D.C.

2) AISC. (1990). *Steel and Composite Beams with Web Openings*, American Institute of Steel Construction, Chicago, IL.

3) Arizumi, Y., Hamada, S., Oshiro, T. (Nov-1988). *"Behavior Study of Curved Composite Box Girders,"* J. of Structural Engineering, ASCE, 114(11), 2555-2573.

4) Cheung, M. S., Foo, S. H. C. (Feb-1995). *"Design of Horizontally Curved Composite Box-Girder Bridges-A Simplified Approach,"* Canadian J. of Civil Engineering, 22 (1), 93-105.

5) Galdos, N. H., Shelling, D. R., Sahin, M. A. (June-1993). *"Methodology for Impact Factor of Horizontally Curved Box Bridges,"* J. of Structural Engineering, ASCE,119 (6), 1917-1934.

6) Guohao, Li. (1987). *Analysis of Box Girder and Truss Bridges*, China Academic Publishers, Springer-Verlag.

7) Hsu, Y. T., Fu, C. C., Shelling, D. R. (1990). *"An Improved Horizontally-curved Beam Element,"* J. of Computers and Structures. 34(2), 313-318.

8) Huan, C., Bezley, S. E., Huang, J. (Oct-1992). *"Free Vibration Analysis of Curved Thin-walled Girder Bridges,"* J. of Structural Engineering, ASCE, 118(10), 2890-2910.

9) Huang, D., Wang, T., Shahawy, M. (Sep-1995). *"Vibration of Thin-Walled Box-Girder Bridges Excited by Vehicles,"* J. of Structural Engineering, 121(90), 1330-1337.

10) Kollbrunner, C.F., and Basler, K. (1969). *Torsion in Structures. An Engineering Approach*, Springer-Verlag, New York, Heidelberg, Berlin.

11) Nakai, H., and Yoo, C. H. (1988). *Analysis and Design of Curved Steel Bridges*, McGraw Hill, Inc., New York, N.Y.

12) Nakai, H., and Murayama, Y. (1981). *"Distortional Stress Analysis and Design Aid for Horizontally Curved Box Girder Bridges with Diaphragms," Proceedings*, Japanese Society of Civil Engineers, 309, 25-39. (in Japanese).

13) Ng, S. F., Cheung, M. S., Hachem, H. M. (Feb-1993). *"Study of a Curved Continuous Composite Box Girder Bridge,"* Canadian J. of Civil Engineering, 20 (1), 107-119.

14) Razaqpur, A. G., Li, H. G. (1994). *"Refined Analysis of Curved Thin-walled Multicell Box Girders,"* J. of Computers and Structures, 53 (1), 131-142.

15) Shelling, D. R., Galdos, N. H., Sahin, M. A. (Nov-1992). *"Evaluation of Impact Factors for Horizontally Curved Steel Box Girders,"* J. of Structural Engineering, ASCE, 118(11), 3203-3221.

16) Sennah, K., Kennedy, J. B. (May-1998). *"Shear Distribution In Simply Supported Curved Composite Cellular Bridges,"* J. of Bridge Engineering, ASCE, 3 (2), 47-55.

17) Yabuki, T., Arizumi, Y., Vinnakota, S. (May-1995). *"Strength of Thin walled Box Girders Curved in Plan,"* J. of Structural Engineering, ASCE, 121(5), 907-914.

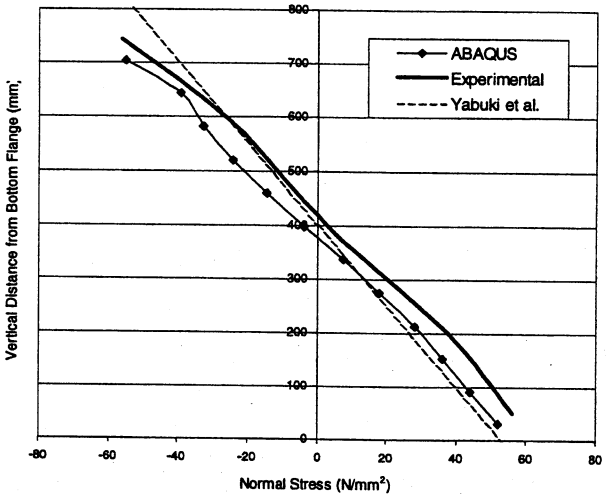

Figure 1: Normal stress Distributions at Center Span Cross-section for Inner Web of Girder M-5 (P=96.58)

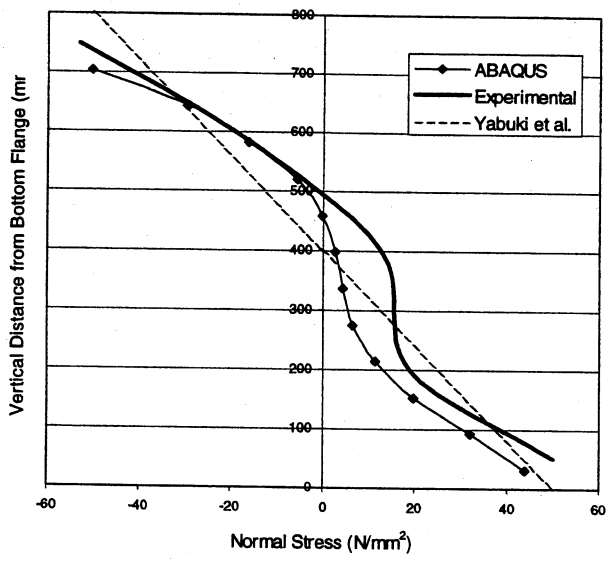

Figure 2: Normal stress Distributions at Center Span Cross-section for Outer Web of Girder M-5

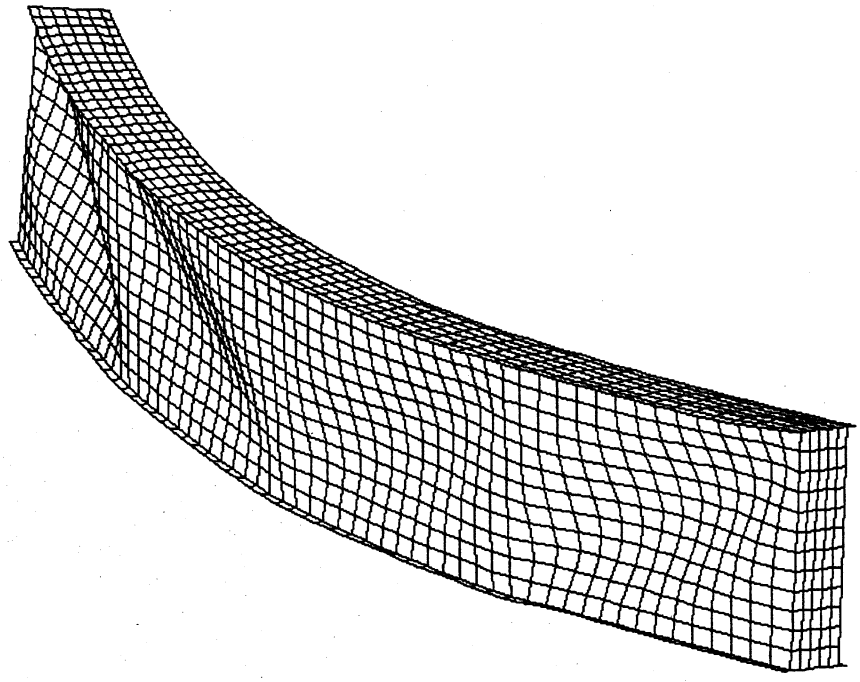

Figure 3: Deformed shape of Verification Girder II (Yabuki et al.)

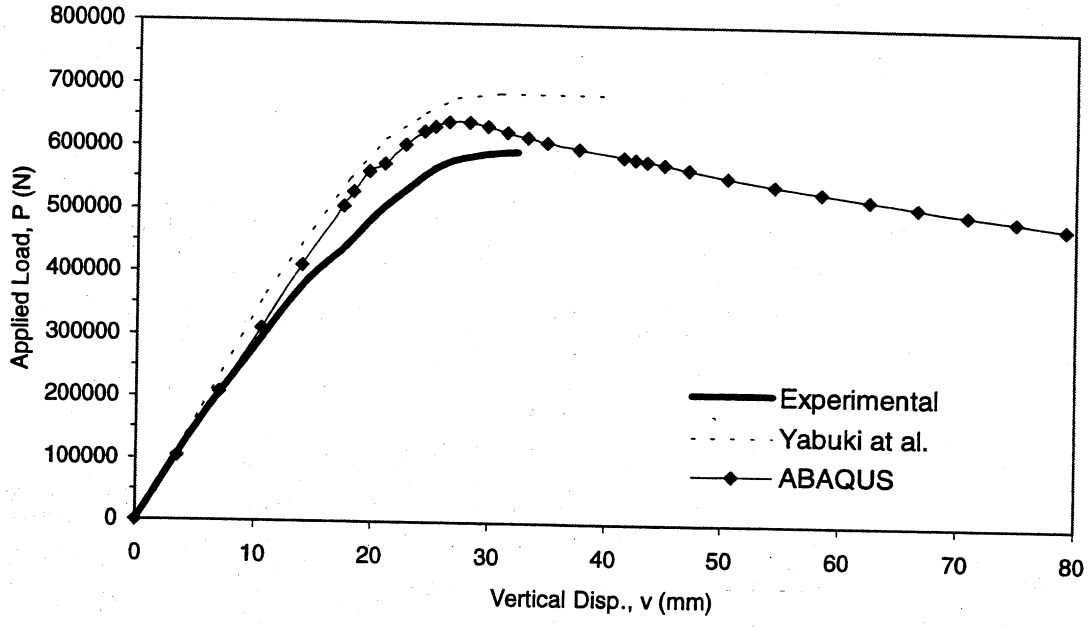

Figure 4: Load-deflection curve for Girder M-3

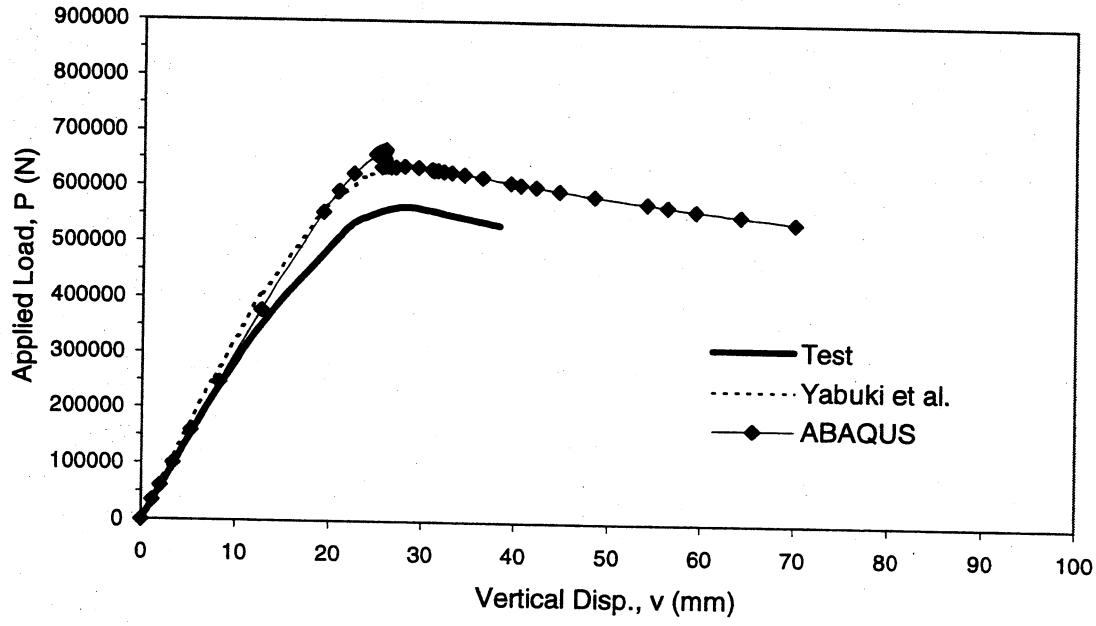

Figure 5: Load-deflection relationship for Girder M-5

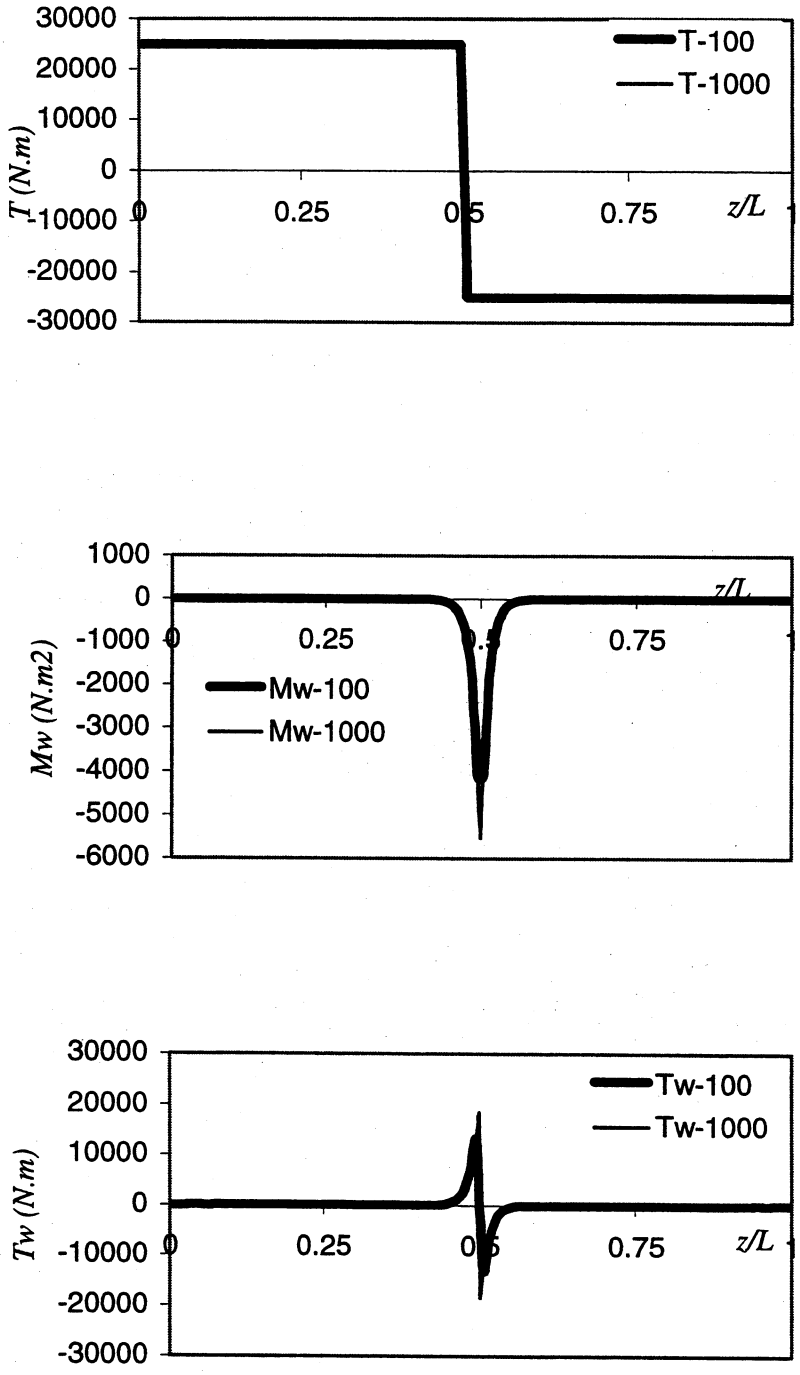

Figure 6: Beam model verification (case of concentrated torque)

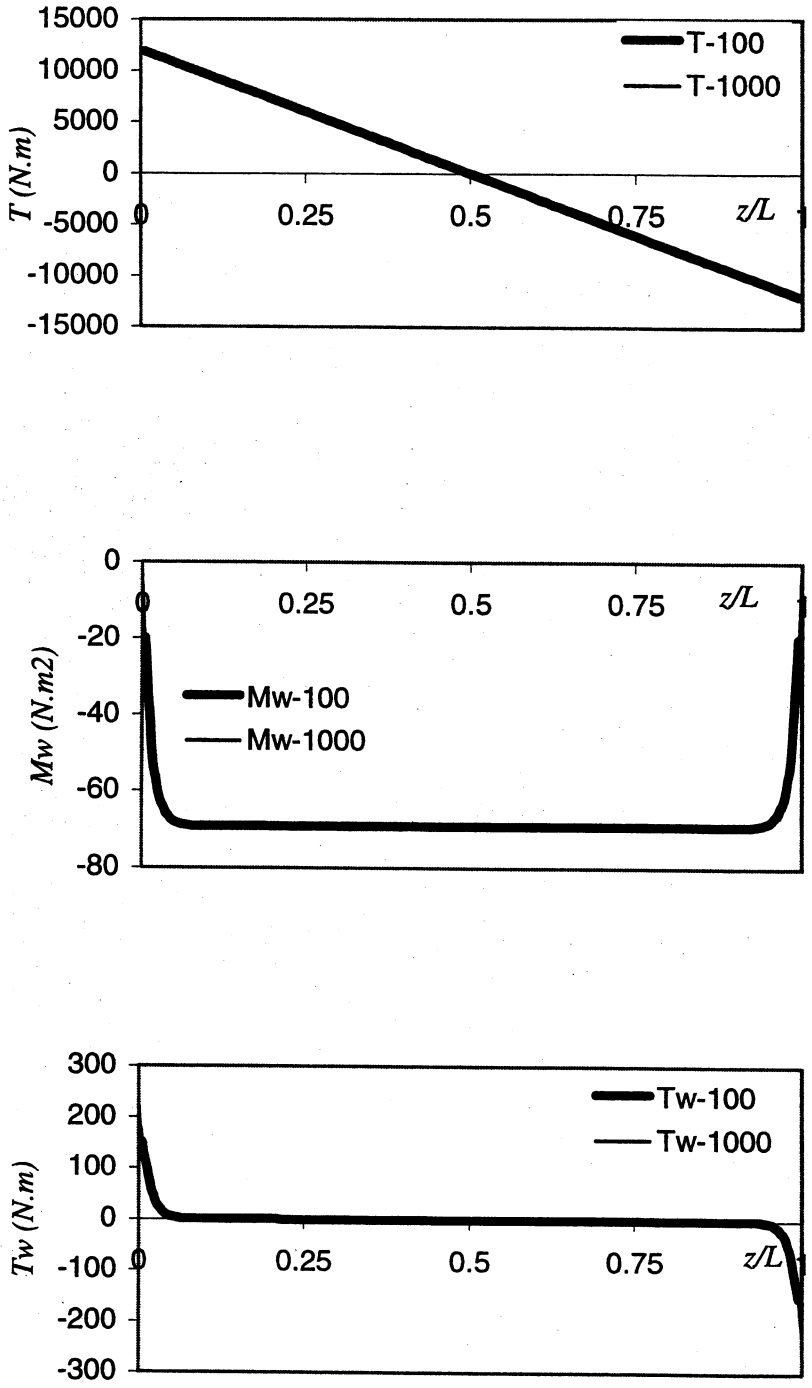

Figure 7: Beam model verification (case of uniformly distributed torque)

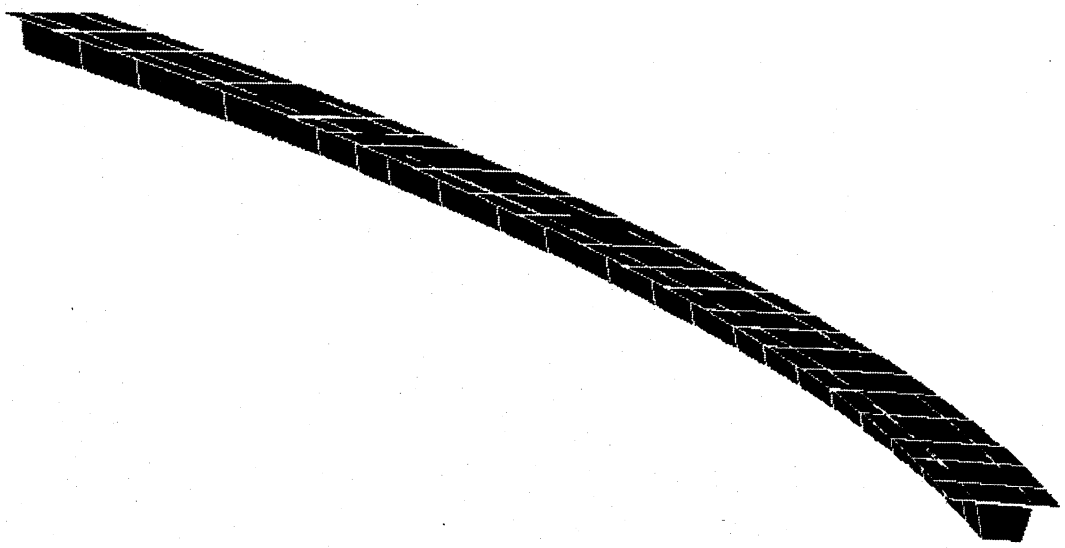

Figure 8: Overall view of the Bridge geometry

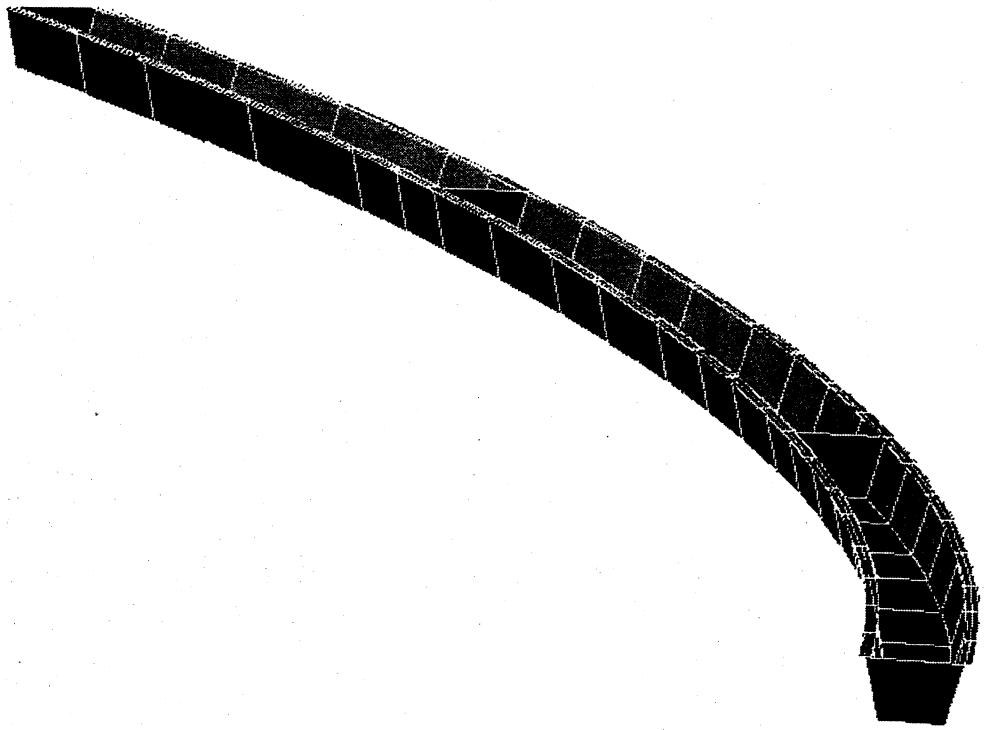

Figure 9: An inside view showing the diaphragms at support locations

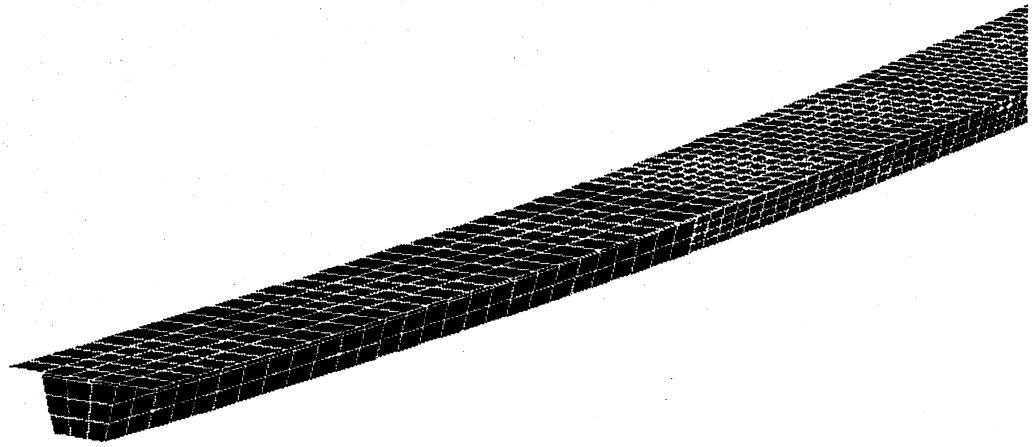

Figure 10: Transition from coarse mesh to fine mesh

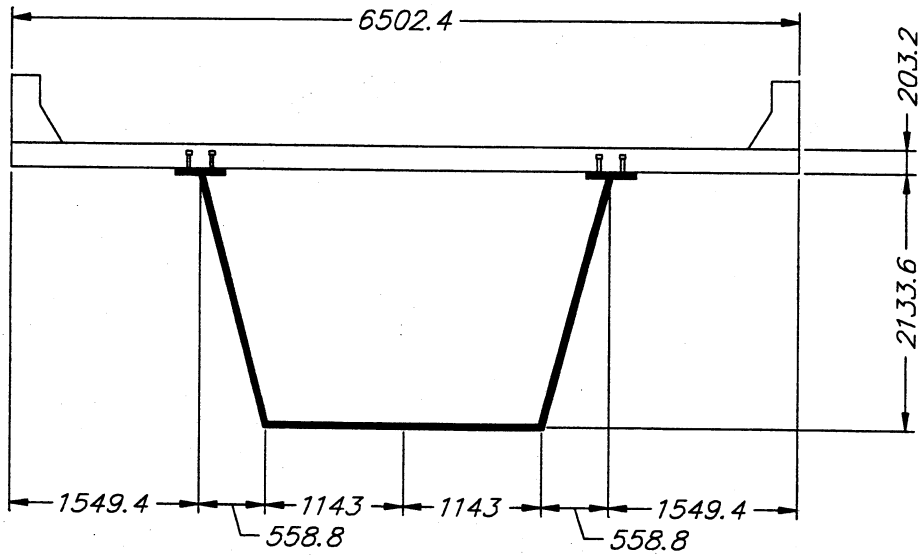

Figure 11: Cross-sectional dimensions for Bridge (dims in mm)

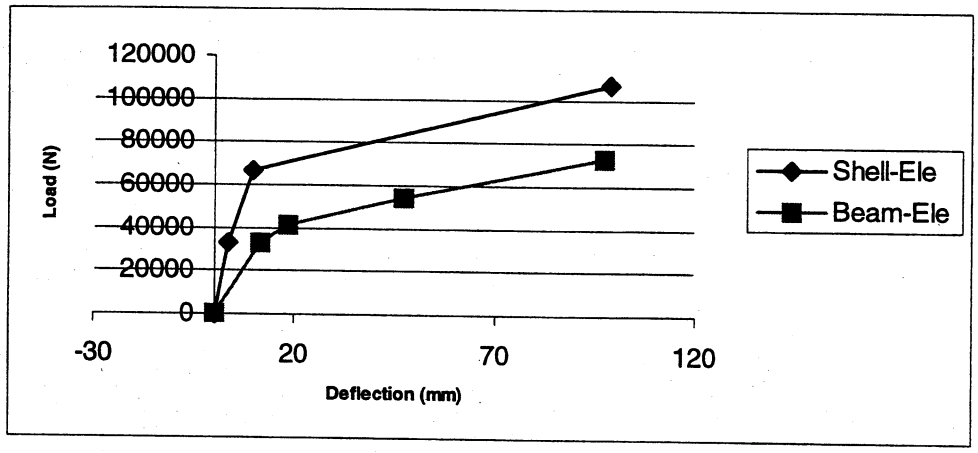

Figure 12: Stiffener study before modification

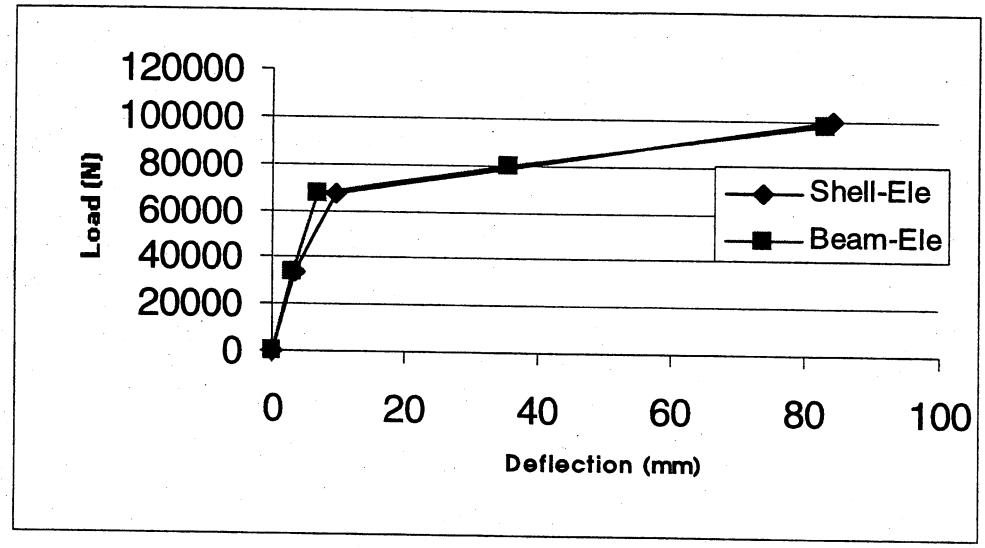

Figure 13: Stiffener study after modification

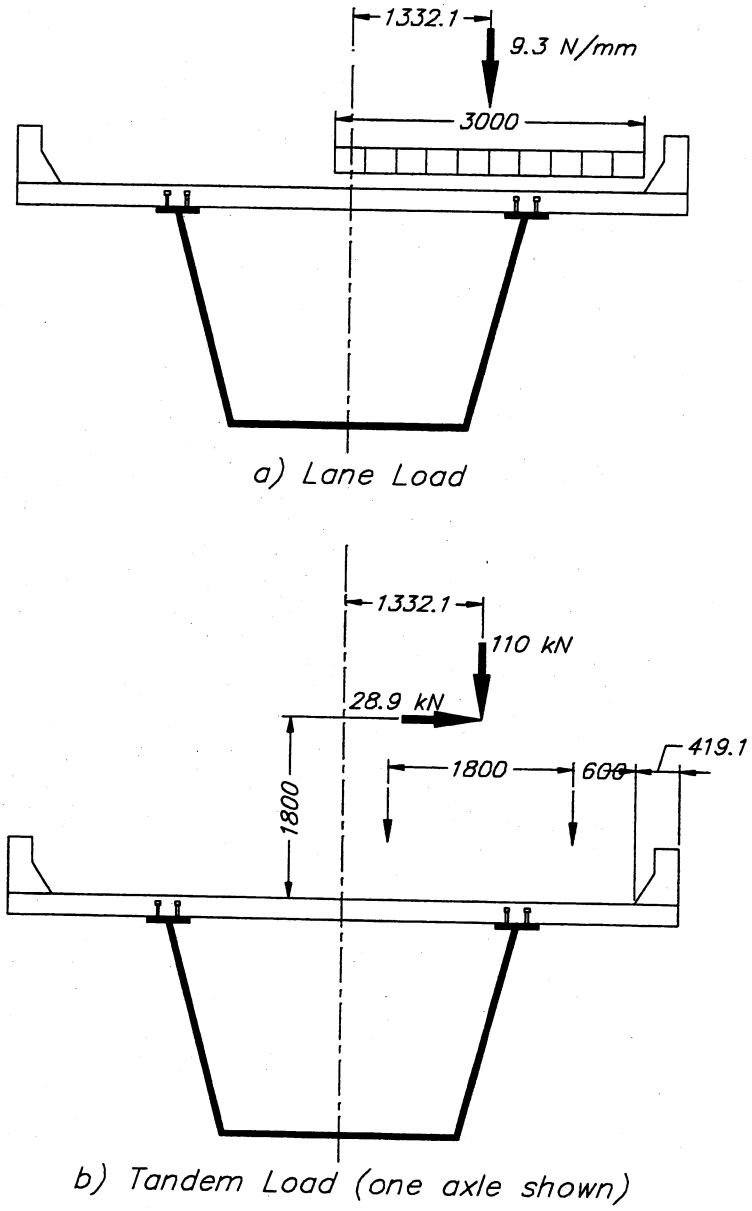

Figure 14: Transverse positioning of live load on Bridge 538

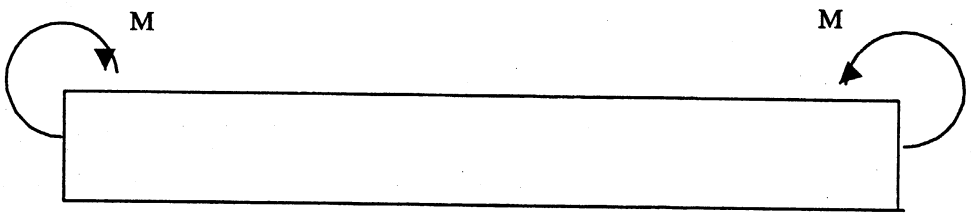

Figure 15: Loading of cross section shell model.

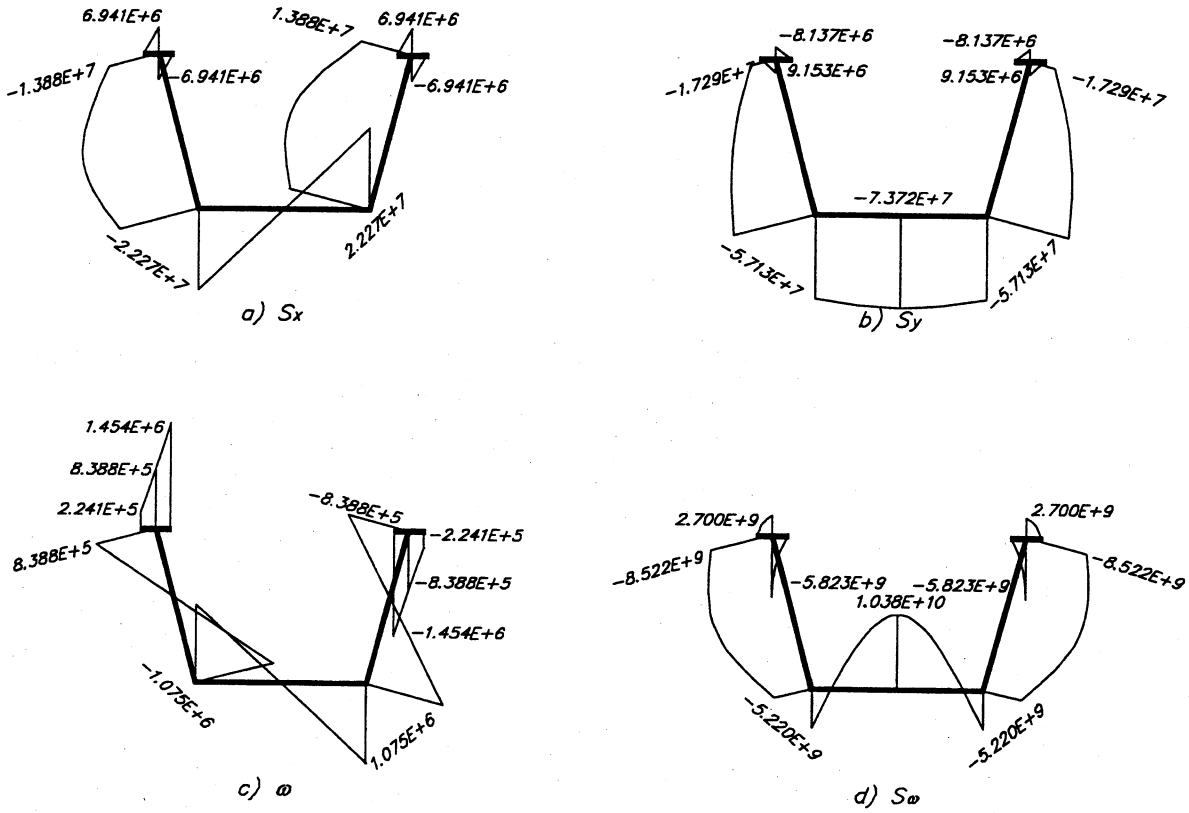

Figure 16: Geometric properties for Brdige 538 (open cross-section without bracing)

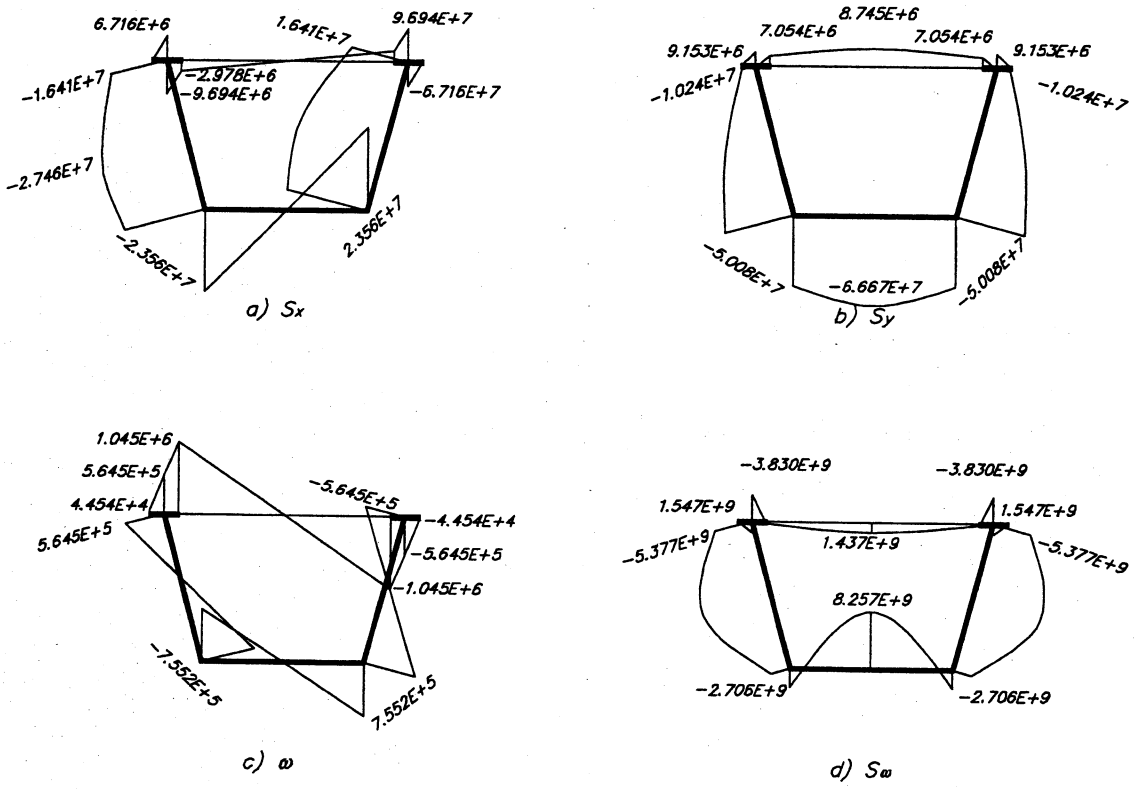

Figure 17: Geometric properties for Brdige 538 (open cross-section with bracing)

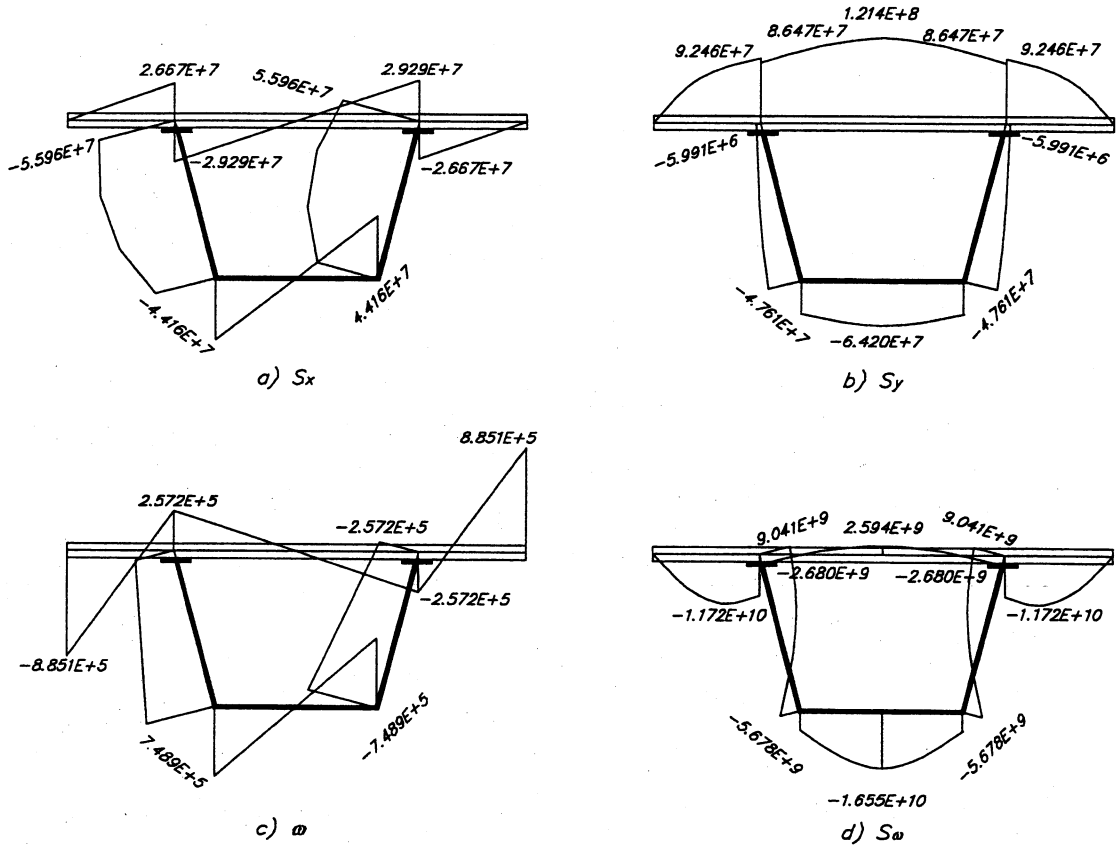

Figure 18: Geometric properties for Brdige 538 (closed cross-section with concrete deck)

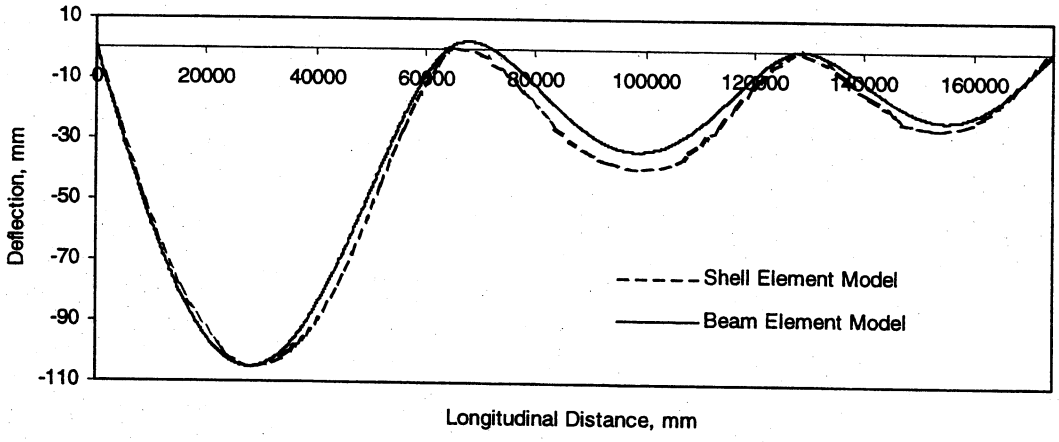

Figure 19: Comparison between deflections obtained by both models

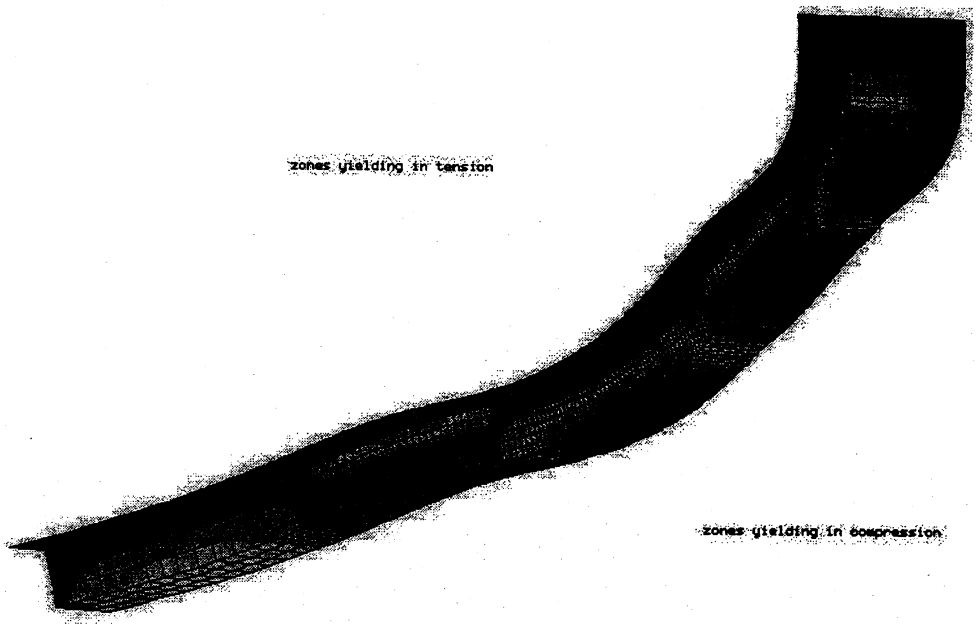

Figure 20: Contours of normal stresses in the longitudinal direction (entire bridge)

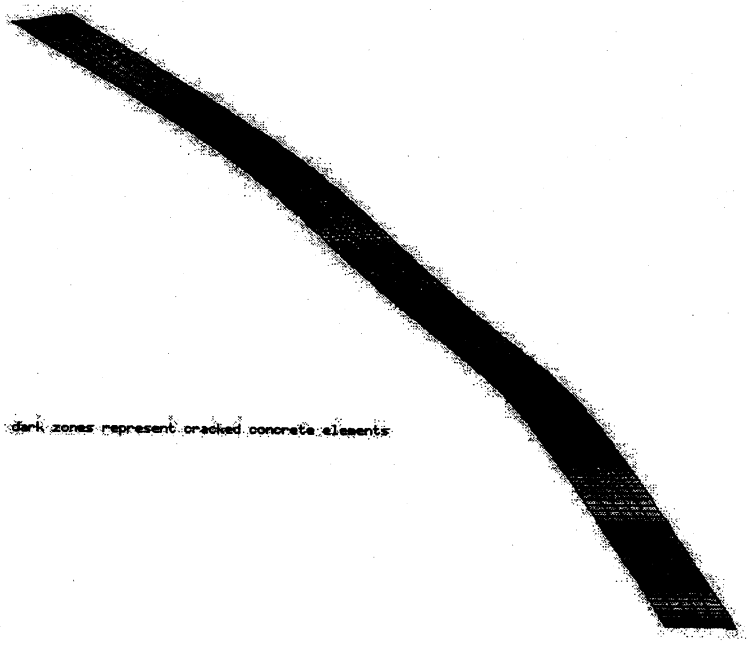

Figure 21: Contours of normal stresses in the longitudinal direction (concrete deck)

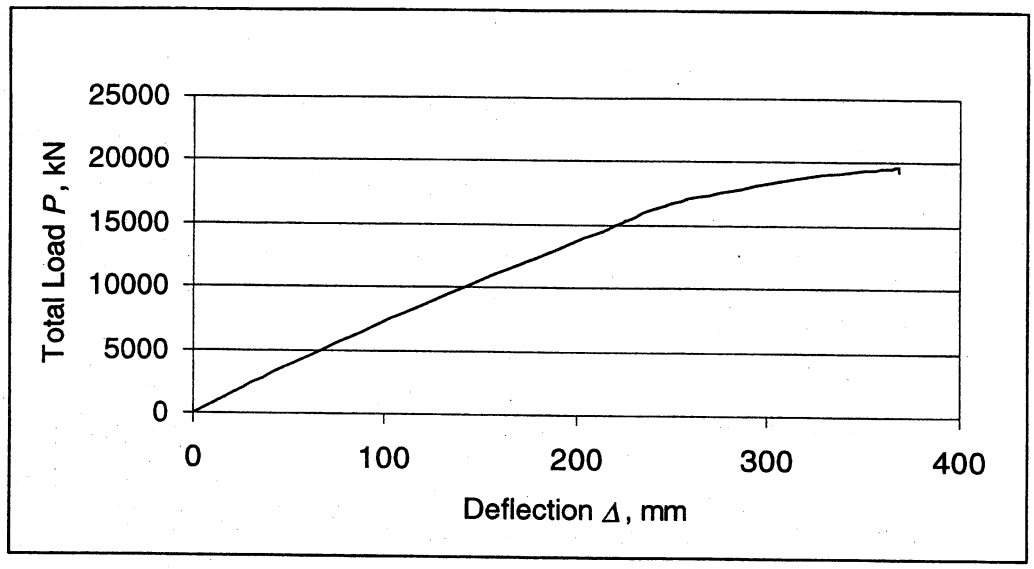

Figure 22: Load-deflection relationship of mid-span point for Bridge 538

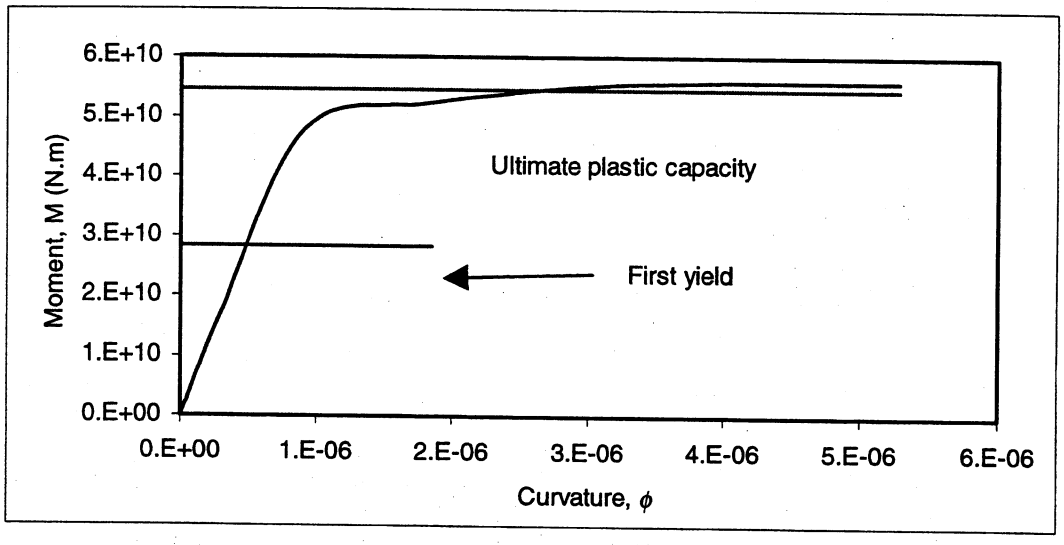

Figure 23: Moment-curvature relationship for cross section model (positive-without a hole)

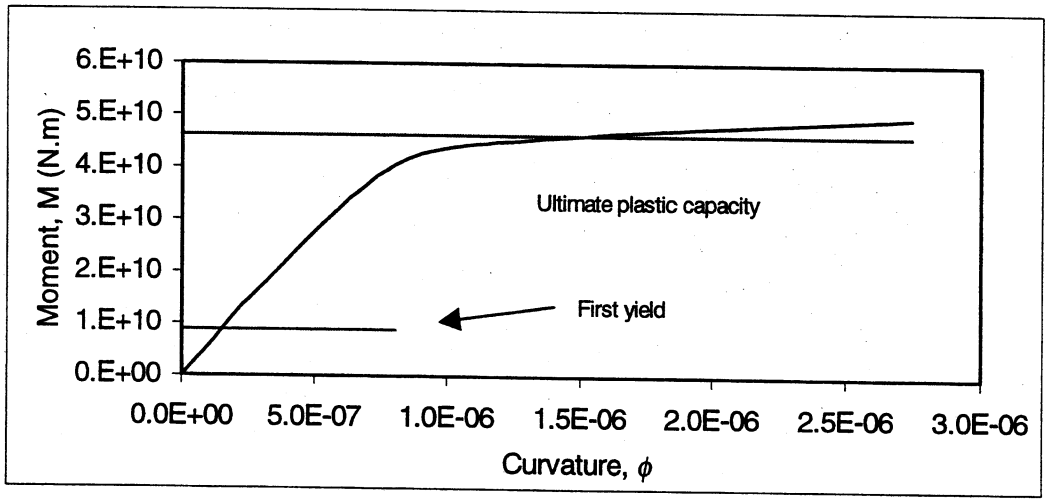

Figure 24: Moment-curvature relationship for cross section model (positive-with a hole)

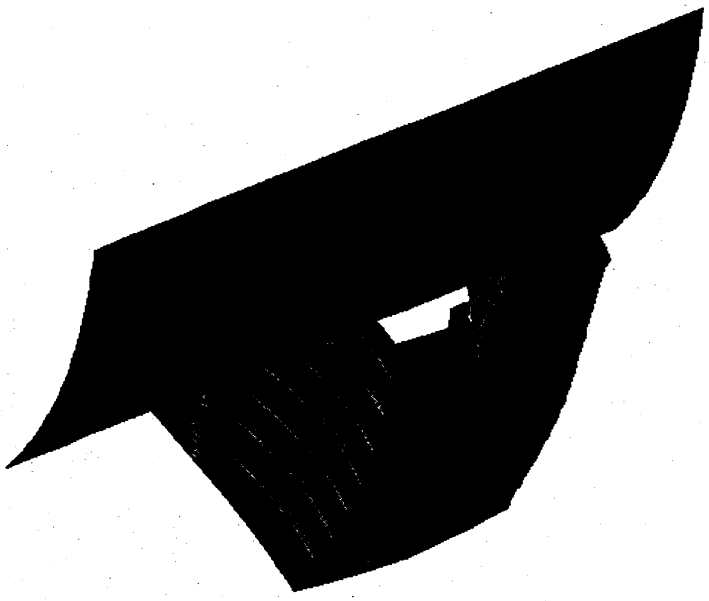

Figure 25: Contours of normal stresses. (positive moment without hole)

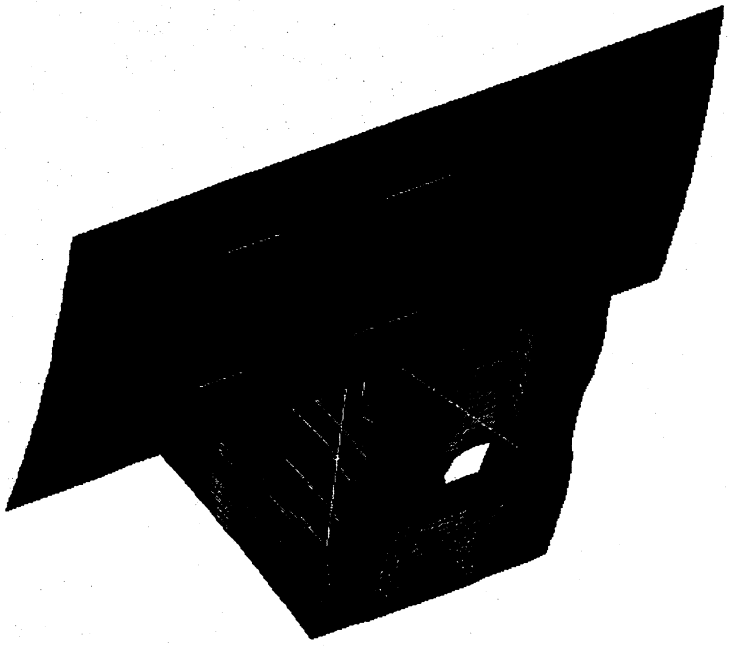

Figure 26: Contours of normal stresses. (positive moment with hole)

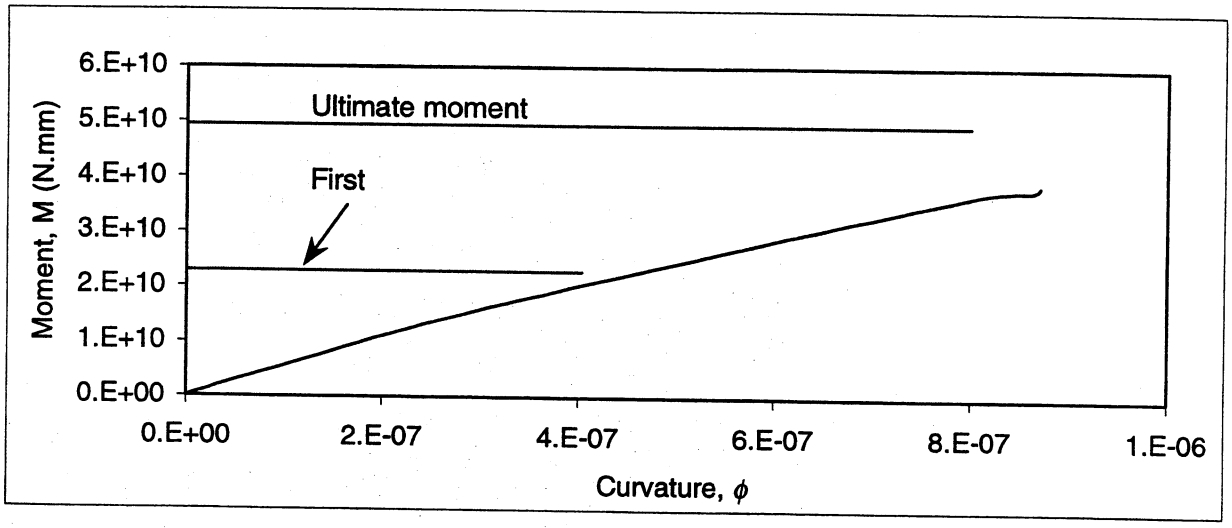

Figure 27: Moment-curvature relationship for cross section model (negative moment-without a hole)

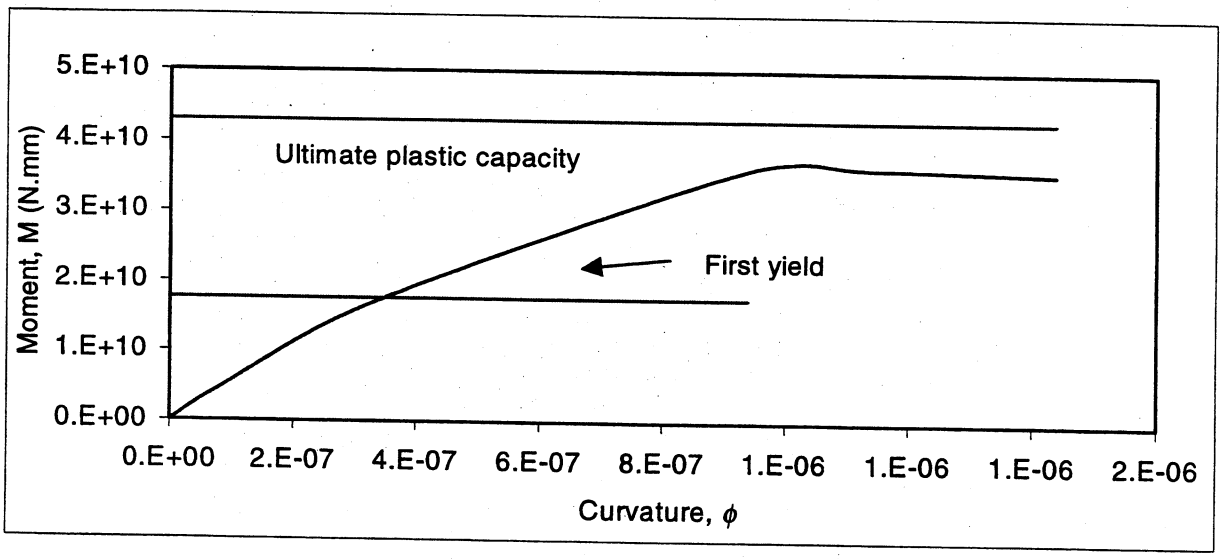

Figure 28: Moment-curvature relationship for cross section model (negative moment-with a hole)

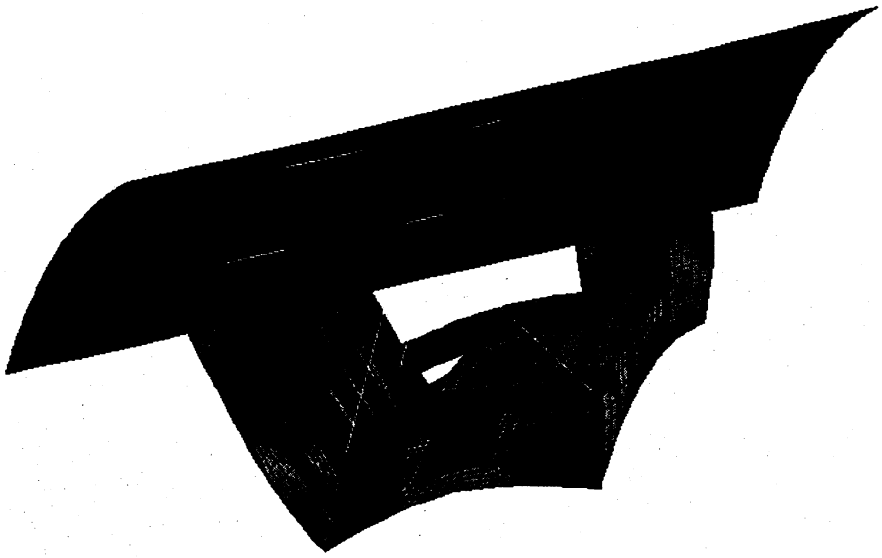

Figure 29: Contours of normal stresses. (negative moment without hole)

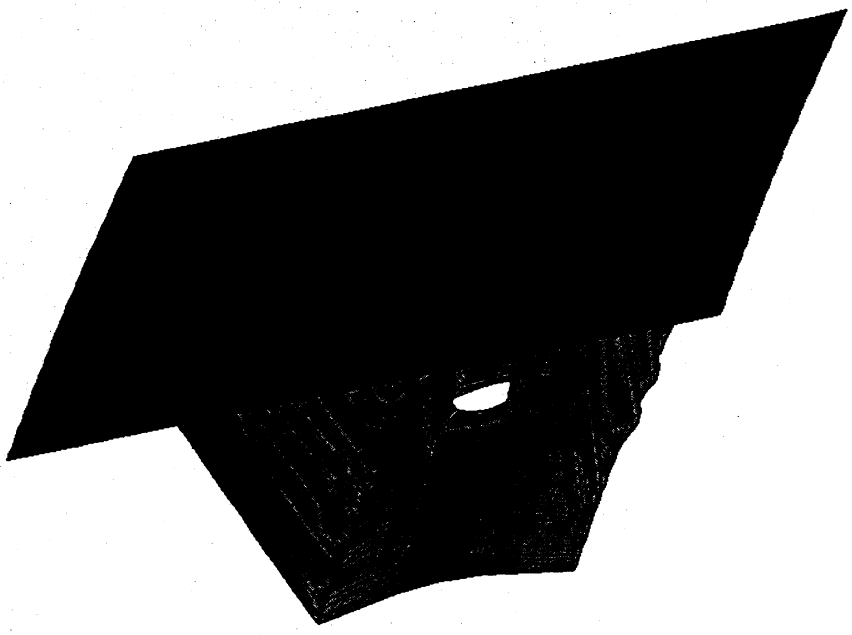

Figure 30: Contours of normal stresses. (negative moment with hole)

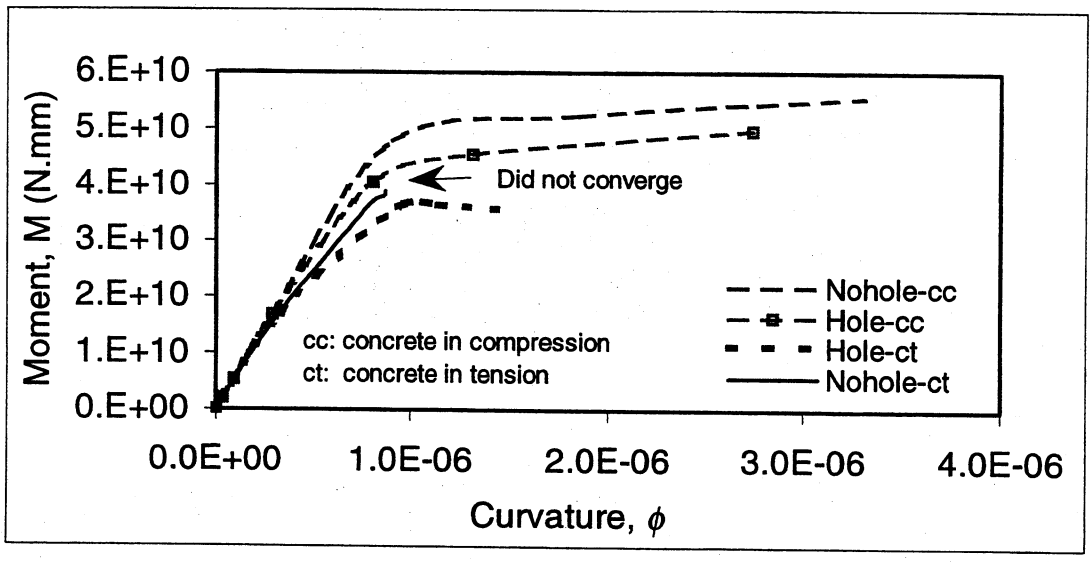

Figure 31: Comparison between moment-curvature relationship for all cases.

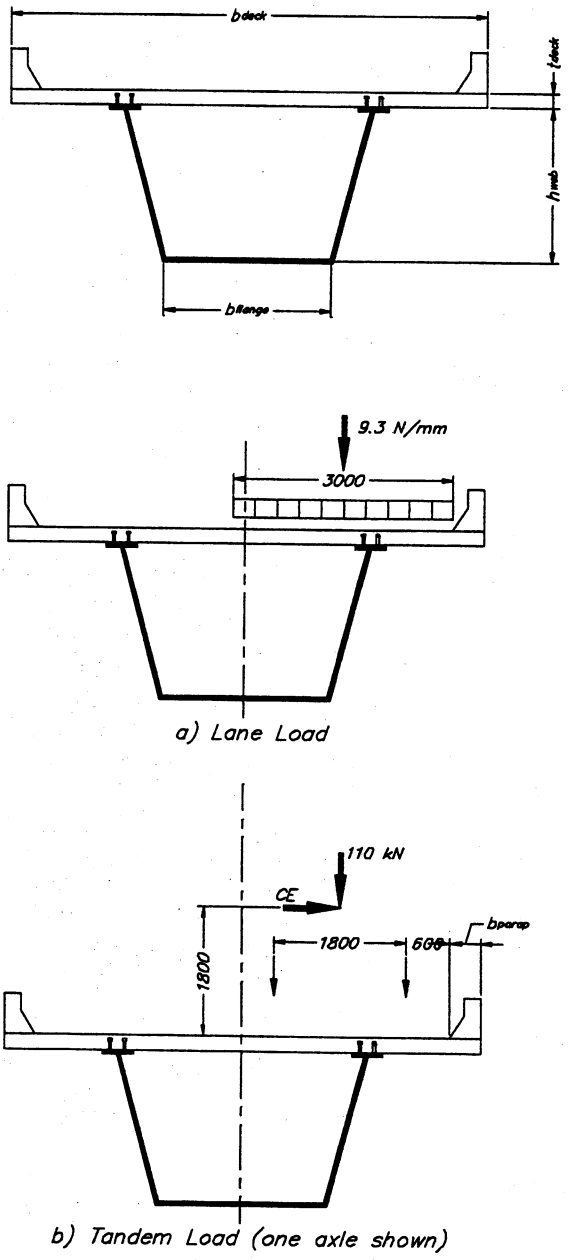

Figure 32: Positioning of live loads for a one-lane bridge

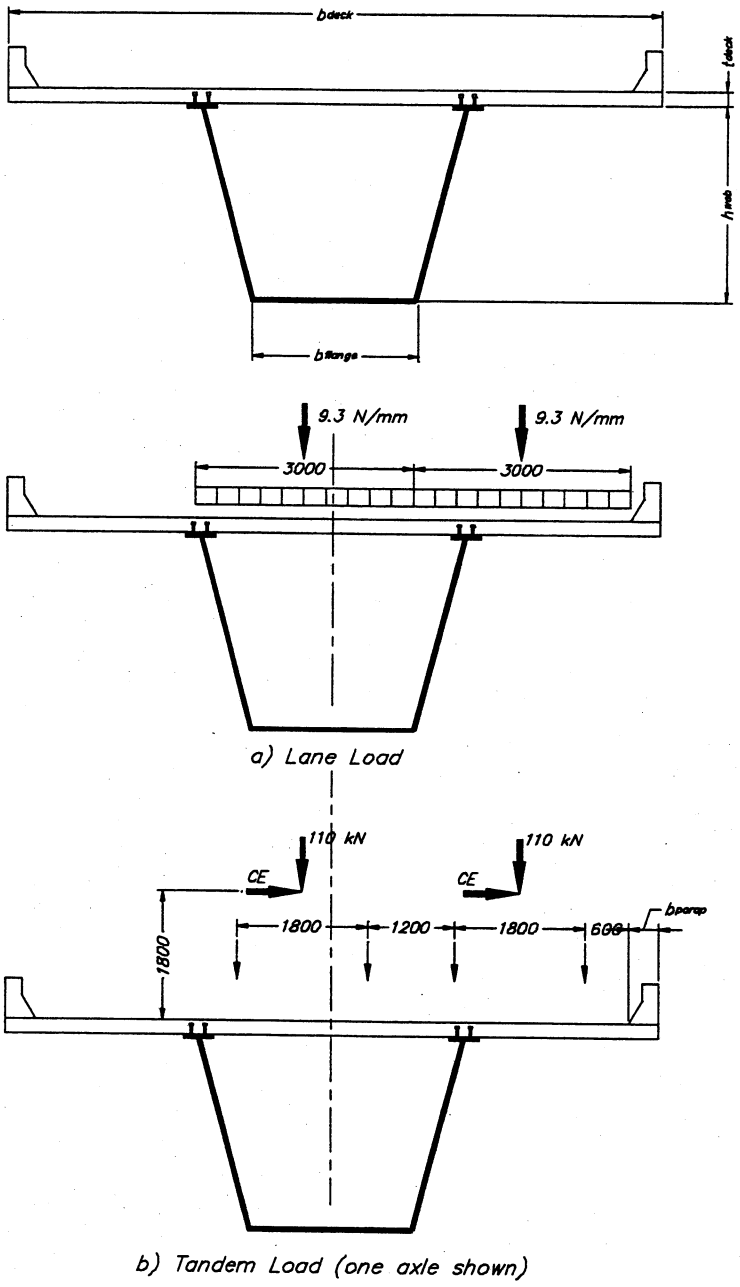

Figure 33: Positioning of live loads for a two-lane bridge

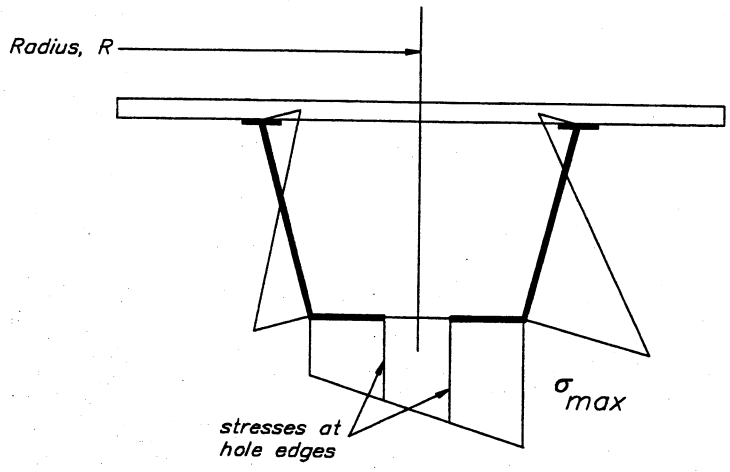

Figure 34: Normal stress distribution at an inner support.

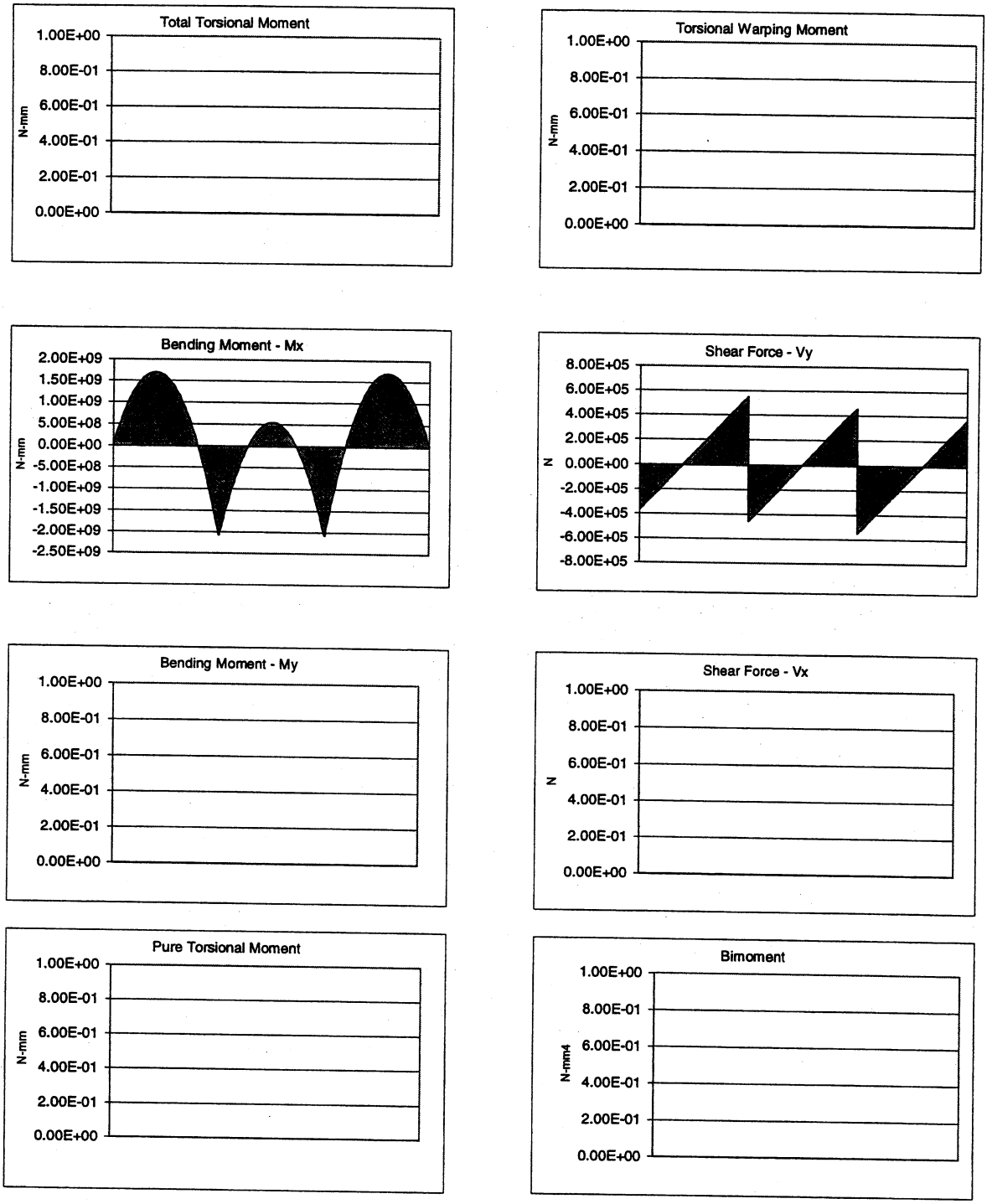

Figure 35: Straining actions due to dead loads (idealized bridge)

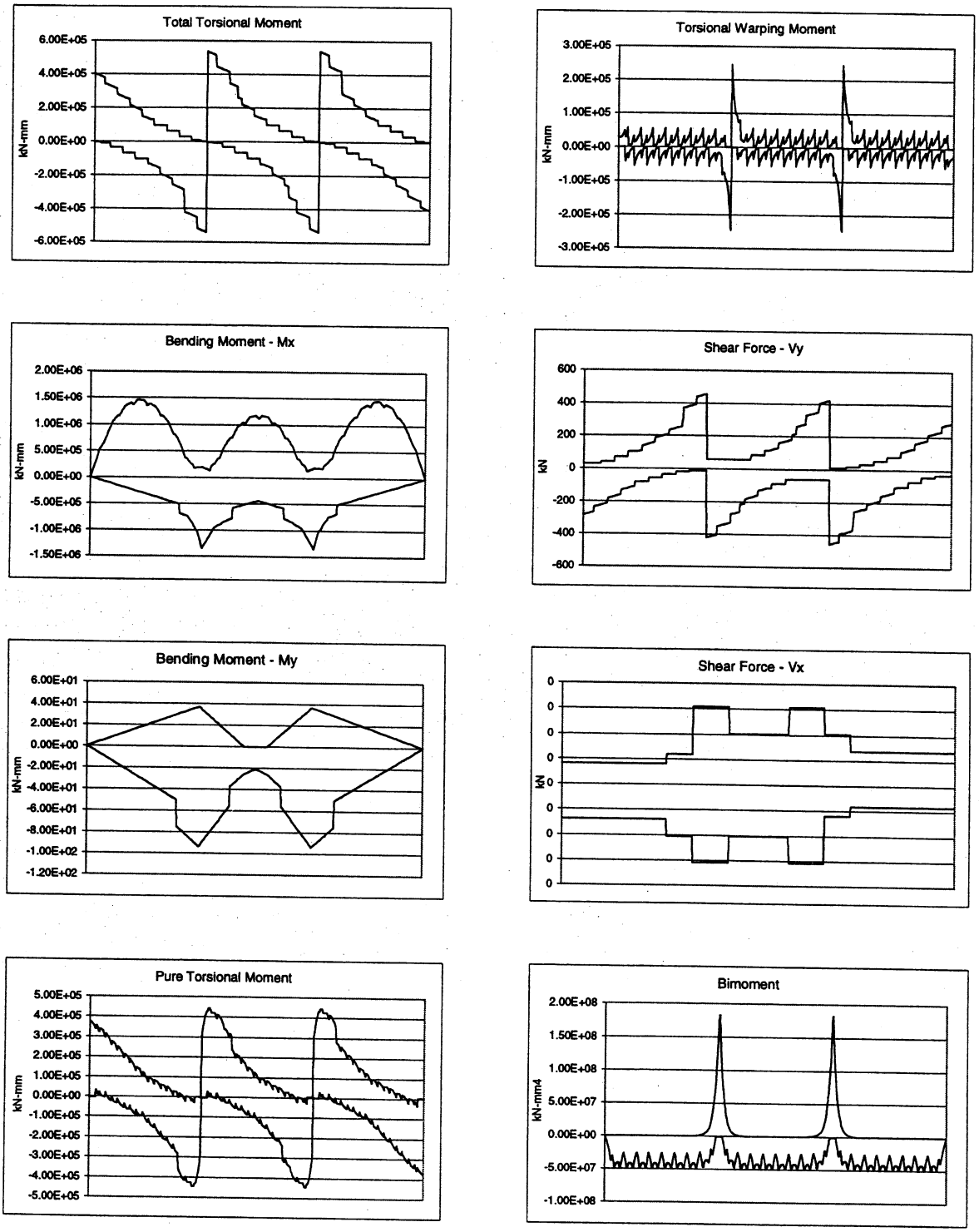

Figure 36: Envelope of straining actions due to live loads (idealized bridge)

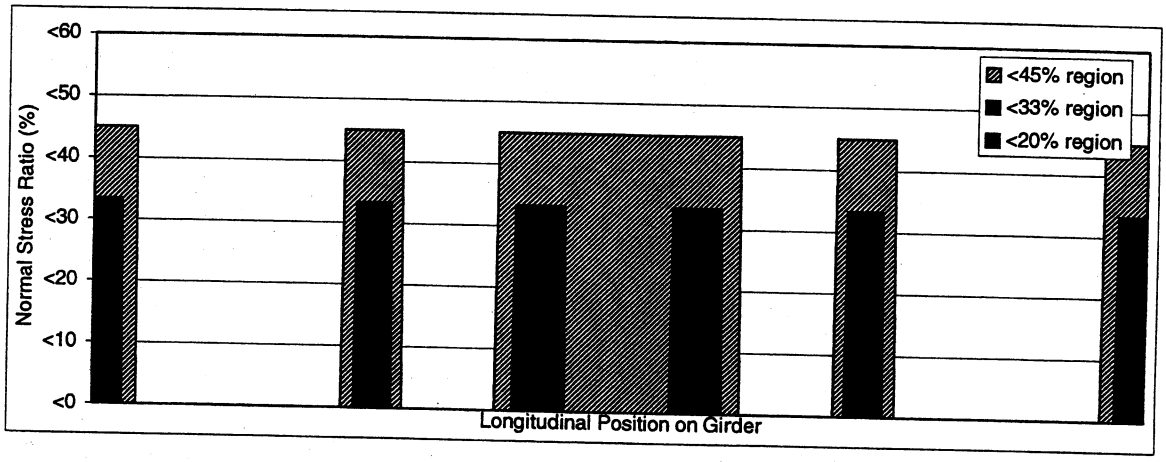

(a)

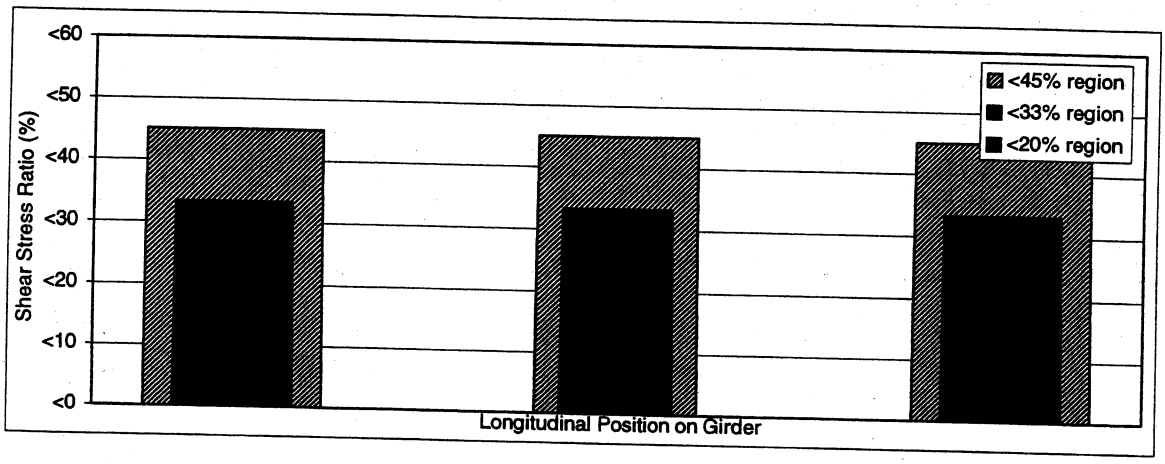

(b)

Figure 37: Low stress regions (a- Approach I, b- Approach II)

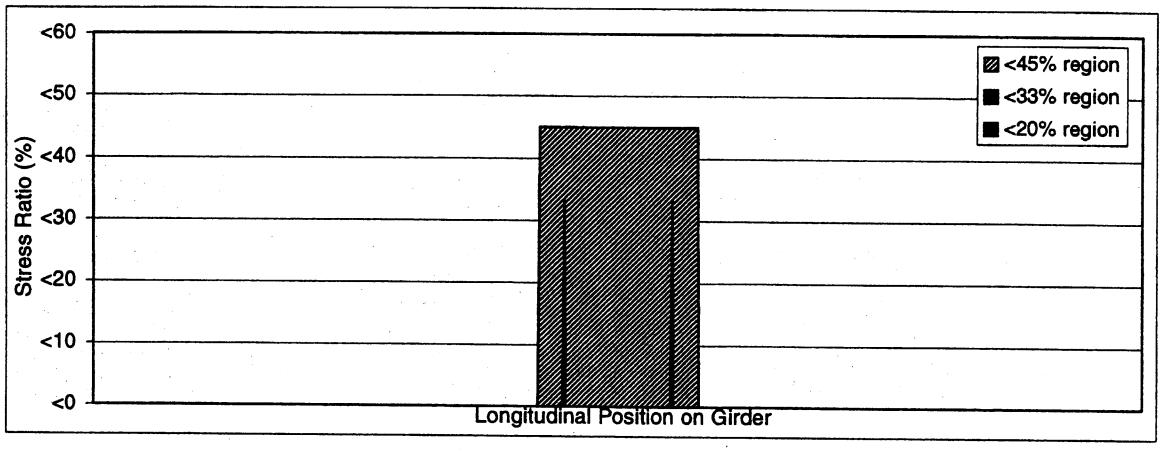

(a)

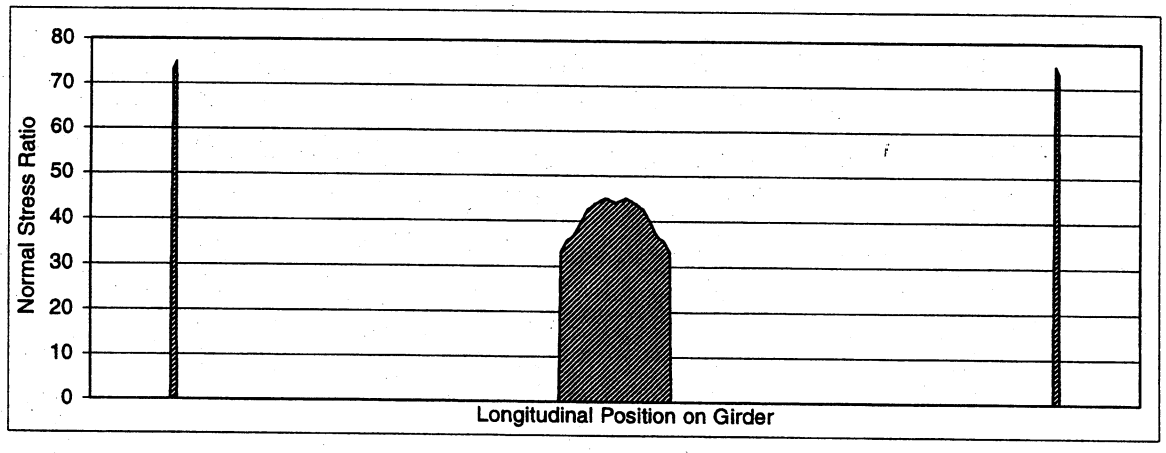

(b)

Figure 38: Low stress regions (a- Approach III, b- Approach IV)

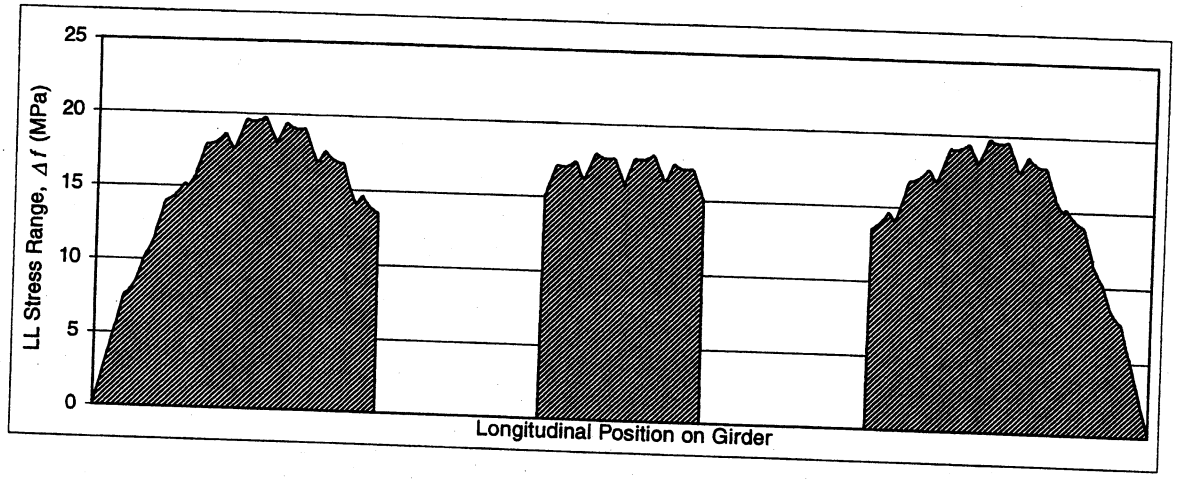

(a)

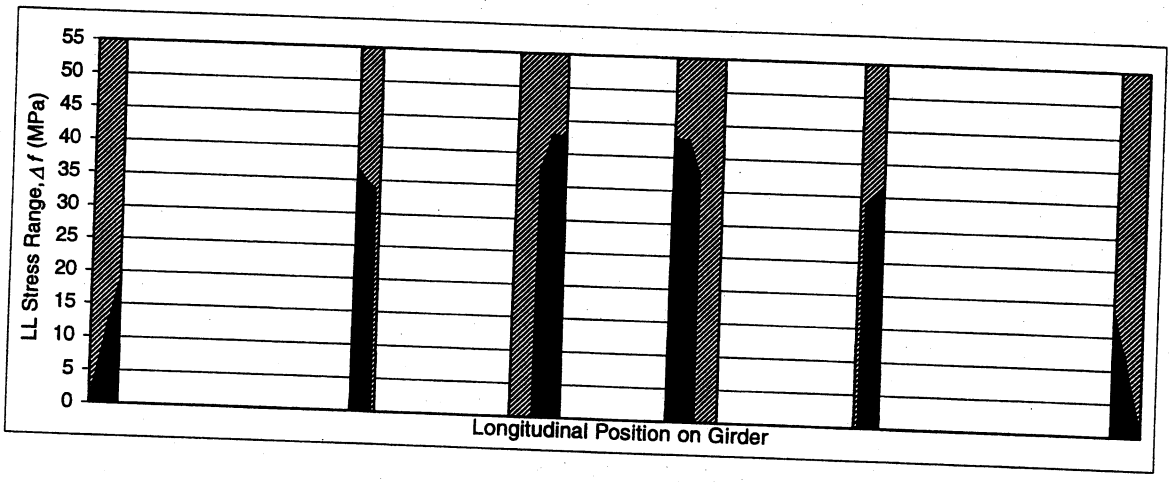

(b)

Figure 39: a- Fatigue stress range, b- Low stress regions following Approach V

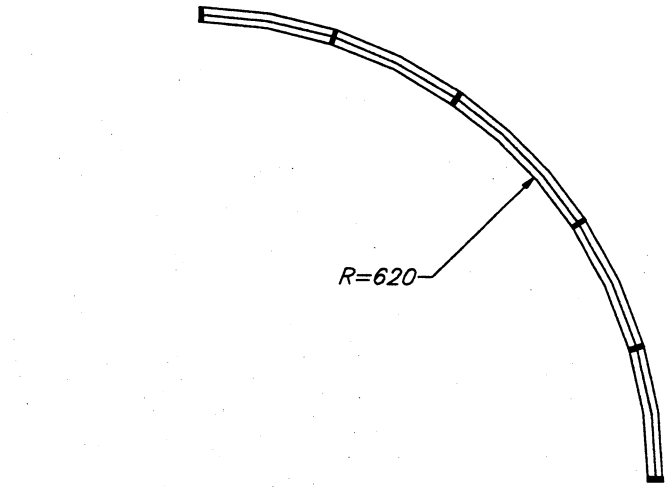

(a) Plan

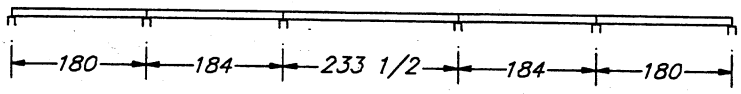

(b) Elevation

Figure 40: Geometry of Bridge 390

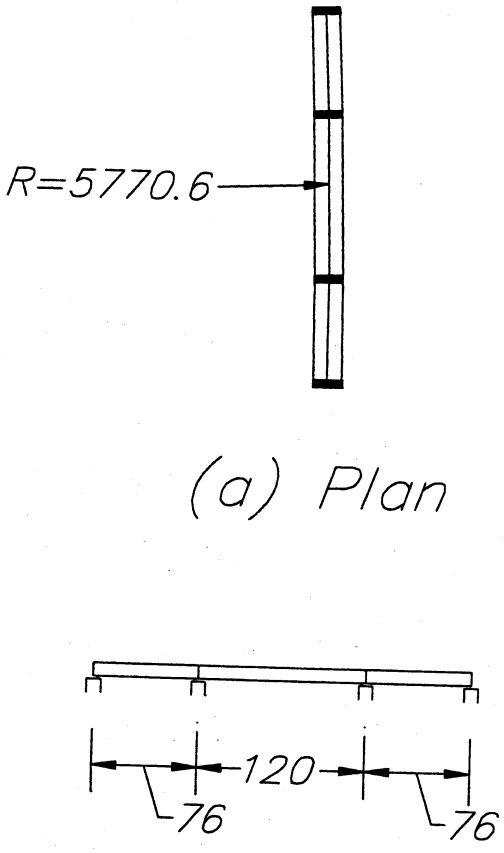

Figure 41: Geometry of Bridge 521

(a) Plan

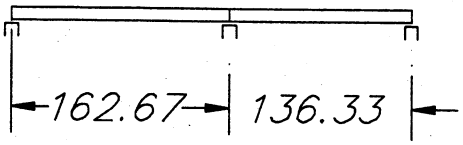

(b) Elevation

Figure 42: Geometry of Bridge 525

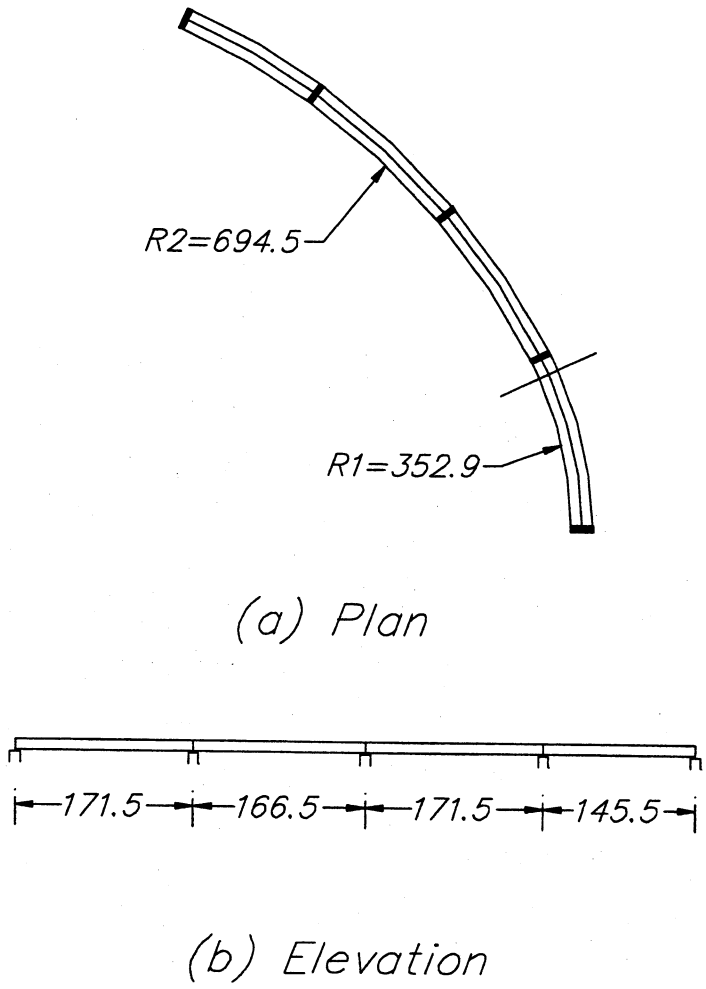

Figure 43: Geometry of Bridge 598

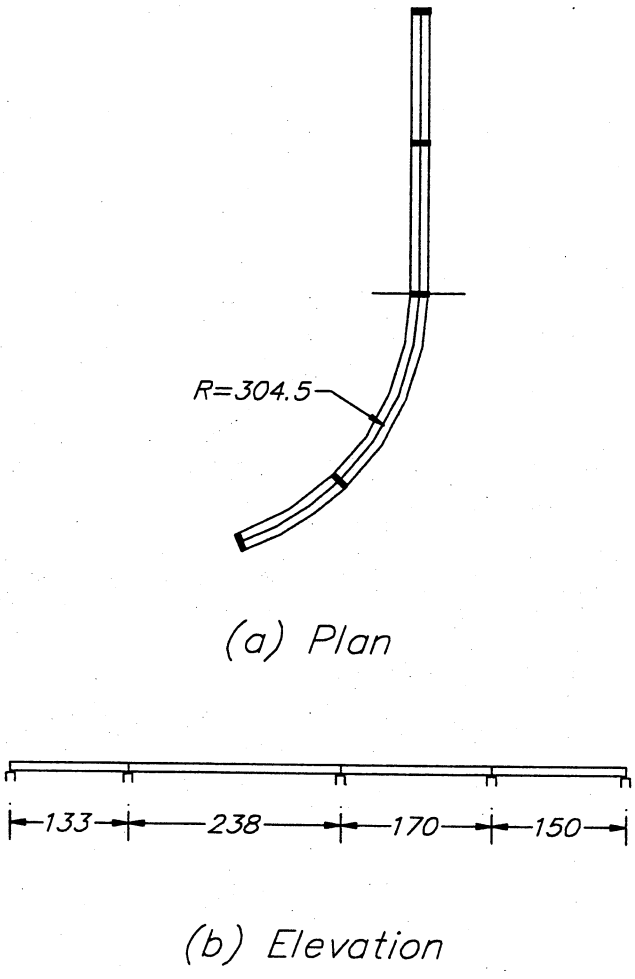

Figure 44: Geometry of Bridge 601

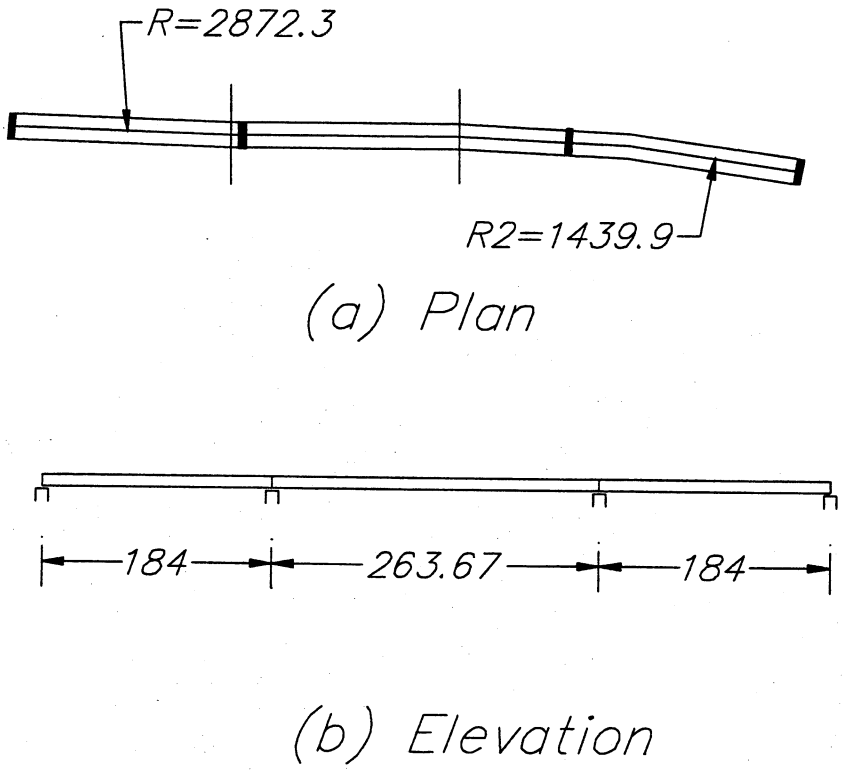

Figure 45: Geometry of Bridge 606

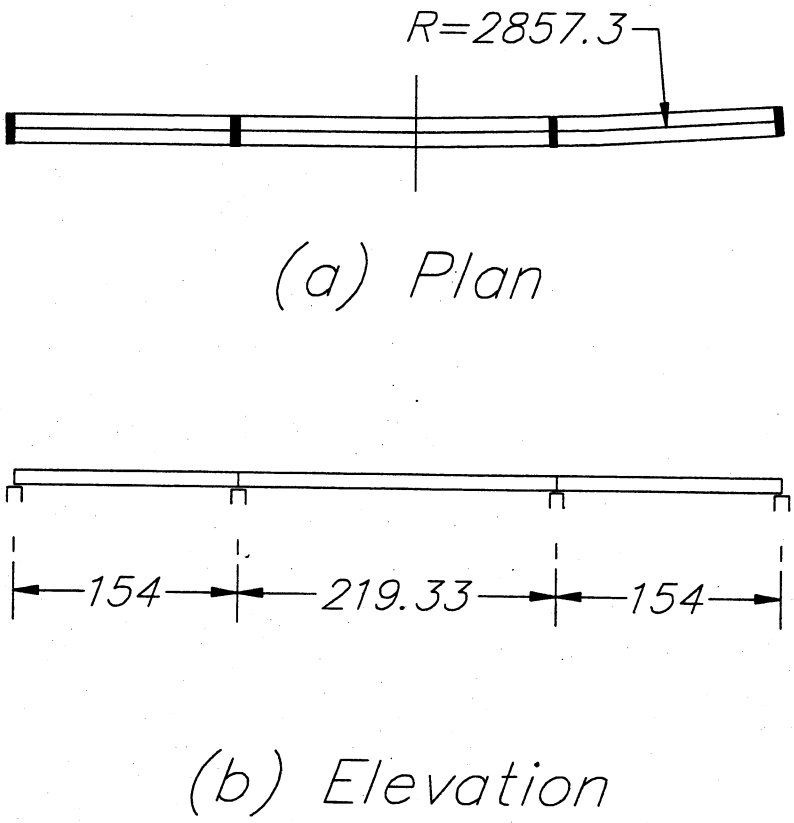

Figure 46: Geometry of Bridge 607

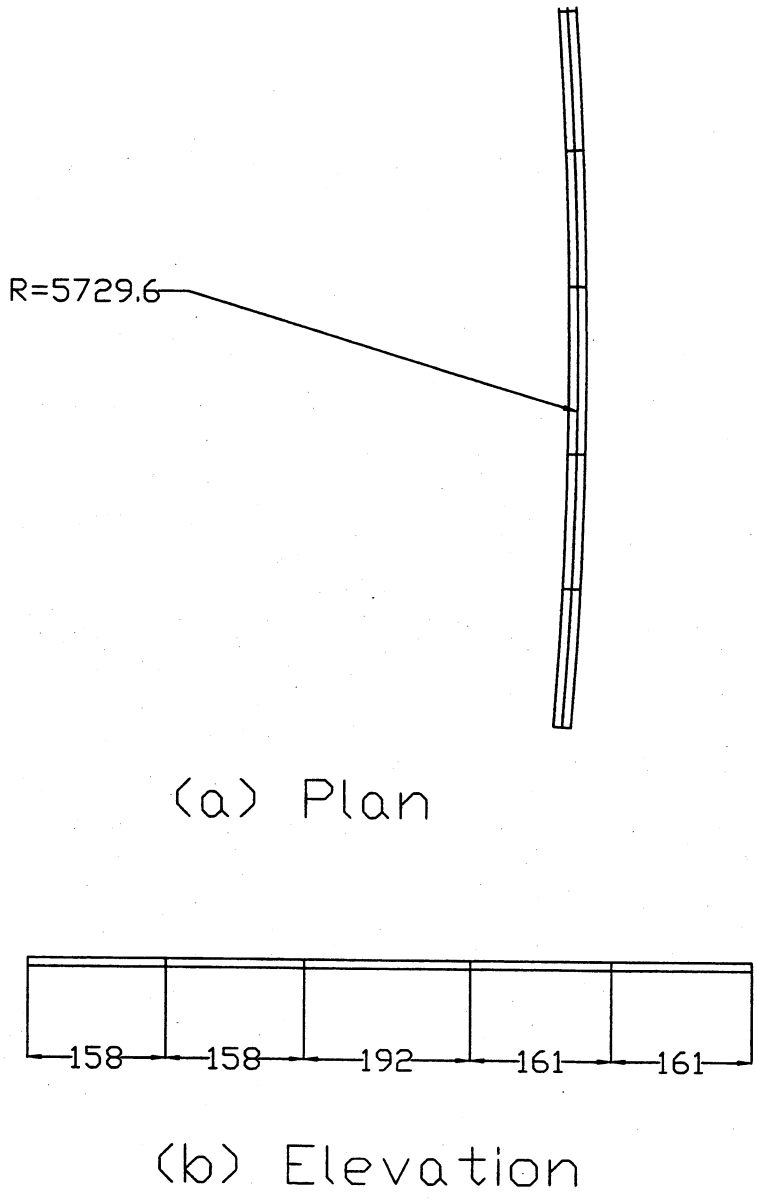

Figure 47: Geometry of Bridge 528

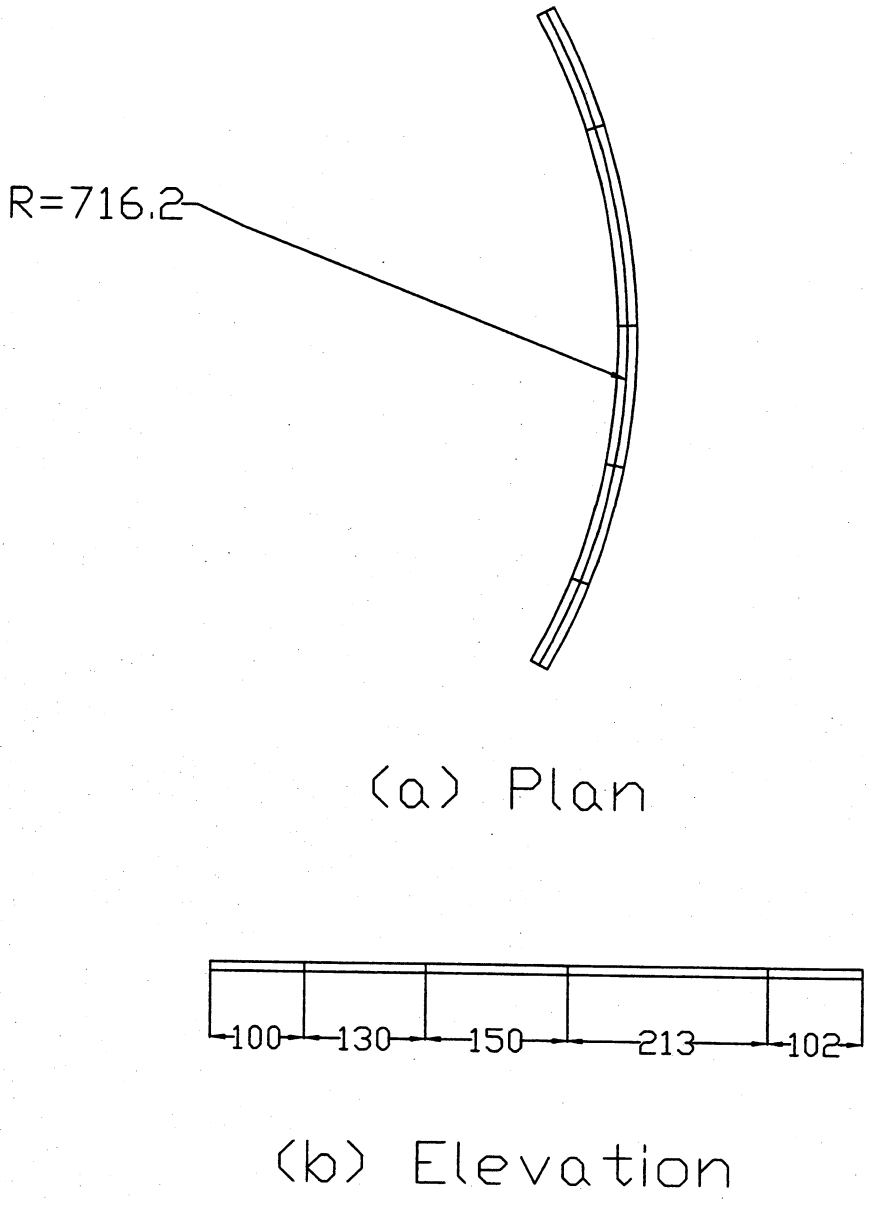

Figure 48: Geometry of Bridge 537

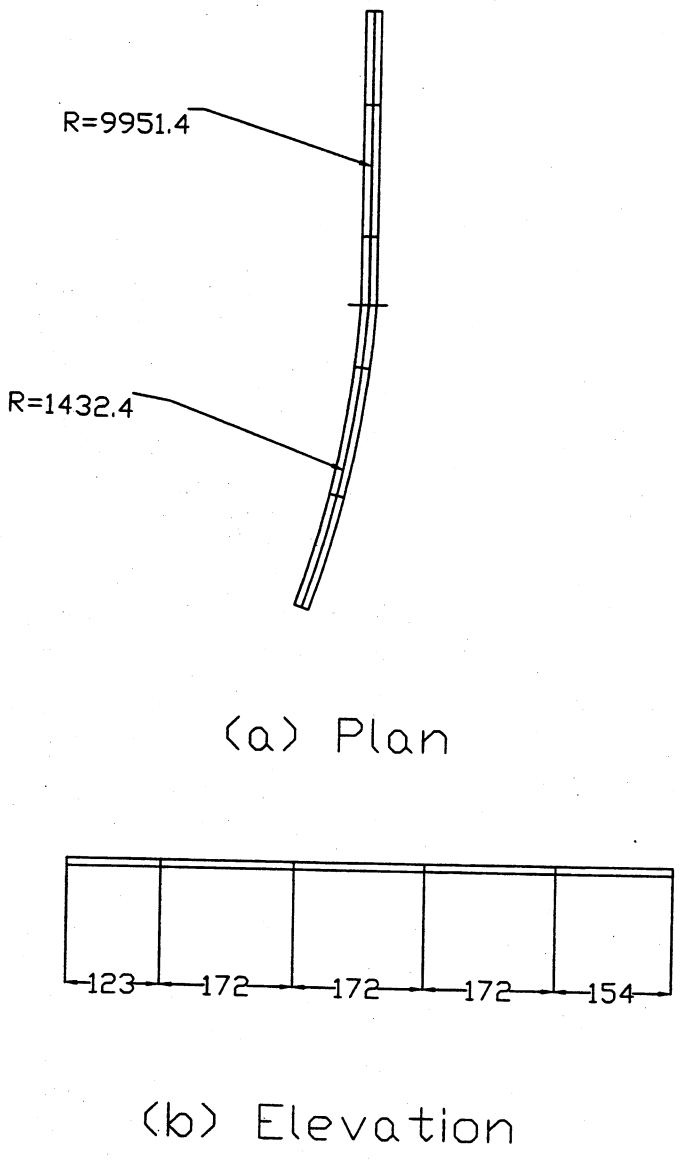

Figure 49: Geometry of Bridge 538a

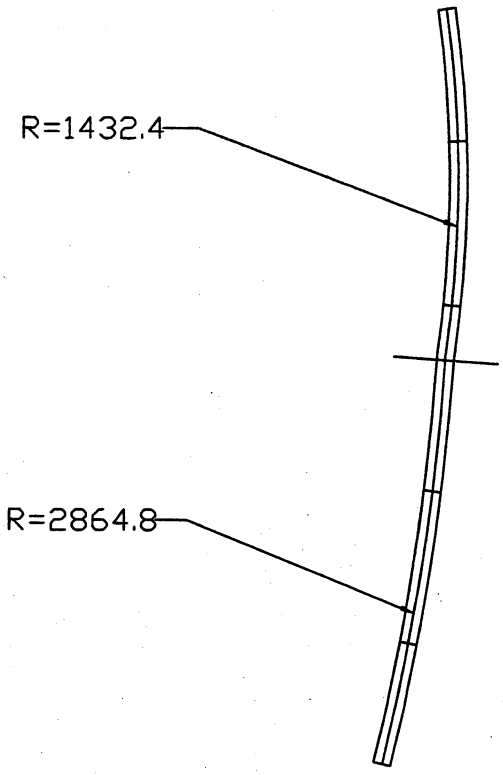

(a) Plan

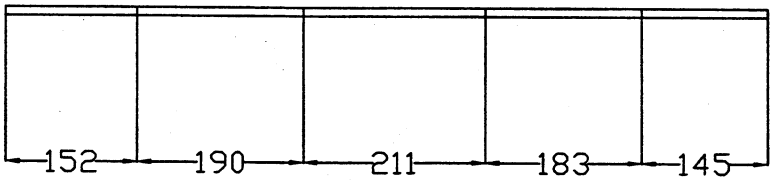

(b) Elevation

Figure 50: Geometry of Bridge 538b

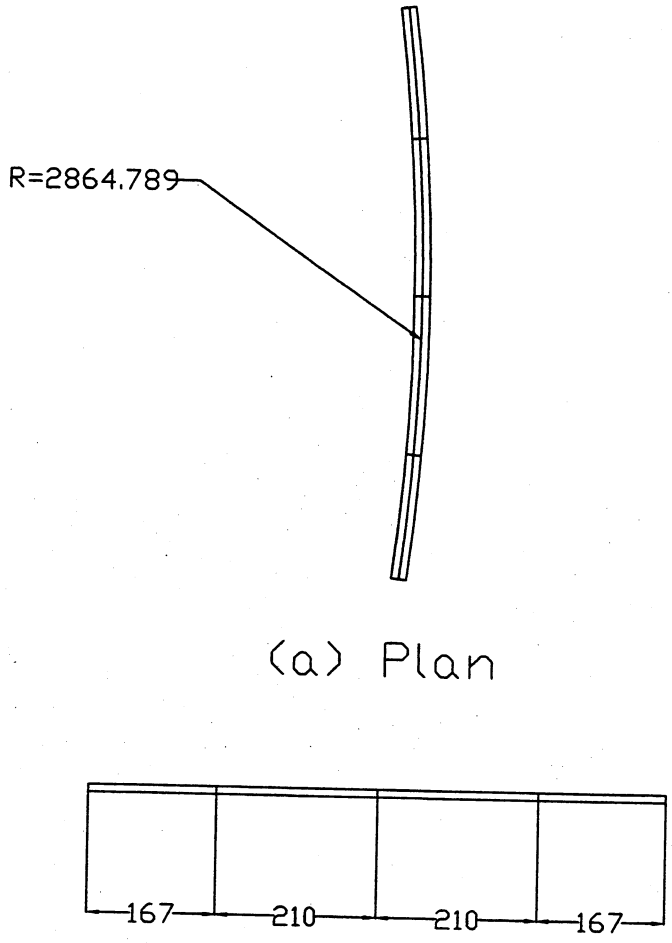

Figure 51: Geometry of Bridge 538c

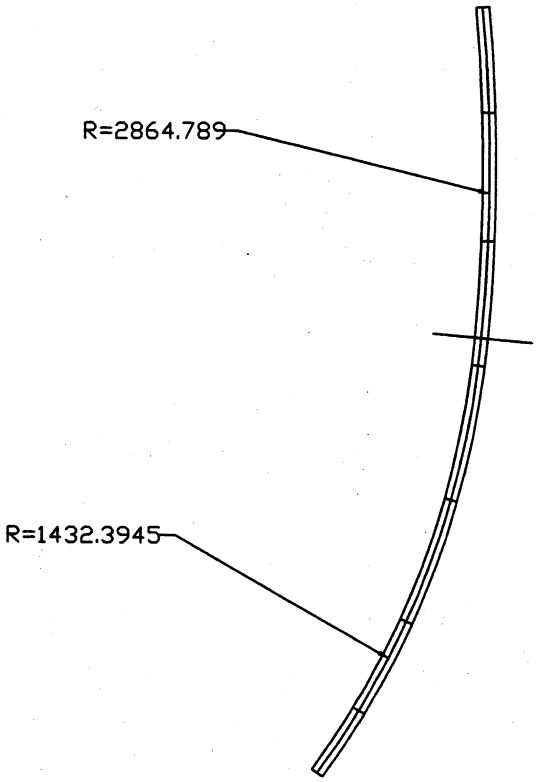

(a) Plan

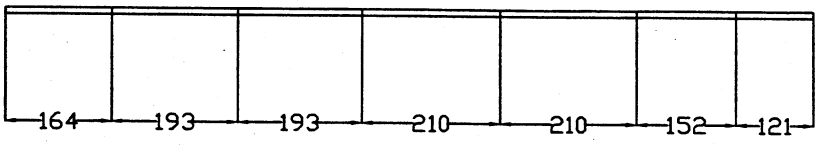

(b) Elevation

Figure 52: Geometry of Bridge 538d

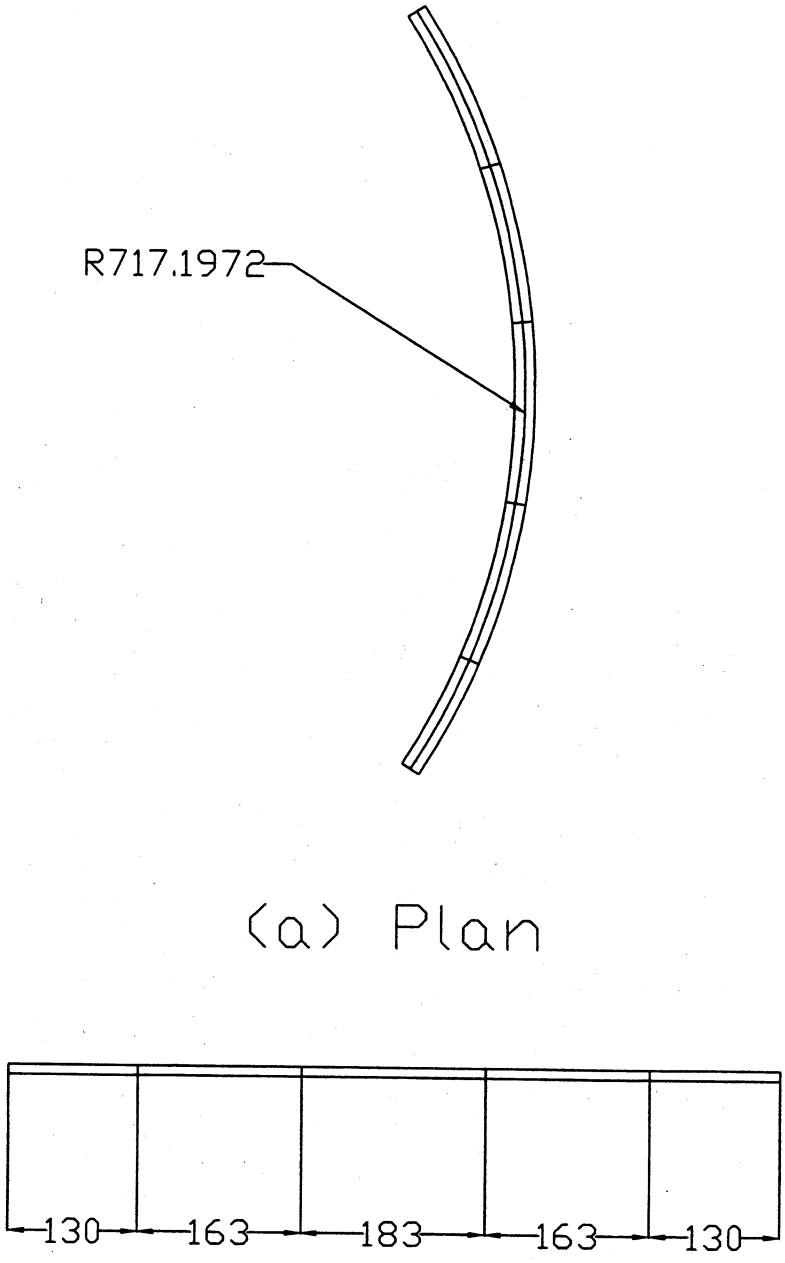

Figure 53: Geometry of Bridge 539

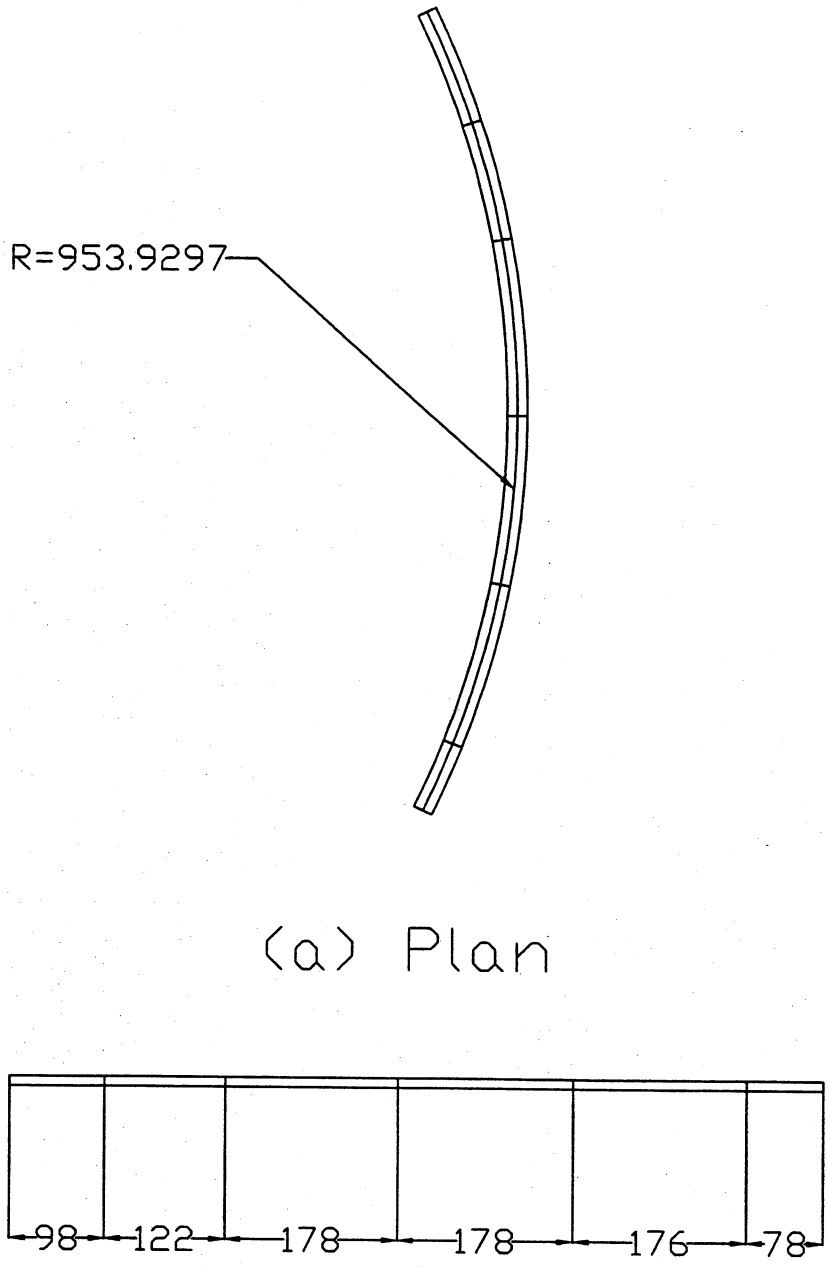

Figure 54: Geometry of Bridge 540

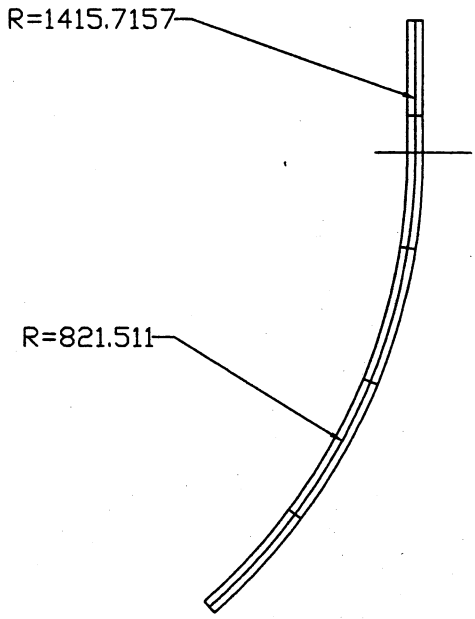

(a) Plan

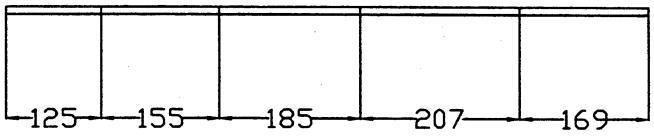

(b) Elevation

Figure 55: Geometry of Bridge 541a

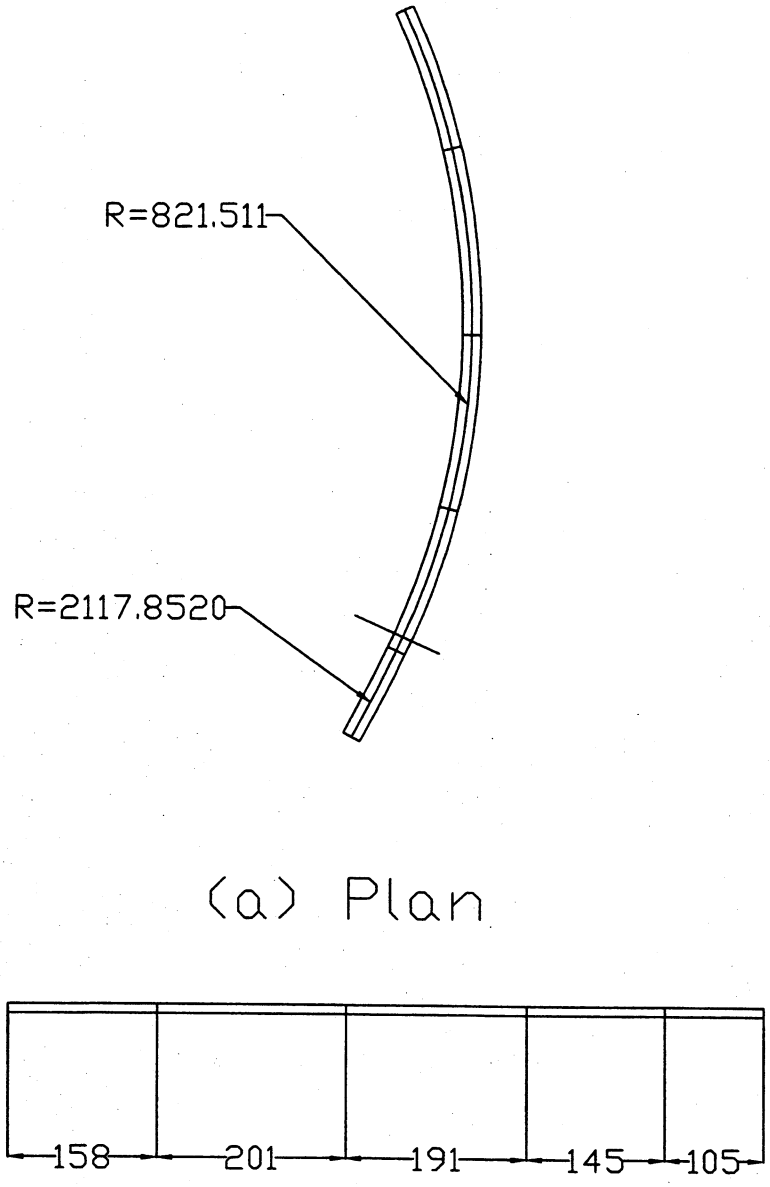

Figure 56: Geometry of Bridge 541b

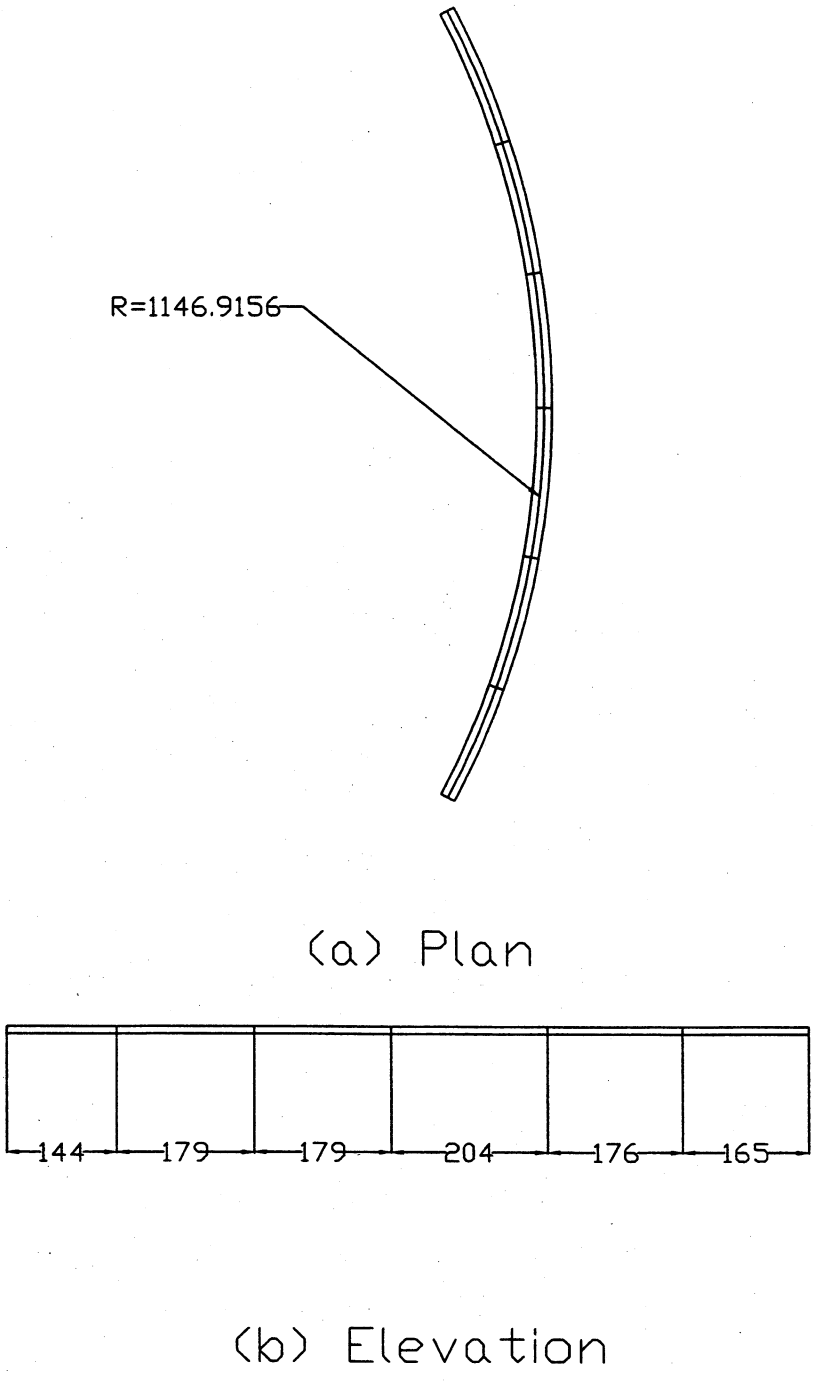

Figure 57: Geometry of Bridge 542a

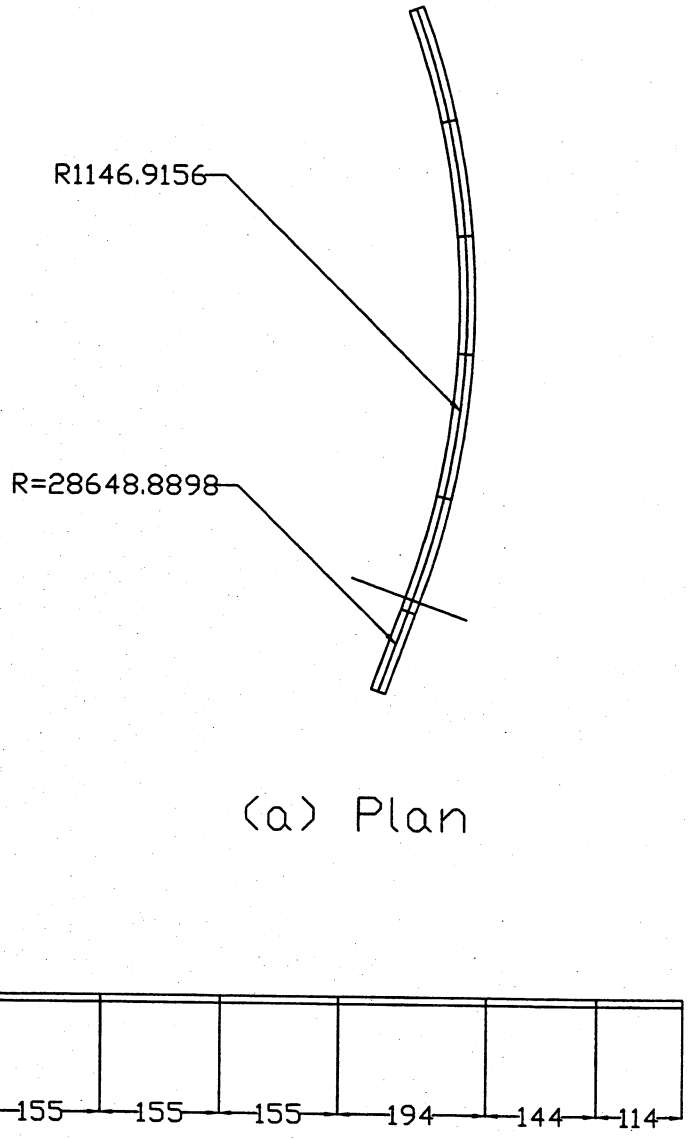

Figure 58: Geometry of Bridge 542b

Table 7-a: Summary of suggested hole locations based on Approach V

BRIDGE	Location	Span-1		Span-2		Span-3		Span-4		Span-5		Span-6		Span-7	
BRIDGE- 528		L=48.1584 m		L=48.1584m		L=58.5216m		L=48.9204m		L=49.9204m					
		meters	%	meters	%	meters	%	meters	%	meters	%				
Hole-1(Beg. of span)	Loc. Beg.	0.00	0.00			8.84	15.10			8.99	18.38				
	Loc. Avg.	1.91	3.96			9.37	16.02			10.13	20.72				
	Loc. End	3.81	7.91			9.91	16.93			11.28	23.05				
	Loc. Len.	3.81	7.91			1.07	1.82			2.29	4.67				
Hole-2(End of span)	Loc. Beg.	8.53	17.72			9.14	15.63			1.00	2.00				
	Loc. Avg.	8.99	18.67			9.53	16.28			2.83	5.67				
	Loc. End	9.45	19.62			9.91	16.93			4.66	9.33				
	Loc. Len.	0.91	1.90			0.76	1.30			3.66	7.33				
BRIDGE- 537		L=30.48 m		L=39.624m		L=45.72m		L=64.9224m		L=31.0896m					
		meters	%	meters	%	meters	%	meters	%	meters	%				
Hole-1(Beg. of span)	Loc. Beg.	0.00	0.00	5.49	13.85	5.94	13.00	10.97	16.90						
	Loc. Avg.	3.20	10.50	7.24	18.27	7.39	16.17	11.43	17.61						
	Loc. End	6.40	21.00	8.99	22.69	8.84	19.33	11.89	18.31						
	Loc. Len.	6.40	21.00	3.51	8.85	2.90	6.33	0.91	1.41						
Hole-2(End of span)	Loc. Beg.	6.25	20.50	6.71	16.92			11.43	17.61	0.00	0.00				
	Loc. Avg.	7.32	24.00	7.09	17.88			12.19	18.78	2.67	8.58				
	Loc. End	8.38	27.50	7.47	18.85			12.95	19.95	5.33	17.16				
	Loc. Len.	2.13	7.00	0.76	1.92			1.52	2.35	5.33	17.16				
BRIDGE- 538a		L=37.338 m		L=52.4256m		L=52.4256m		L=52.4256m		L=46.9392m					
		meters	%	meters	%	meters	%	meters	%	meters	%				
Hole-1(Beg. of span)	Loc. Beg.	0.00	0.00	9.30	17.73										
	Loc. Avg.	2.21	5.92	10.21	19.48										
	Loc. End	4.42	11.84	11.13	21.22										
	Loc. Len.	4.42	11.84	1.83	3.49										
Hole-2(End of span)	Loc. Beg.									0.00	0.00				
	Loc. Avg.									2.06	4.38				
	Loc. End									4.11	8.77				
	Loc. Len.									4.11	8.77				
BRIDGE- 538b		L=46.3296m		L=57.912m		L=64.3128m		L=55.626m		L=44.3484m					
		meters	%	meters	%	meters	%	meters	%	meters	%				
Hole-1(Beg. of span)	Loc. Beg.	0.00	0.00	12.34	21.32	13.11	20.38								
	Loc. Avg.	2.29	4.93	12.80	22.11	13.18	20.50								
	Loc. End	4.57	9.87	13.26	22.89	13.26	20.62								
	Loc. Len.	4.57	9.87	0.91	1.58	0.15	0.24								
Hole-2(End of span)	Loc. Beg.					11.89	18.48	11.73	21.10	0.00	0.00				
	Loc. Avg.					12.34	19.19	12.27	22.05	2.06	4.64				
	Loc. End					12.80	19.91	12.80	23.01	4.11	9.28				
	Loc. Len.					0.91	1.42	1.07	1.92	4.11	9.28				
BRIDGE- 538c		L=50.9016 m		L=64.008m		L=64.008m		L=50.9016m							
		meters	%	meters	%	meters	%	meters	%						
Hole-1(Beg. of span)	Loc. Beg.	0.00	0.00	13.87	21.67										
	Loc. Avg.	2.06	4.04	14.25	22.26										
	Loc. End	4.11	8.08	14.63	22.86										
	Loc. Len.	4.11	8.08	0.76	1.19										
Hole-2(End of span)	Loc. Beg.					13.87	21.67	0.00	0.00						
	Loc. Avg.					14.25	22.26	2.06	4.04						
	Loc. End					14.63	22.86	4.11	8.08						
	Loc. Len.					0.76	1.19	4.11	8.08						
BRIDGE- 538d		L=49.9872m		L=58.8264m		L=58.8264m		L=64.008m		L=64.008m		L=46.3296m		L=36.8808m	
		meters	%	meters	%	meters	%	meters	%	meters	%	meters	%	meters	%
Hole-1(Beg. of span)	Loc. Beg.	0.00	0.00											8.38	22.73
	Loc. Avg.	2.21	4.42											8.46	22.93
	Loc. End	4.42	8.84											8.53	23.14
	Loc. Len.	4.42	8.84											0.15	0.41
Hole-2(End of span)	Loc. Beg.							15.54	24.29	8.53	13.33	7.16	15.46	0.00	0.00
	Loc. Avg.							15.62	24.40	9.91	15.48	8.76	18.91	2.36	6.40
	Loc. End							15.70	24.52	11.28	17.62	10.36	22.37	4.72	12.81
	Loc. Len.							0.15	0.24	2.74	4.29	3.20	6.91	4.72	12.81

Table 7-b: Summary of suggested hole locations based on Approach V

BRIDGE	Location	Span-1		Span-2		Span-3		Span-4		Span-5		Span-6		Span-7	
BRIDGE- 539		L=39.624m		L=49.6824m		L=55.9308m		L=49.6824m		L=39.624m					
		meters	%	meters	%	meters	%	meters	%	meters	%				
Hole-1(Beg. of span)	Loc. Beg.	0.00	0.00	9.91	19.94	10.97	19.62								
	Loc. Avg.	1.98	5.00	10.74	21.63	11.28	20.16								
	Loc. End	3.96	10.00	11.58	23.31	11.58	20.71								
	Loc. Len.	3.96	10.00	1.68	3.37	0.61	1.09								
Hole-2(End of span)	Loc. Beg.					10.97	19.62	9.91	19.94	0.00	0.00				
	Loc. Avg.					11.28	20.16	10.74	21.63	1.98	5.00				
	Loc. End					11.58	20.71	11.58	23.31	3.96	10.00				
	Loc. Len.					0.61	1.09	1.68	3.37	3.96	10.00				
BRIDGE- 540		L=29.8704m		L=37.338m		L=54.2544m		L=54.2544m		L=53.6448m		L=23.7744m			
		meters	%	meters	%	meters	%	meters	%	meters	%	meters	%		
Hole-1(Beg. of span)	Loc. Beg.	0.00	0.00	4.42	11.84							14.17	59.62		
	Loc. Avg.	2.59	8.67	6.32	16.94							15.24	64.10		
	Loc. End	5.18	17.35	8.23	22.04							16.31	68.59		
	Loc. Len.	5.18	17.35	3.81	10.20							2.13	8.97		
Hole-2(End of span)	Loc. Beg.	4.42	14.80			9.30	17.13			8.23	15.34	0.00	0.00		
	Loc. Avg.	4.95	16.58			9.75	17.98			9.60	17.90	2.21	9.29		
	Loc. End	5.49	18.37			10.21	18.82			10.97	20.45	4.42	18.59		
	Loc. Len.	1.07	3.57			0.91	1.69			2.74	5.11	4.42	18.59		
BRIDGE- 541a		L=38.2524m		L=47.3964m		L=56.5404m		L=63.0936m		L=51.6636m					
		meters	%	meters	%	meters	%	meters	%	meters	%				
Hole-1(Beg. of span)	Loc. Beg.	0.00	0.00	8.08	17.04	9.11	16.12	12.04	19.08	14.02	27.14				
	Loc. Avg.	2.51	6.57	9.68	20.42	10.04	17.76	12.80	20.29	14.17	27.43				
	Loc. End	5.03	13.15	11.28	23.79	10.97	19.41	13.56	21.50	14.33	27.73				
	Loc. Len.	5.03	13.15	3.20	6.75	1.86	3.29	1.52	2.42	0.30	0.59				
Hole-2(End of span)	Loc. Beg.	9.30	24.30					12.80	20.29	0.00	0.00				
	Loc. Avg.	9.75	25.50					13.87	21.98	2.51	4.87				
	Loc. End	10.21	26.69					14.94	23.67	5.03	9.73				
	Loc. Len.	0.91	2.39					2.13	3.38	5.03	9.73				
BRIDGE- 541b		L=48.3108m		L=61.2648m		L=58.3692m		L=44.3484m		L=32.1564m					
		meters	%	meters	%	meters	%	meters	%	meters	%				
Hole-1(Beg. of span)	Loc. Beg.	0.00	0.00	12.50	20.40										
	Loc. Avg.	2.21	4.57	13.18	21.52										
	Loc. End	4.42	9.15	13.87	22.64										
	Loc. Len.	4.42	9.15	1.37	2.24										
Hole-2(End of span)	Loc. Beg.			13.56	22.14	8.23	14.10	5.18	11.68	0.00	0.00				
	Loc. Avg.			13.87	22.64	9.60	16.45	7.01	15.81	13.49	41.94				
	Loc. End			14.17	23.13	10.97	18.80	8.84	19.93	26.97	83.89				
	Loc. Len.			0.61	1.00	2.74	4.70	3.66	8.25	26.97	83.89				
BRIDGE- 542a		L=43.8912m		L=54.5592m		L=54.5592m		L=62.1792m		L=53.7972m		L=50.4444m			
		meters	%	meters	%	meters	%	meters	%	meters	%	meters	%		
Hole-1(Beg. of span)	Loc. Beg.	0.00	0.00	10.97	20.11	11.89	21.79	12.80	20.59			9.75	19.34		
	Loc. Avg.	2.29	5.21	11.89	21.79	12.27	22.49	13.03	20.96			10.44	20.69		
	Loc. End	4.57	10.42	12.80	23.46	12.65	23.18	13.26	21.32			11.13	22.05		
	Loc. Len.	4.57	10.42	1.83	3.35	0.76	1.40	0.46	0.74			1.37	2.72		
Hole-2(End of span)	Loc. Beg.			11.58	21.23			11.58	18.63	13.56	25.21	0.00	0.00		
	Loc. Avg.			11.66	21.37			11.96	19.24	14.33	26.63	2.59	5.14		
	Loc. End			11.73	21.51			12.34	19.85	15.09	28.05	5.18	10.27		
	Loc. Len.			0.15	0.28			0.76	1.23	1.52	2.83	5.18	10.27		
BRIDGE- 542b		L=47.244m		L=47.244m		L=47.244m		L=59.1312m		L=43.8912m		L=34.7472m			
		meters	%	meters	%	meters	%	meters	%	meters	%	meters	%		
Hole-1(Beg. of span)	Loc. Beg.	0.00	0.00	12.65	26.77	8.08	17.10	10.06	17.01	15.24	34.72	6.86	19.74		
	Loc. Avg.	2.21	4.68	13.18	27.90	8.69	18.39	10.90	18.43	15.39	35.07	7.39	21.27		
	Loc. End	4.42	9.35	13.72	29.03	9.30	19.68	11.73	19.85	15.54	35.42	7.92	22.81		
	Loc. Len.	4.42	9.35	1.07	2.26	1.22	2.58	1.68	2.84	0.30	0.69	1.07	3.07		
Hole-2(End of span)	Loc. Beg.	9.45	20.00	7.92	16.77			8.53	14.43	5.94	13.54	0.00	0.00		
	Loc. Avg.	10.21	21.61	8.46	17.90			9.75	16.49	7.79	17.74	2.51	7.24		
	Loc. End	10.97	23.23	8.99	19.03			10.97	18.56	9.63	21.94	5.03	14.47		
	Loc. Len.	1.52	3.23	1.07	2.26			2.44	4.12	3.69	8.40	5.03	14.47		

APPENDIX A

CALCULATION OF WARPING CONSTANT

In this appendix a summary of the derivation for the calculation of the warping constant, $I_{\omega\omega}$, is given. The details can be found in the literature (Nakai and Yoo – 1988, Guohao – 1987)

For a closed section as the one shown in Fig. 59, the applied torque, T, causes shear stress, τ. In the case of thin walled sections, it can be assumed that τ is uniformly distributed across the thickness of the wall, t. The relationship between T and τ can be determined by integrating the resultant shear flow, $q = \tau \,.\, t$, along the perimeter of the cell as follows:

$$T = \oint \rho_S \cdot q \cdot ds$$

Knowing that the shear flow is constant along the perimeter of the cell, the previous equation reduces to

$$T = 2 \cdot q \cdot A_c$$

since

$$A_c = \frac{1}{2} \oint \rho_S \cdot ds$$

where A_c is the area enclosed by the cell.

A relationship can be established between the location of the shear center and the centroid of the cross-section as follows:

$$\rho_S = \rho_O - x_S \sin\beta + y_S \cos\beta$$

where ρ_S and ρ_O are the perpendicular distances from any point on the perimeter to the shear center and the centroid, respectively. The distance between the shear center and the centroid horizontally is x_s and vertically is y_s. β is the angle between ρ_S and the horizontal axis.

Due to warping normal stresses and strains develop in the cross-section. The normal strain can be determined by studying the shear strain γ_{zs} where

$$\gamma_{zs} = \frac{\partial \eta}{\partial z} + \frac{\partial w}{\partial s}$$

the tangential deformation η is related to the angle of twist θ

$$\eta = \theta \cdot \rho_S$$

Unlike open sections where the shear strain is equal to zero because of the assumption that plane sections remain plane, shear strain in closed cross sections, γ_c, is given as

$$\gamma_C = \frac{\left(\frac{2A_c}{\oint (ds/t)} \right)}{t} \theta'$$

by defining a new variable, , ψ, as

$$\psi = \frac{2A_c}{\oint (ds/t)}$$

the shear strain equation becomes

$$\gamma_{zs} = \frac{\psi}{t}\theta' = \rho_s \frac{\partial \theta}{\partial z} + \frac{\partial w}{\partial s}$$

by rearranging the integration of the previous formula, we get the following expression for the longitudinal (out of plane) displacement w is

$$w = -\theta' \int_0^s \left(\rho_S - \frac{\psi}{t} \right) ds + w_o$$

and by defining a warping function ω as follows

$$w = -\omega\theta'$$

we now have a formula for the ω as

$$\omega = \int_0^s \left(\rho_S - \frac{\psi}{t}\right) ds + \omega_1(0)$$

in which $\omega_1(0)$ is the integration constant. This constant can be found using equilibrium of forces associated with normal stresses. We know that due to warping

$$N = \int_F \sigma \cdot dF = 0$$

$$M_x = \int_F y\sigma \cdot dF = 0$$

$$M_y = \int_F x\sigma \cdot dF = 0$$

where $dF = t\, ds$. The equation for ω can be viewed as consisting of two parts, one is the closed section part of ω and the other is the open section part. This is illustrated in Fig. 60.

The normal stress σ can be determined from the normal strain using Hooke's law

$$\sigma(s,z) = Ew' = -E\omega(s)\theta''$$

which leads to

$$\int_F \omega \cdot dF = 0 \quad : \quad \omega_1(0) = -\frac{1}{F}\int_F \omega_1(s) \cdot dF = 0$$

Since warping calculations require the knowledge of the shear center location, it is important to find this location first. This is achieved by using the relationship between the shear center location and the centroid location in the following manner:

$$\rho_S \cdot ds = \rho_O \cdot ds - x_S ds \sin\beta + y_S ds \cos\beta$$

$$\rho_S \cdot ds = \rho_O \cdot ds - x_S dy + y_S dx$$

by integrating both sides we get

$$\omega = \omega_S = \omega_O - x_S y + y_S x$$

Using equilibrium again (moment equilibrium), we get

$$\int_F y\omega \cdot dF = 0 \quad : \quad x_S = -\frac{I_{y\omega_O}}{I_{yy}}$$

$$\int_F x\omega \cdot dF = 0 \quad : \quad y_S = -\frac{I_{x\omega_O}}{I_{xx}}$$

where $I_{x\omega o}$ and $I_{y\omega o}$ are the section integrals.

$$I_{x\omega_O} = \int_F x \cdot \omega_O \cdot dF \quad \text{and} \quad I_{y\omega_O} = \int_F y \cdot \omega_O \cdot dF$$

I_{xx} and I_{yy} are the moments of inertia of the cross-section.

The moment which develops due to the normal warping stresses is called the bimoment. It is given by the following equation

$$M_\omega = \int_F \omega\sigma \cdot dF = -EI_{\omega\omega}\theta''$$

from which the normal warping stresses can be calculated as

$$\sigma = \frac{M_\omega}{I_{\omega\omega}}\omega$$

These relationships define the warping constant $I_{\omega\omega}$ as

$$I_{\omega\omega} = \int_F \omega \cdot \omega \cdot dF$$

The warping torsional moment is given as

$$T_\omega = -EI_{\omega\omega}\theta'''$$

which leads to the following relationship with the bimoment

$$T_\omega = M'_\omega$$

Shear stress caused by the T_ω is given by the following equation

$$\tau = -\frac{T_\omega}{tI_{\omega\omega}}S_\omega(s)$$

where S_ω is the static moment with respect to warping (sometimes referred to as the sectoral moment). This quantity is analogous to the first moment of area used in shear stress calculations due to shear forces. The value of the sectoral moment was evaluated at different locations in the cross section according to the following equation:

$$S_\omega(s) = F_\omega(s) - \frac{1}{(ds/t)}\oint F_\omega(s)\frac{ds}{t}$$

where

$$F_\omega(s) = \int_0^s \omega(s) \cdot t \cdot ds$$

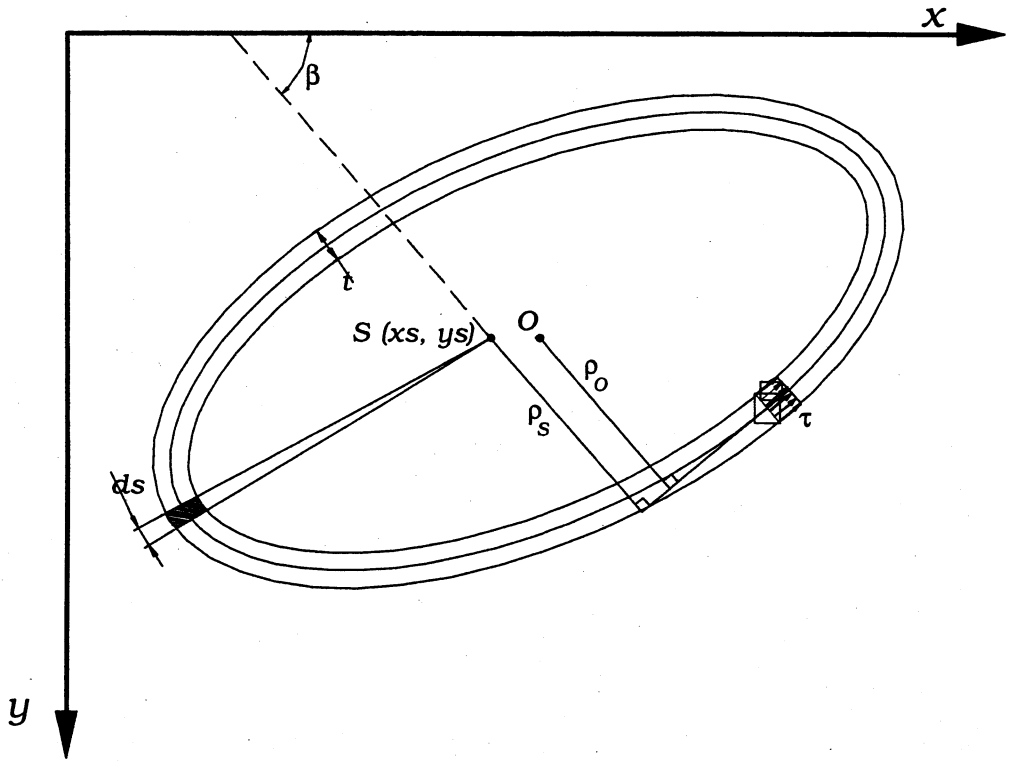

Figure 59: Closed thin-walled cross-section

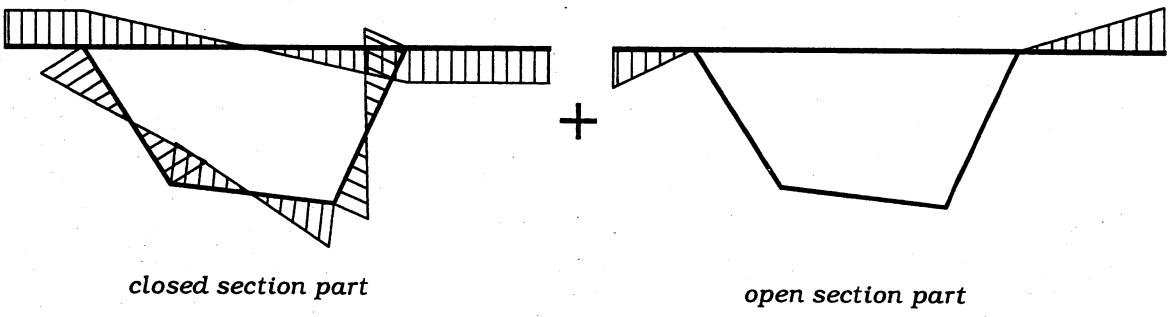

Figure 60: ω diagrams of closed and open section parts

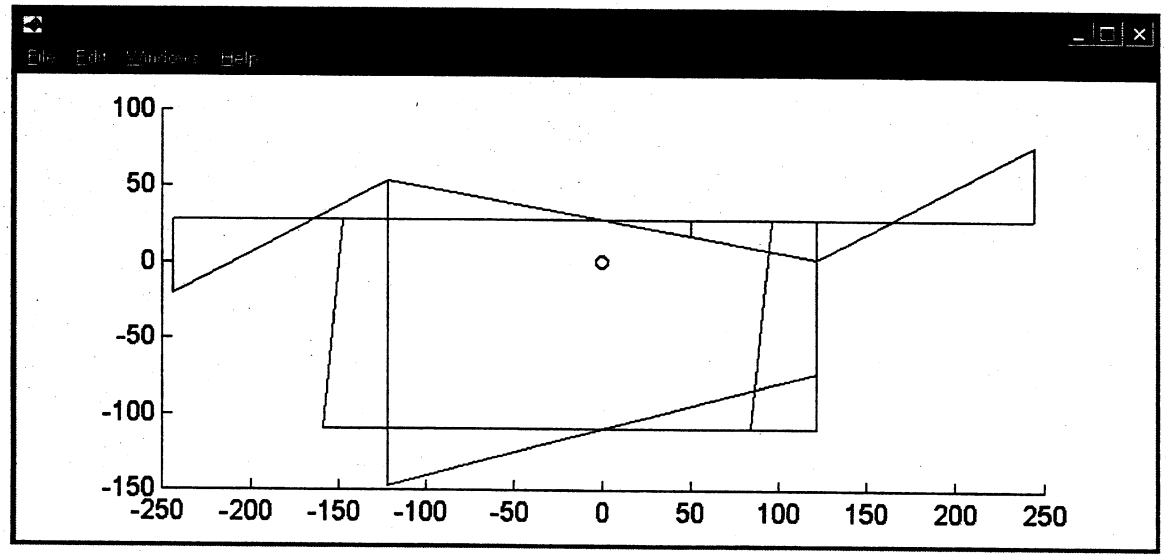

Figure 61: Program plot of warping function (ω)

APPENDIX B

STRAINING ACTIONS FOR STUDIED BRIDGES

The straining actions of the nineteen existing bridges upon which the locations of minimally stressed cross sections were determined are given in this appendix. These straining actions are obtained from the beam element model. Each of the studied bridges has two sets of straining actions diagrams. The first set shows the straining actions due to dead loads acting on a quasi-open steel cross section. The other set is obtained from live load cases, which act on a closed composite cross section. Eight diagrams are provided in each set. These are:

- Shear force in the y-direction (vertical shear), V_y
- Shear force in the x-direction (horizontal shear), V_x
- Bending moment (about the x-axis), M_x
- Bending moment (about the y-axis), M_y
- Bimoment, M_ω
- Total torsional moment (about the longitudinal axis), T_{total}. Also the following two torsional moment components are obtained :
    - Pure torsional moment component, T_s
    - Warping torsional moment component, T_ω

The horizontal axis in these figures represents the longitudinal position on the bridge line. To determine the location from the figures, the ordinate needs to be multiplied by the element length provided in Table 6.

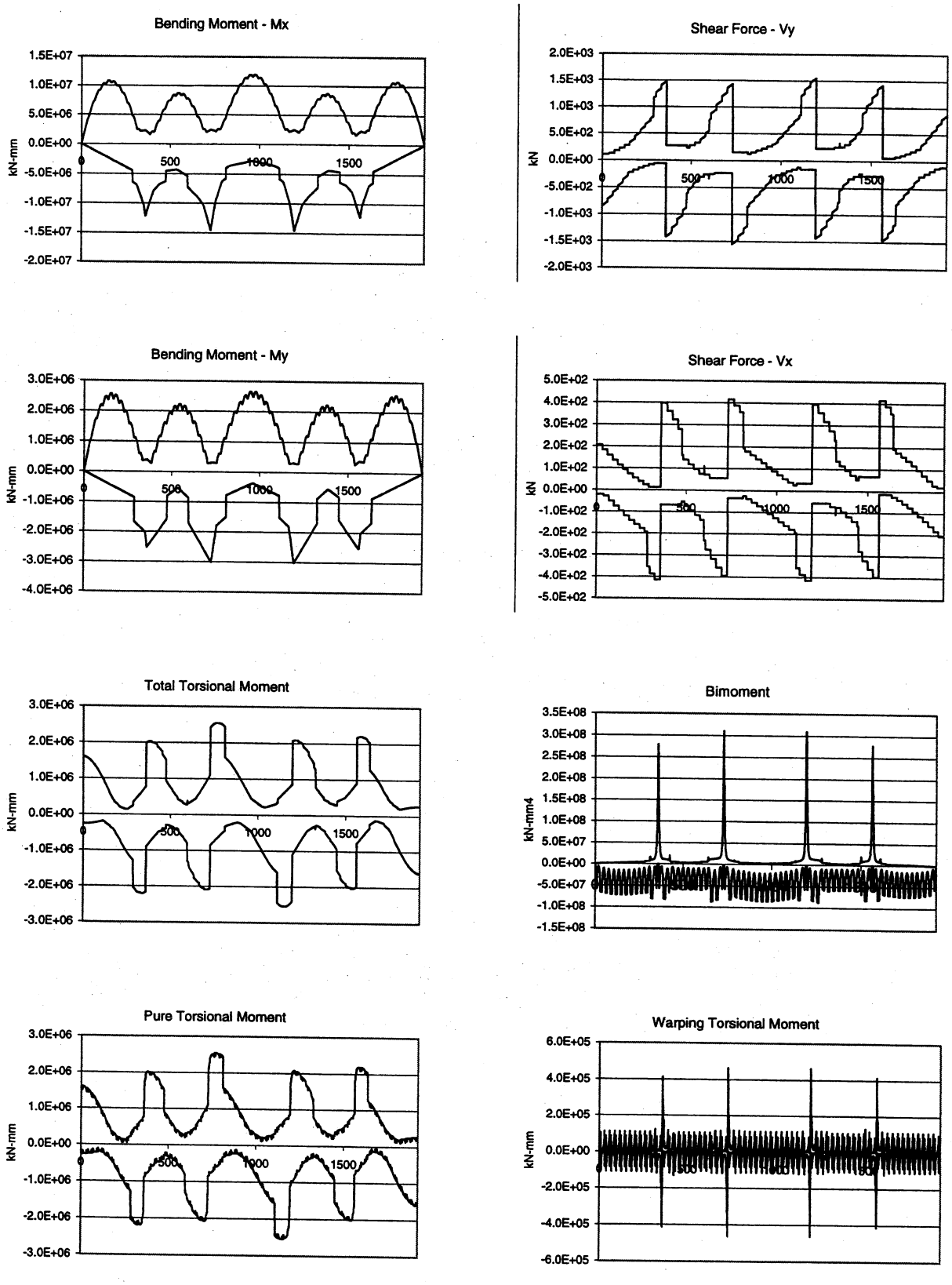

Figure 62: Straining actions for Br. 390 (Live load envelope)

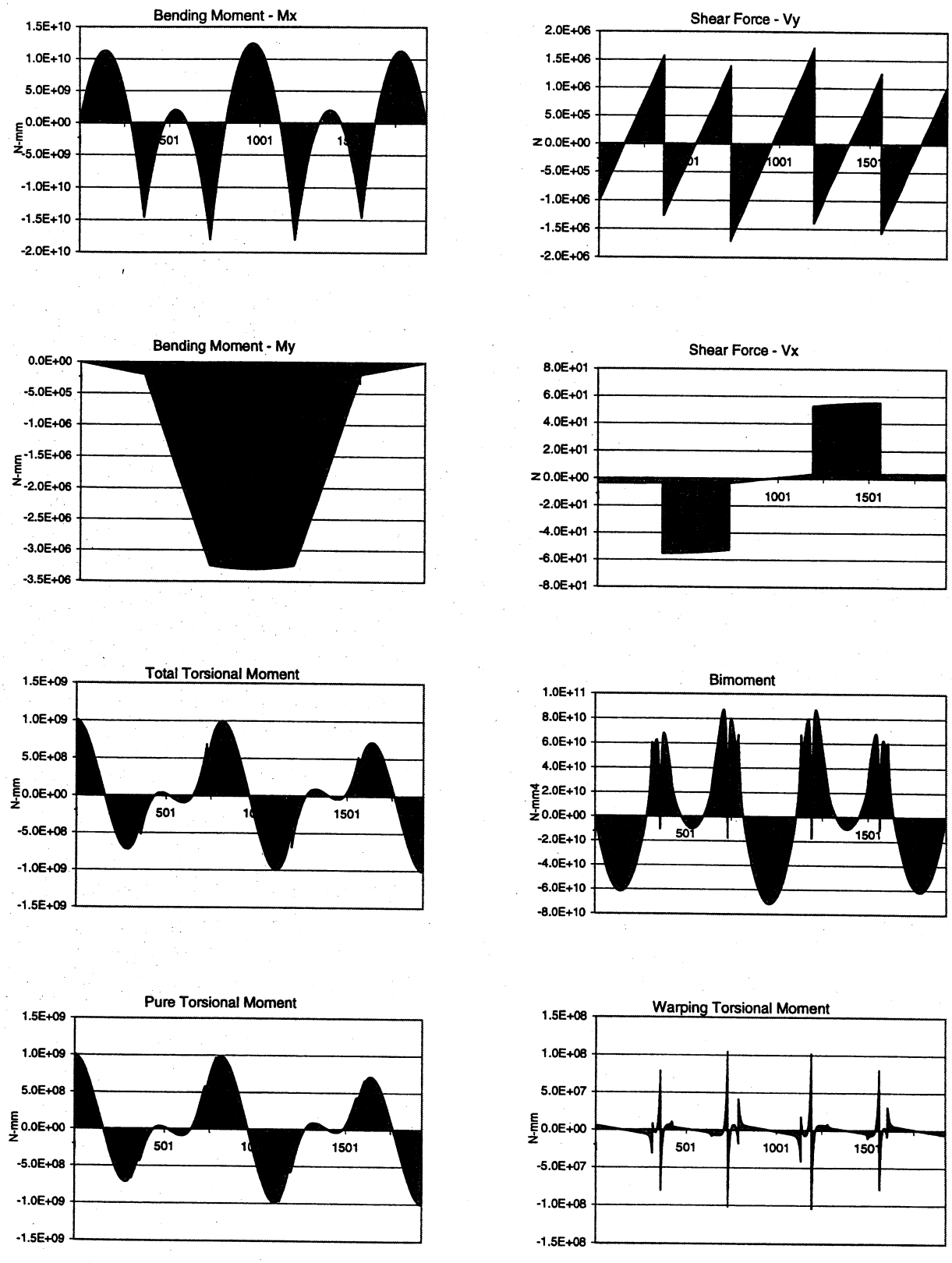

Figure 63: Straining actions for Br. 390 (Dead load)

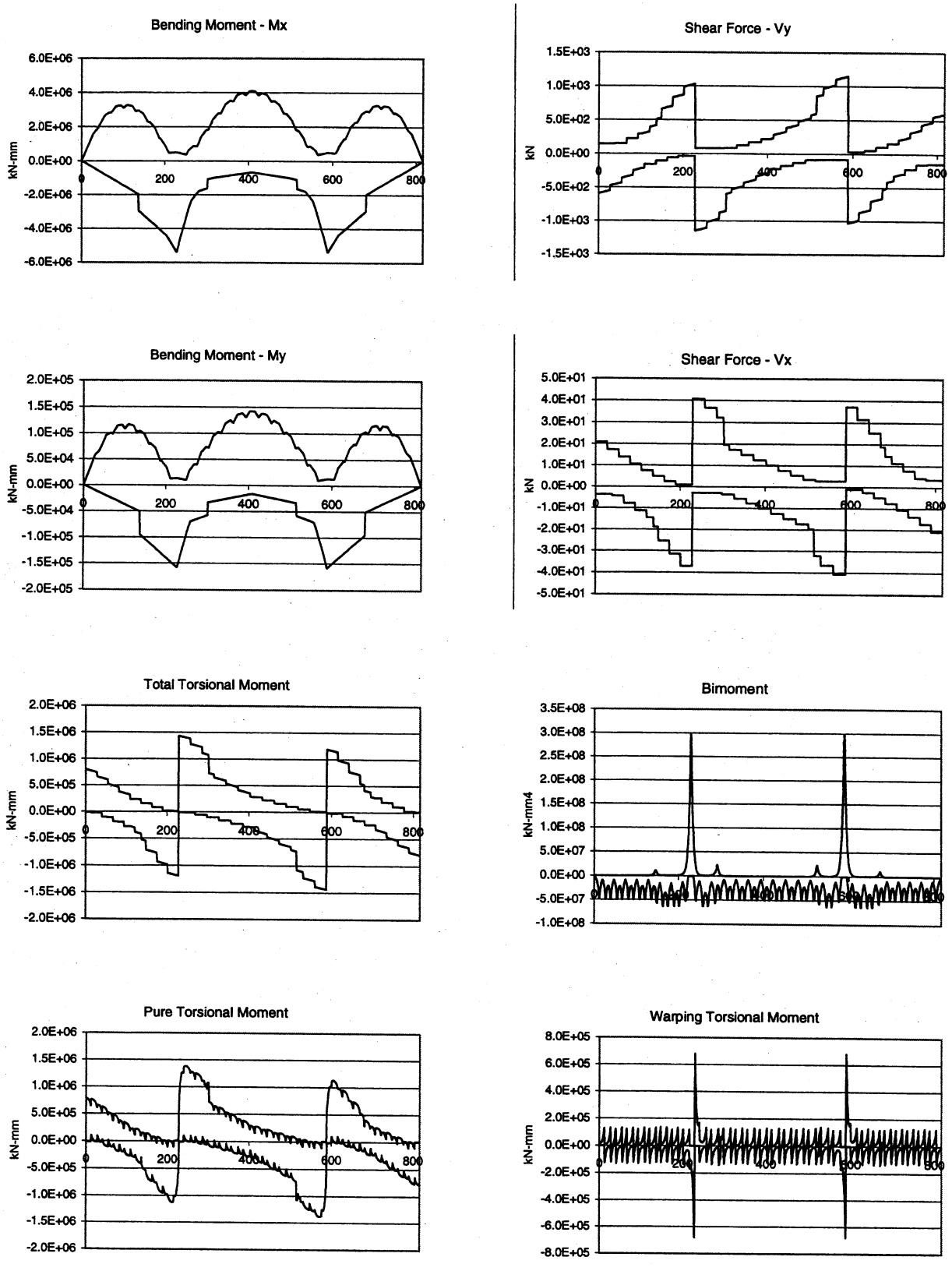

Figure 64: Straining actions for Br. 521 (Live load envelope)

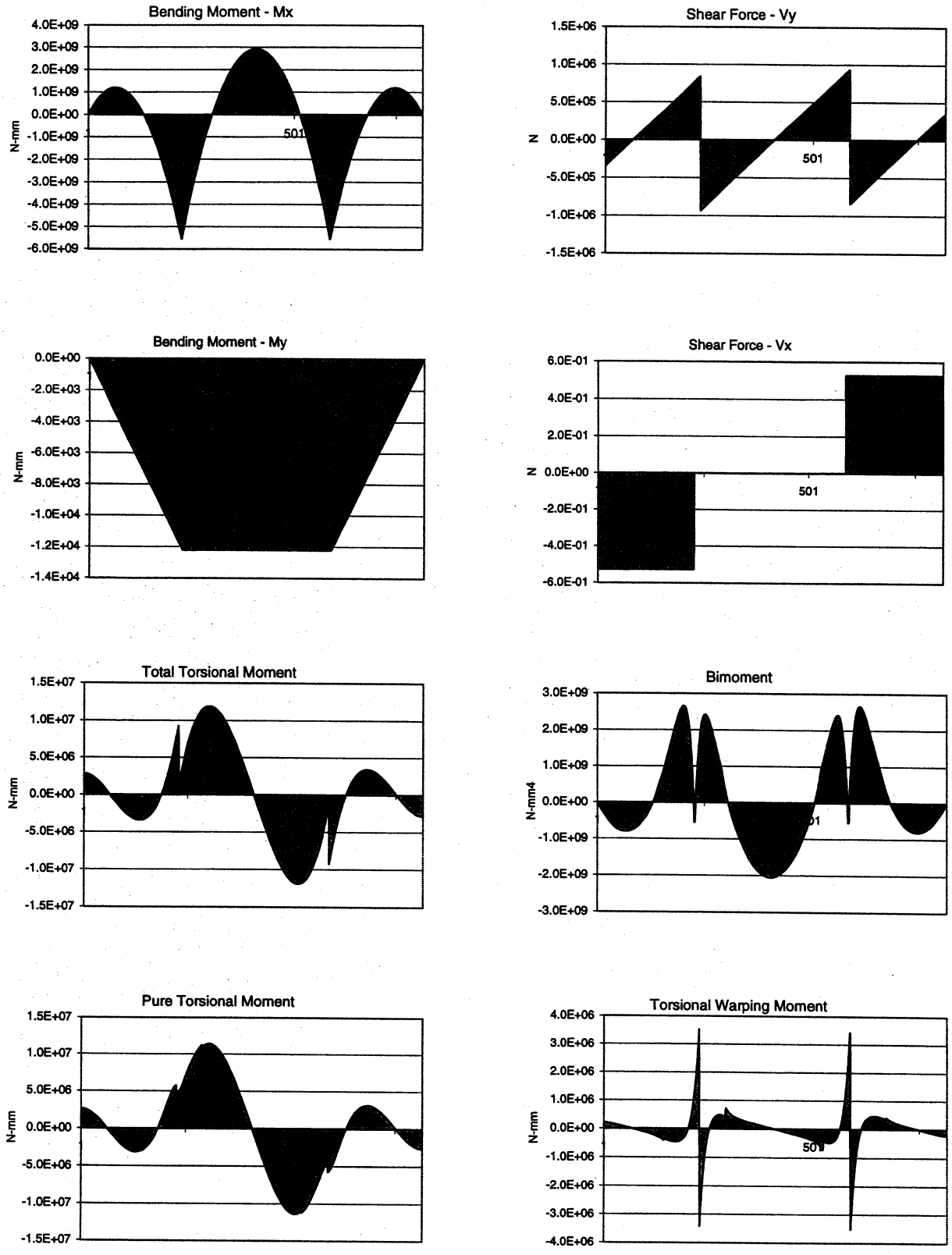

Figure 65: Straining actions for Br. 521 (Dead load)

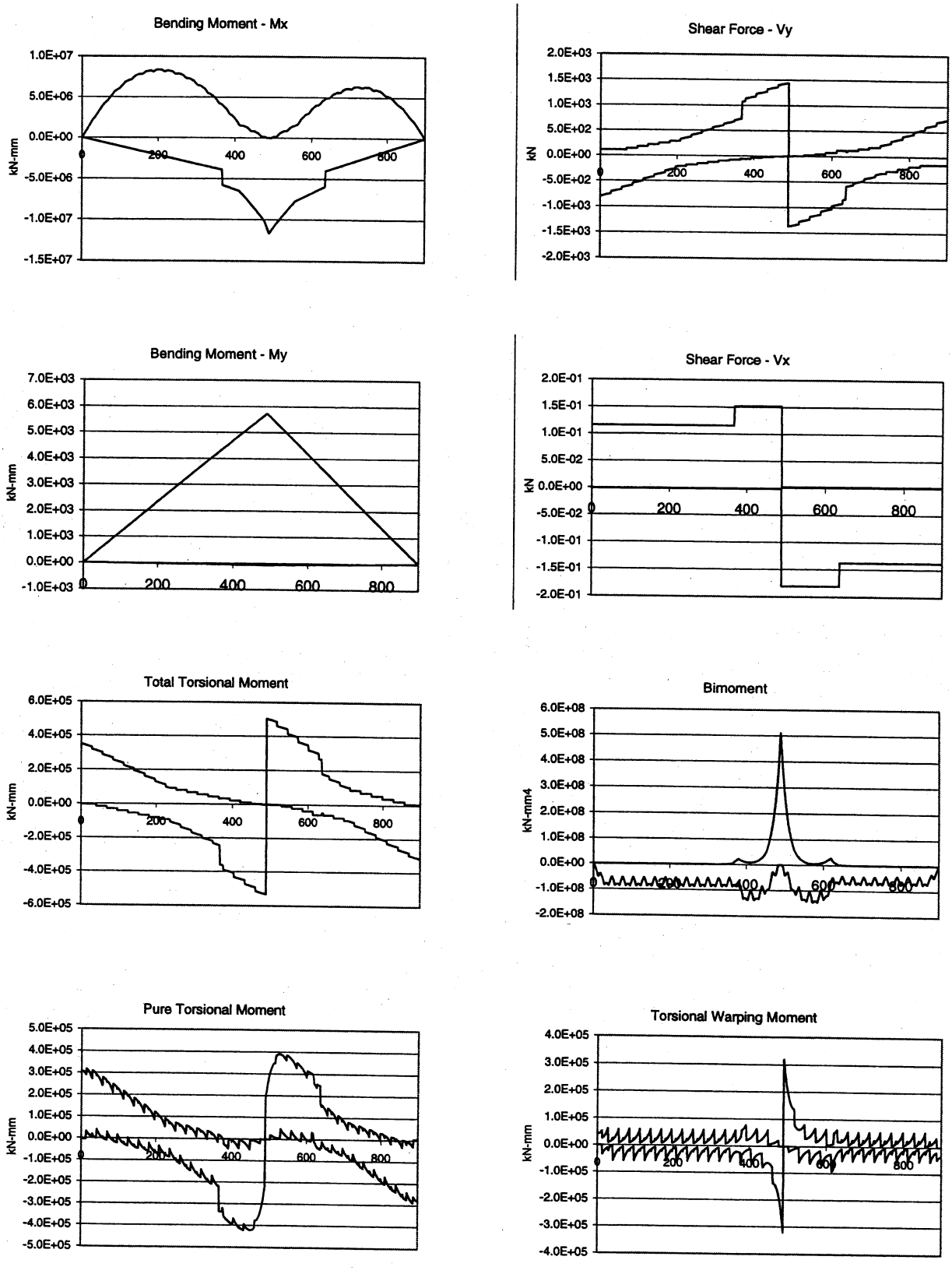

Figure 66: Straining actions for Br. 525 (Live load envelope)

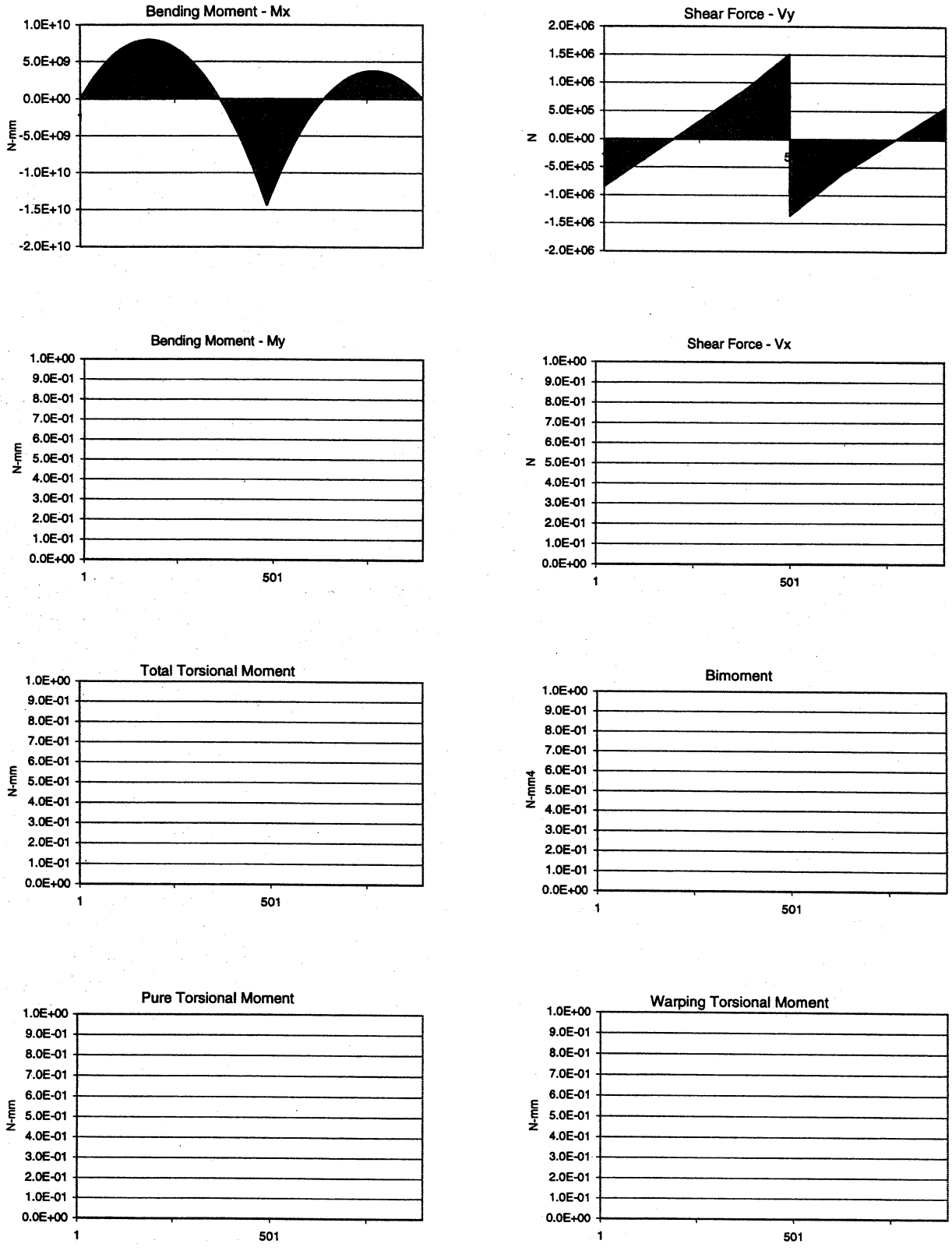

Figure 67: Straining actions for Br. 525 (Dead load)

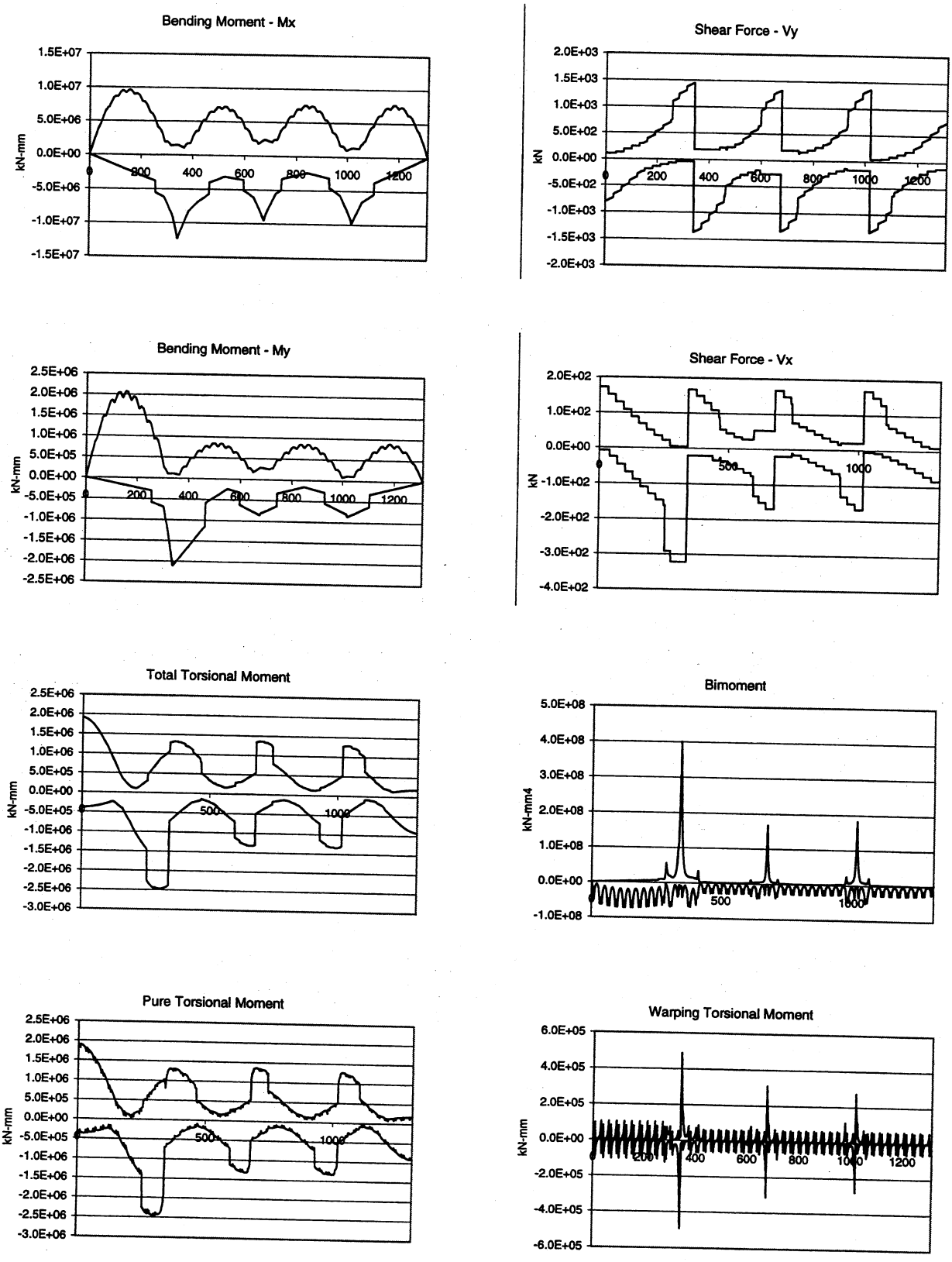

Figure 68: Straining actions for Br. 598 (Live load envelope)

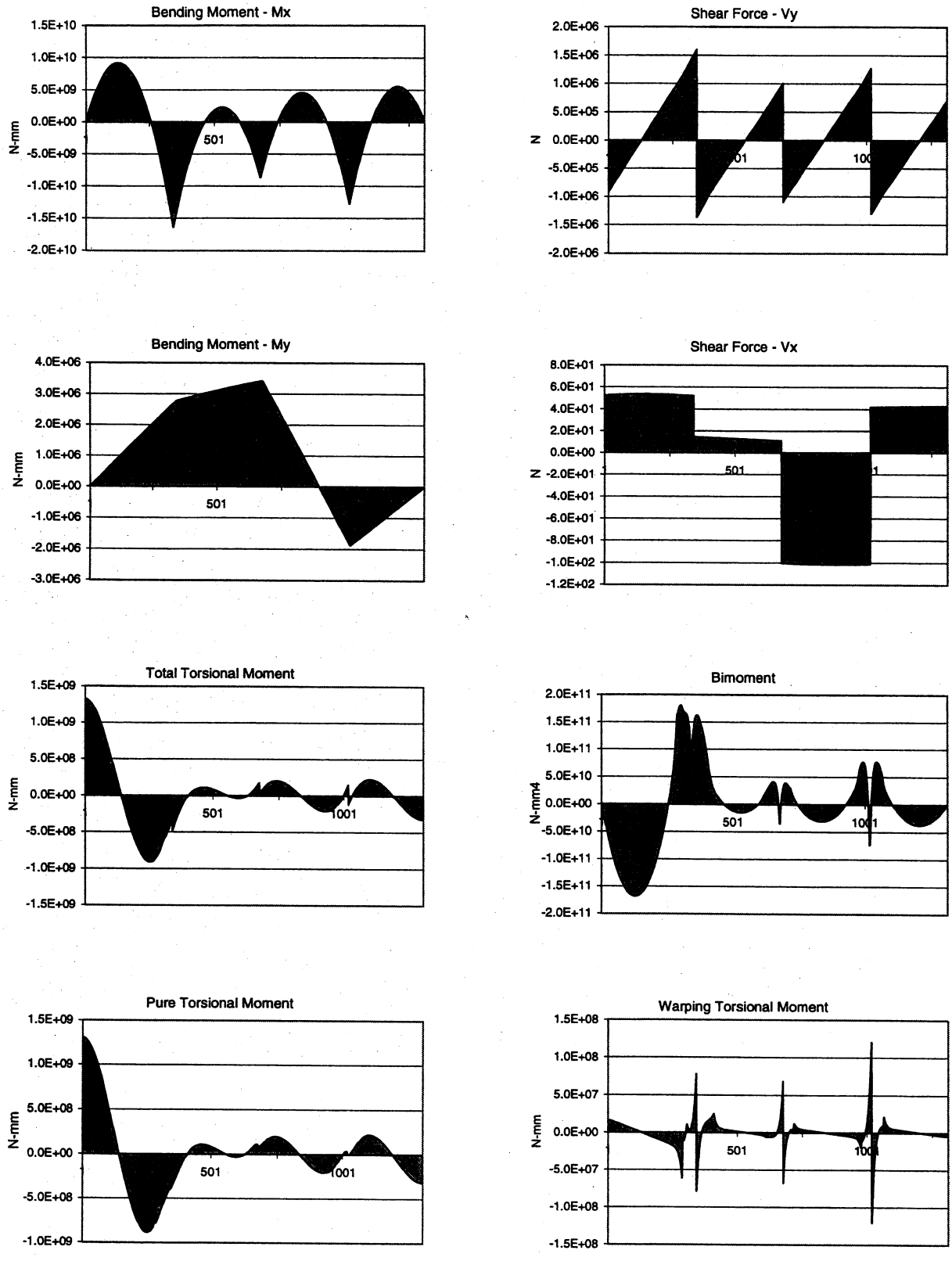

Figure 69: Straining actions for Br. 598 (Dead load)

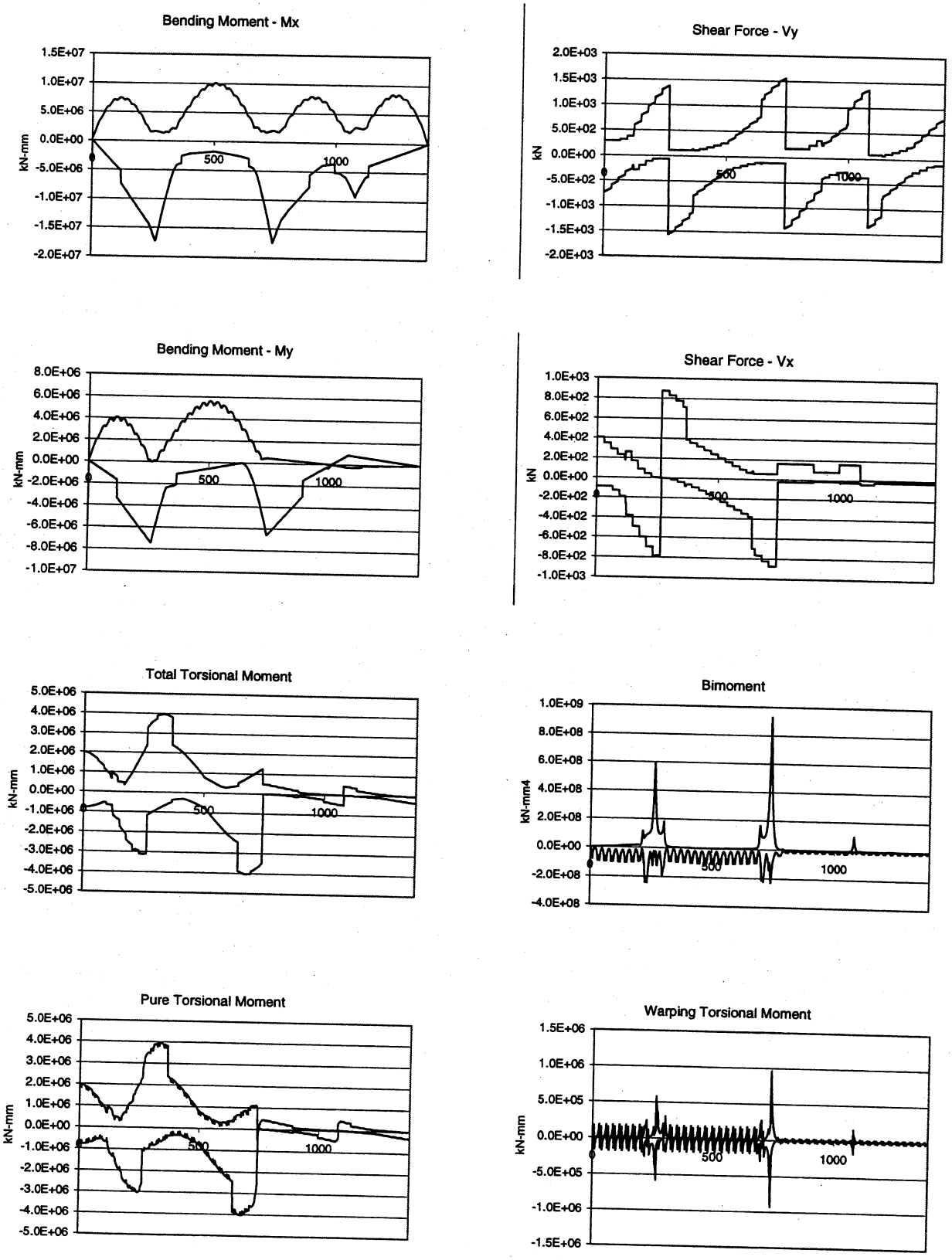

Figure 70: Straining actions for Br. 601 (Live load envelope)

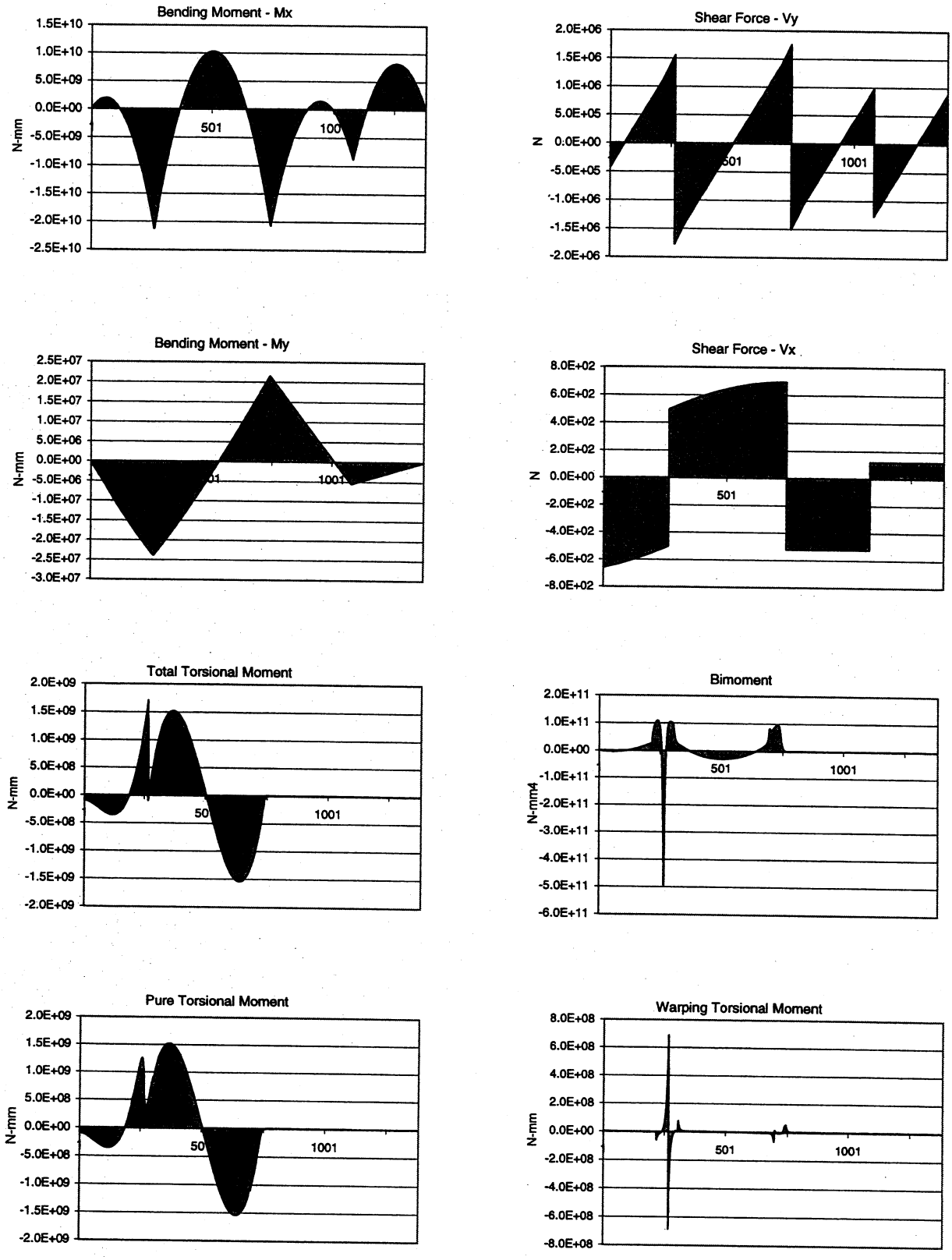

Figure 71: Straining actions for Br. 601 (Dead load)

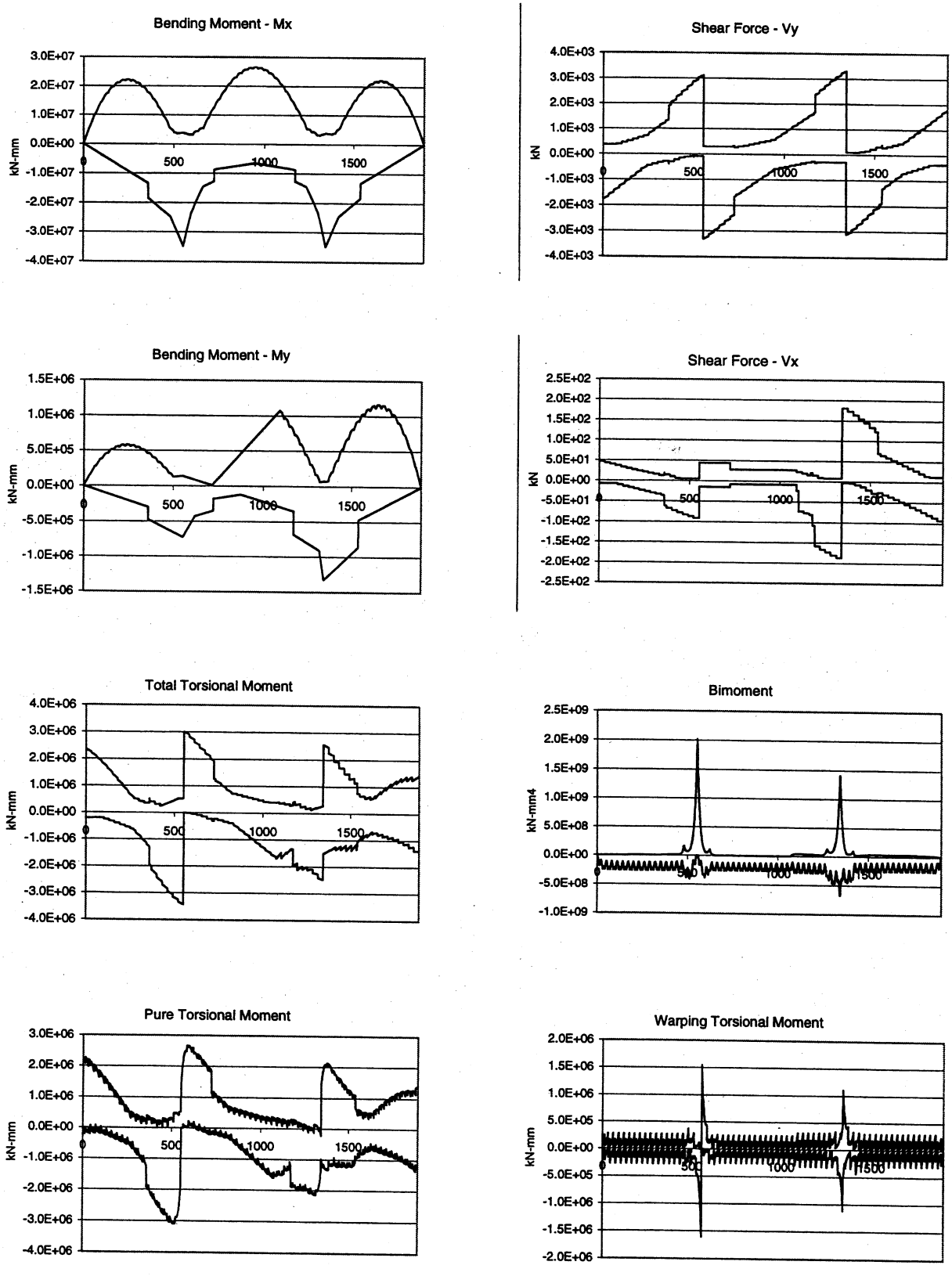

Figure 72: Straining actions for Br. 606 (Live load envelope)

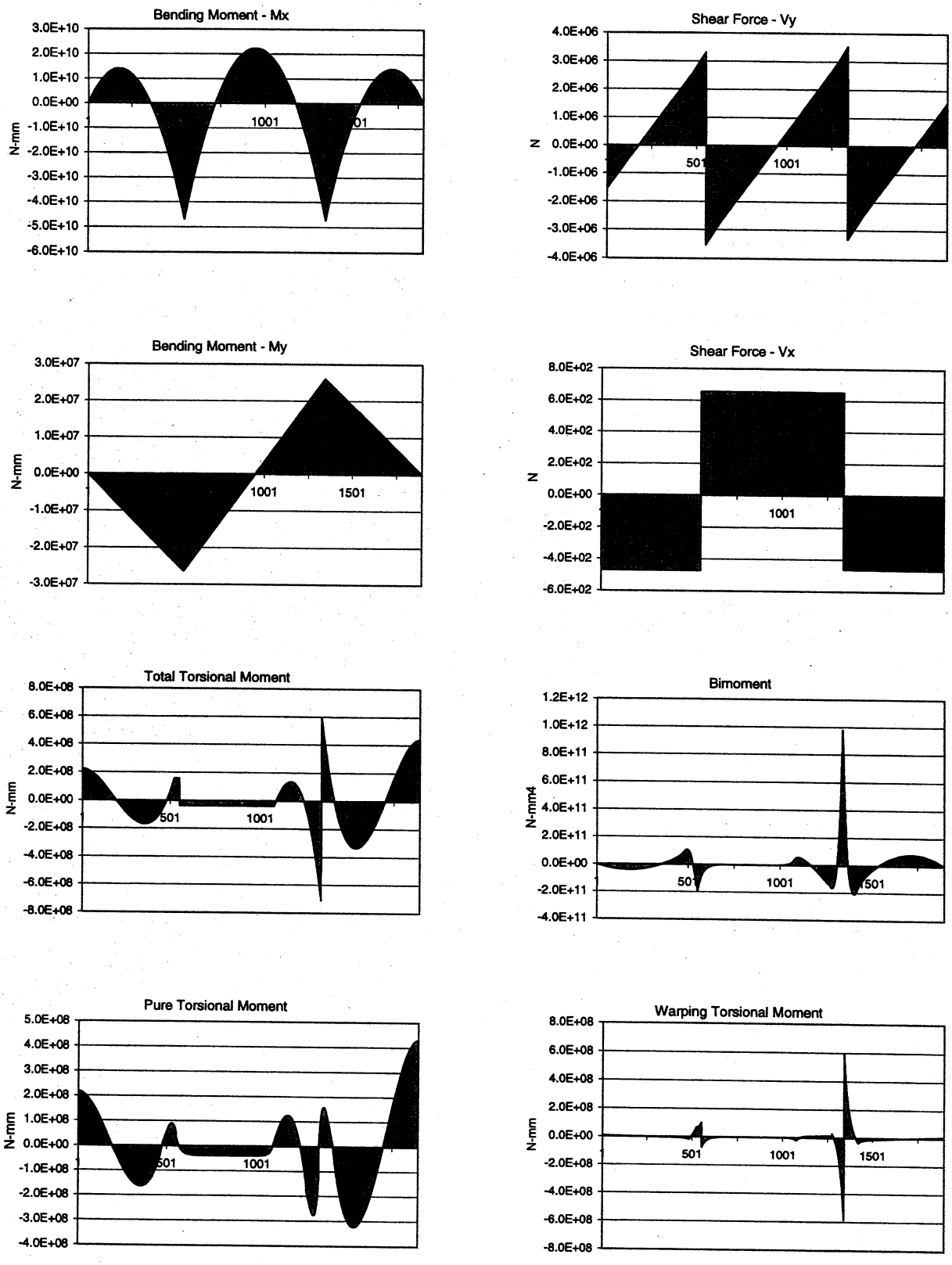

Figure 73: Straining actions for Br. 606 (Dead load)

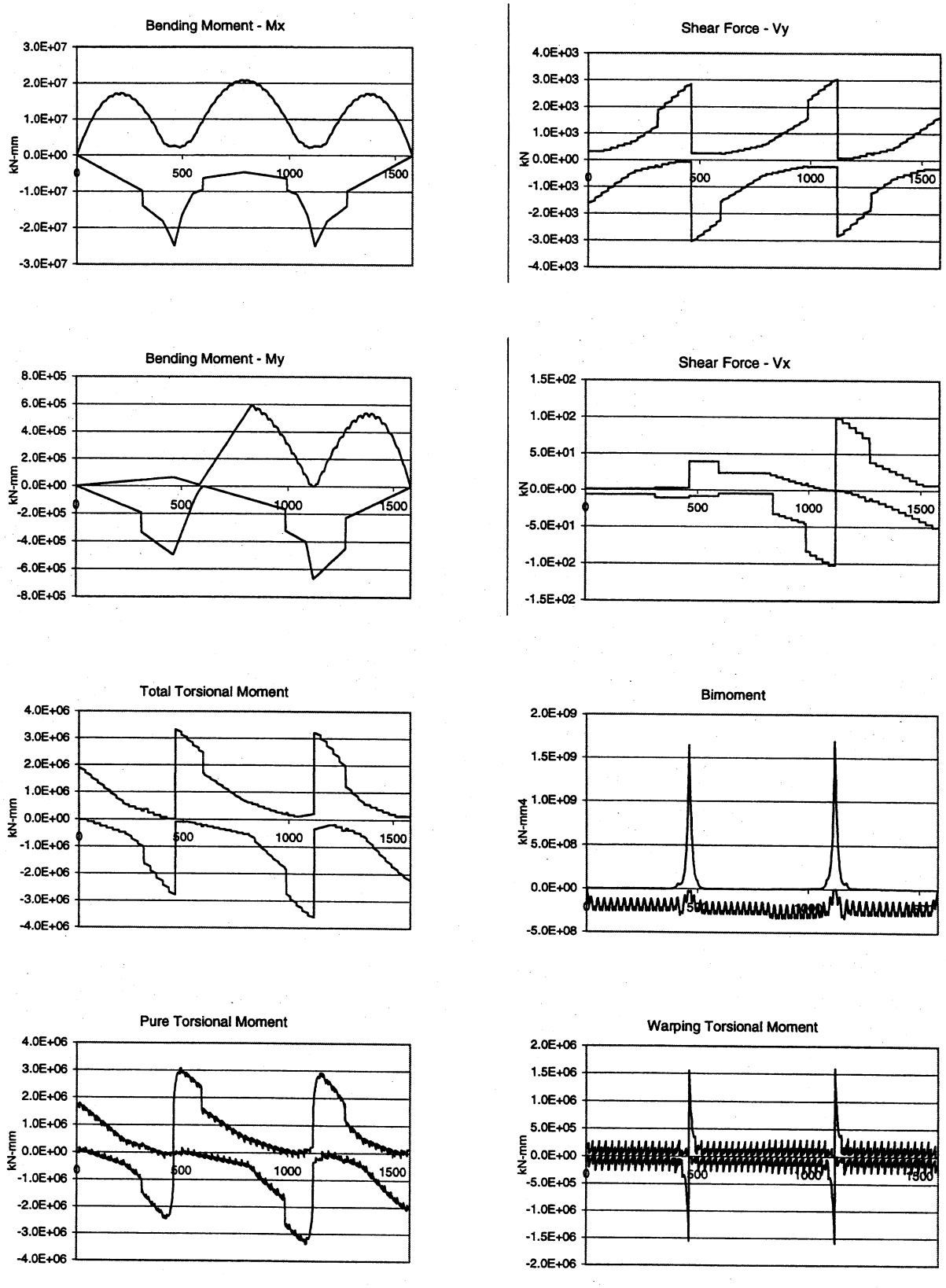

Figure 74: Straining actions for Br. 607 (Live load envelope)

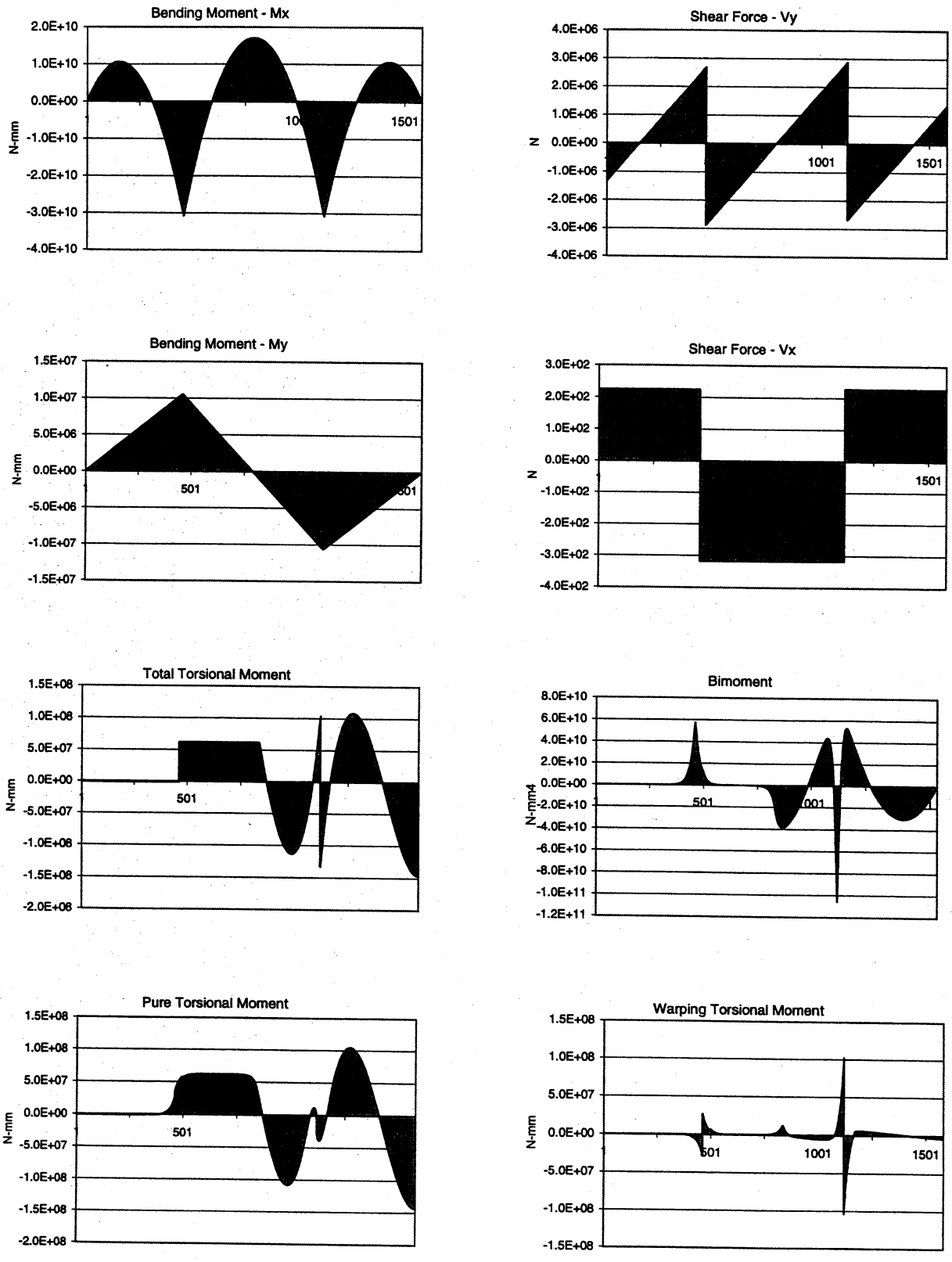

Figure 75: Straining actions for Br. 607 (Dead load)

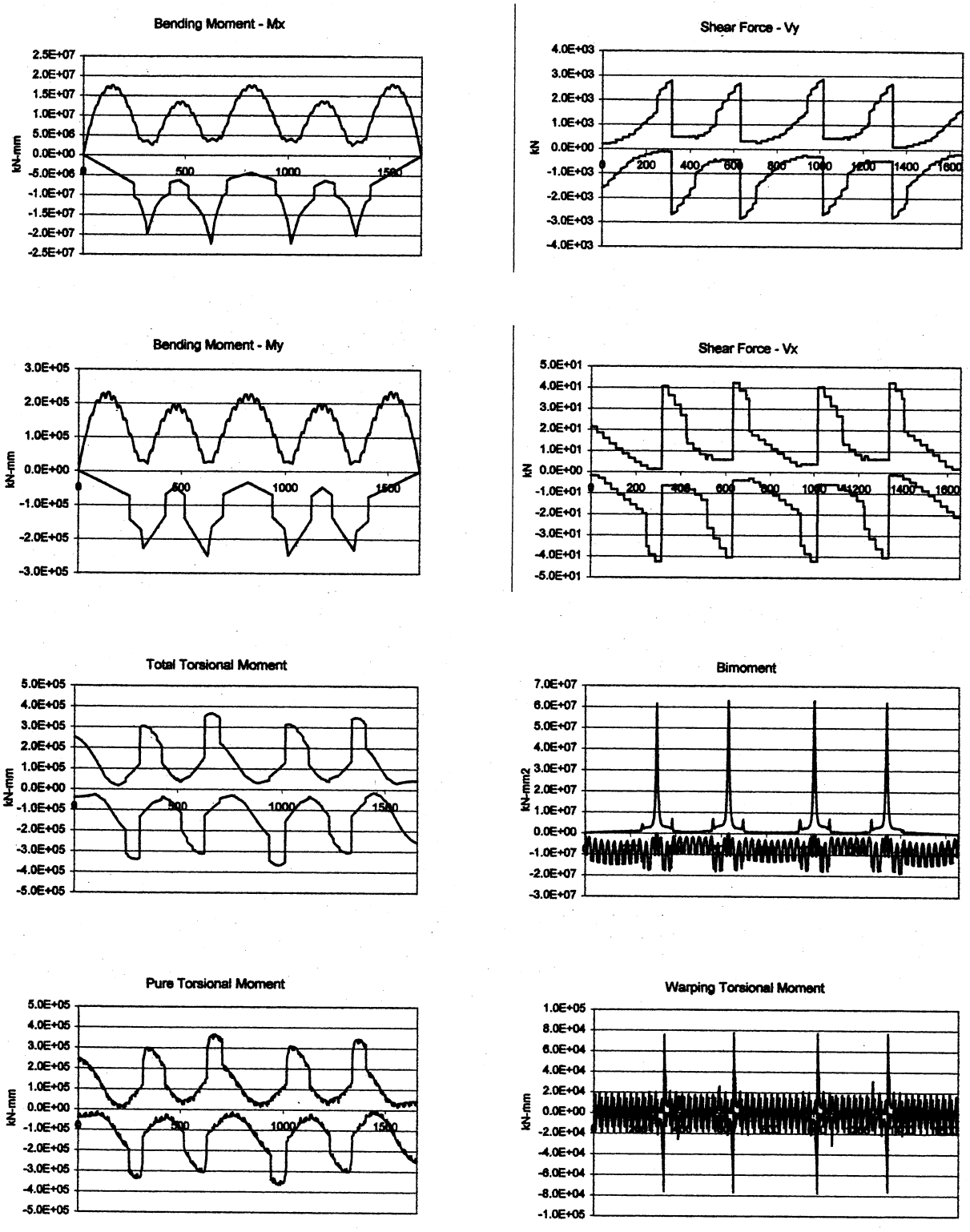

Figure 76: Straining actions for Br.528 (Live load envelope)

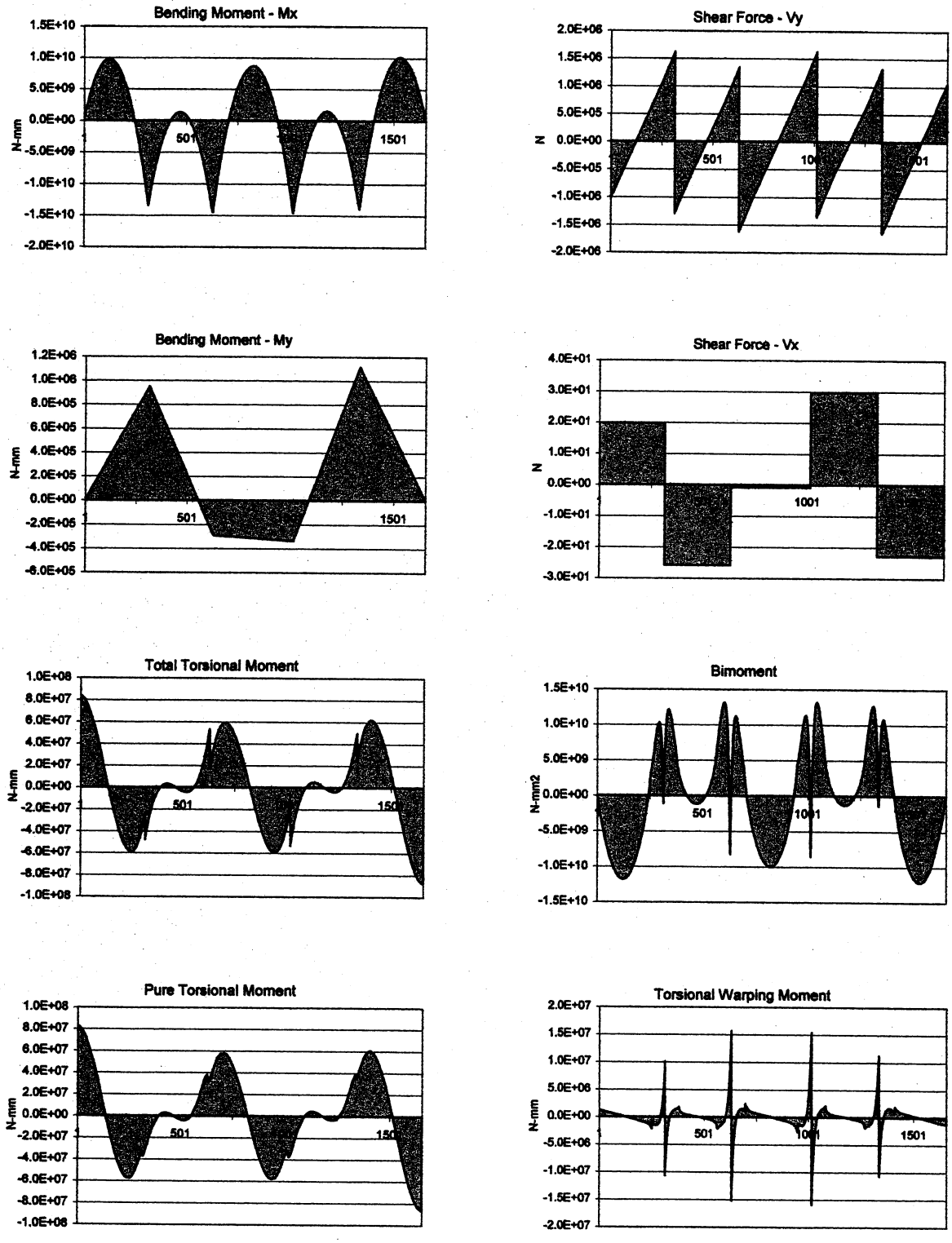

Figure 77: Straining actions for Br.528 (Dead load)

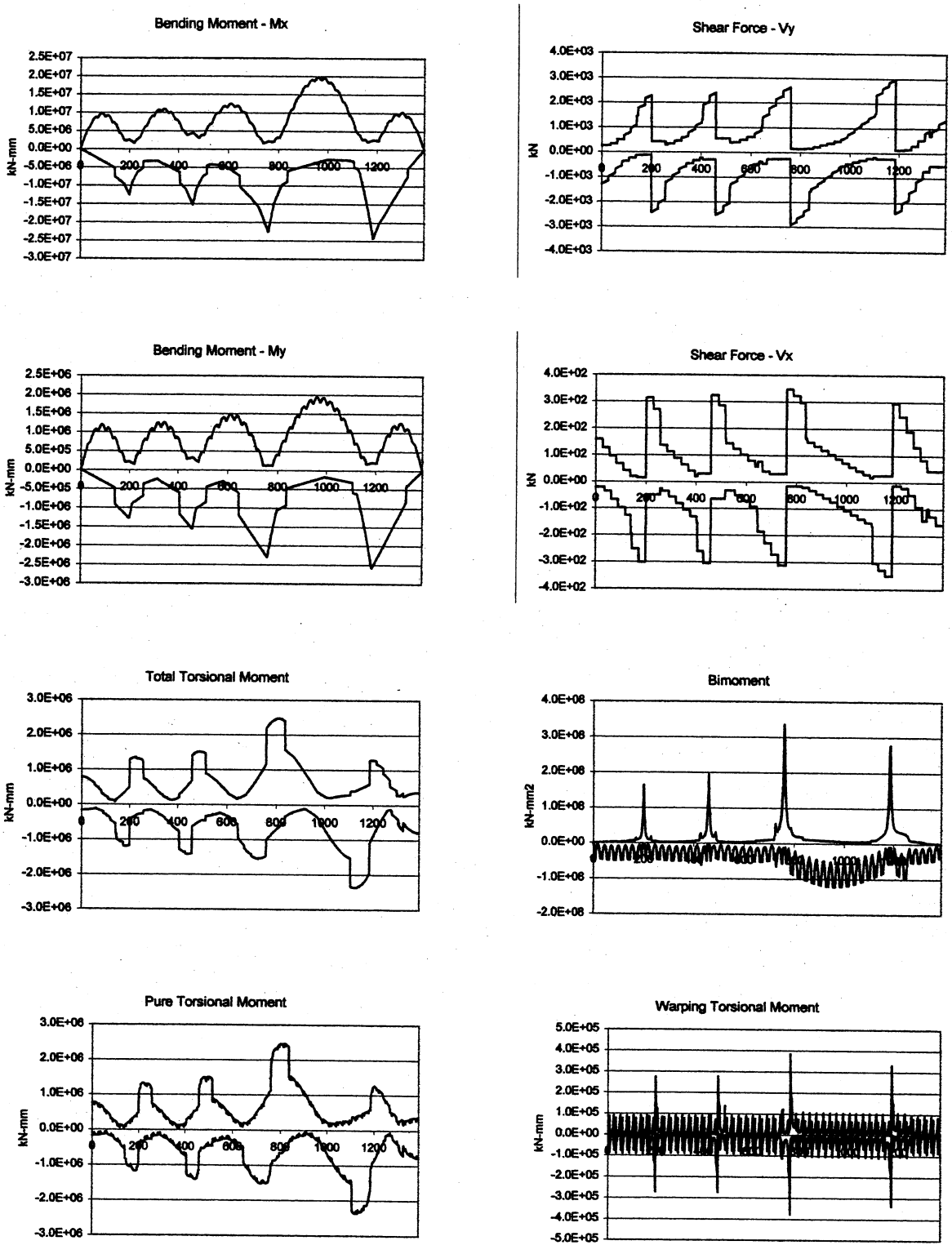

Figure 78: Straining actions for Br.537 (Live load envelope)

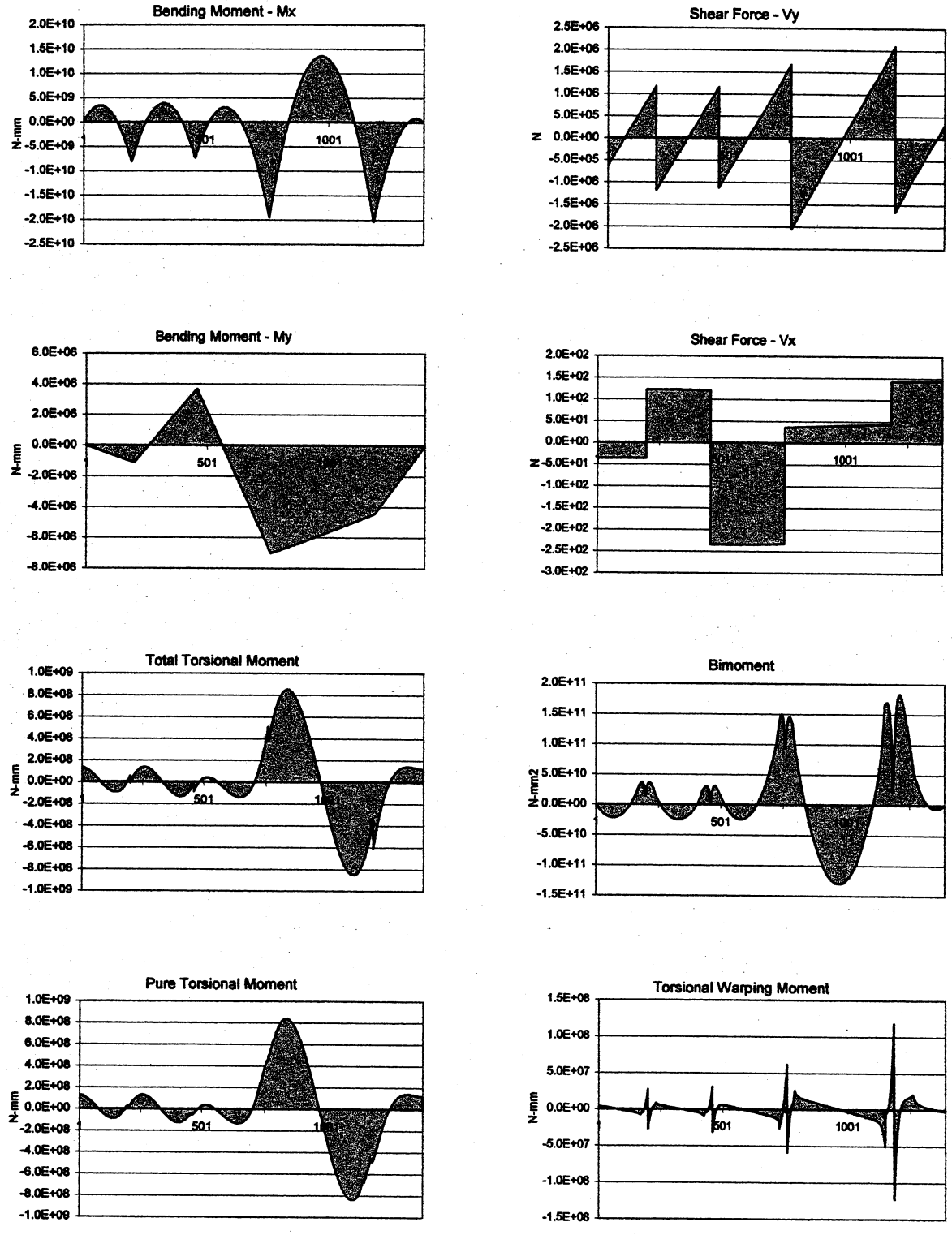

Figure 79: Straining actions for Br.537 (Dead load)

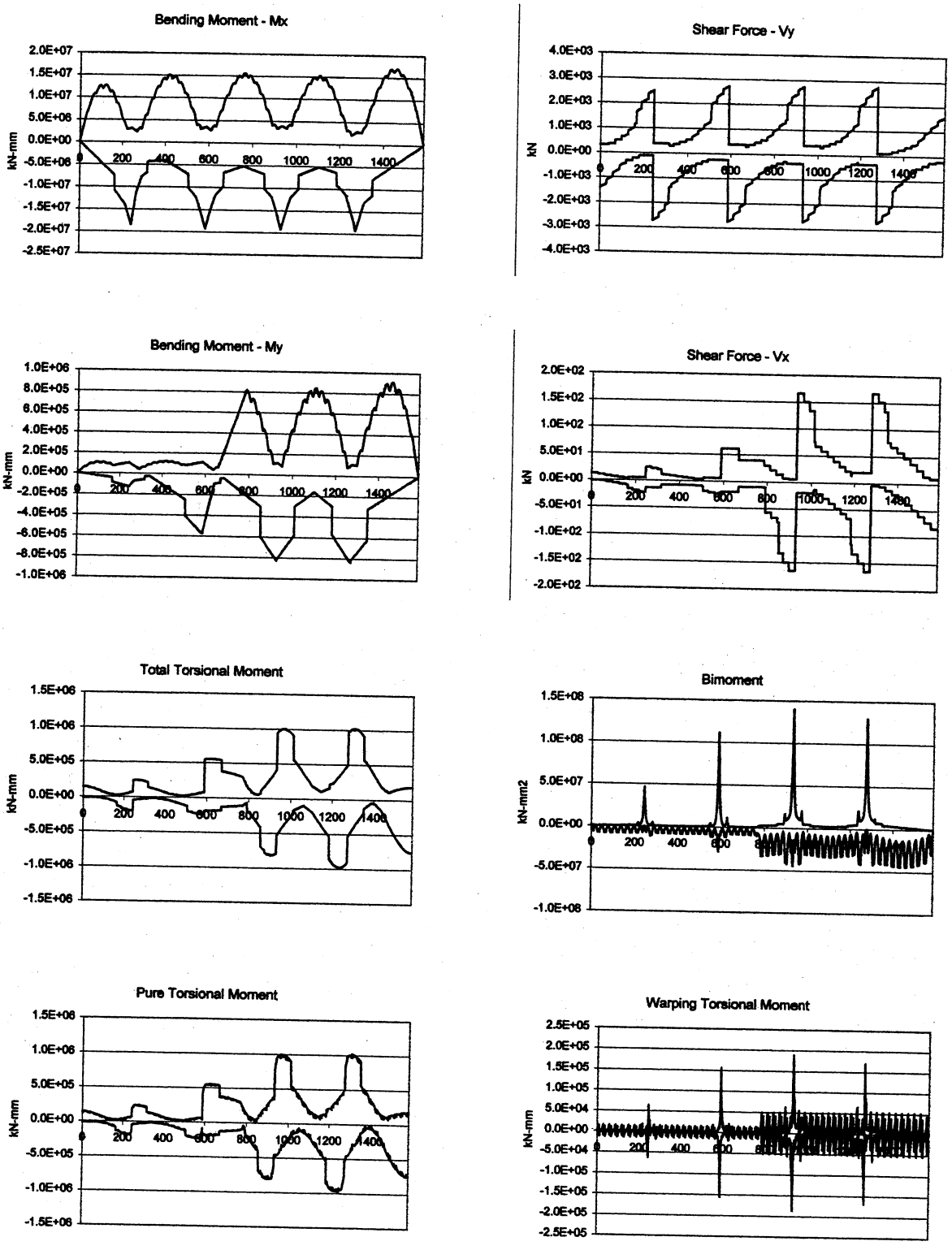

Figure 80: Straining actions for Br.538a (Live load envelope)

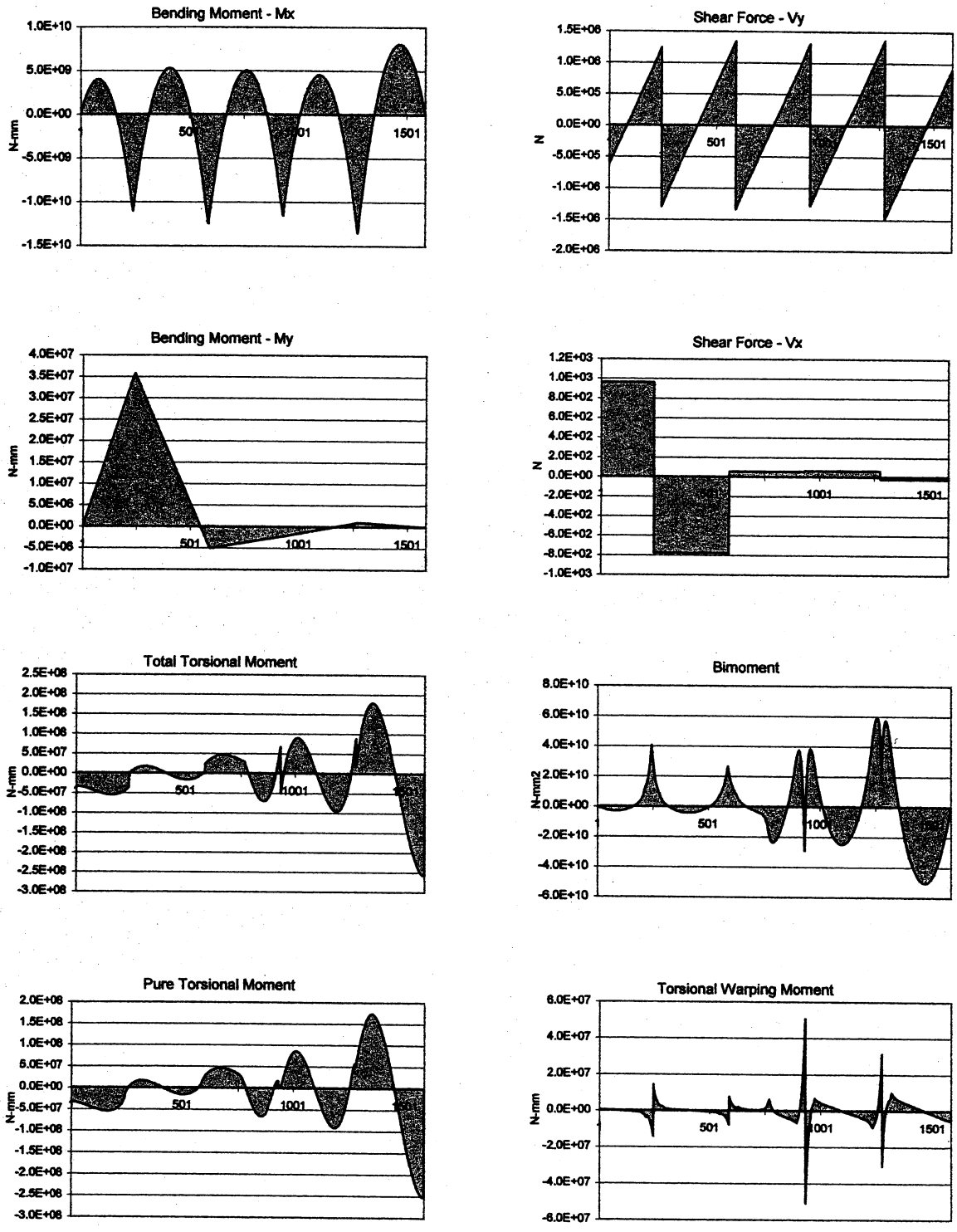

Figure 81: Straining actions for Br.538a (Dead load)

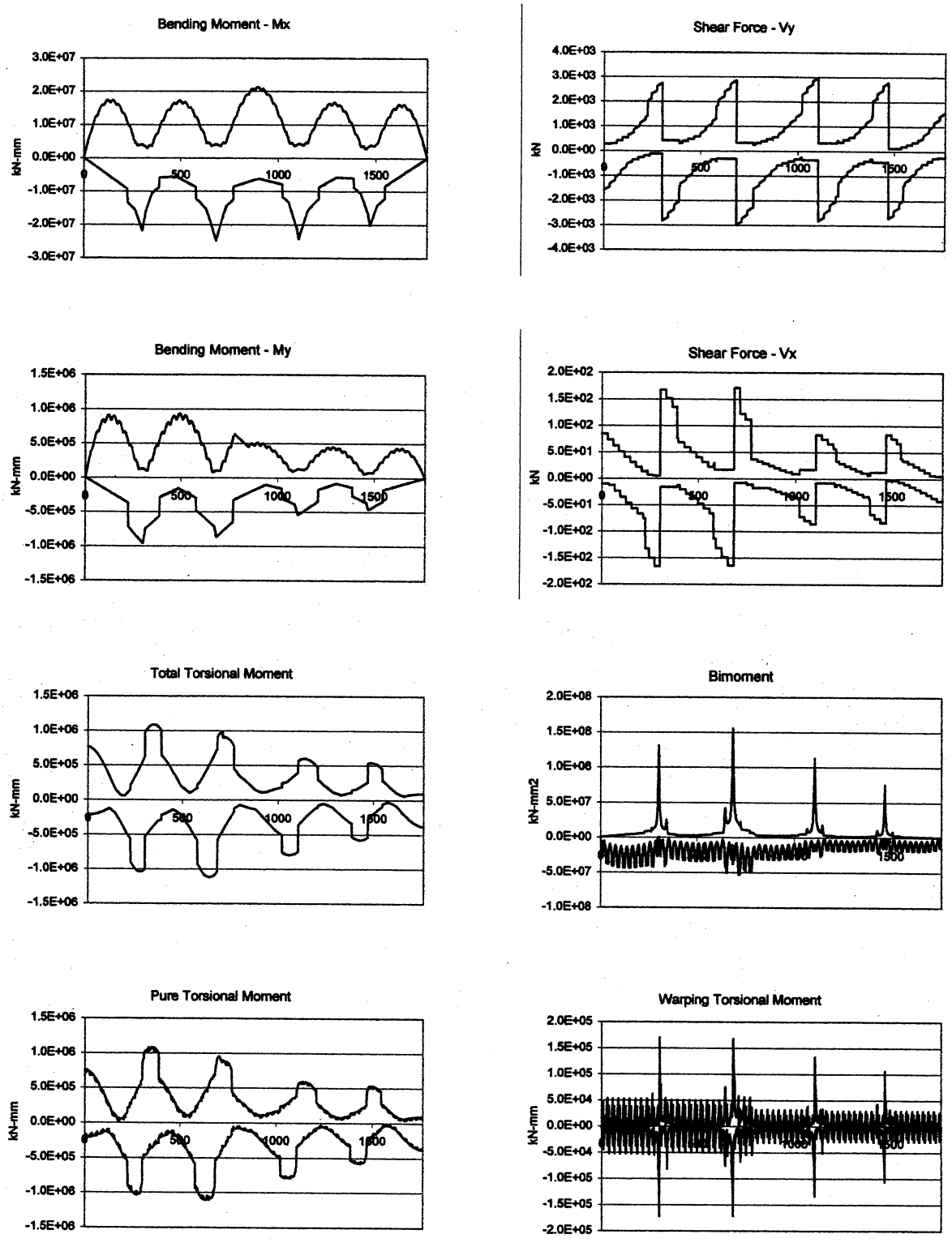

Figure 82: Straining actions for Br.538b (Live load envelope)

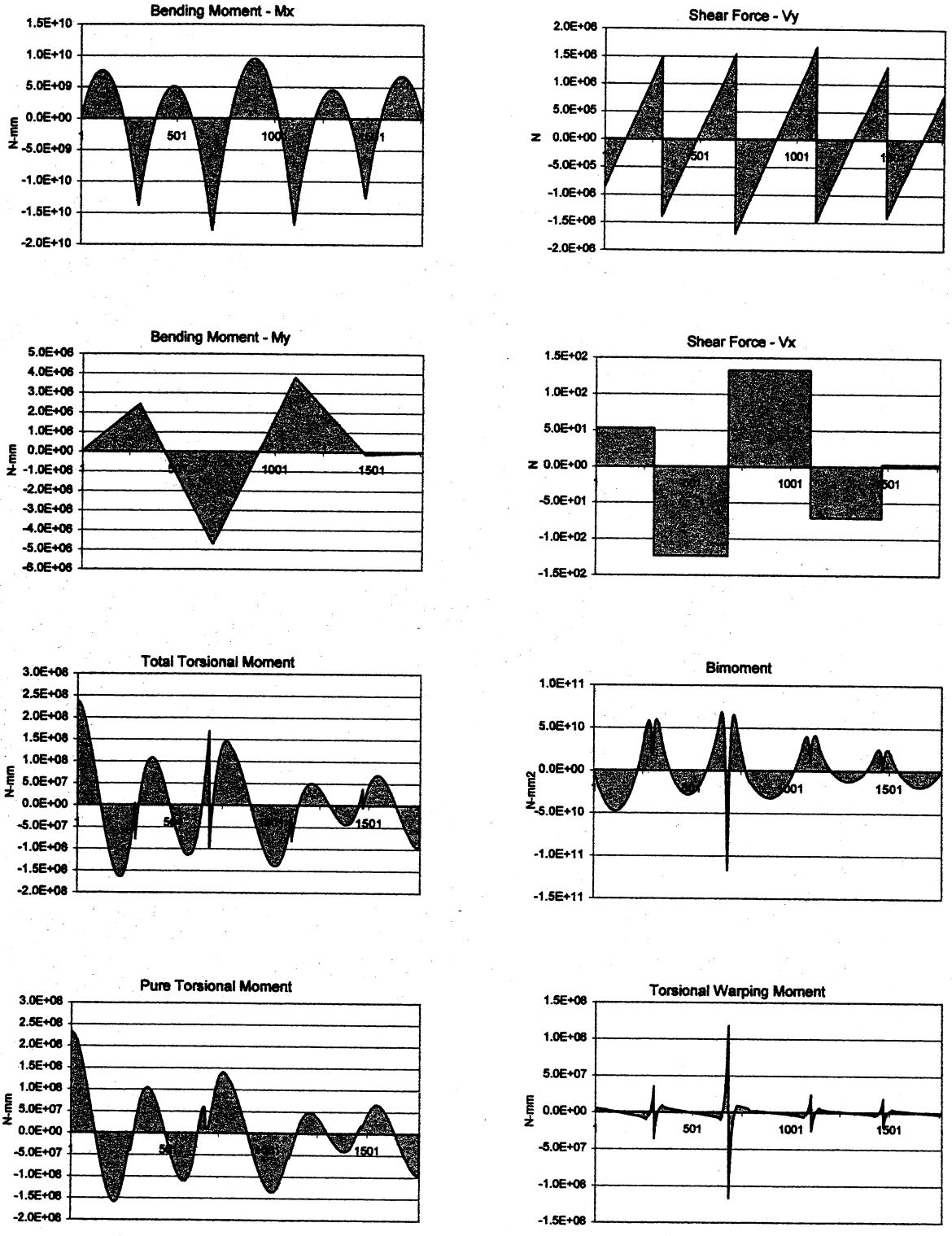

Figure 83: Straining actions for Br.538b (Dead load)

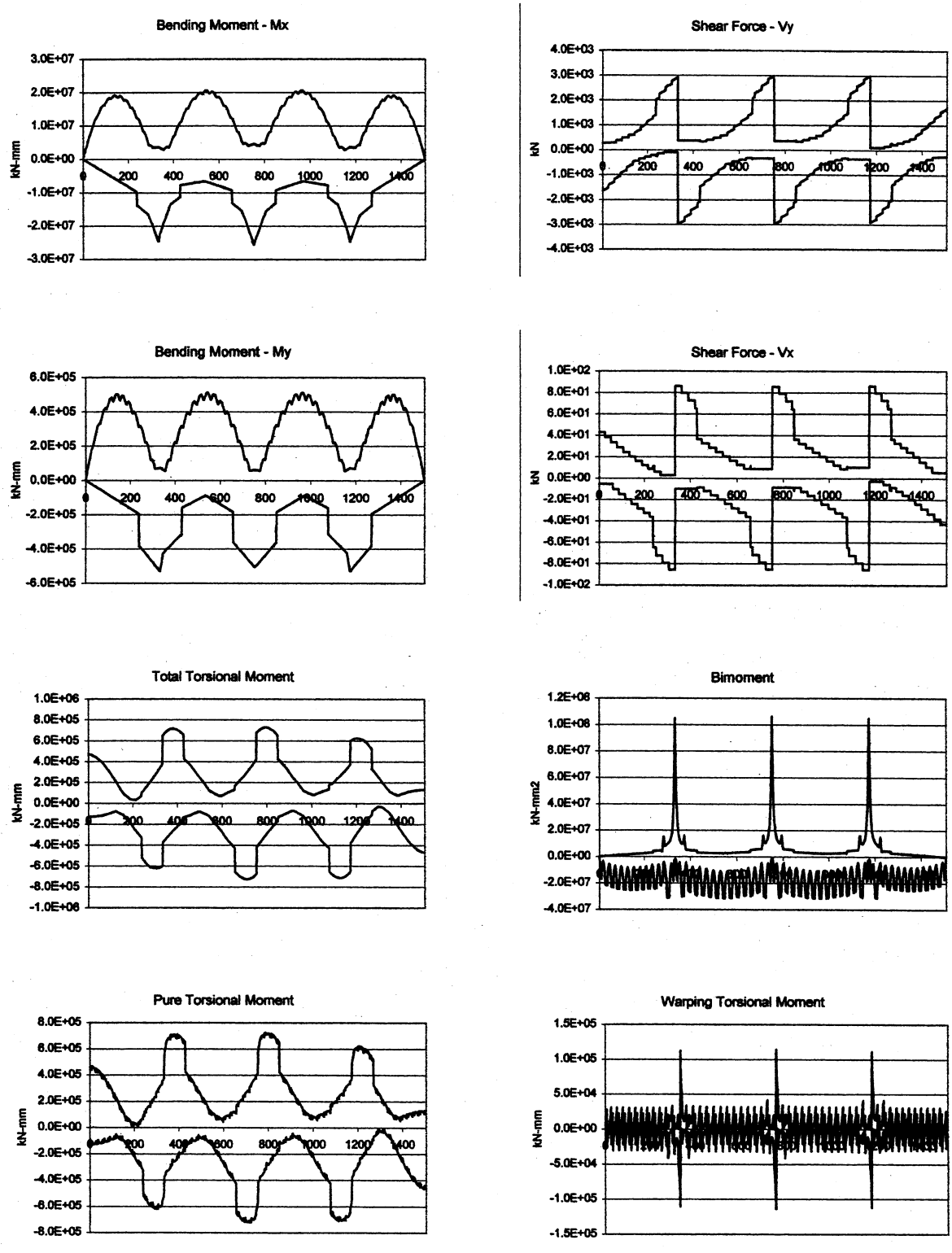

Figure 84: Straining actions for Br.538c (Live load envelope)

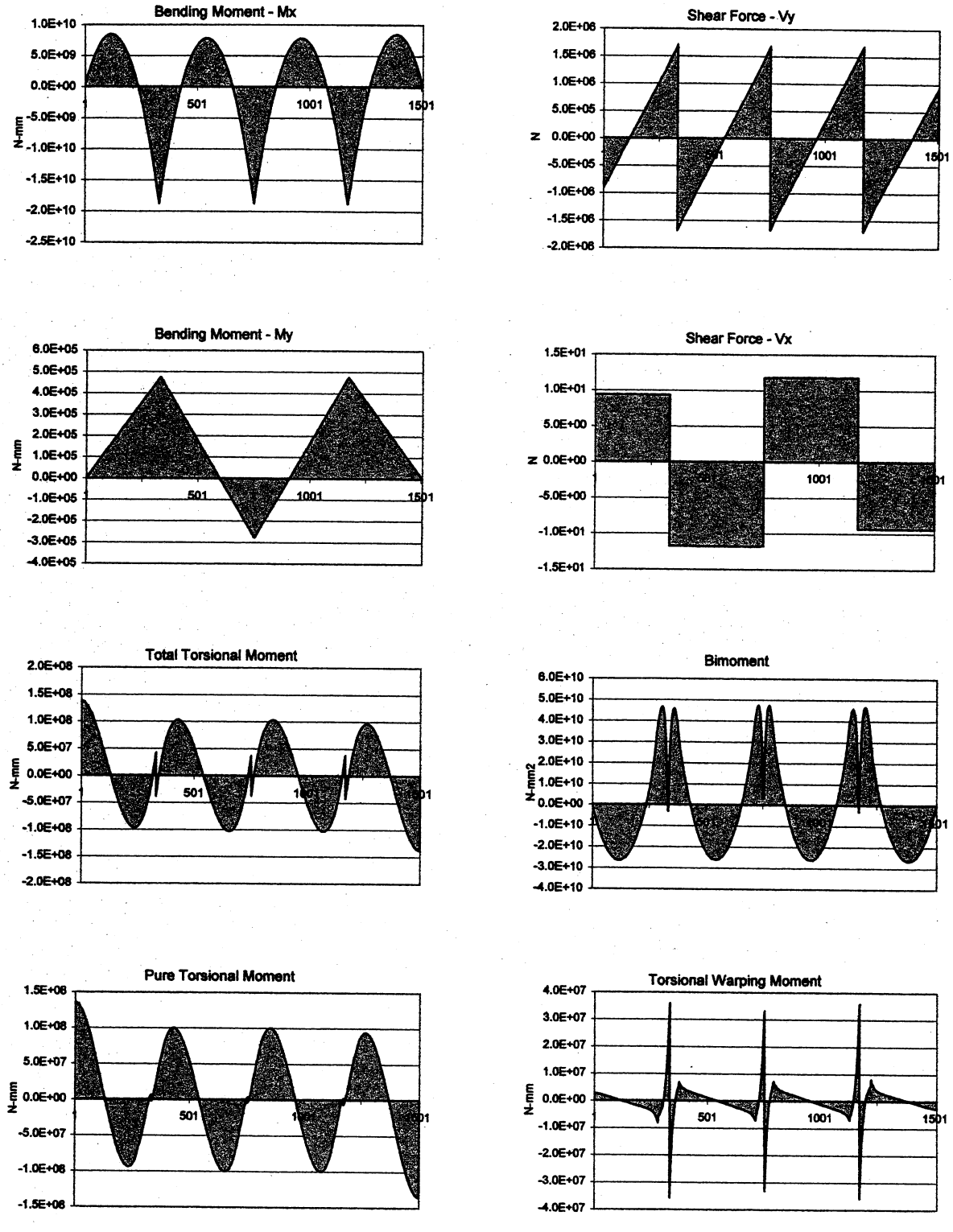

Figure 85: Straining actions for Br.538c (Dead load)

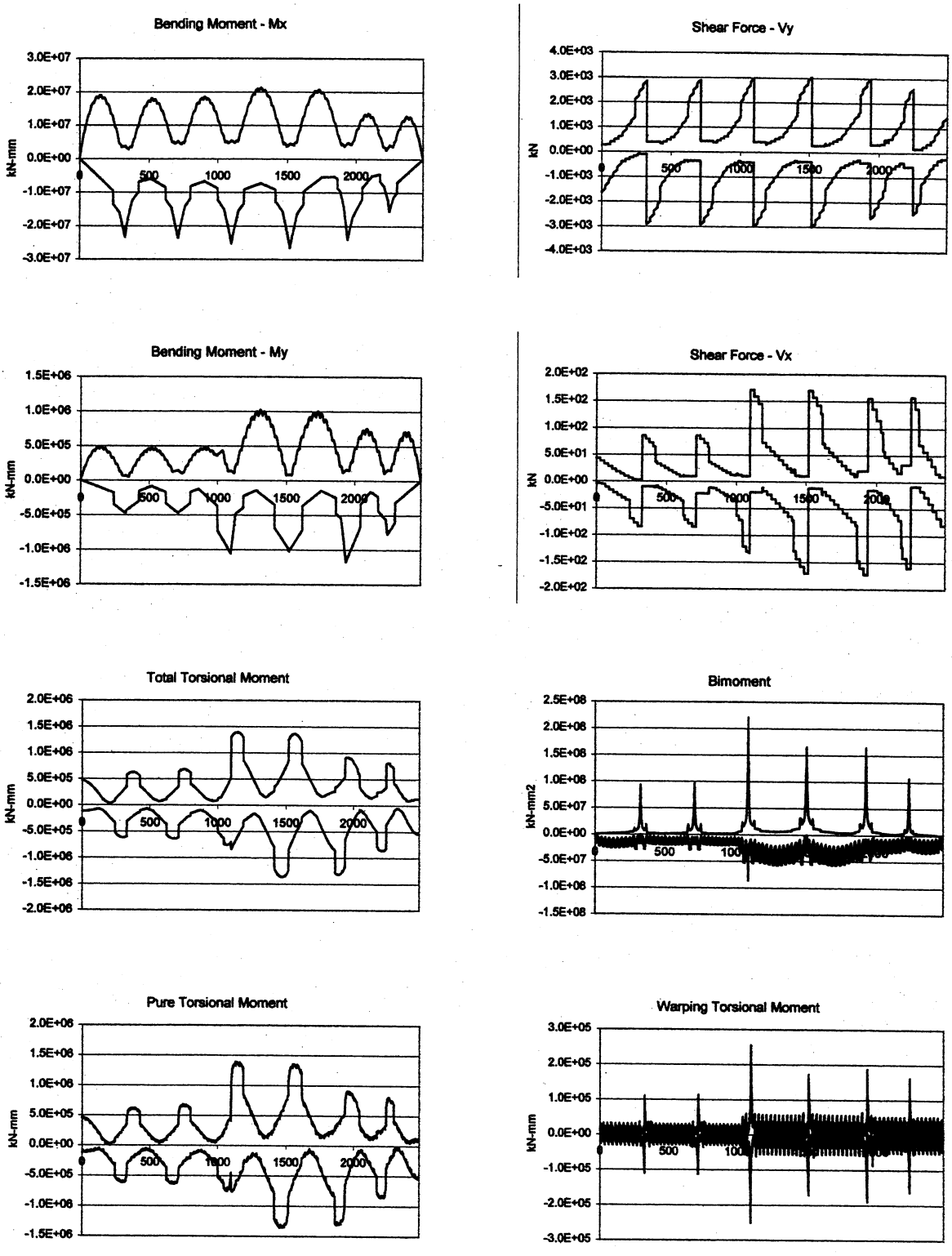

Figure 86: Straining actions for Br.538d (Live load envelope)

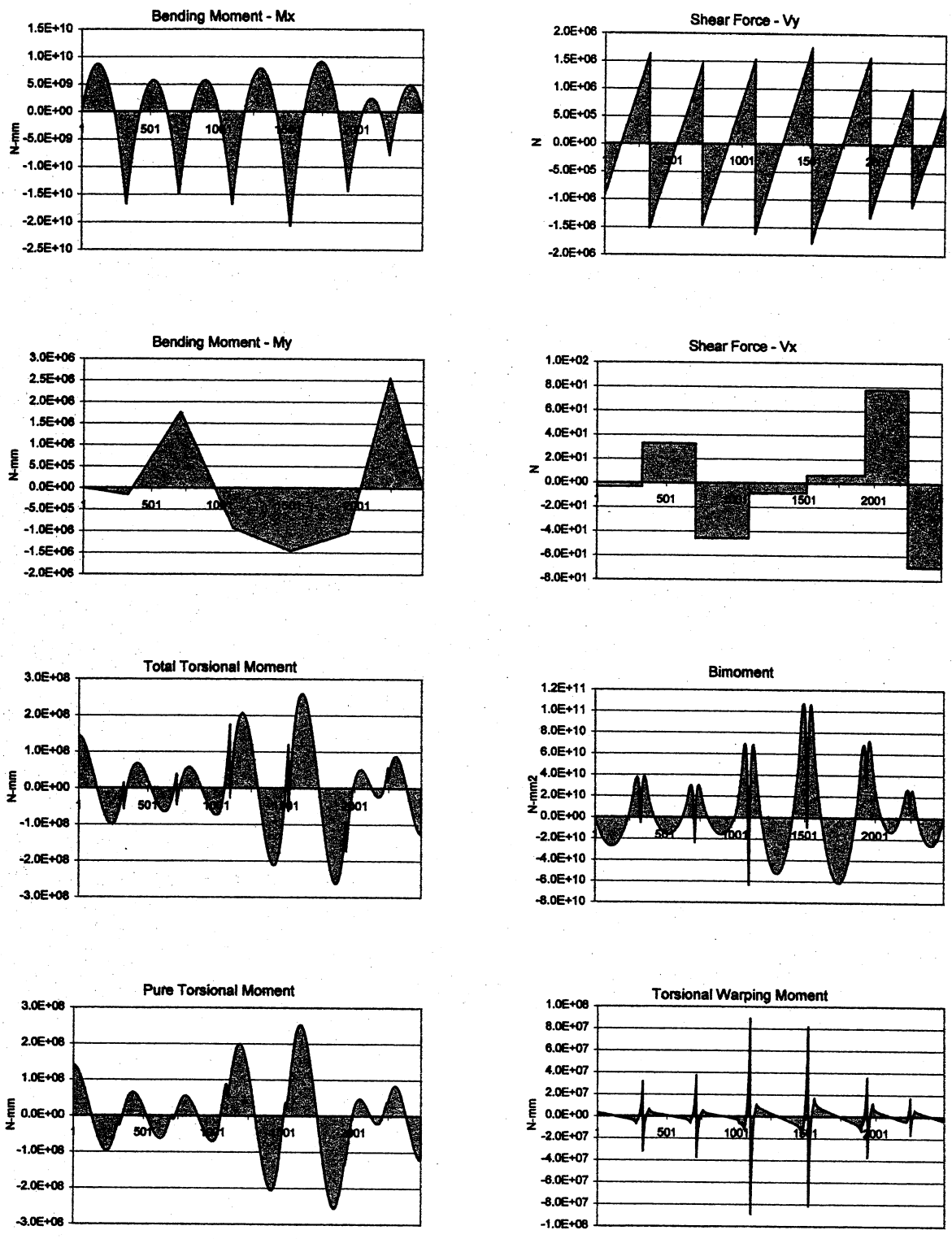

Figure 87: Straining actions for Br.538d (Dead load)

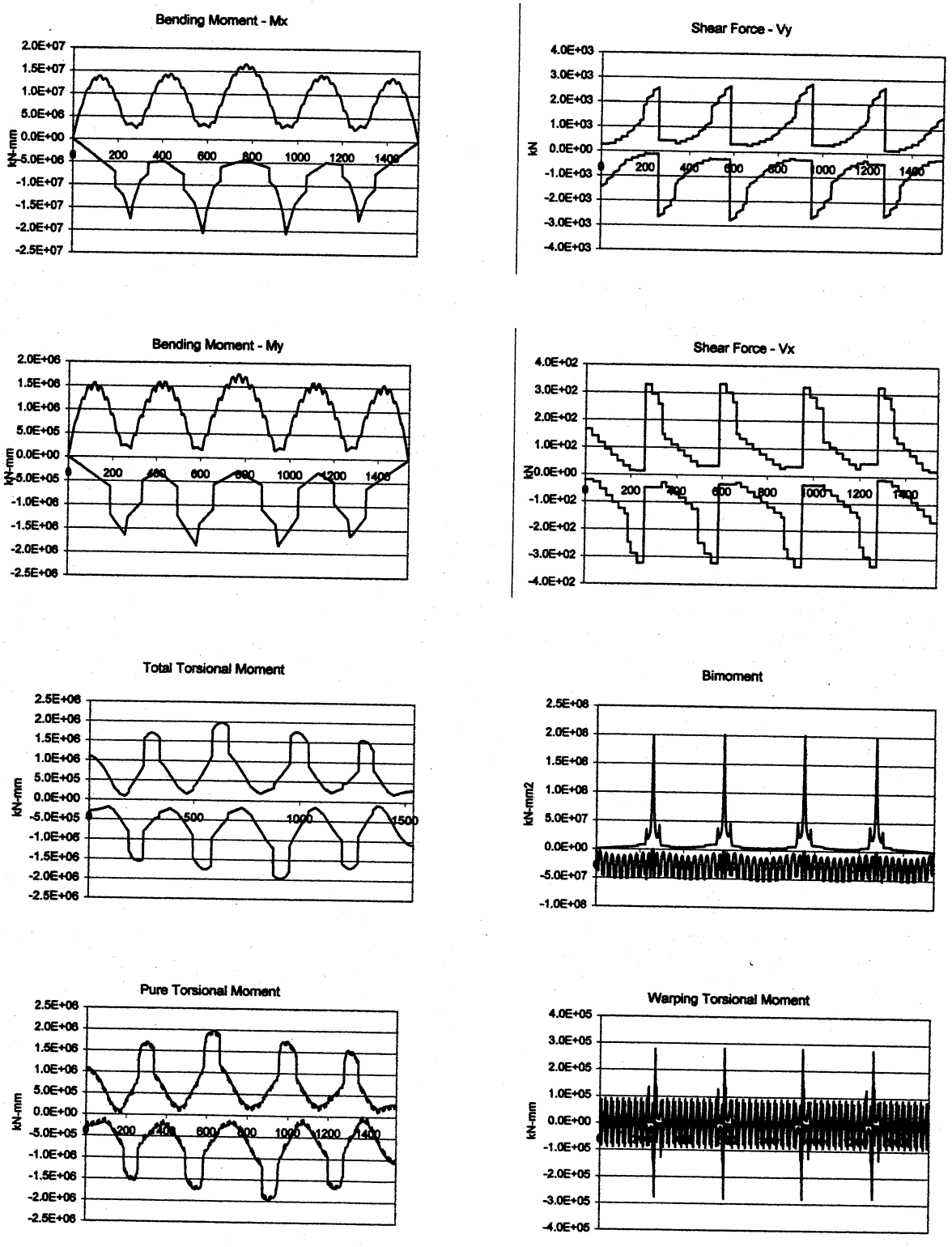

Figure 88: Straining actions for Br.539 (Live load envelope)

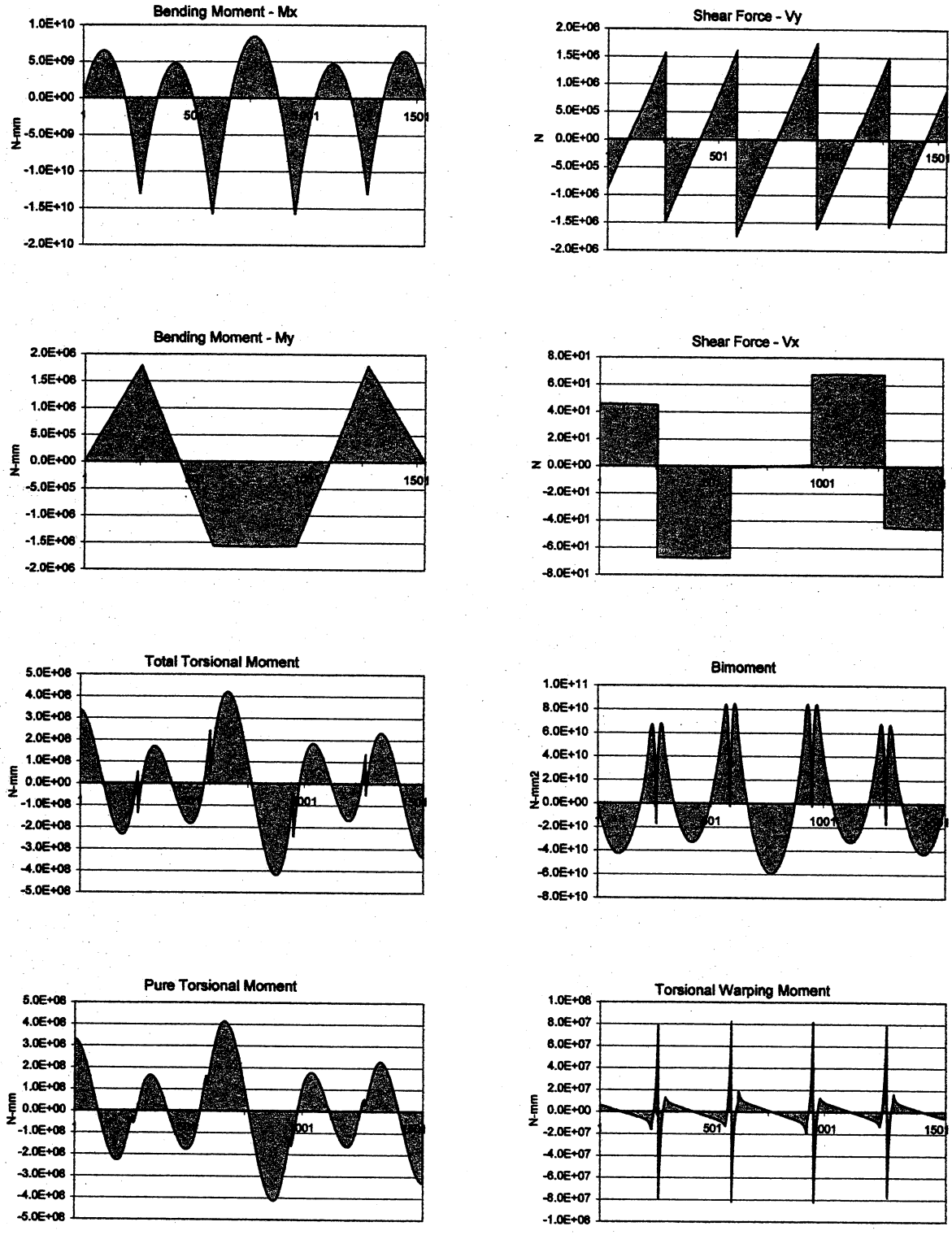

Figure 89: Straining actions for Br.539 (Dead load)

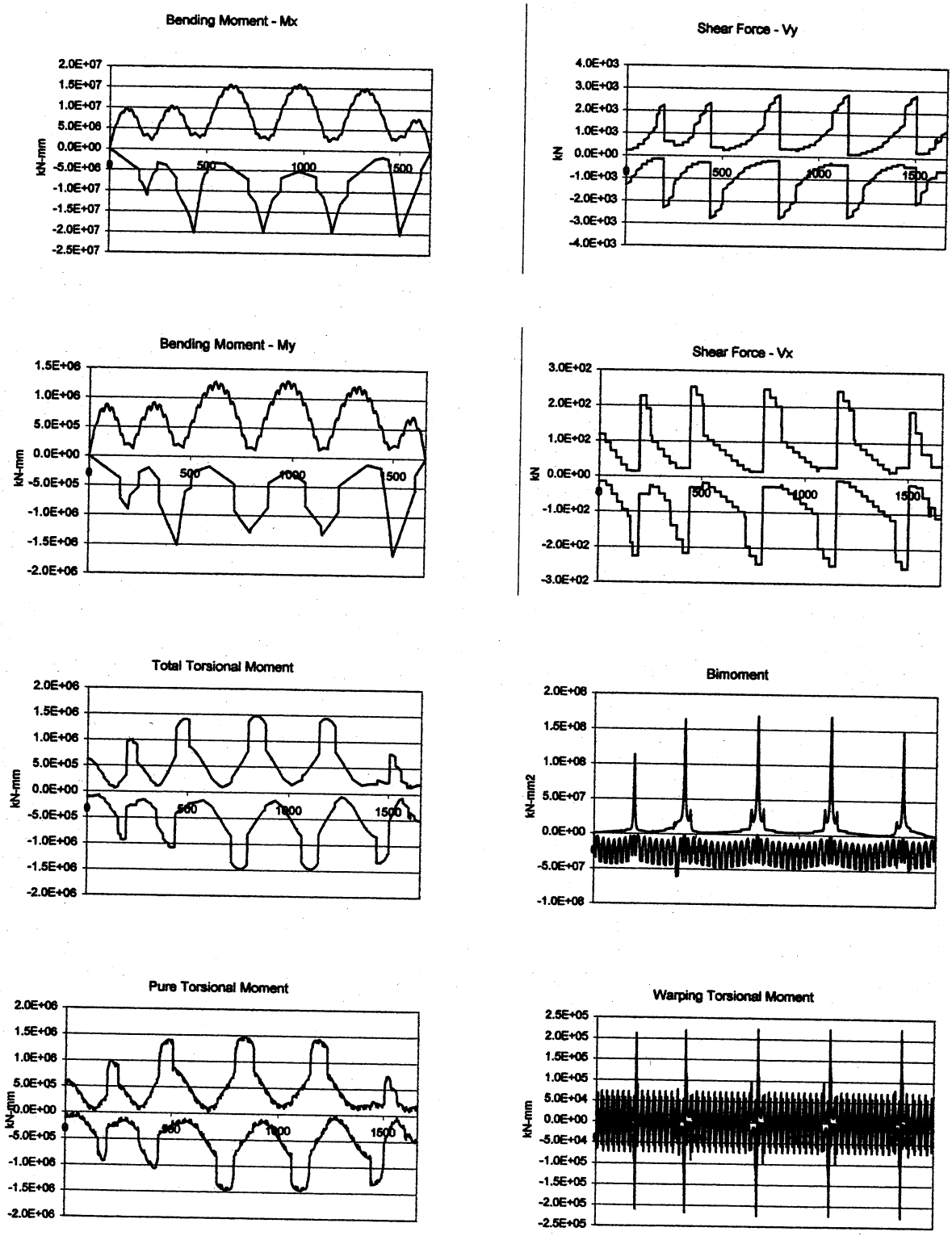

Figure 90: Straining actions for Br.540 (Live load envelope)

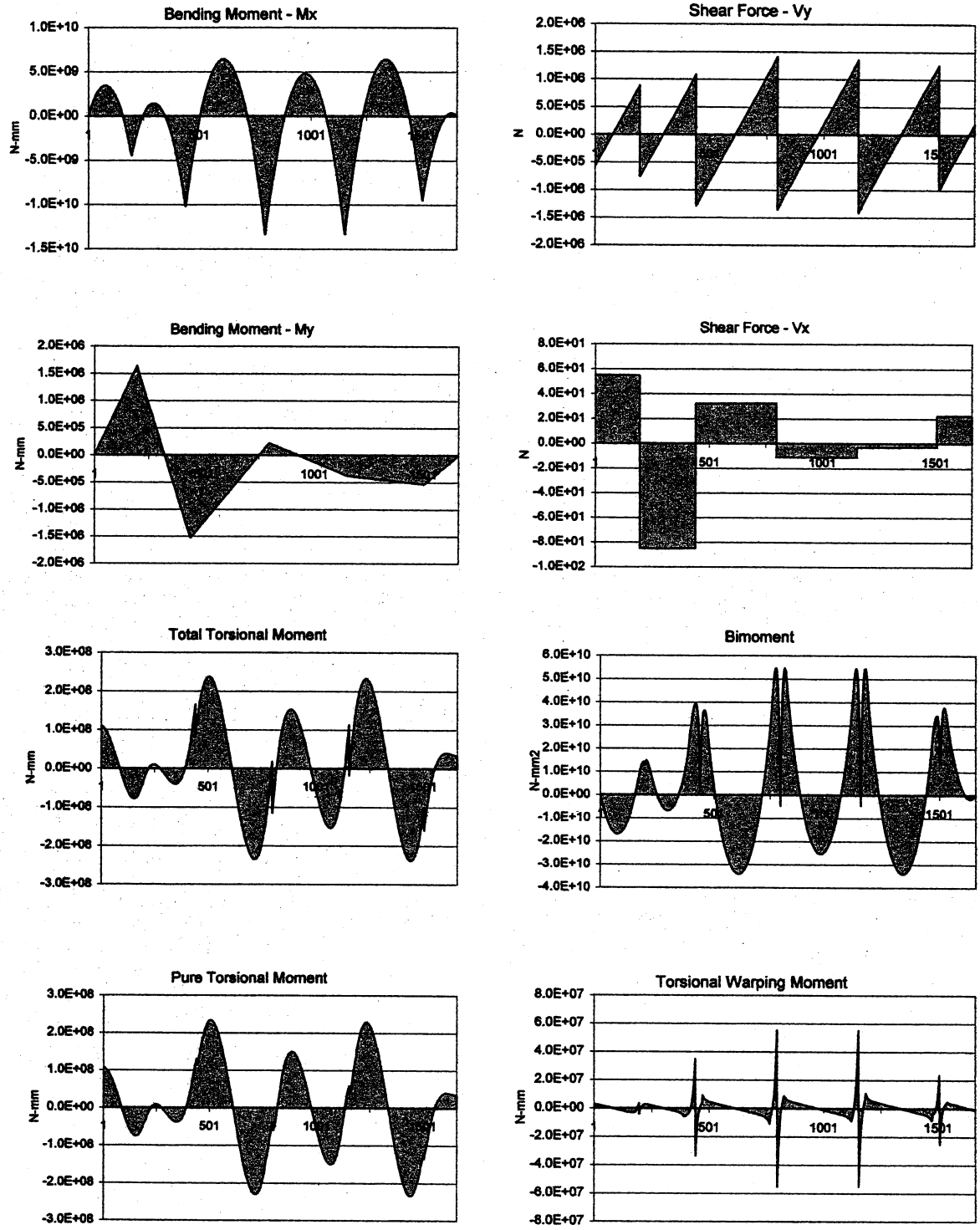

Figure 91: Straining actions for Br.540 (Dead load)

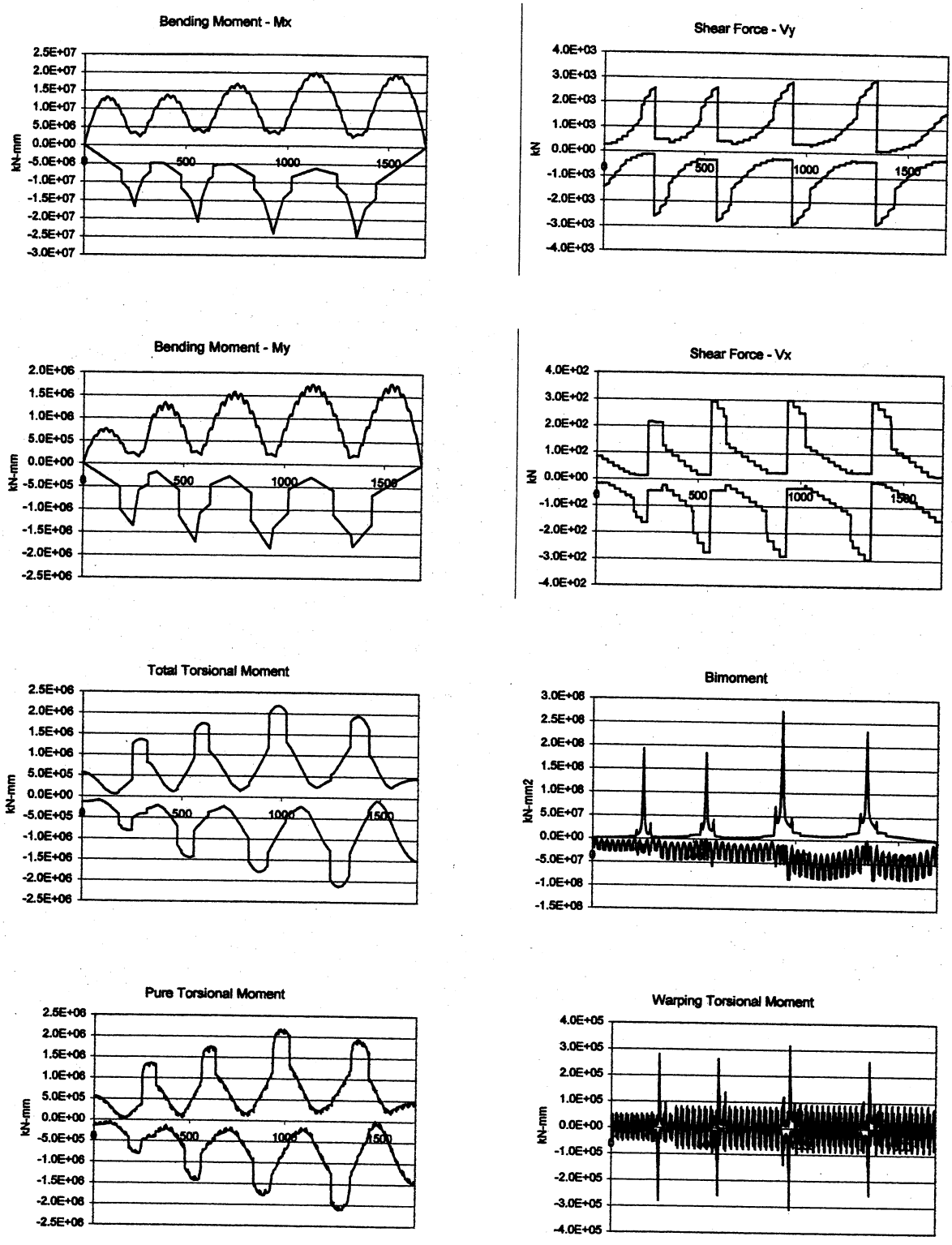

Figure 92: Straining actions for Br.541a (Live load envelope)

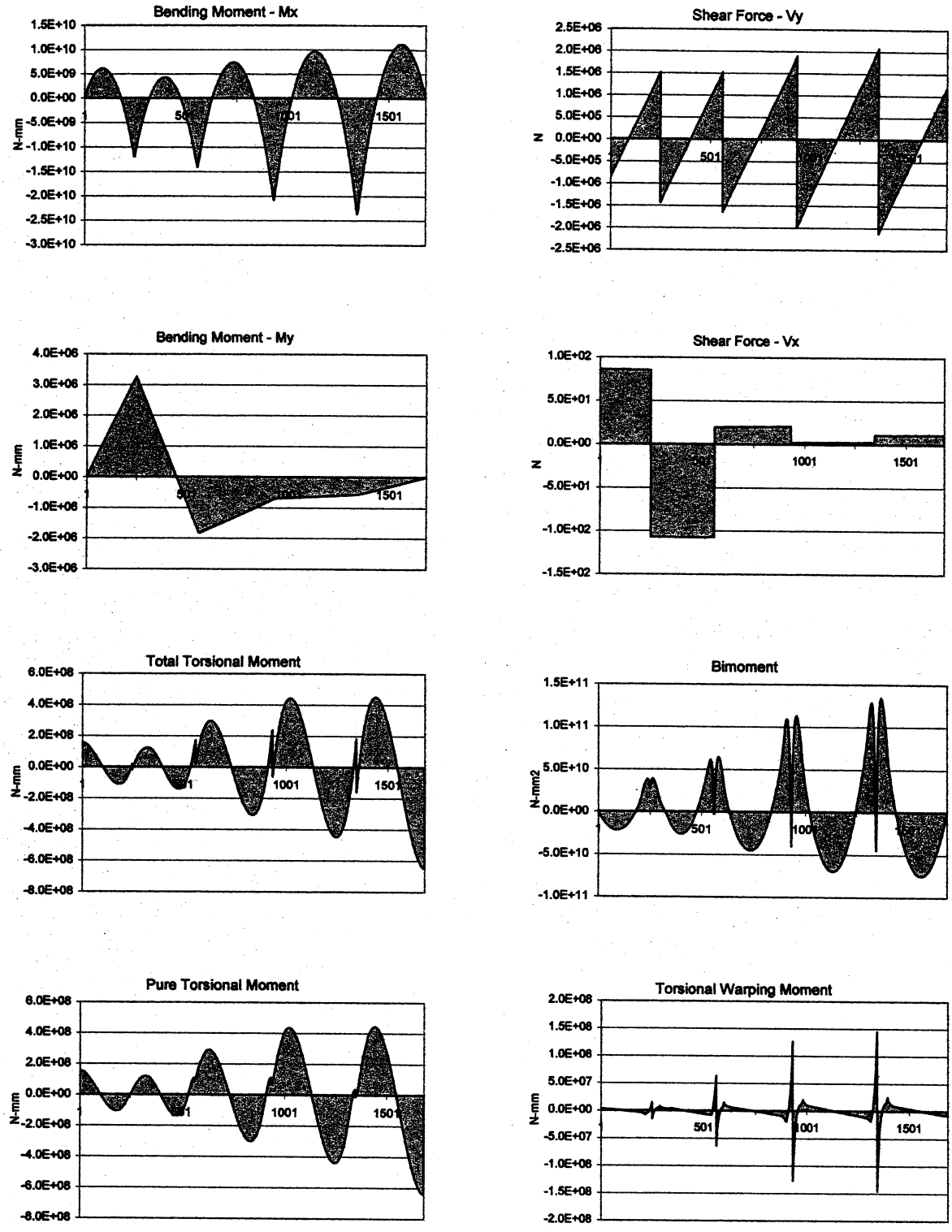

Figure 93: Straining actions for Br.541a (Dead load)

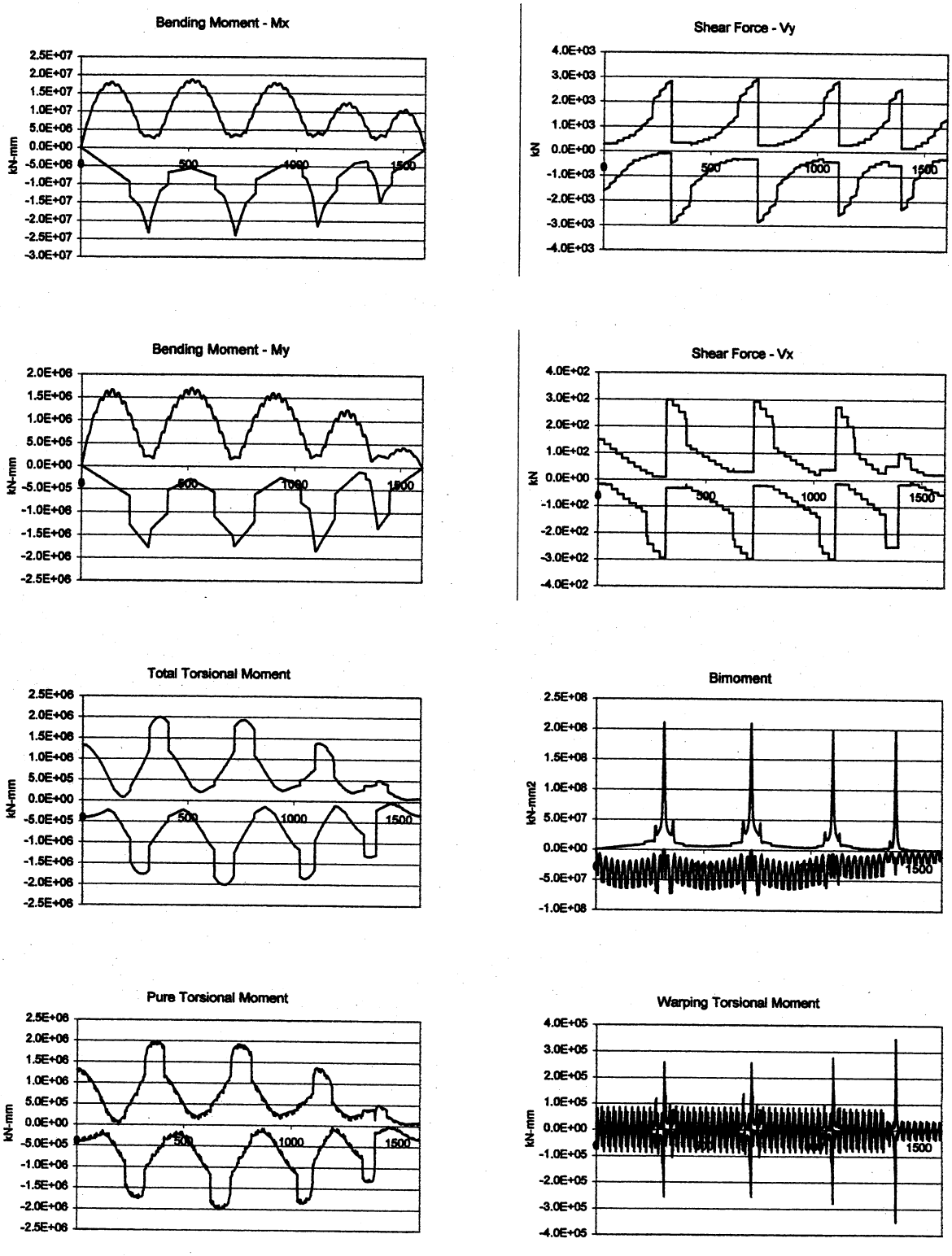

Figure 94: Straining actions for Br.541b (Live load envelope)

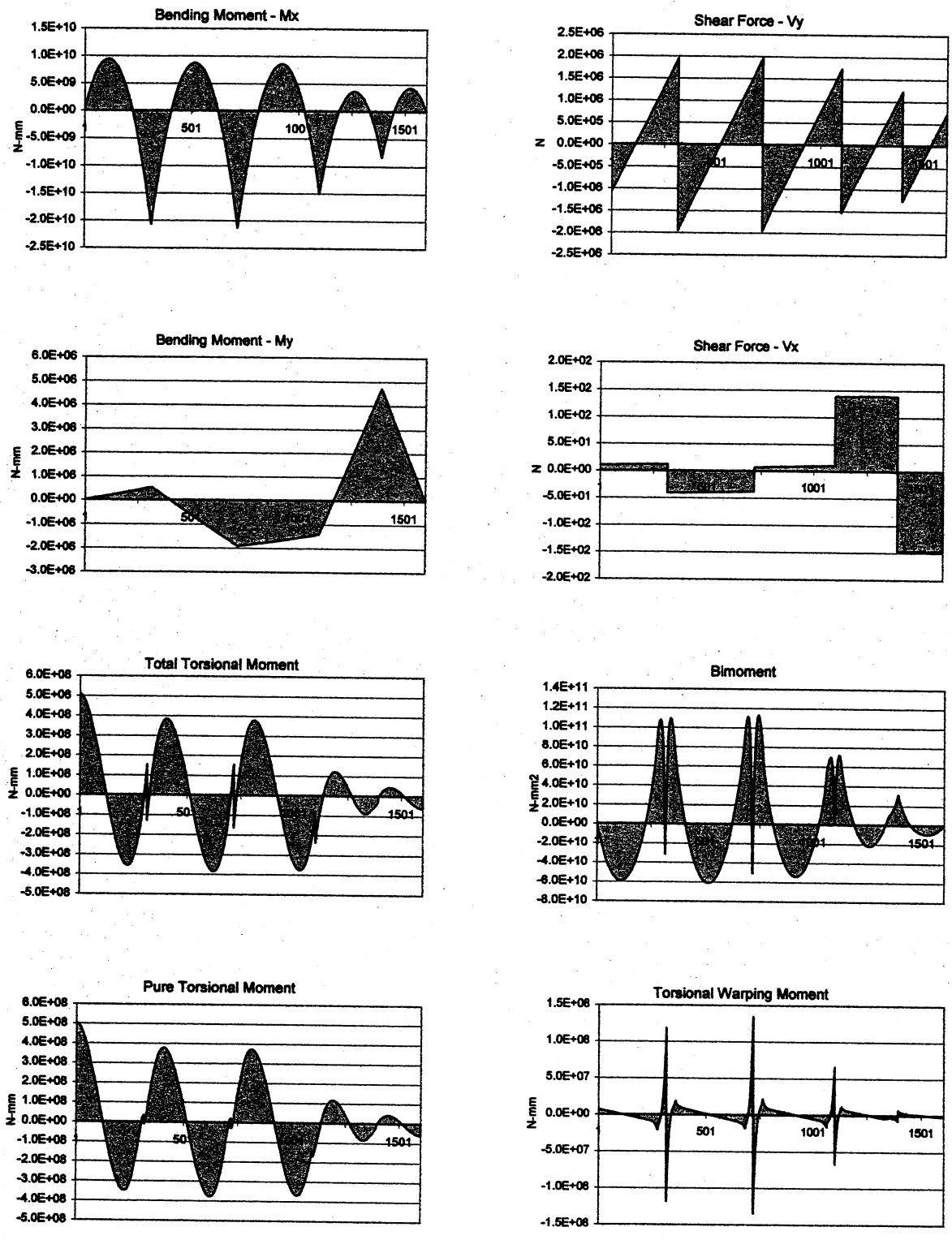

Figure 95: Straining actions for Br.541b (Dead load)

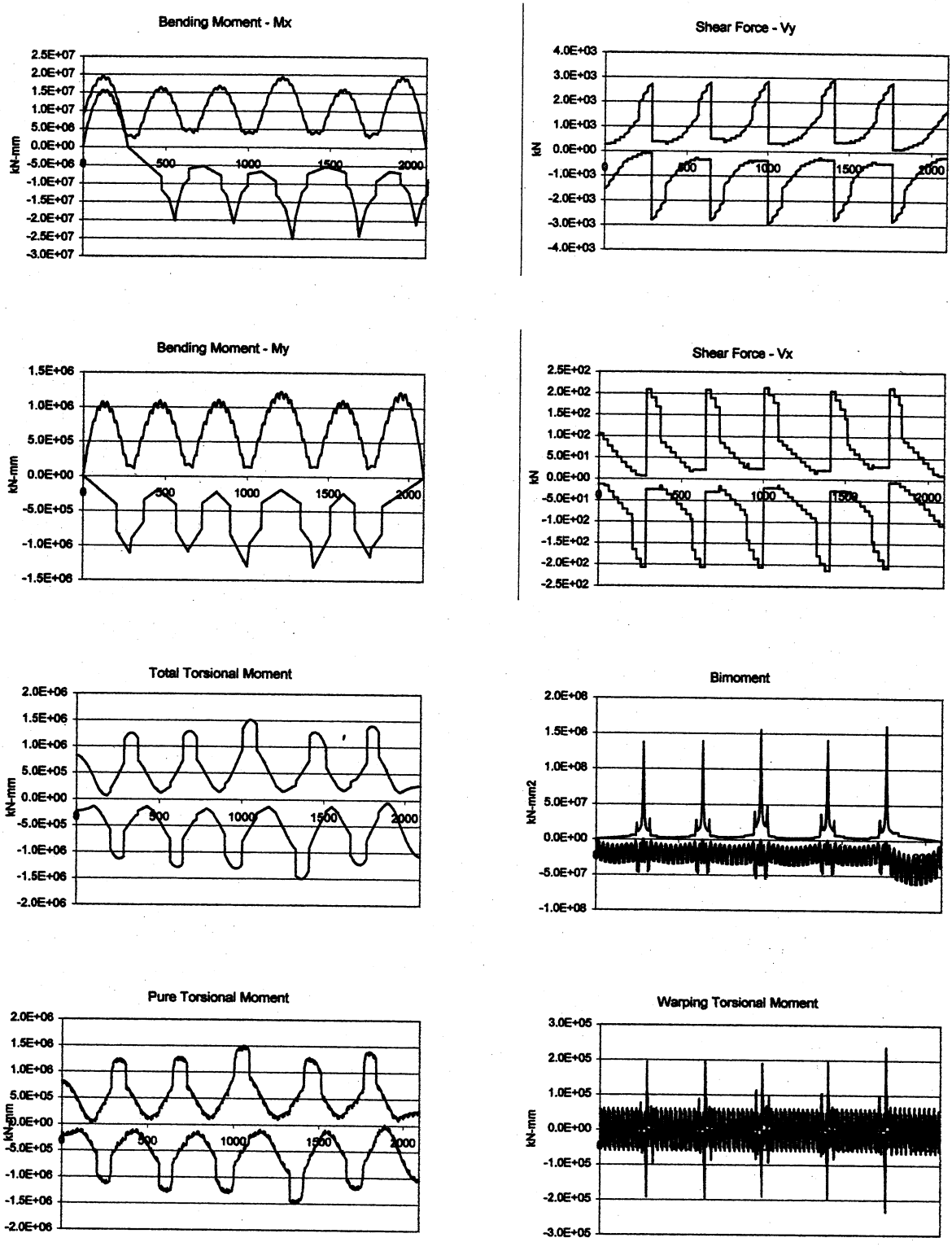

Figure 96: Straining actions for Br.542a (Live load envelope)

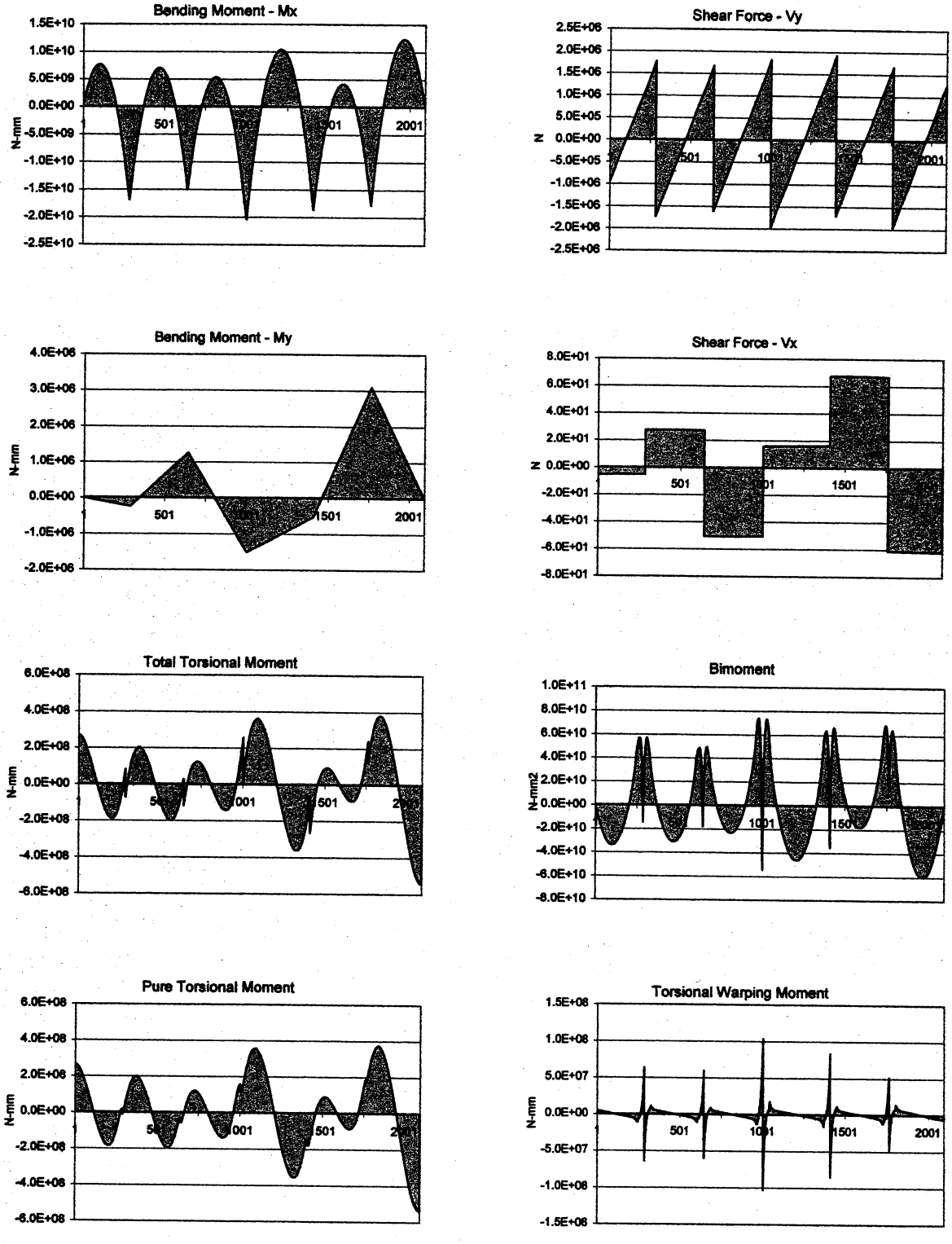

Figure 97: Straining actions for Br.542a (Dead load)

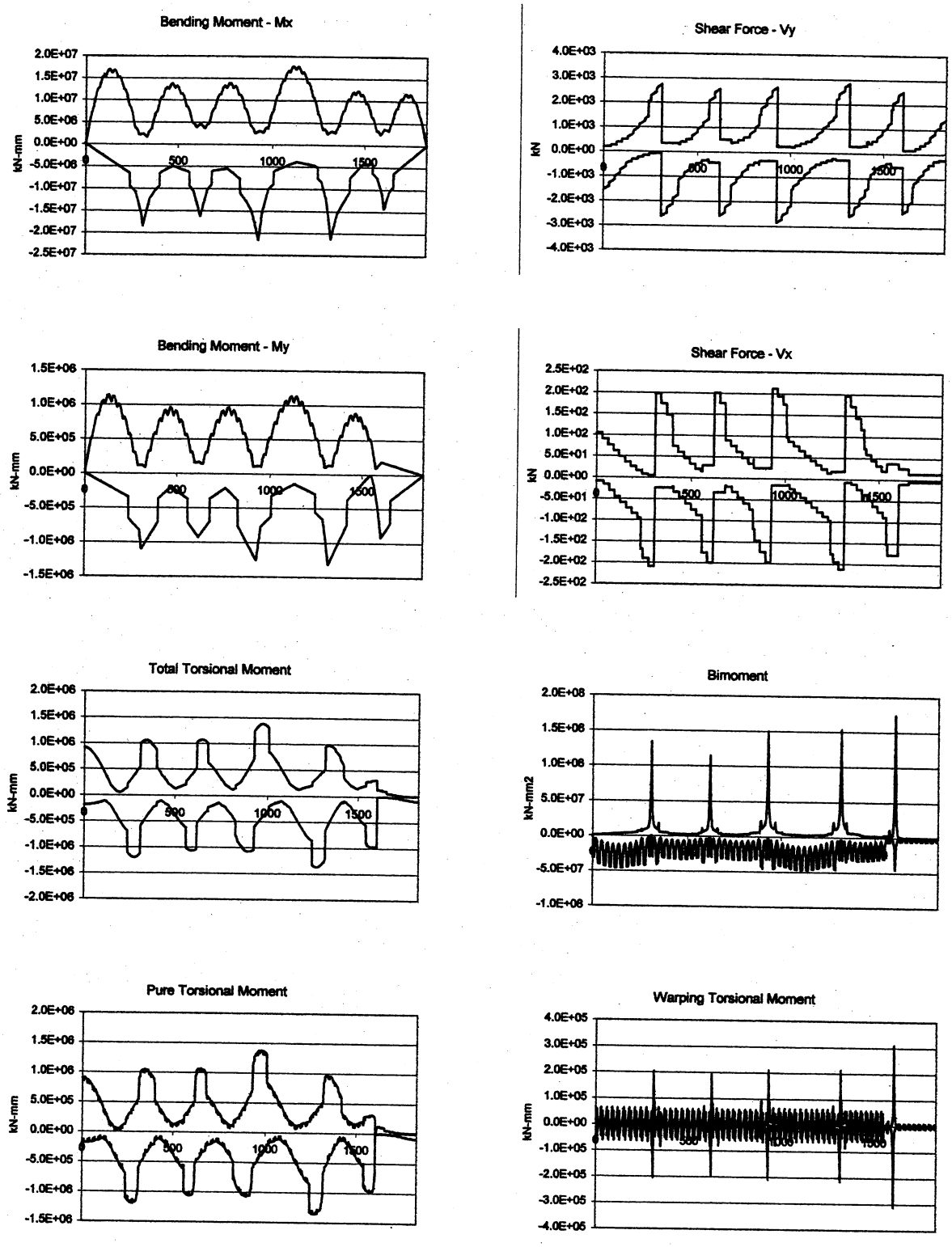

Figure 98: Straining actions for Br.542b (Live load envelope)

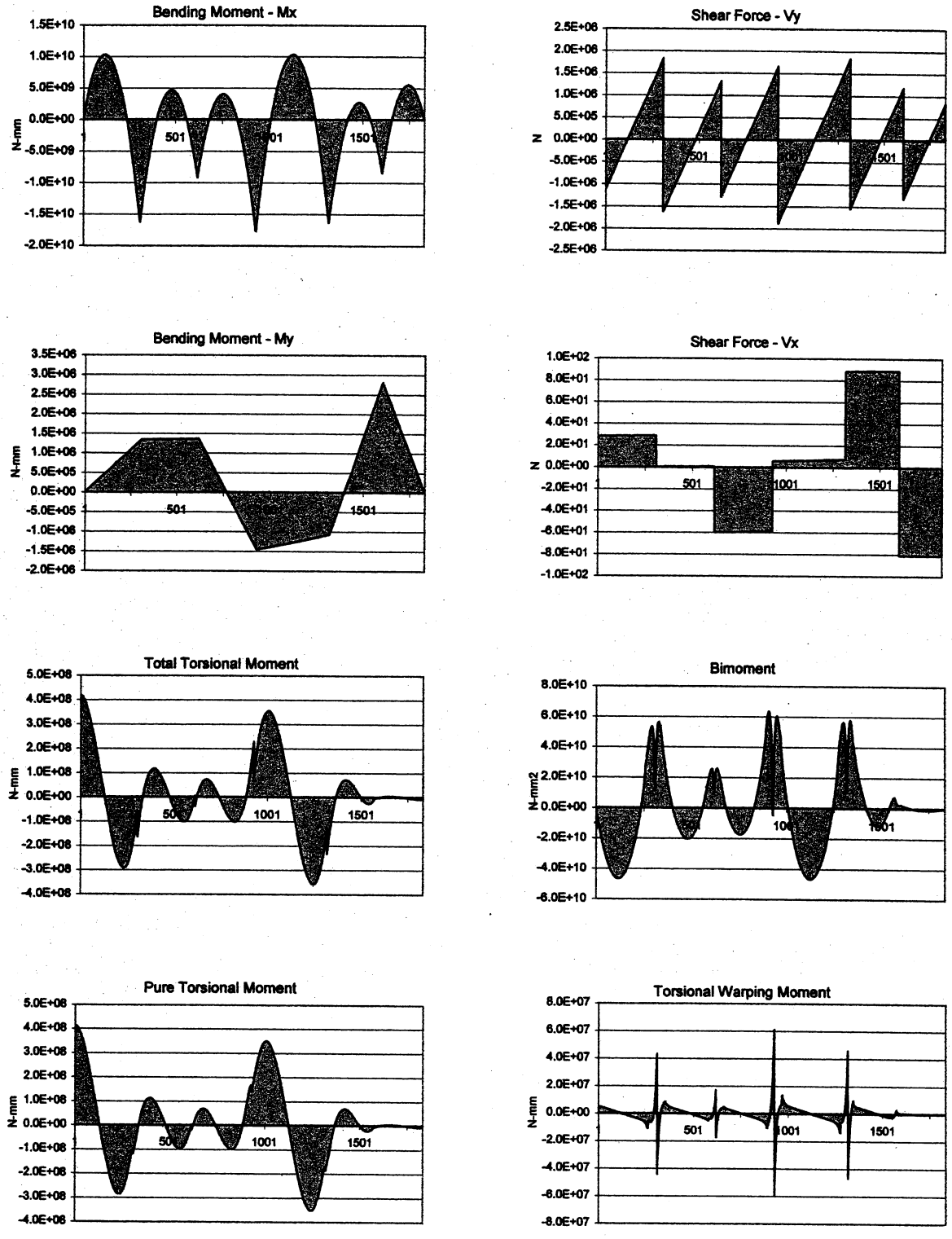

Figure 99: Straining actions for Br.542b (Dead load)

APPENDIX C

BEAM ELEMENT MODEL STUDY RESULTS

The results of the hole location study are given in this appendix. For each one of the nineteen analyzed bridges, 8 figures are given. The first two figures show calculations based on schemes I and II (see page 50 for definition). The following two figures show regions based on schemes III and IV, while the region based on scheme V is shown in the next set. Finally, a byproduct of this study is the warping stresses in box girder bridges. For each bridge, a figure showing the normal warping stress as a percentage of the maximum normal stress is given. Also shear warping stress percentages are also presented.

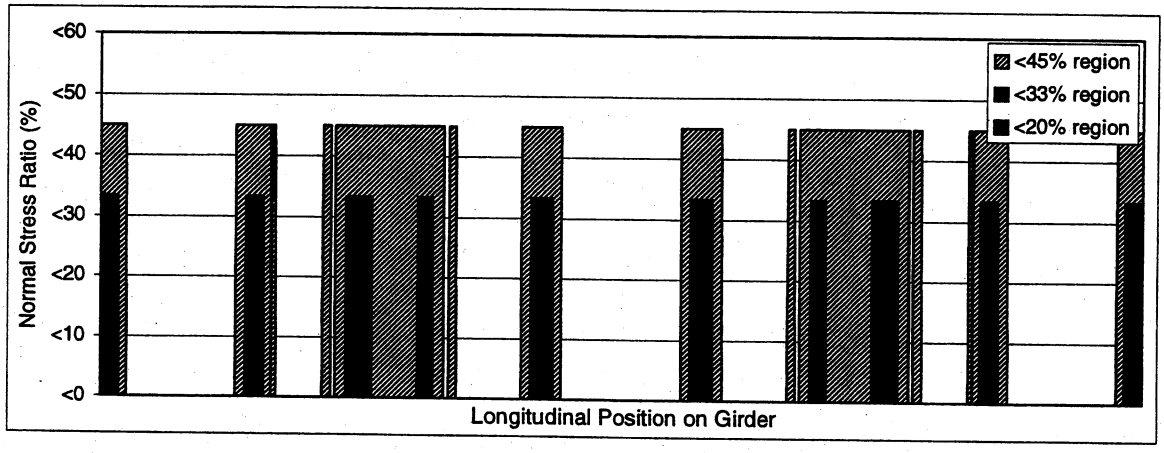

(a)

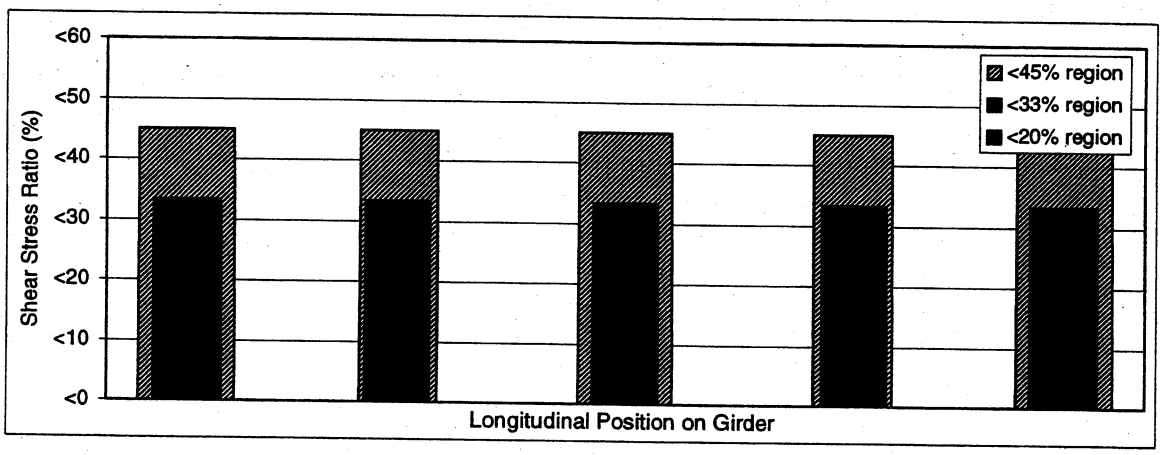

(b)

Figure 100: Regions of low stresses for Br. 390 (a-Approach I, b-Approach II)

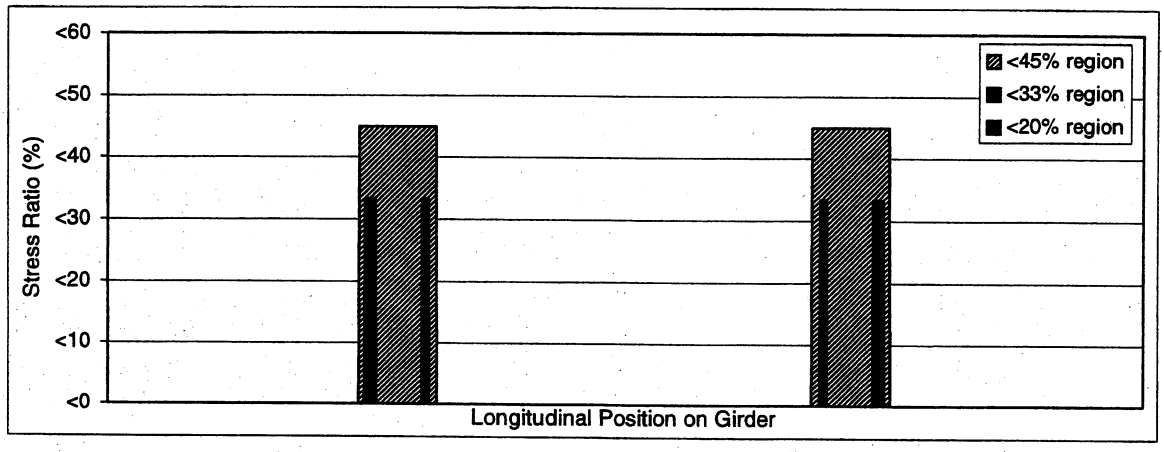

(a)

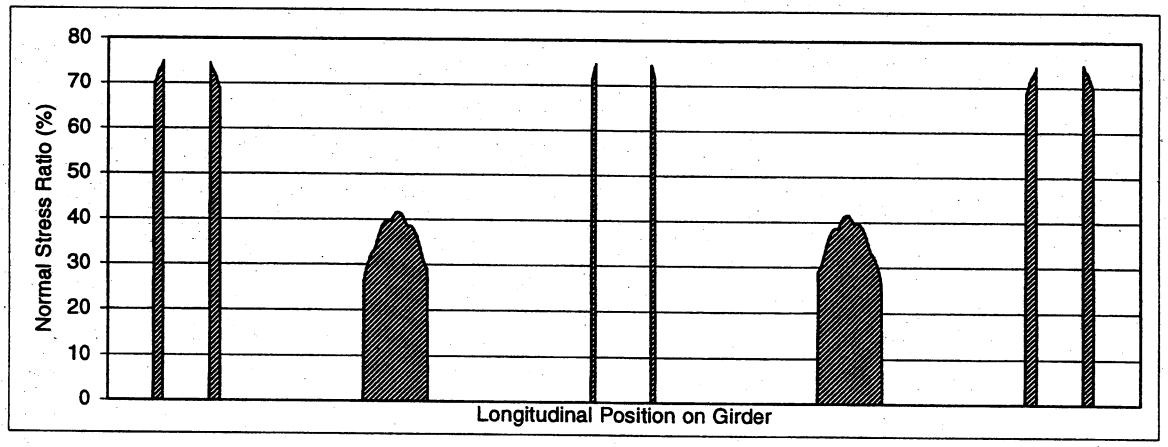

(b)

Figure 101: Regions of low stresses for Br. 390 (a-Approach III, b-Approach IV)

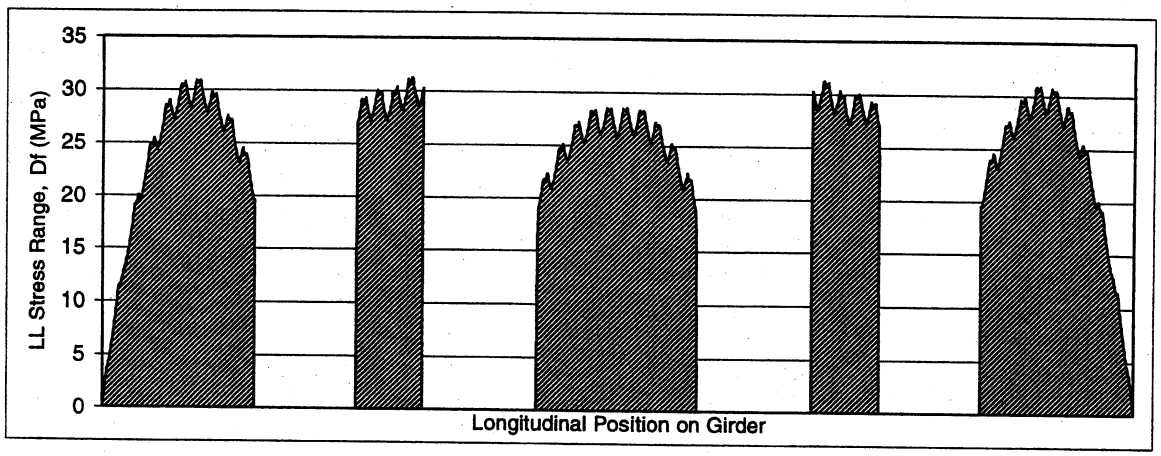

(a)

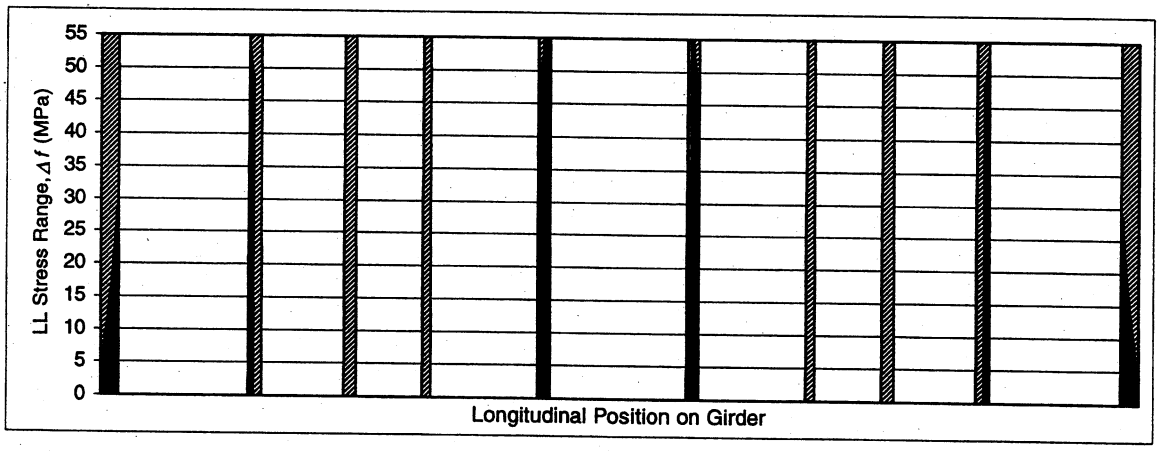

(b)

Figure 102: Br. 390 (a- Live load fatigue stress range,b- Low stress regions according to Approach V)

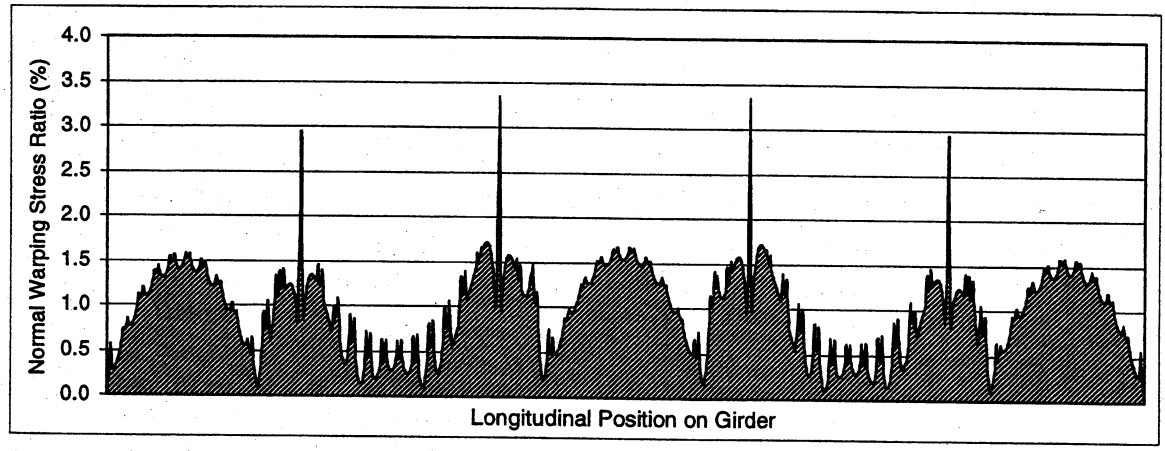

(a)

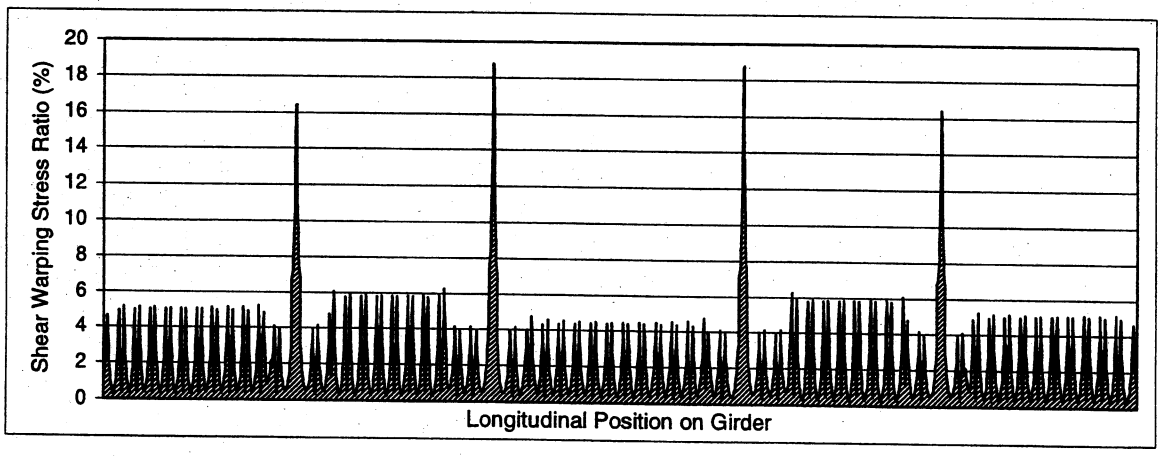

(b)

Figure 103: Warping stress ratios for Br. 390. a) σ_w/σ_T, b) τ_w/τ_T

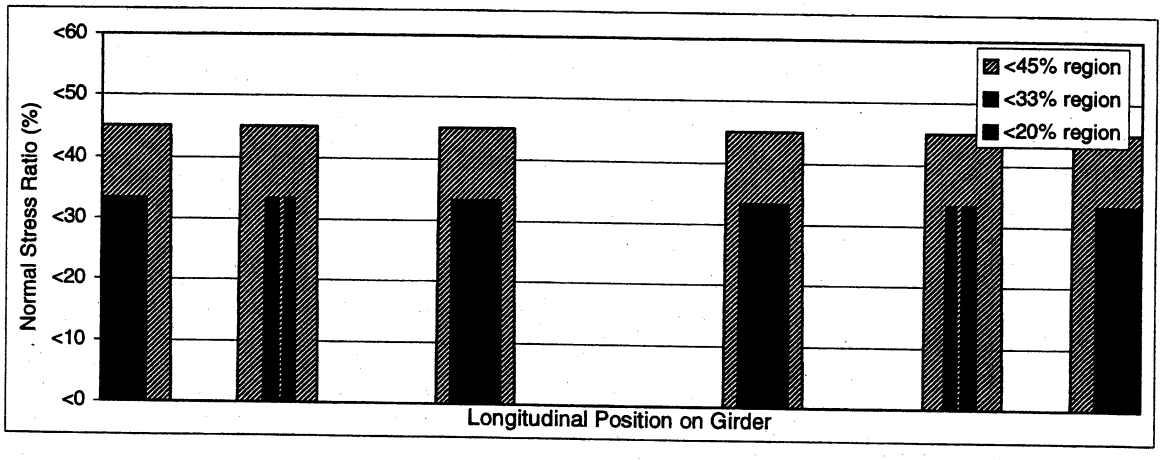

(a)

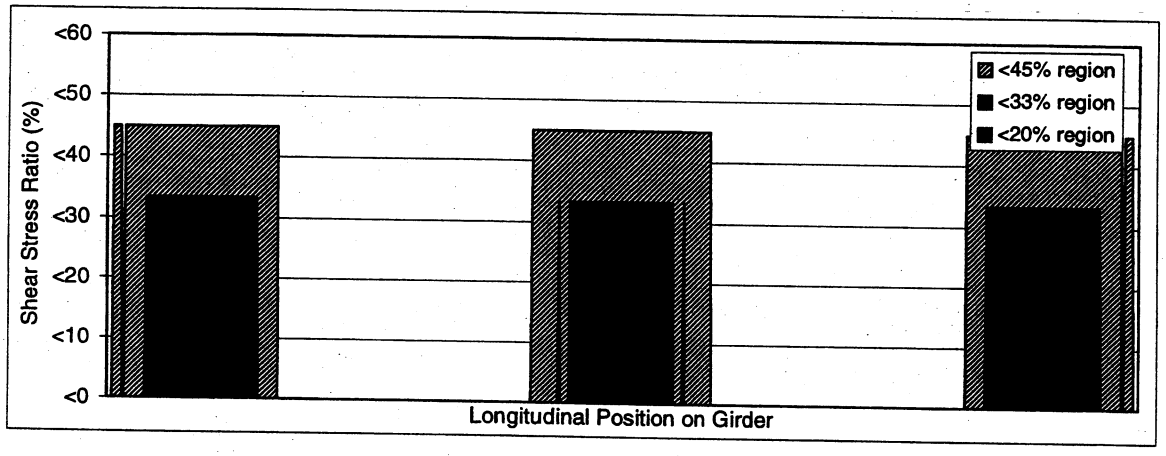

(b)

Figure 104: Regions of low stresses for Br. 521 (a-Approach I, b-Approach II)

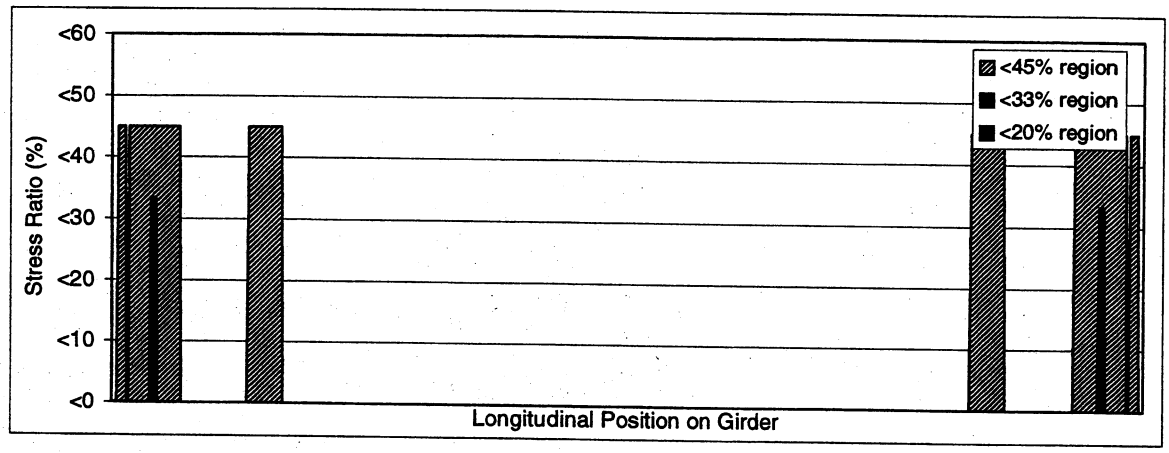

(a)

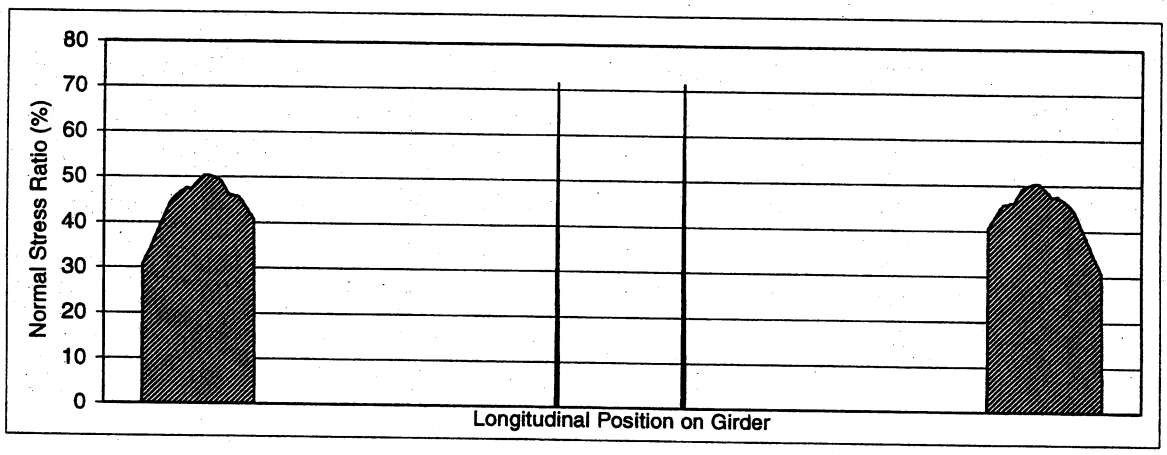

(b)

Figure 105: Regions of low stresses for Br. 521 (a-Approach III, b-Approach IV)

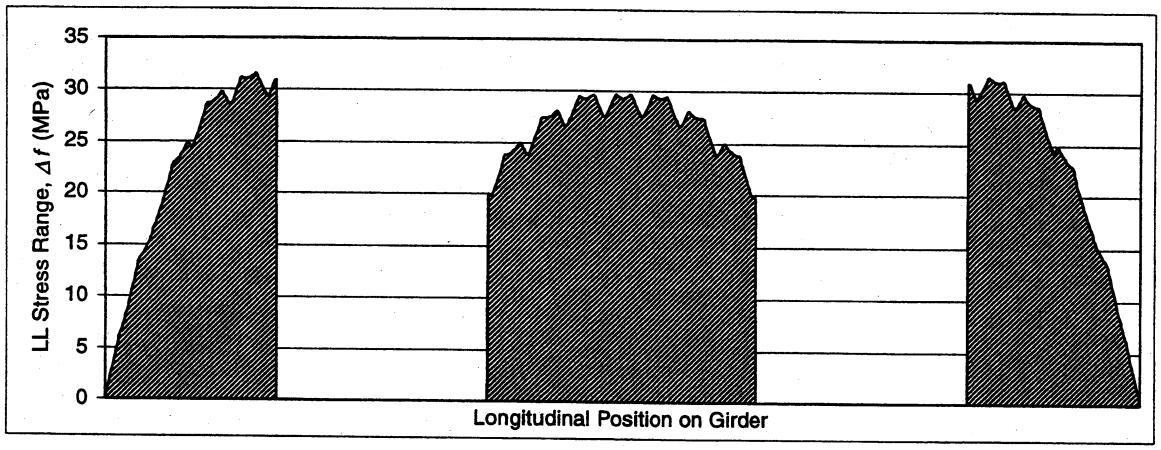

(a)

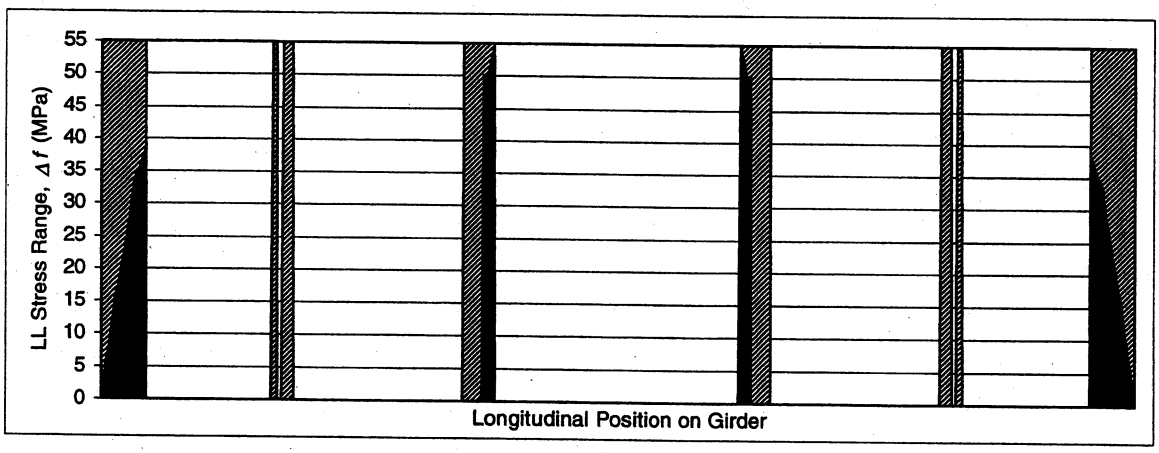

(b)

Figure 106: Br. 521 (a- Live load fatigue stress range,b- Low stress regions according to Approach V)

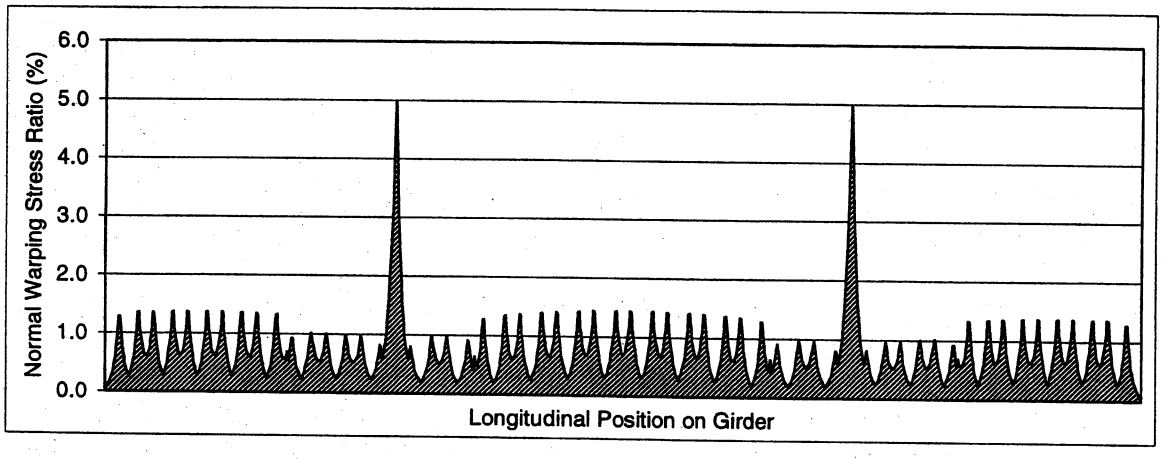

(a)

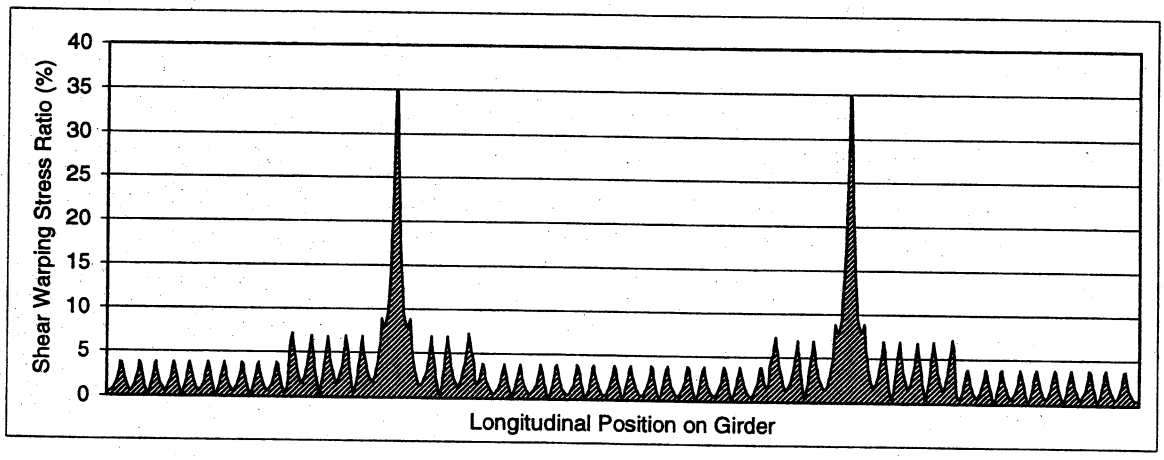

(b)

Figure 107: Warping stress ratios for Br. 521. a) σ_w/σ_T, b) τ_w/τ_T

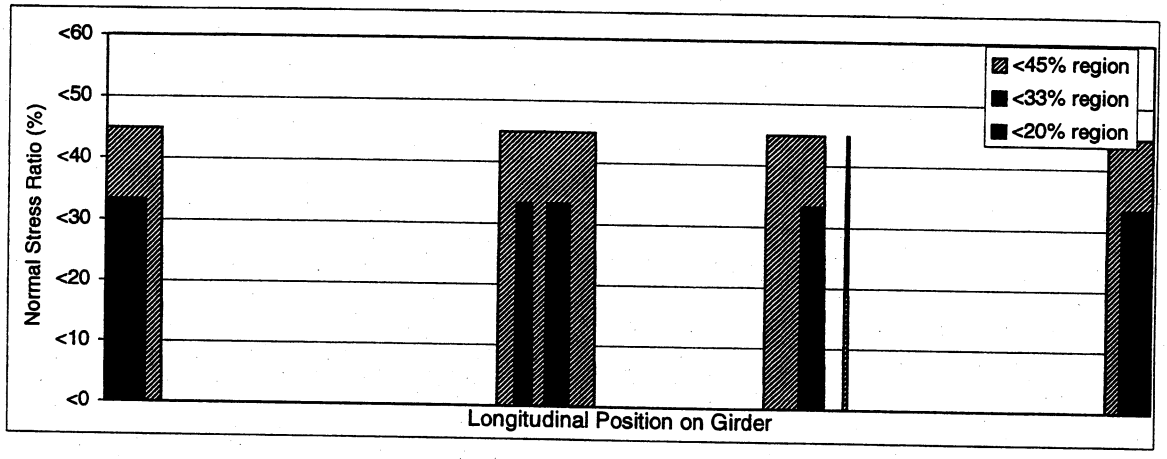

(a)

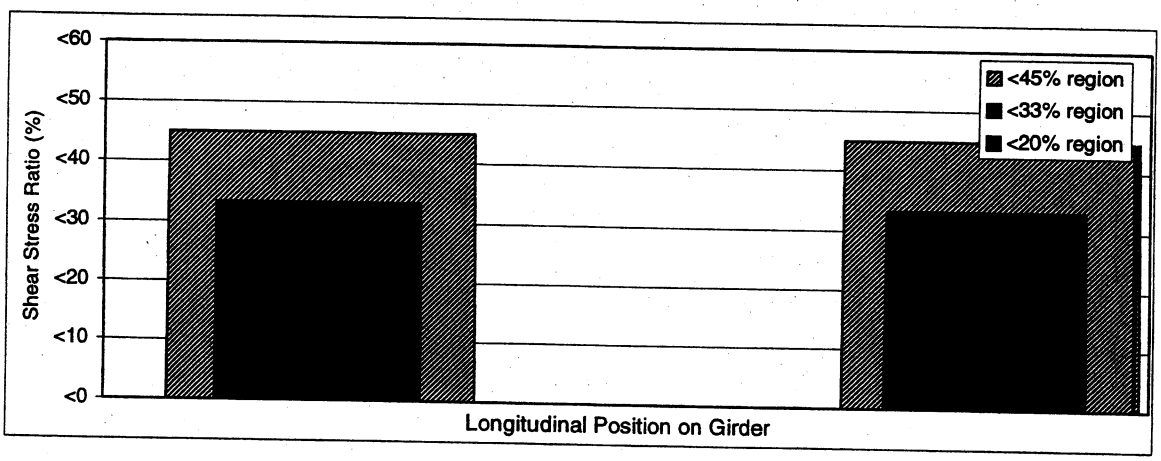

(b)

Figure 108: Regions of low stresses for Br. 525 (a-Approach I, b-Approach II)

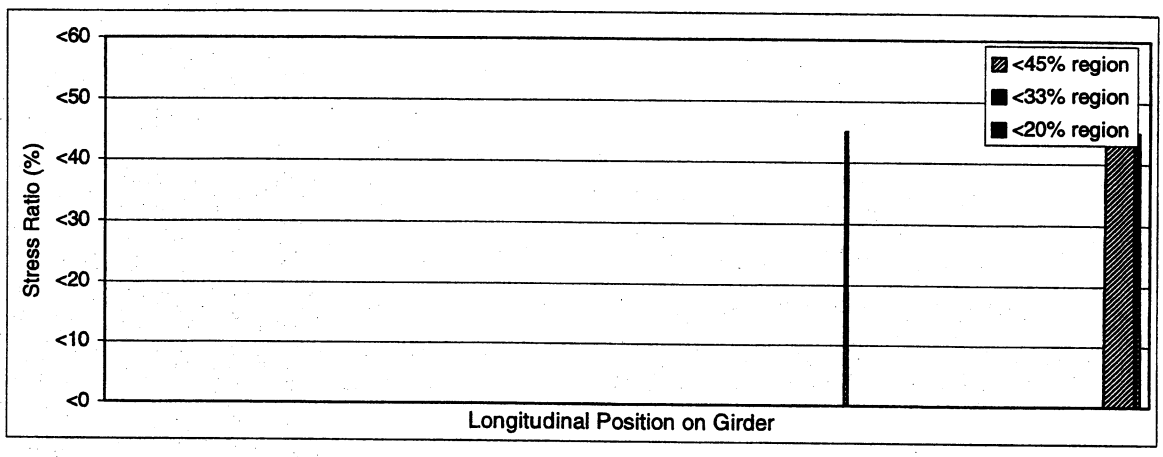

(a)

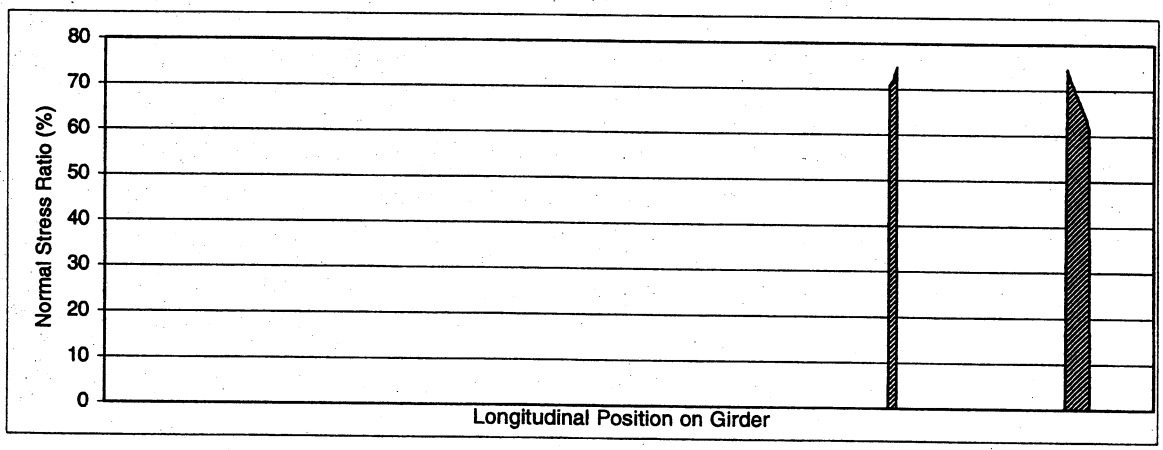

(b)

Figure 109: Regions of low stresses for Br. 525 a-Approach III, b-Approach IV)

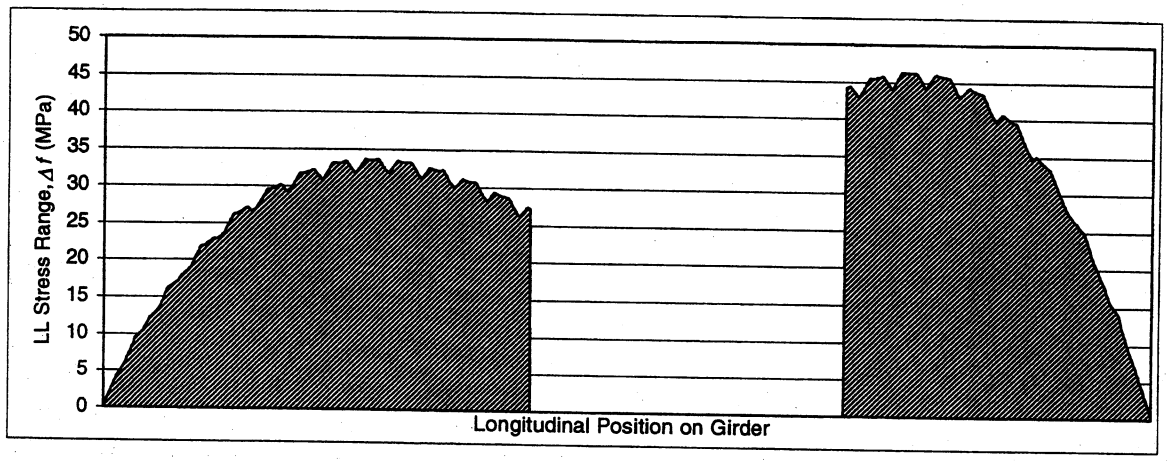

(a)

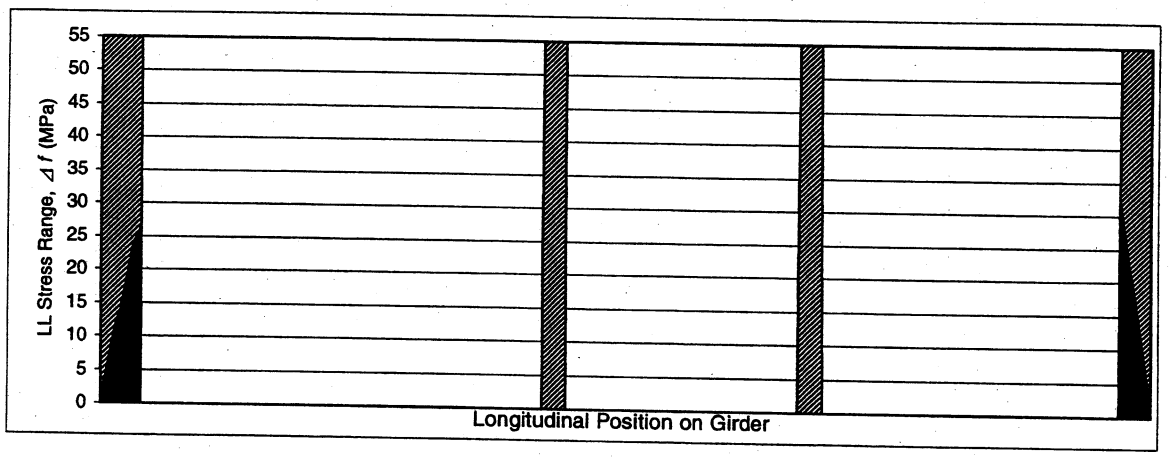

(b)

Figure 110: Br. 525 (a- Live load fatigue stress range,b- Low stress regions according to Approach V)

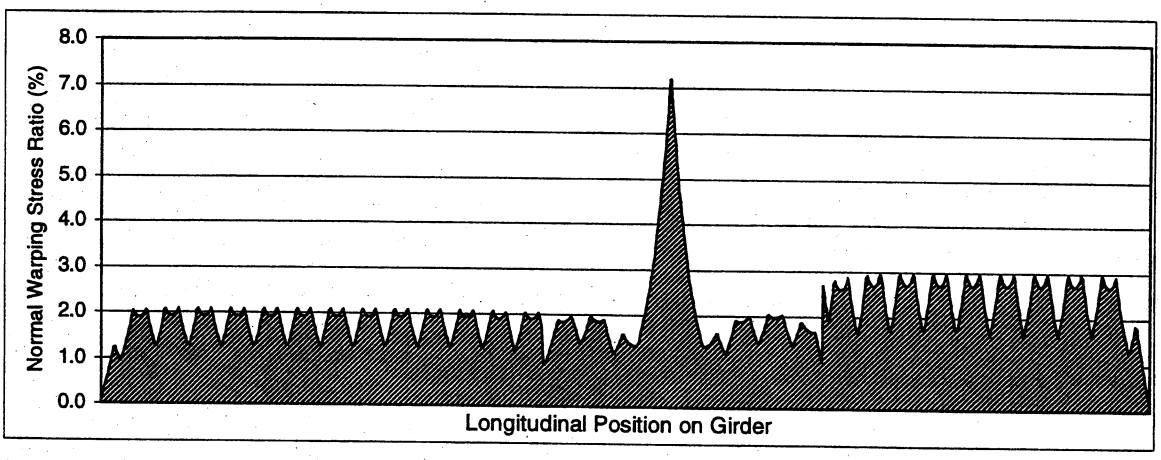

(a)

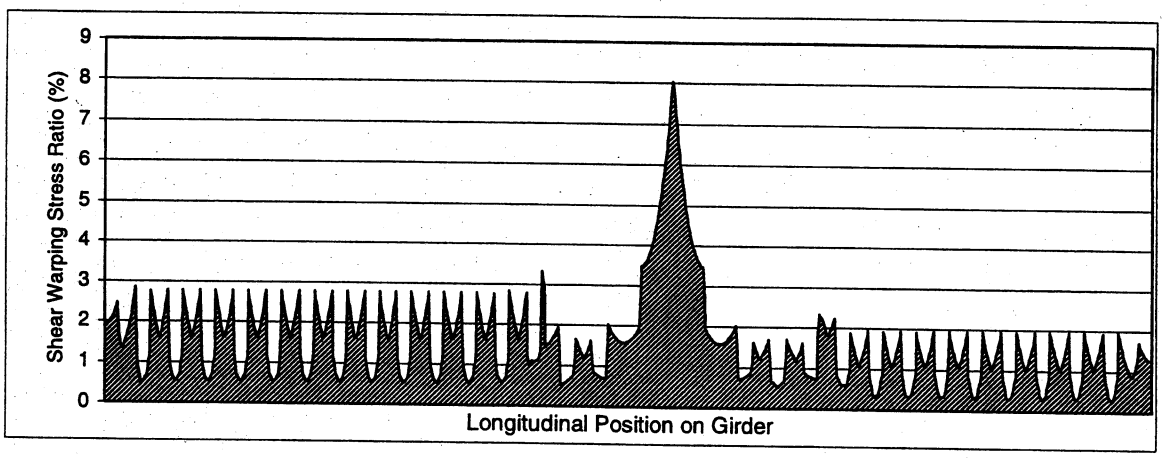

(b)

Figure 111: Warping stress ratios for Br. 525. a) σ_w/σ_T, b) τ_w/τ_T

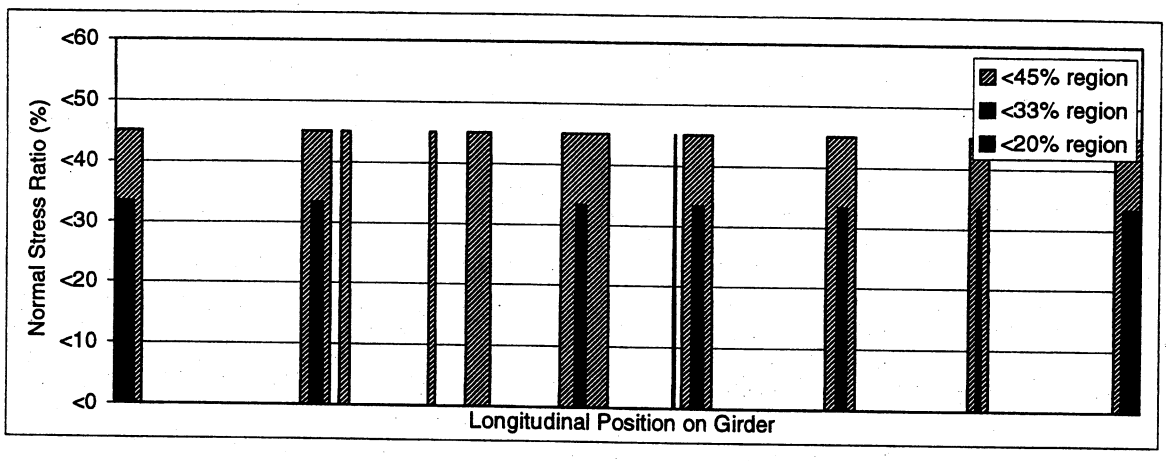

(a)

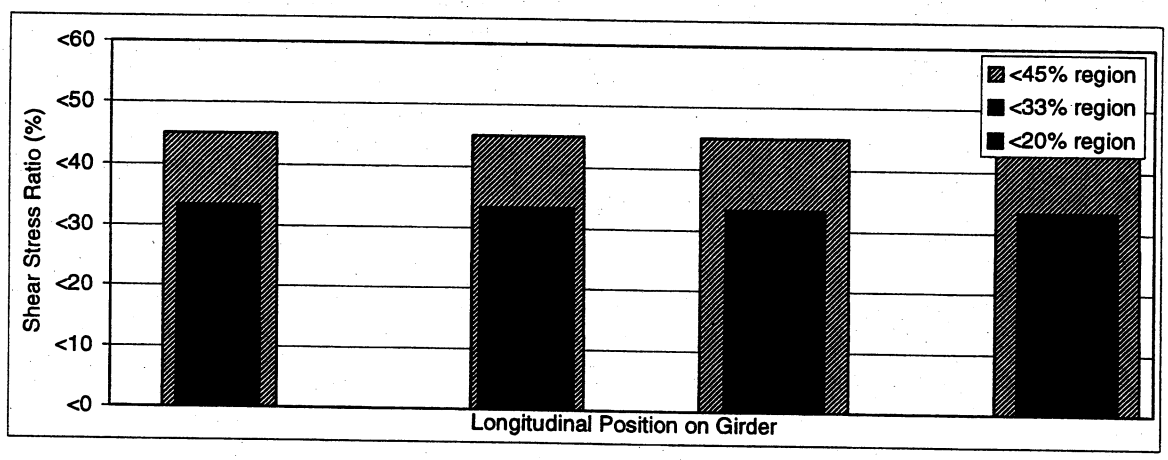

(b)

Figure 112: Regions of low stresses for Br. 598 (a-Approach I, b-Approach II)

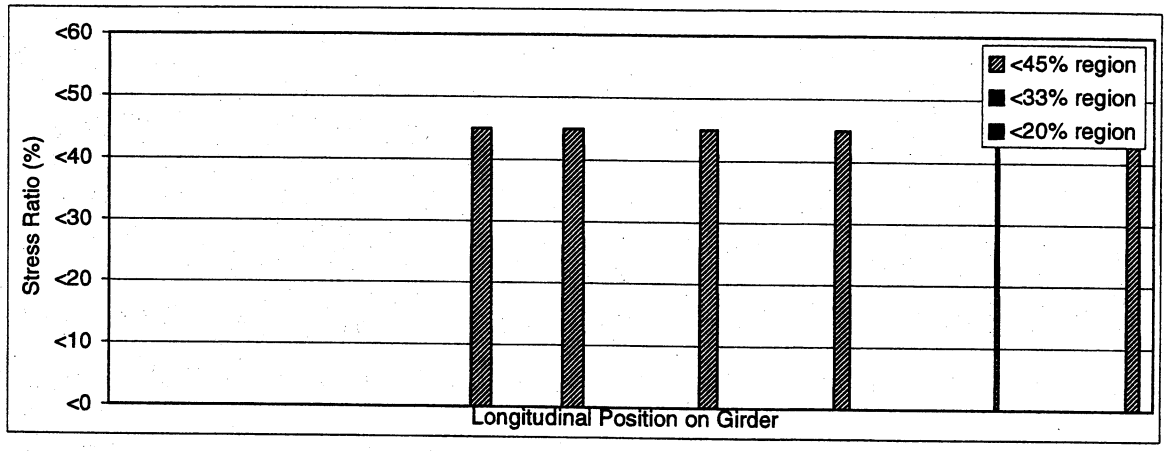

(a)

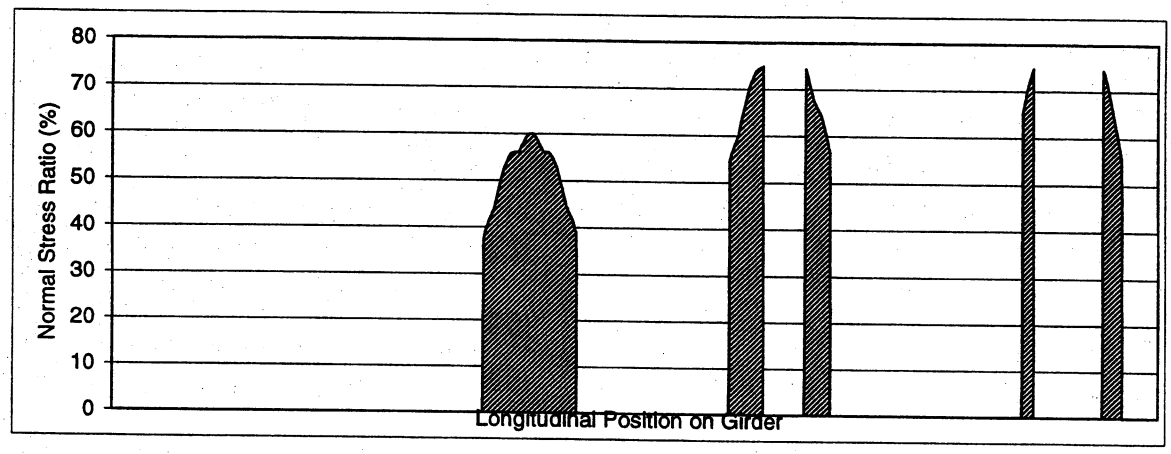

(b)

Figure 113: Regions of low stresses for Br. 598 (a-Approach III, b-Approach IV)

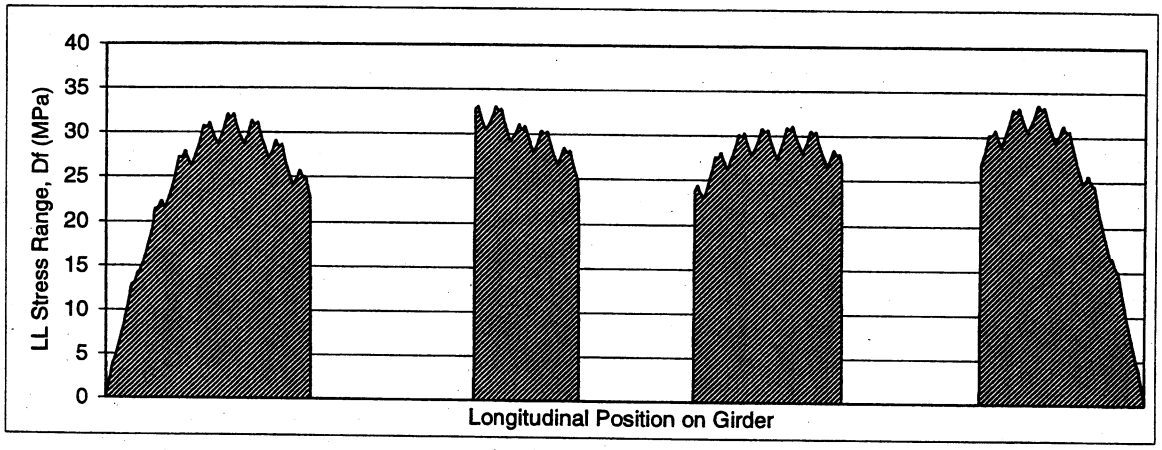

(a)

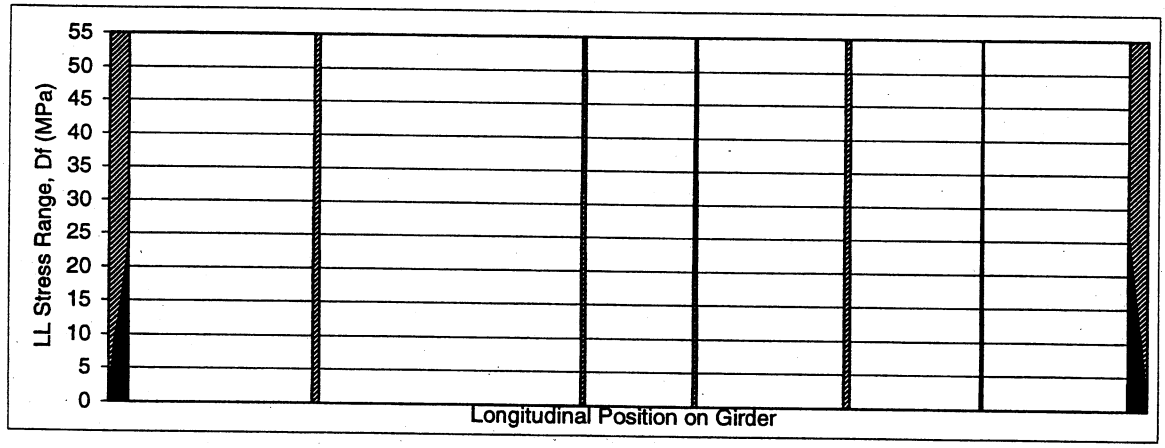

(b)

Figure 114: Br. 598 (a- Live load fatigue stress range,b- Low stress regions according to Approach V)

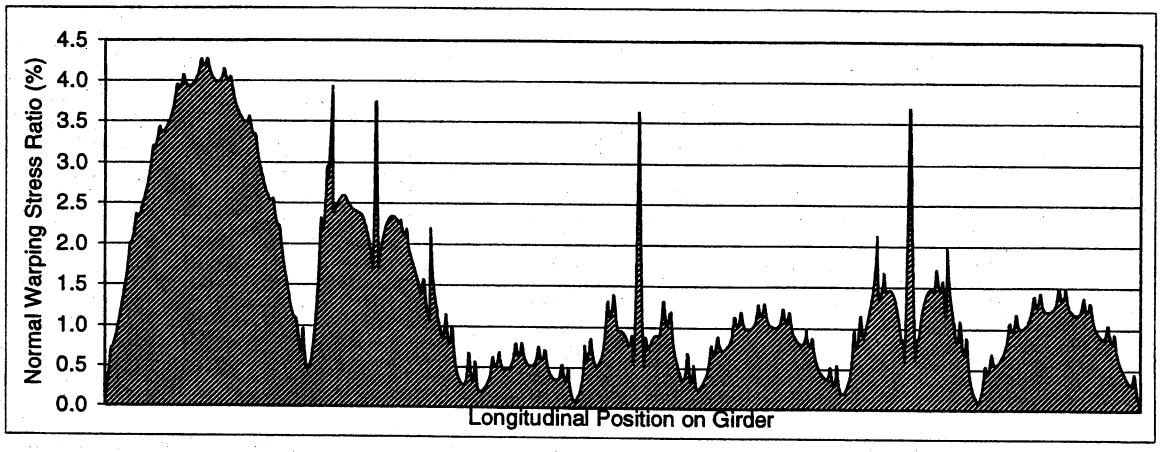

(a)

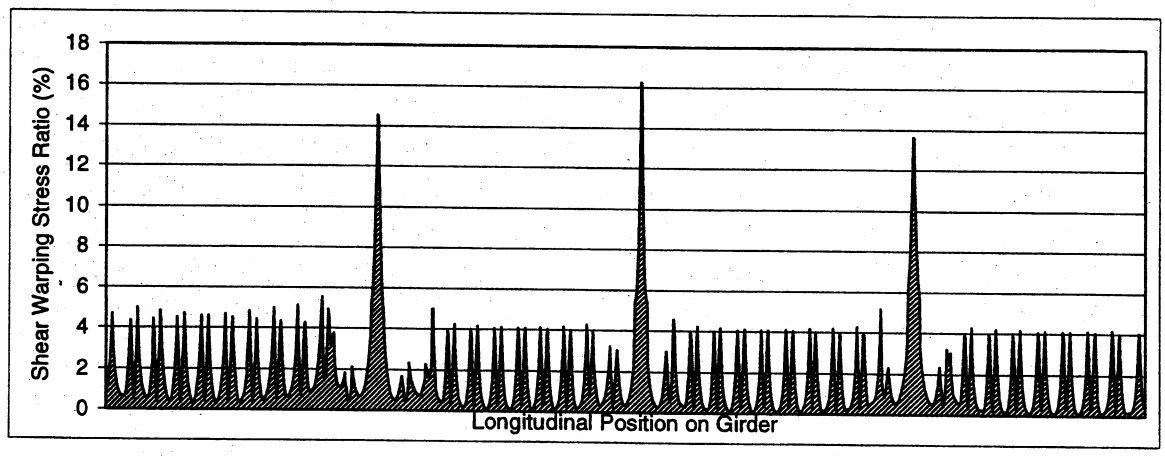

(b)

Figure 115: Warping stress ratios for Br. 598. a) σ_w/σ_T, b) τ_w/τ_T

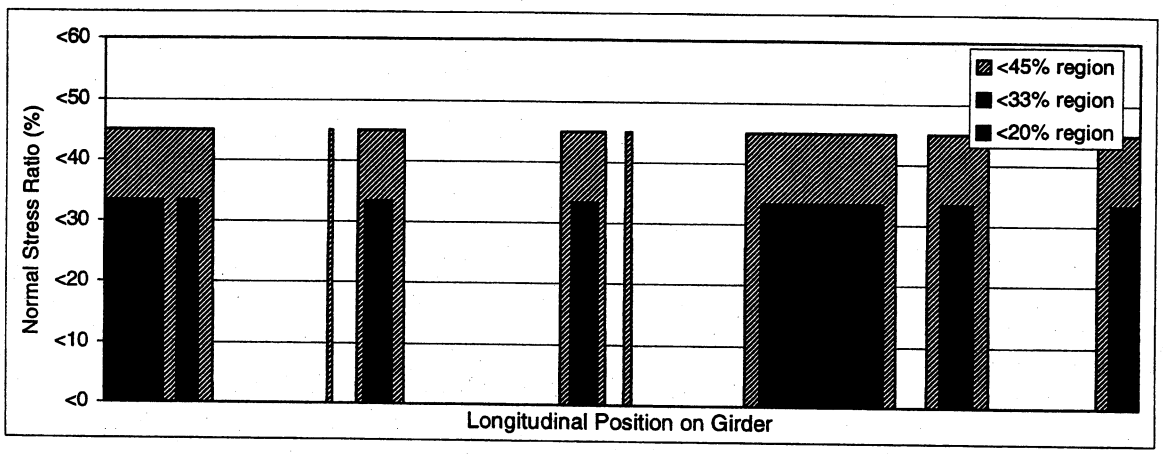

(a)

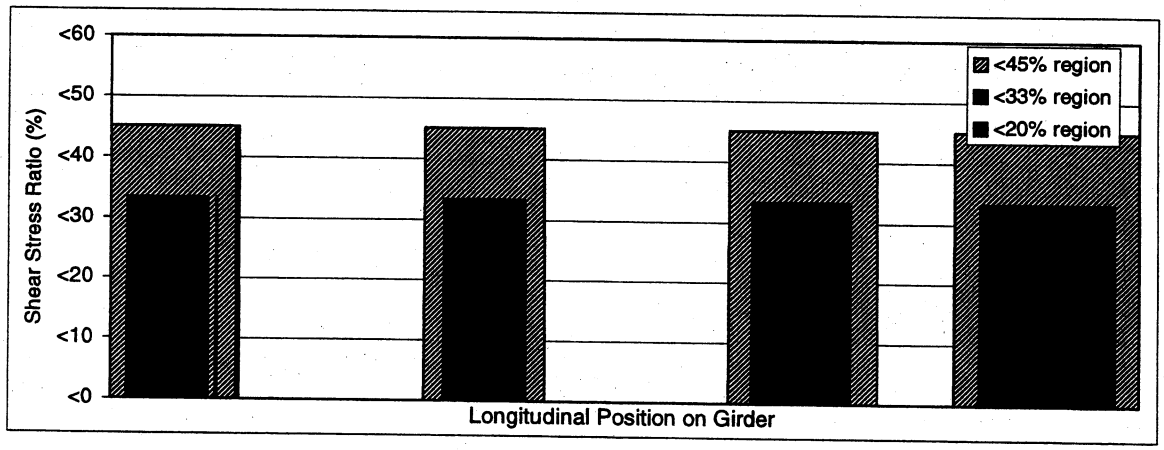

(b)

Figure 116: Regions of low stresses for Br. 601 (a-Approach I, b-Approach II)

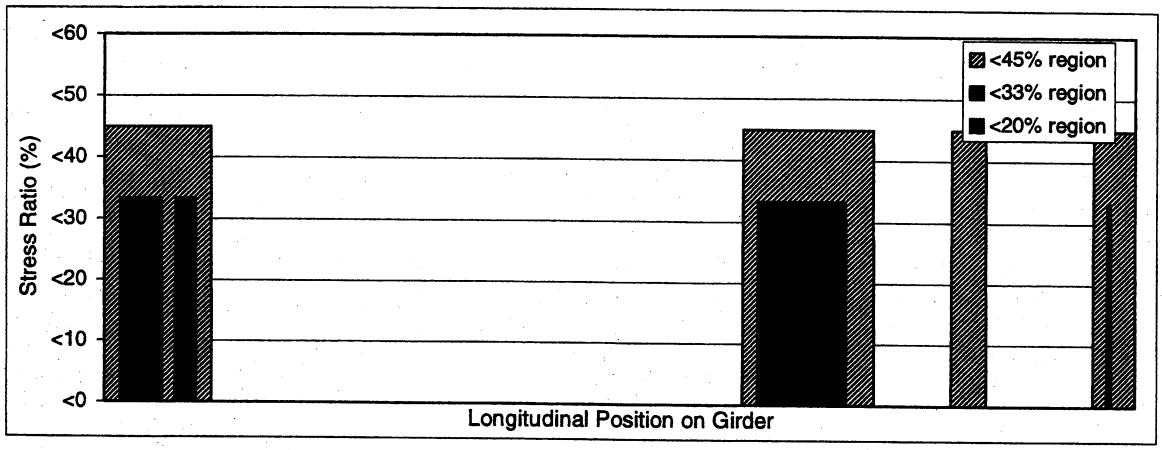

(a)

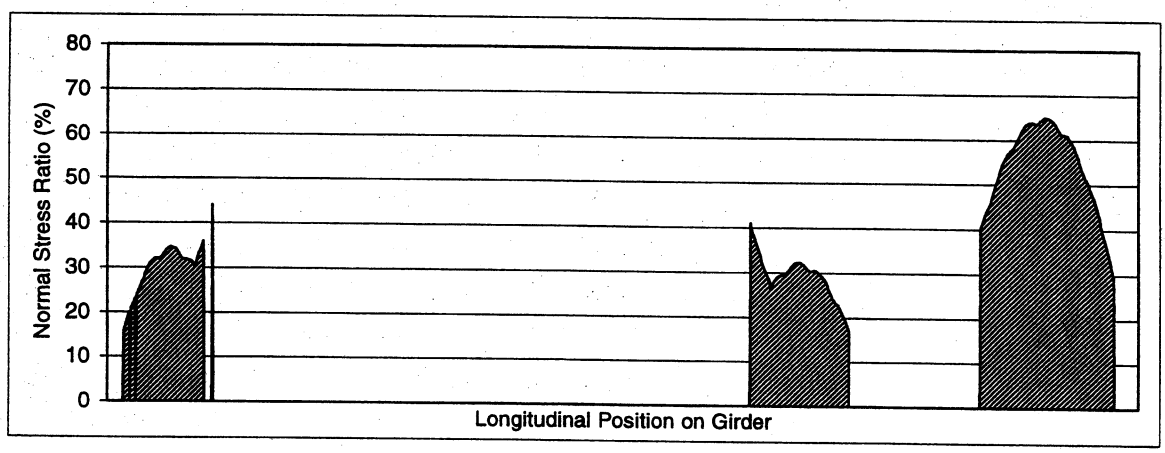

(b)

Figure 117: Regions of low stresses for Br. 601 (a-Approach III, b-Approach IV)

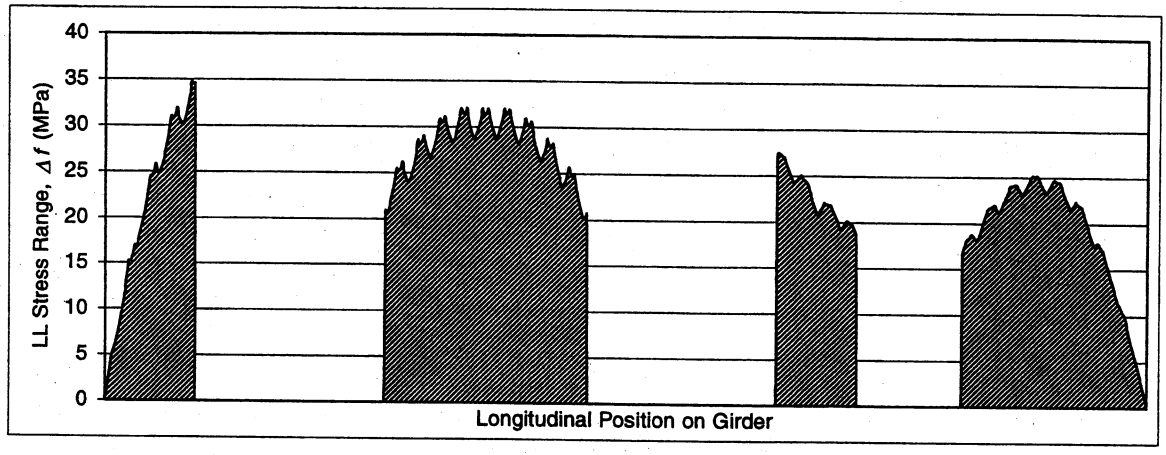

(a)

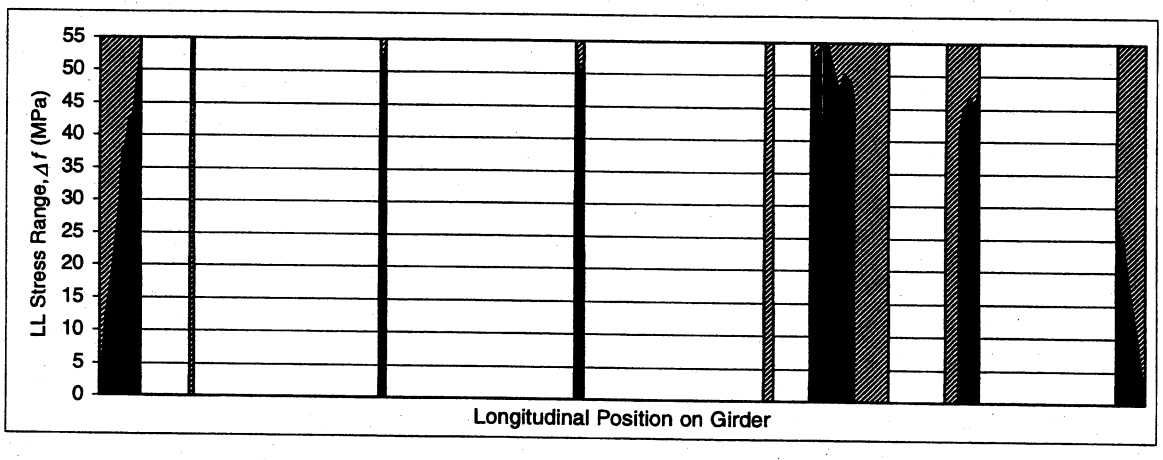

(b)

Figure 118: Br. 601 (a- Live load fatigue stress range,b- Low stress regions according to Approach V)

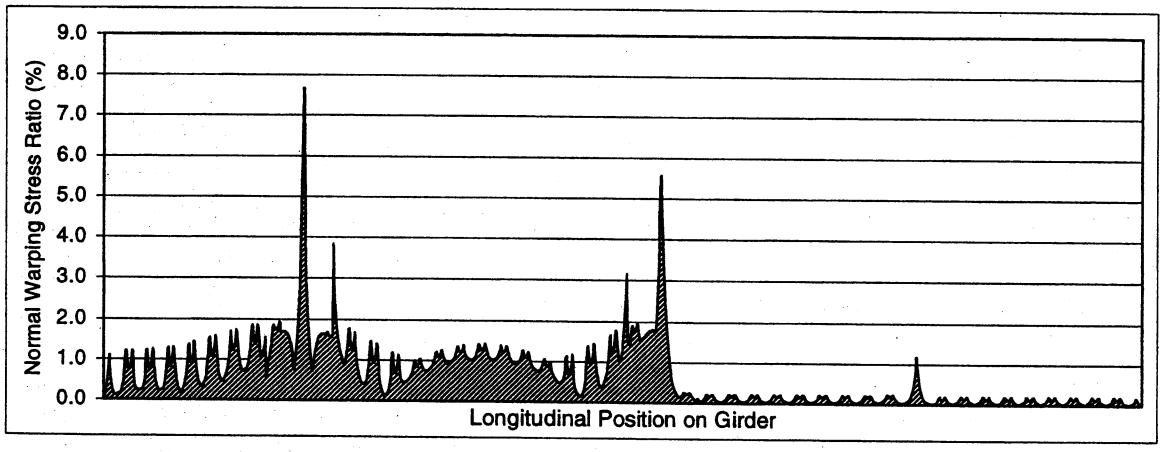

(a)

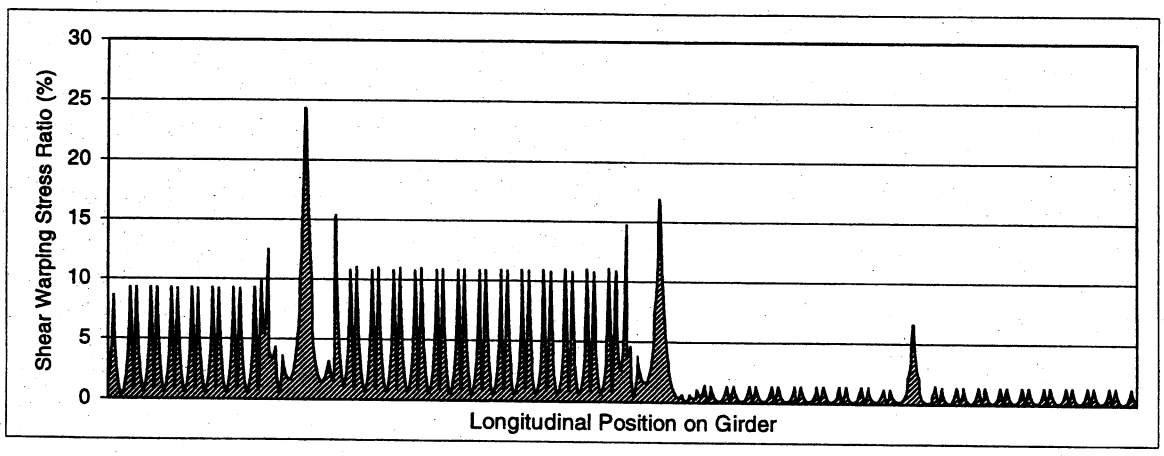

(b)

Figure 119: Warping stress ratios for Br. 601. a) σ_w/σ_T, b) τ_w/τ_T

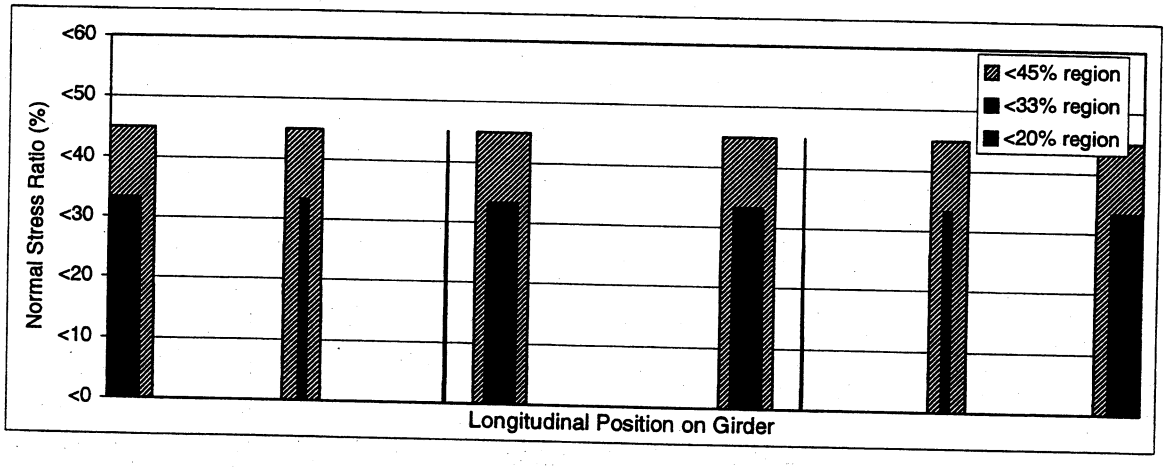

(a)

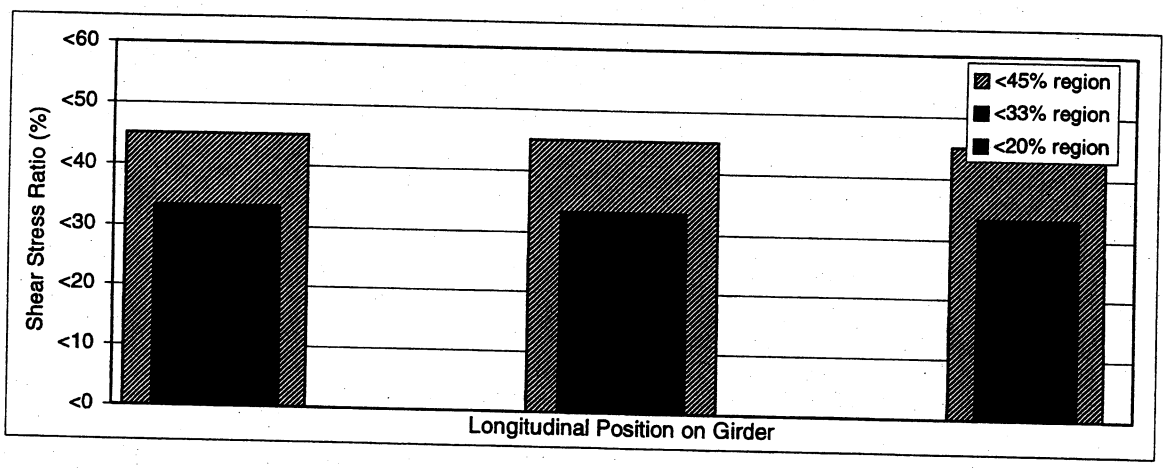

(b)

Figure 120: Regions of low stresses for Br. 606 (a-Approach I, b-Approach II)

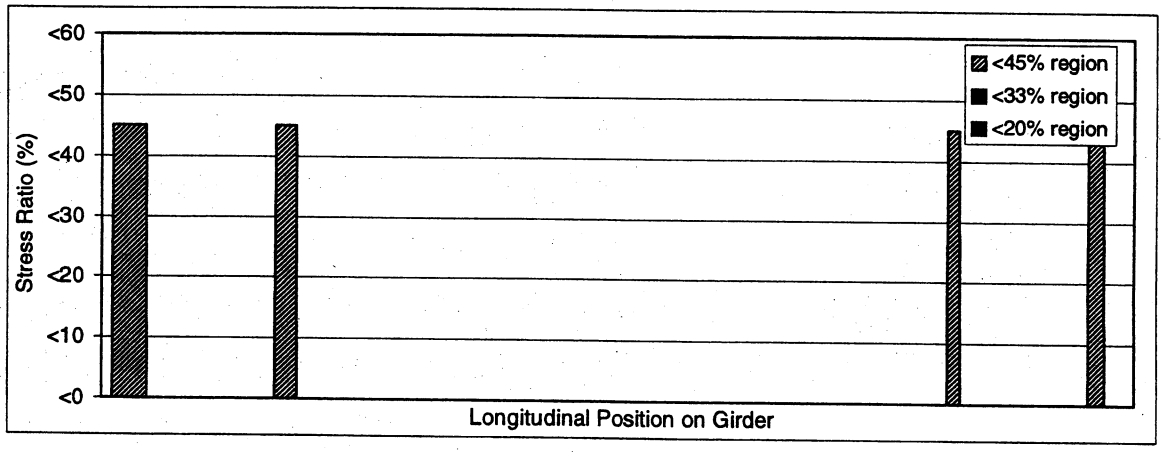

(a)

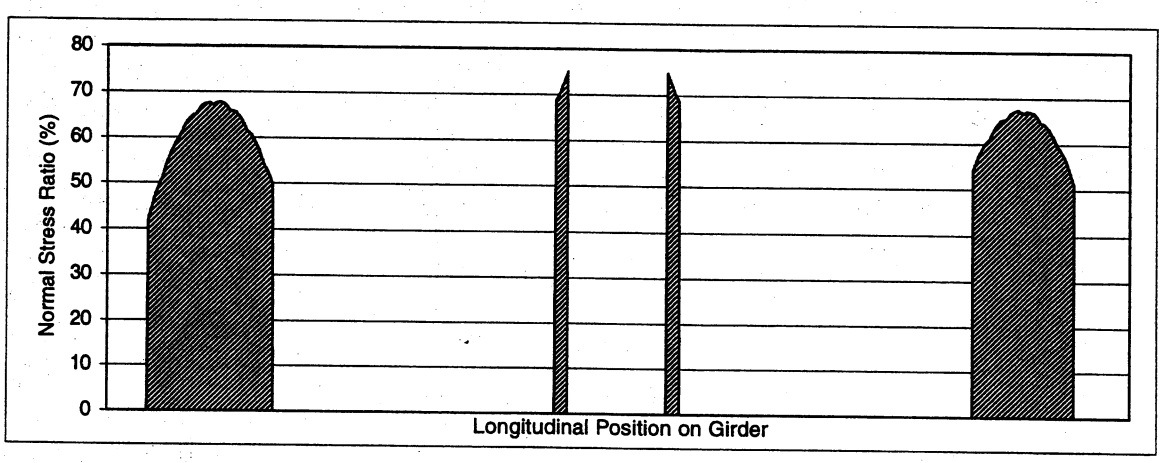

(b)

Figure 121: Regions of low stresses for Br. 606 (a-Approach III, b-Approach IV)

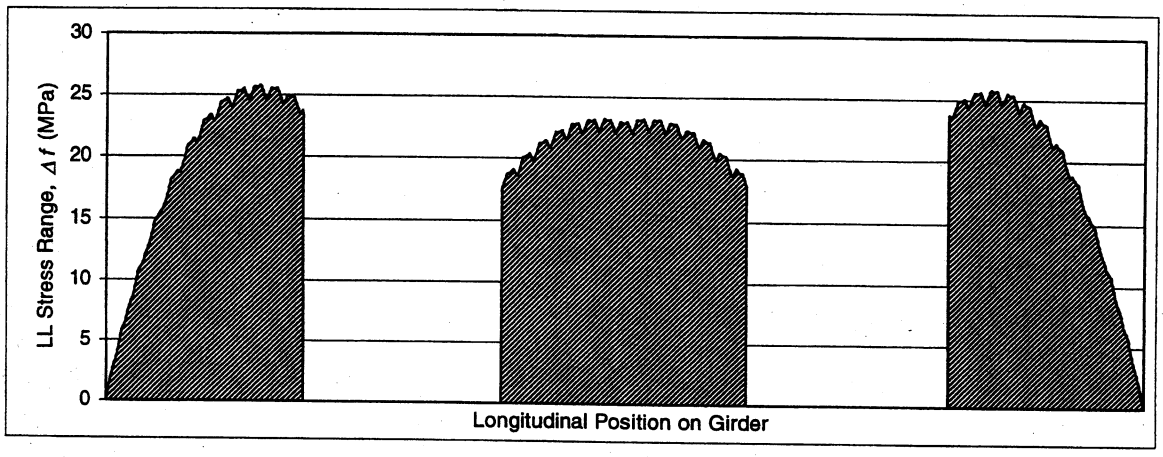

(a)

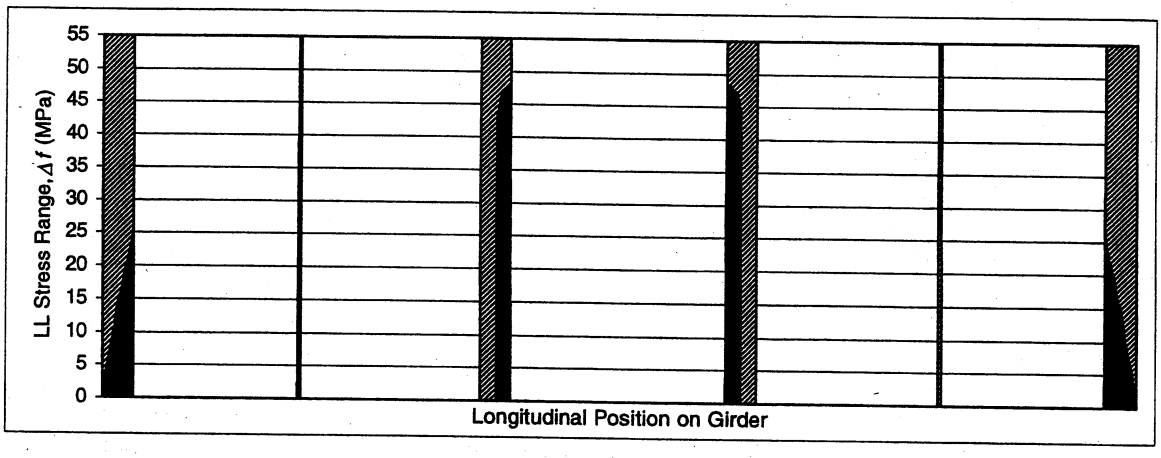

(b)

Figure 122: Br. 606 (a- Live load fatigue stress range,b- Low stress regions according to Approach V)

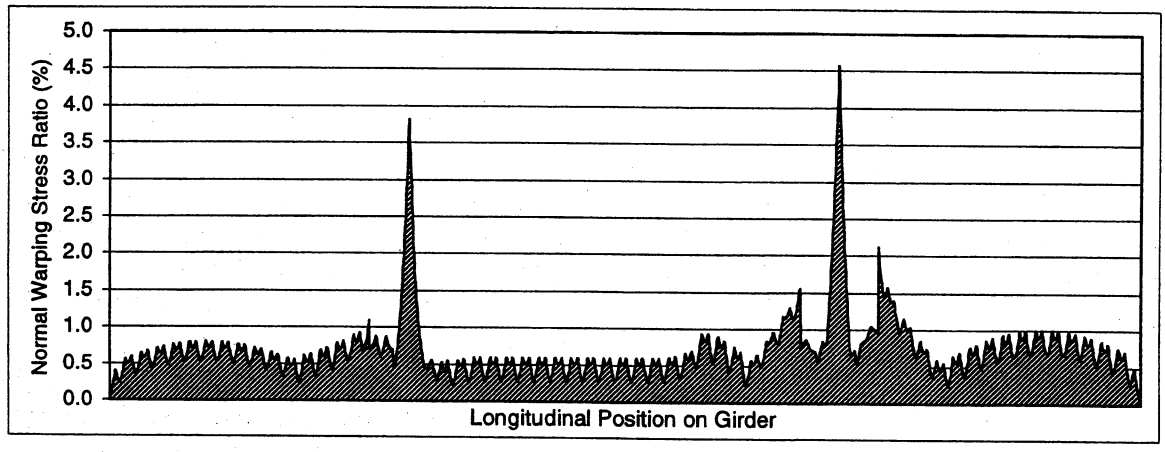

(a)

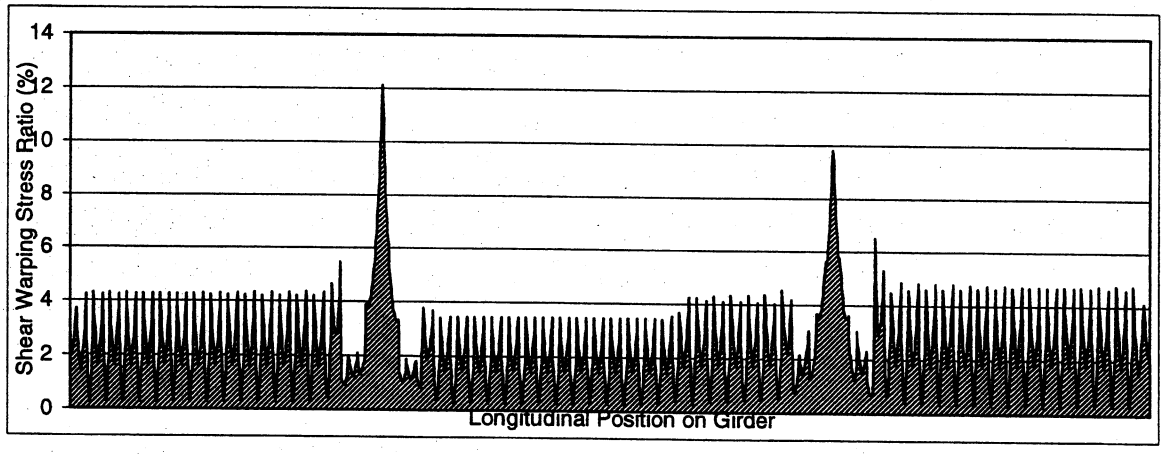

(b)

Figure 123: Warping stress ratios for Br. 606. a) σ_w/σ_T, b) τ_w/τ_T

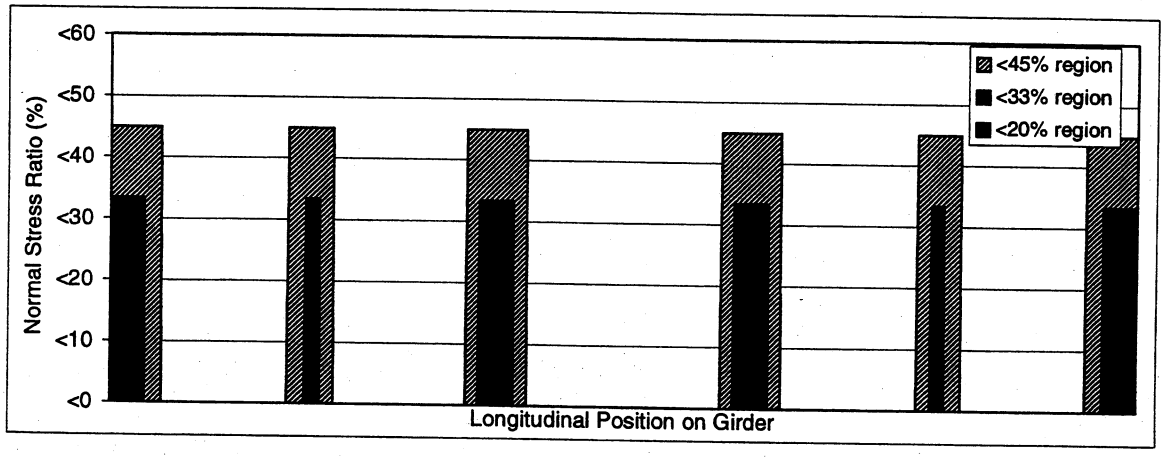

(a)

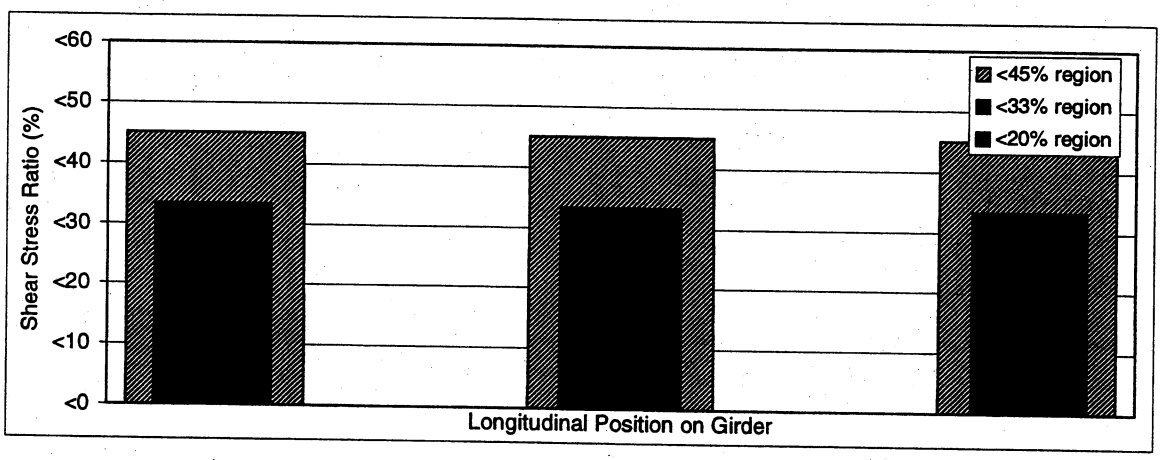

(b)

Figure 124: Regions of low stresses for Br. 607 (a-Approach I, b-Approach II)

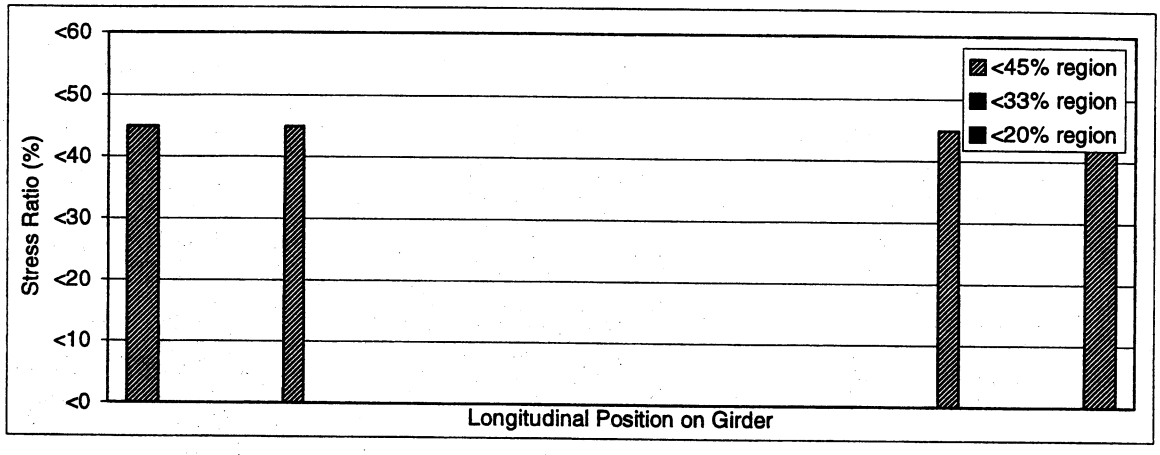

(a)

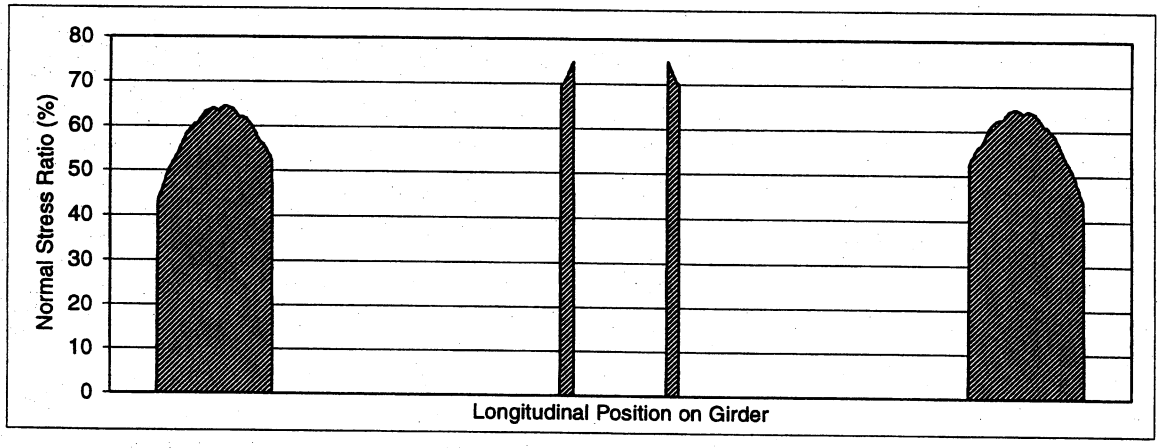

(b)

Figure 125: Regions of low stresses for Br. 607 (a-Approach III, b-Approach IV)

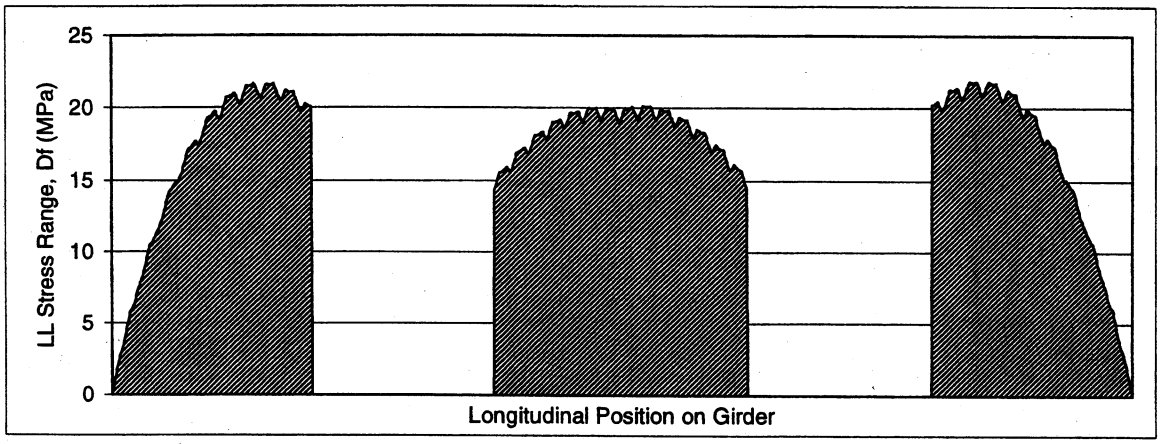

(a)

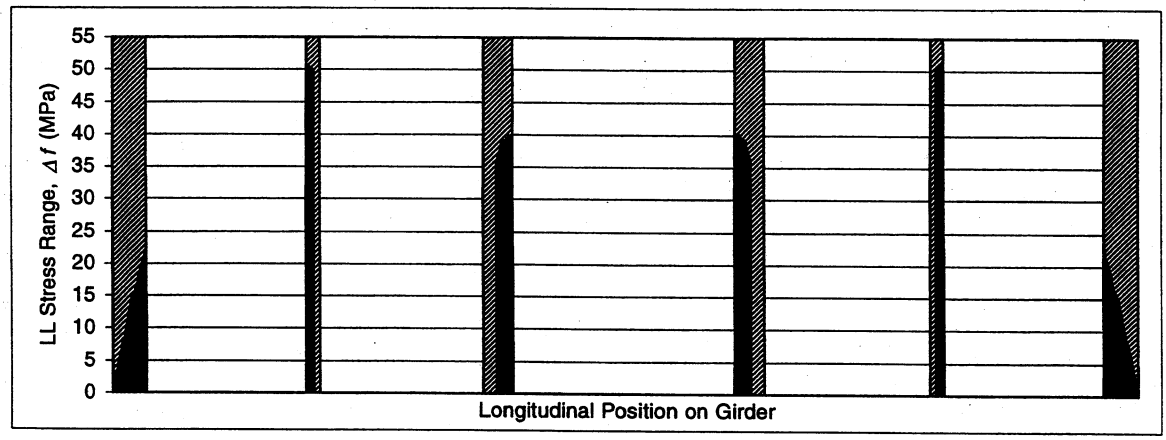

(b)

Figure 126: Br. 607 (a- Live load fatigue stress range,b- Low stress regions according to Approach V)

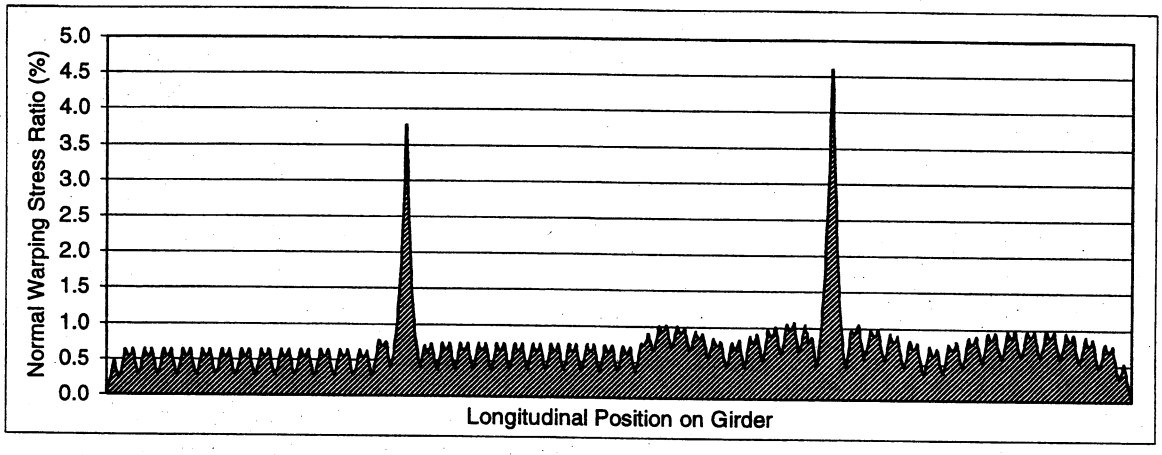

(a)

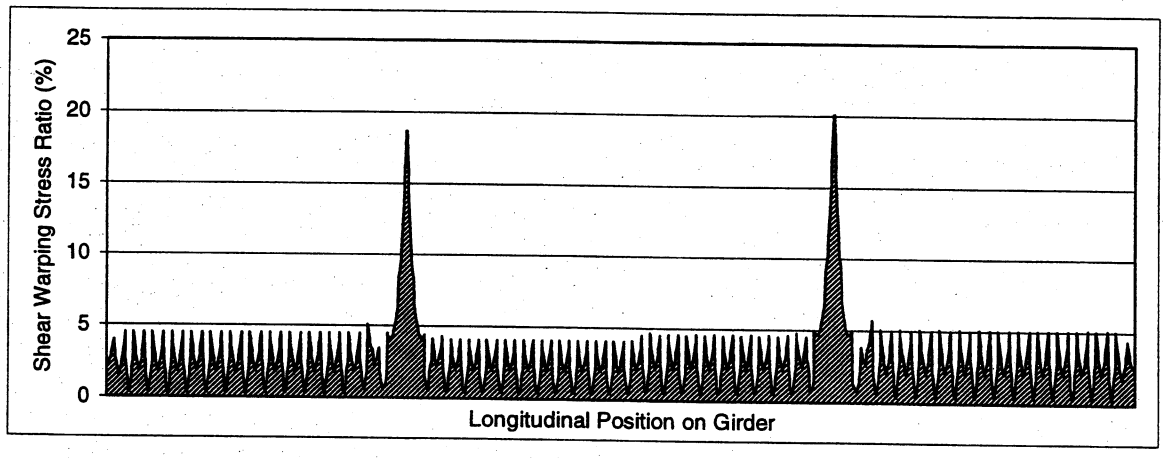

(b)

Figure 127: Warping stress ratios for Br. 607. a) σ_w/σ_T, b) τ_w/τ_T

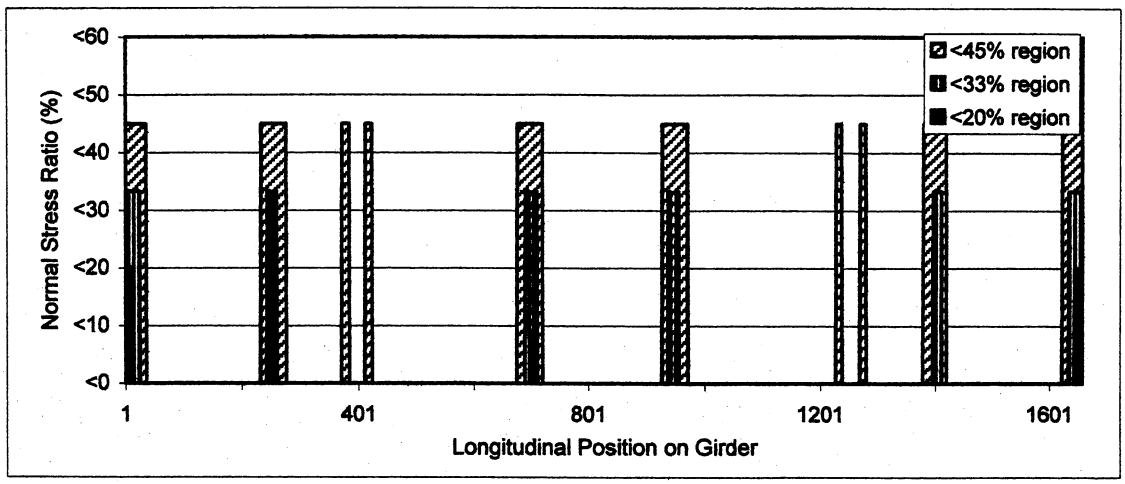

(a)

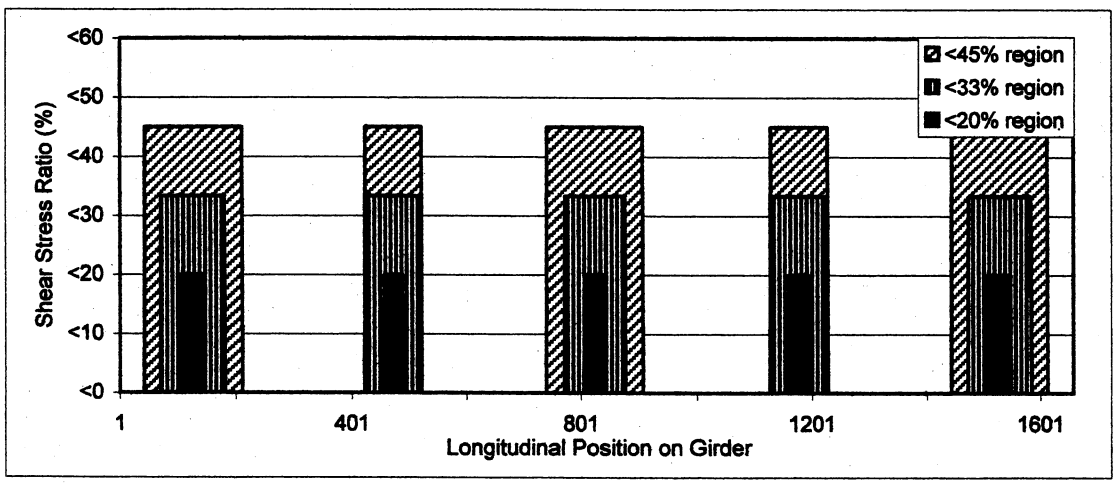

(b)

Figure 128: Regions of low stresses for Br.528 (a-Approach I, b-Approach II)

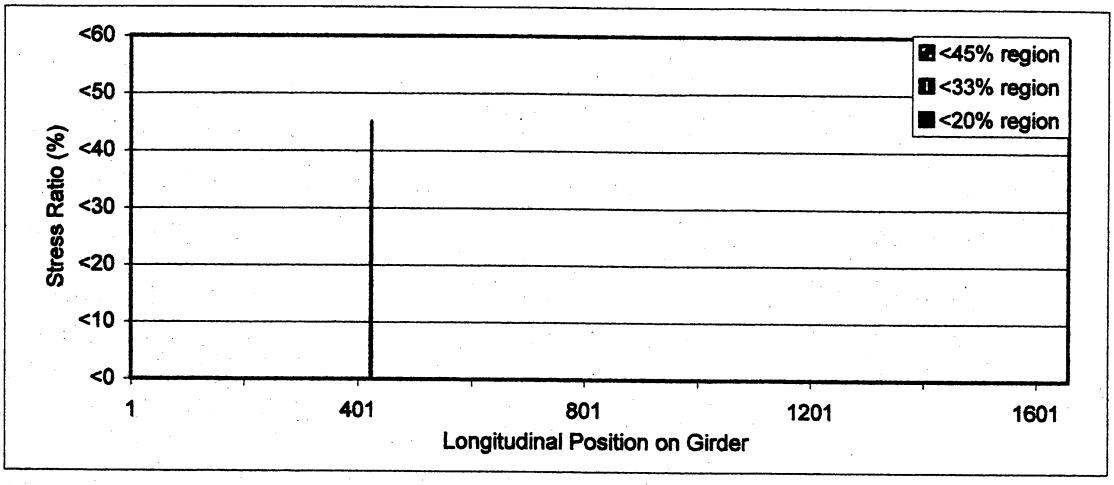

(a)

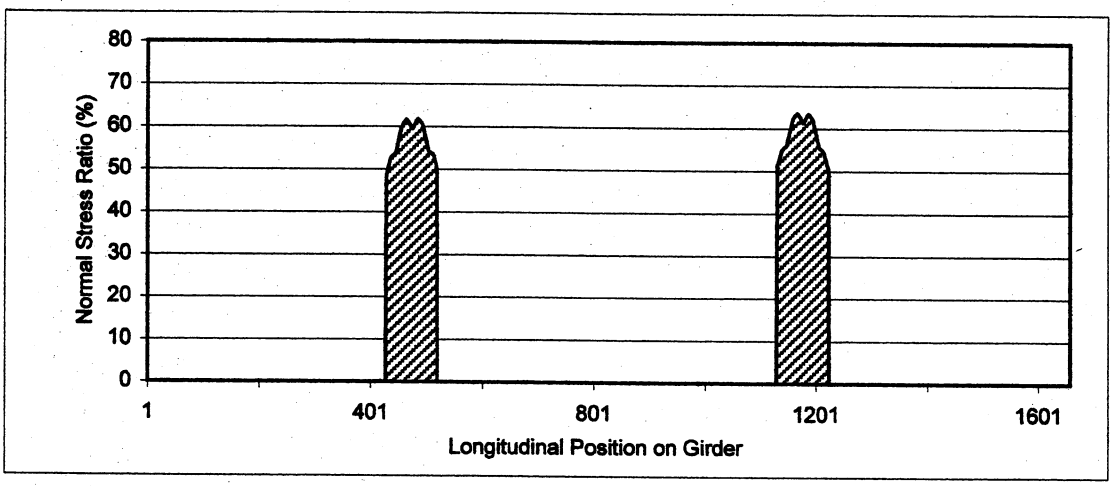

(b)

Figure 129: Regions of low stresses for Br.528 (a-Approach III, b-Approach IV)

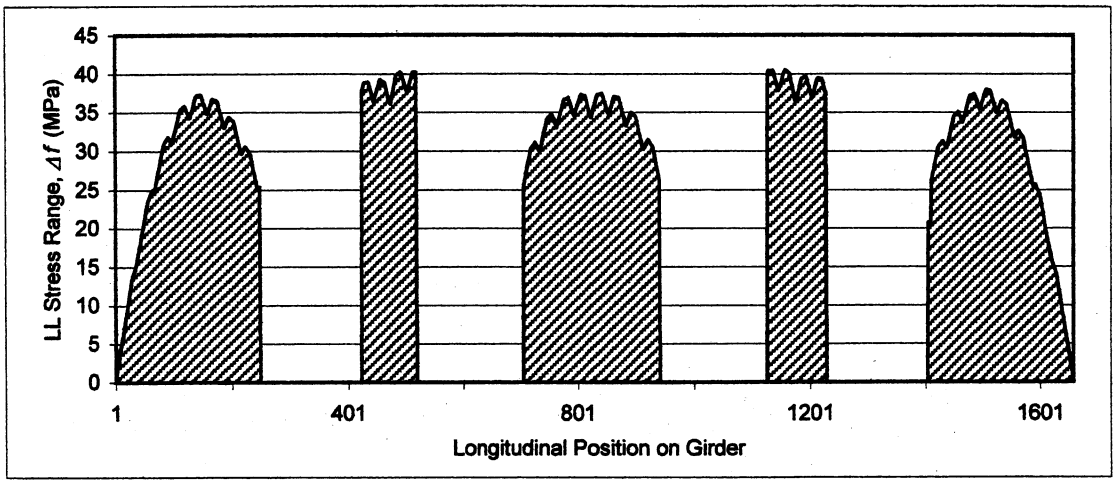

(a)

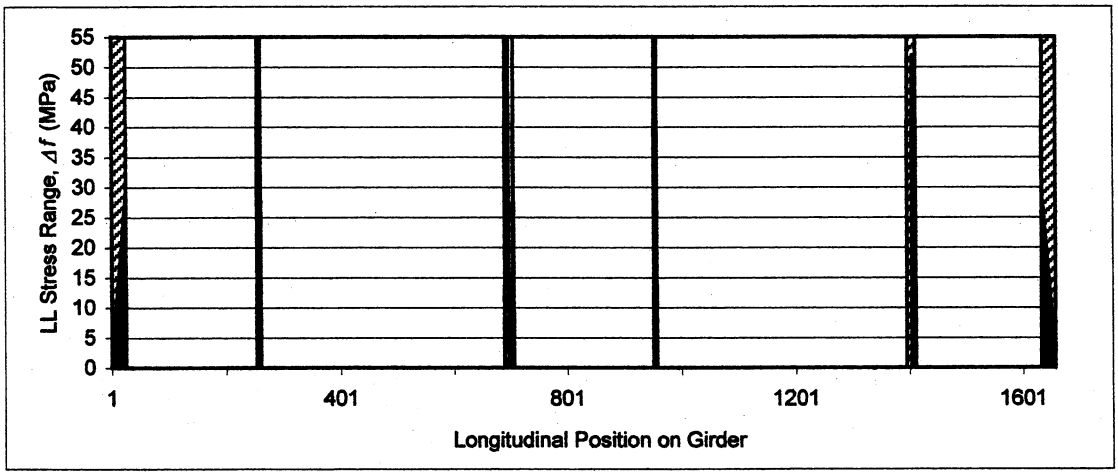

(b)

Figure 130: Br.528 (a-Live load fatigue stress range, b-Low stress regions according to Approach V)

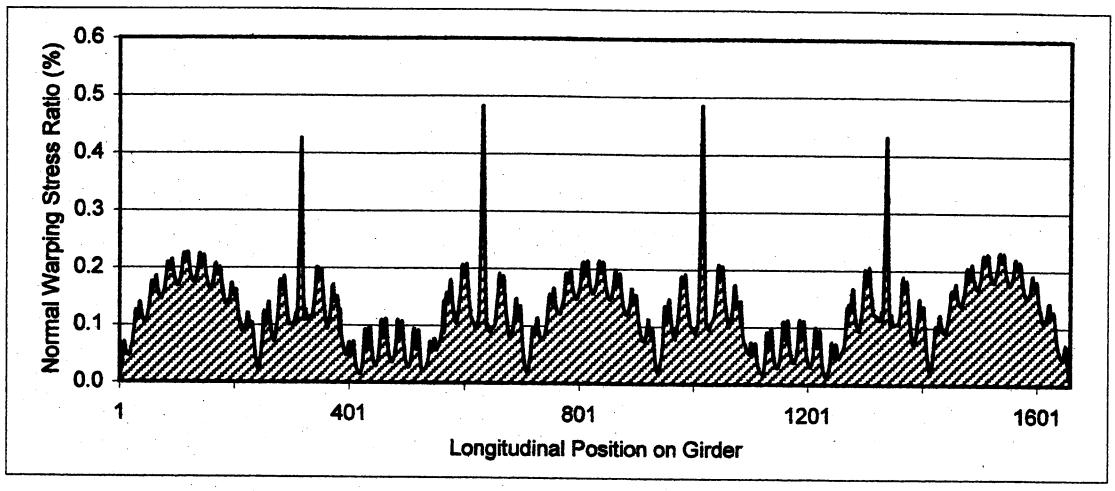

(a)

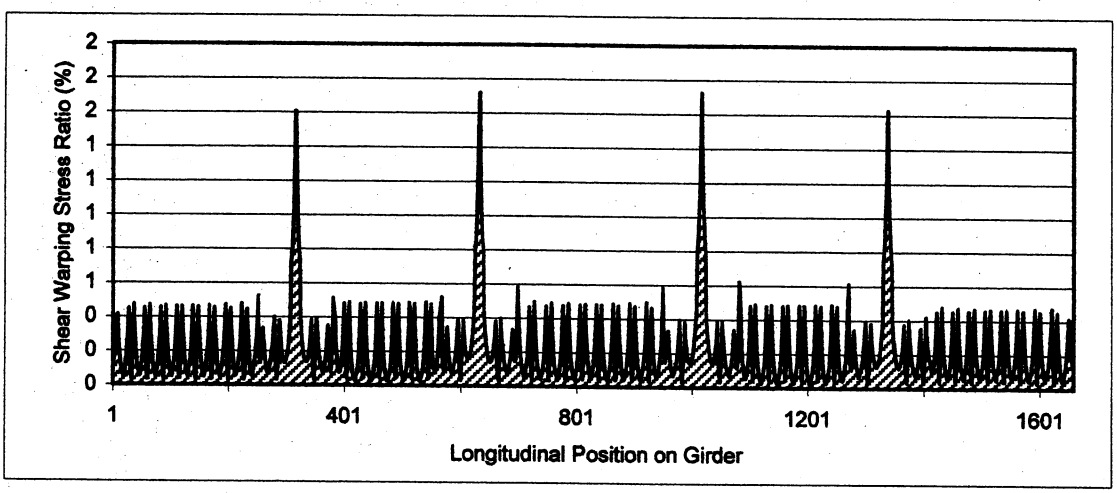

(b)

Figure 131: Warping stress ratios for Br.528
a) σ_ω / σ_T, b) τ_ω / τ_T)

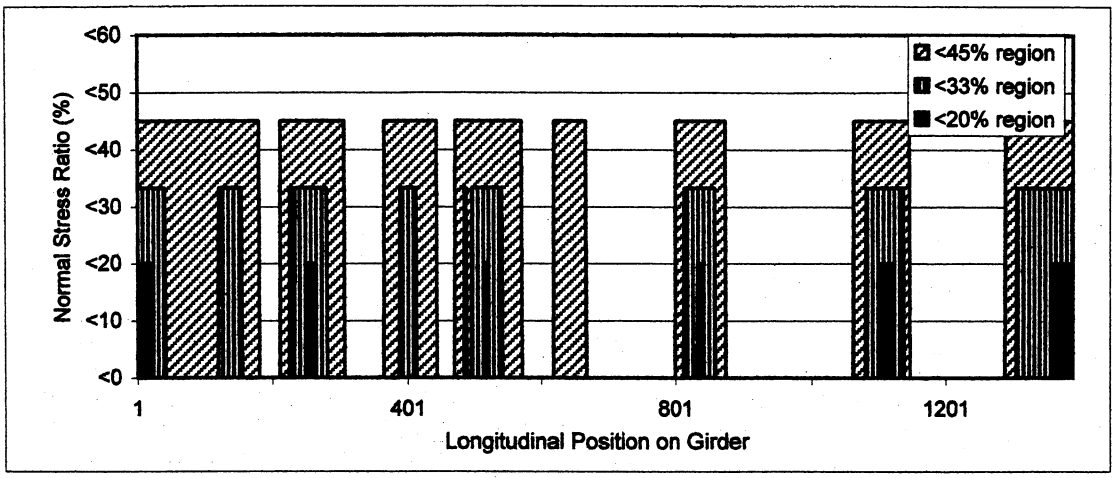

(a)

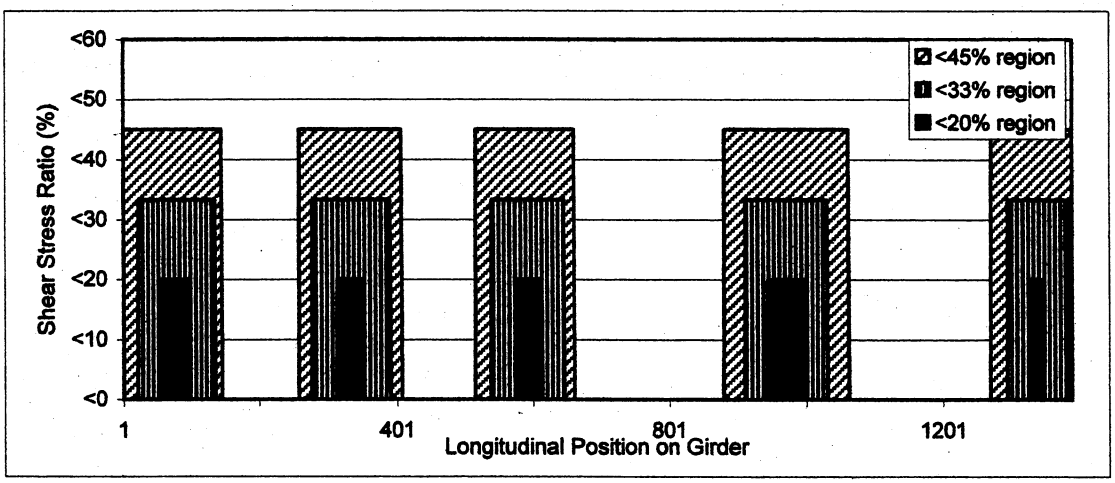

(b)

Figure 132: Regions of low stresses for Br.537 (a-Approach I, b-Approach II)

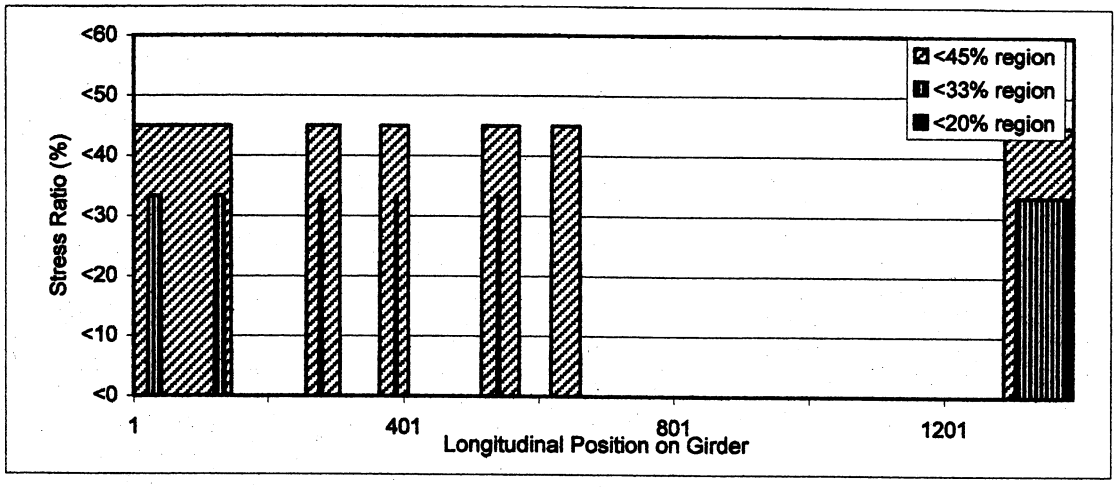

(a)

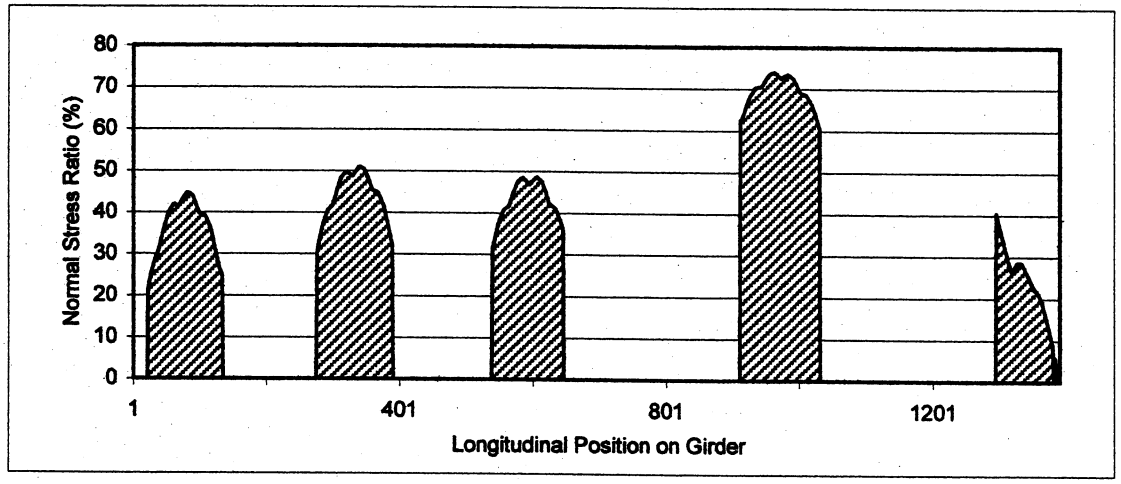

(b)

Figure 133: Regions of low stresses for Br.537 (a-Approach III, b-Approach IV)

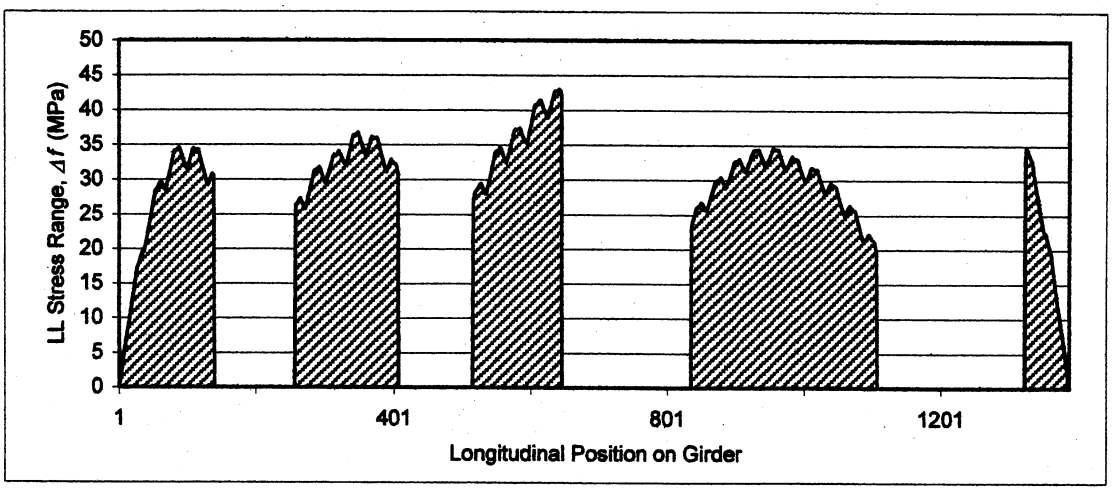

(a)

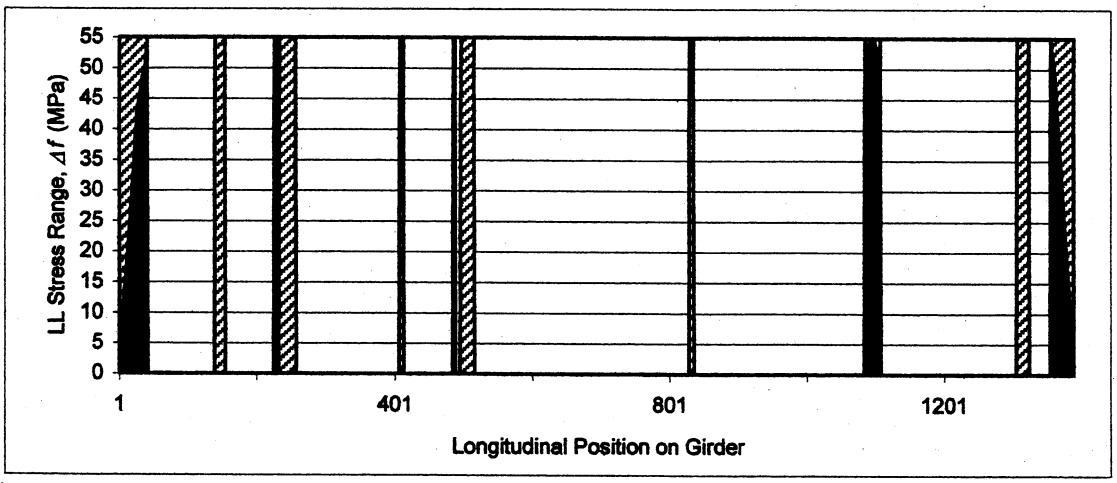

(b)

Figure 134: Br.537 (a-Live load fatigue stress range, b-Low stress regions according to Approach V)

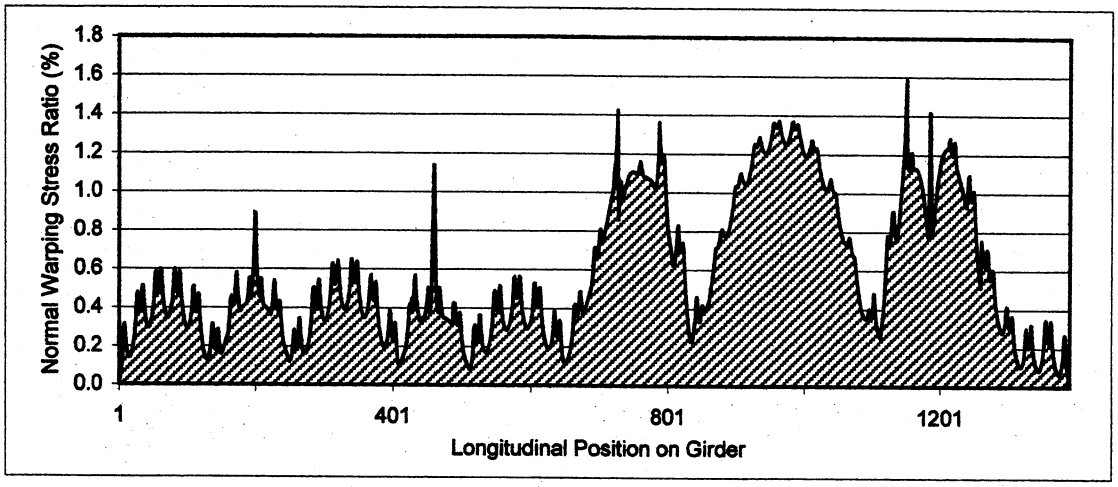

(a)

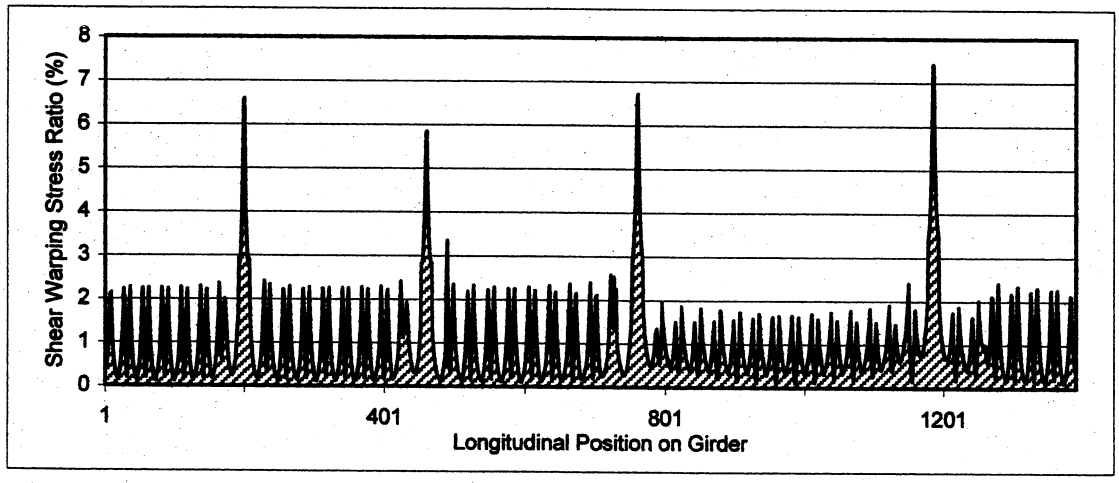

(b)

Figure 135: Warping stress ratios for Br.537
a) σ_ω / σ_T, b) τ_ω / τ_T)

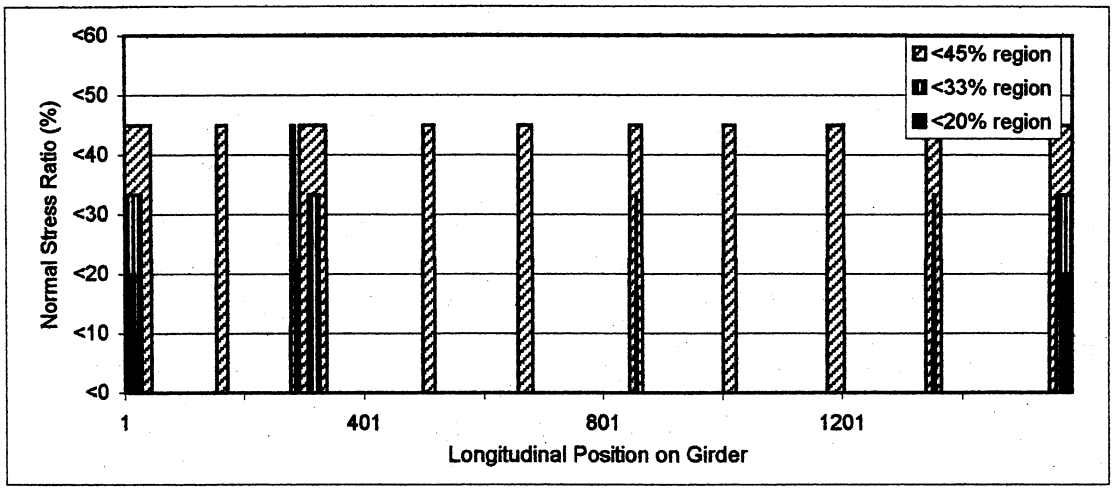

(a)

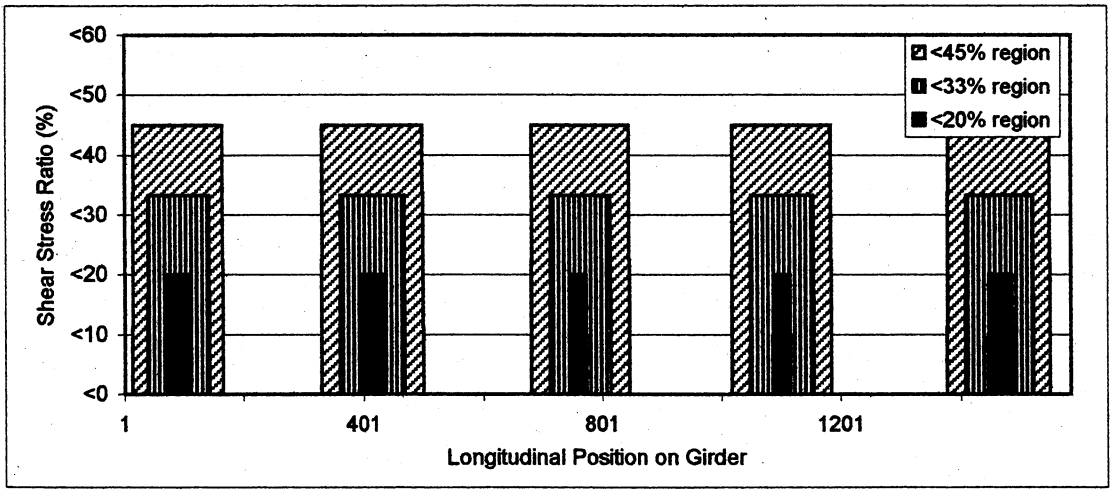

(b)

Figure 136: Regions of low stresses for Br.538a (a-Approach I, b-Approach II)

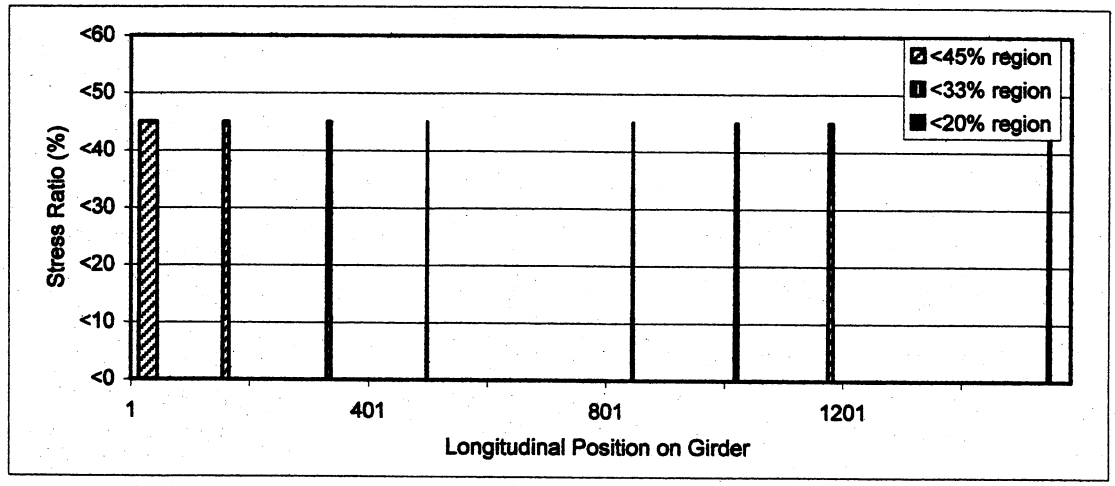

(a)

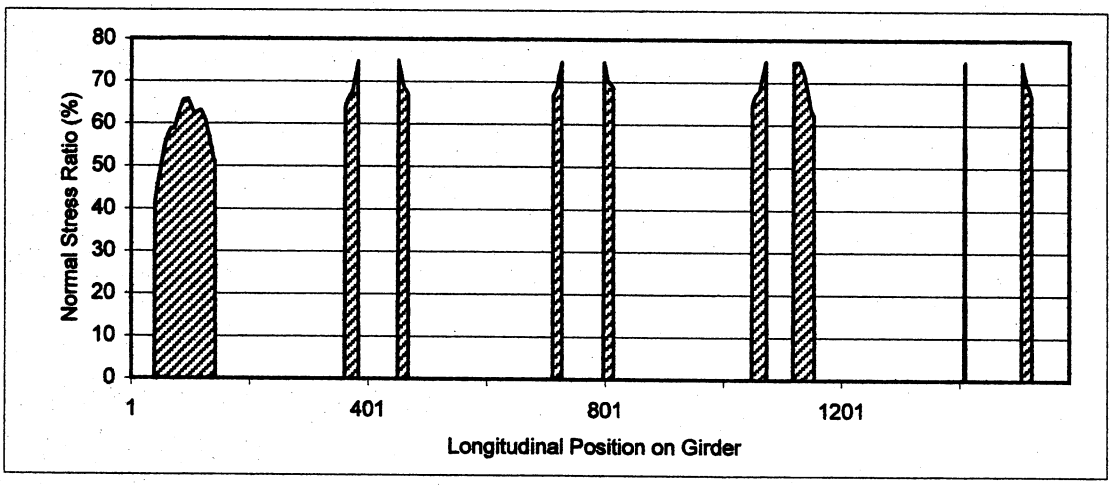

(b)

Figure 137: Regions of low stresses for Br.538a (a-Approach III, b-Approach IV)

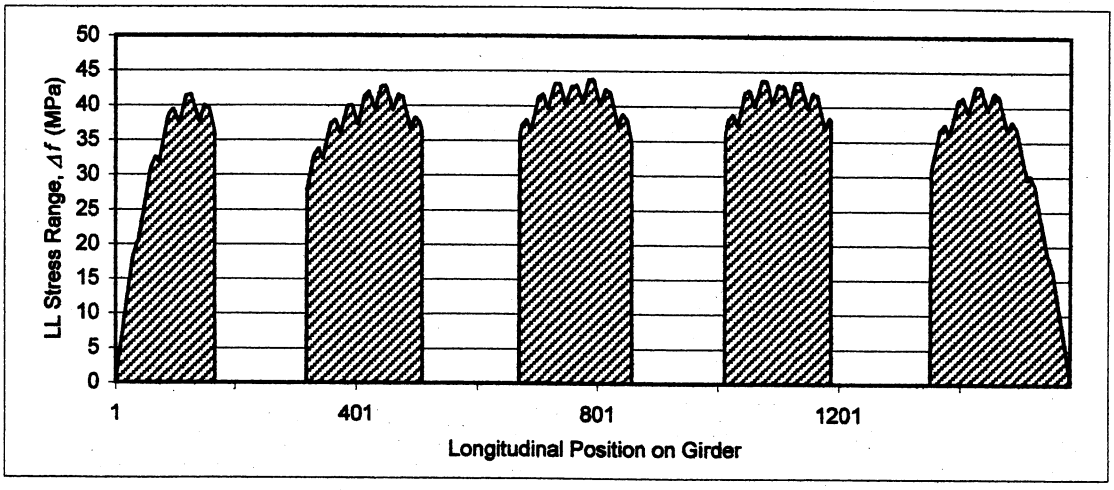

(a)

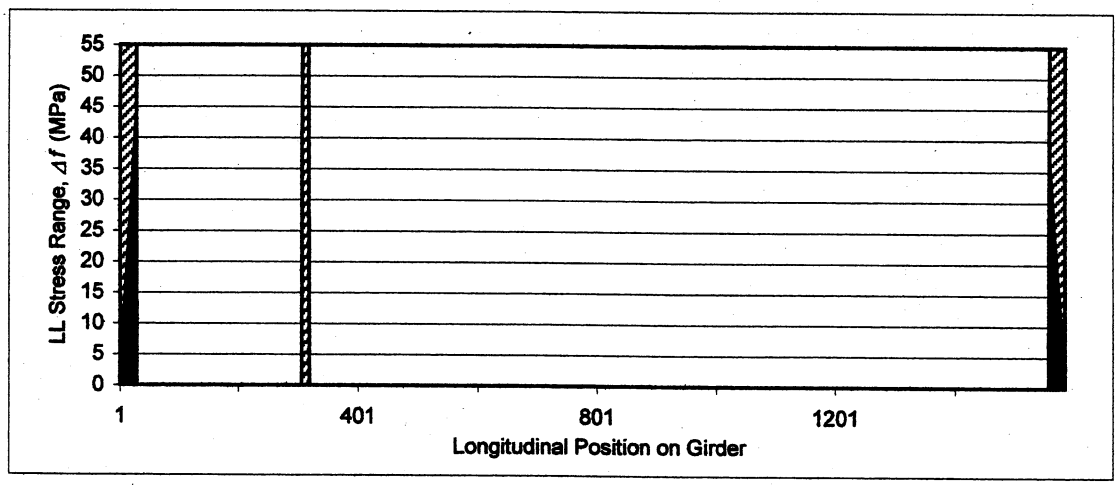

(b)

Figure 138: Br.538a (a-Live load fatigue stress range, b-Low stress regions according to Approach V)

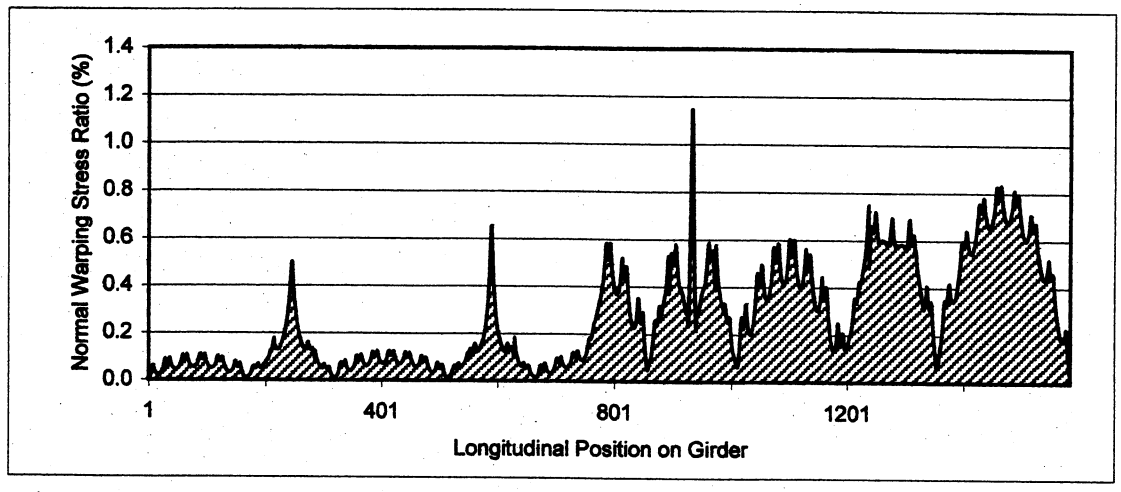

(a)

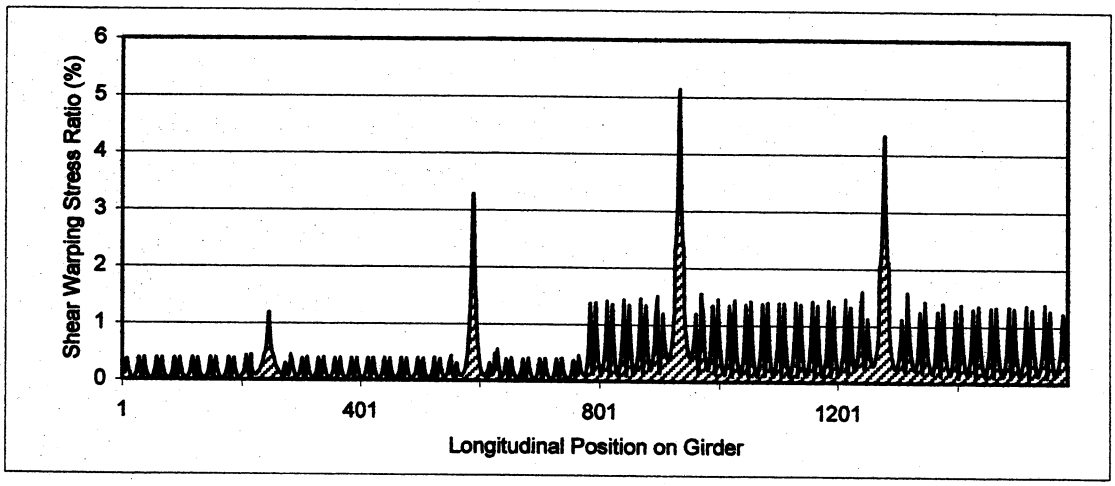

(b)

Figure 139: Warping stress ratios for Br.538a
a) σ_ω / σ_T, b) τ_ω / τ_T)

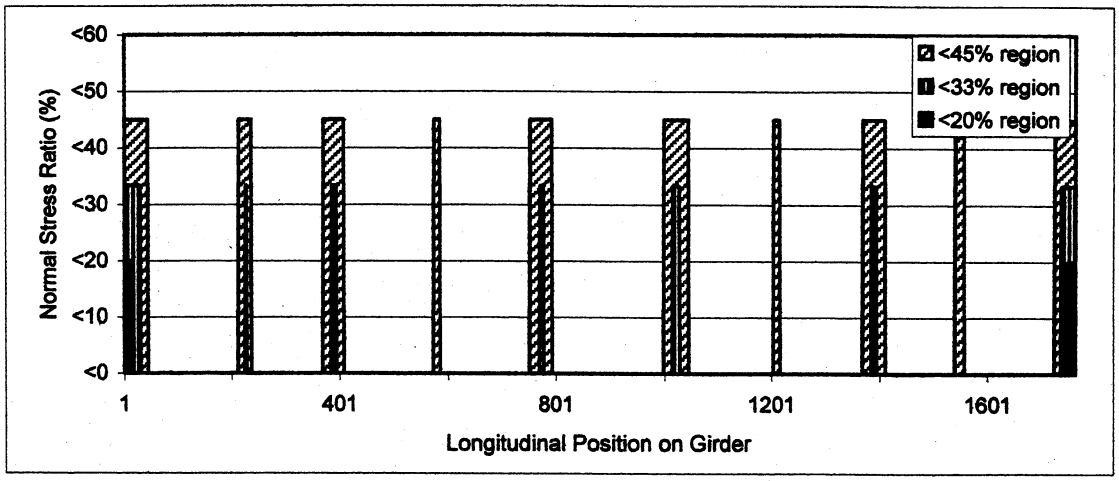

(a)

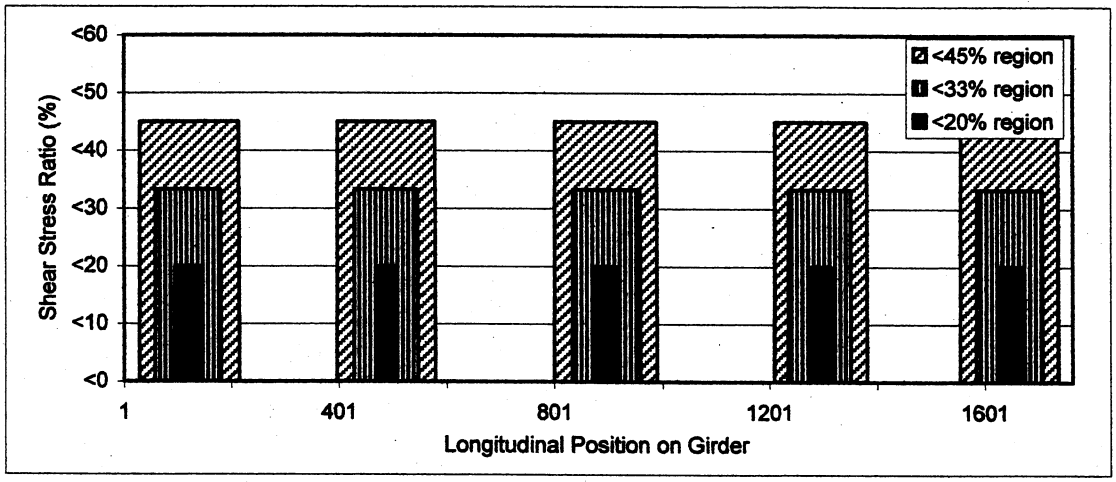

(b)

Figure 140: Regions of low stresses for Br.538b (a-Approach I, b-Approach II)

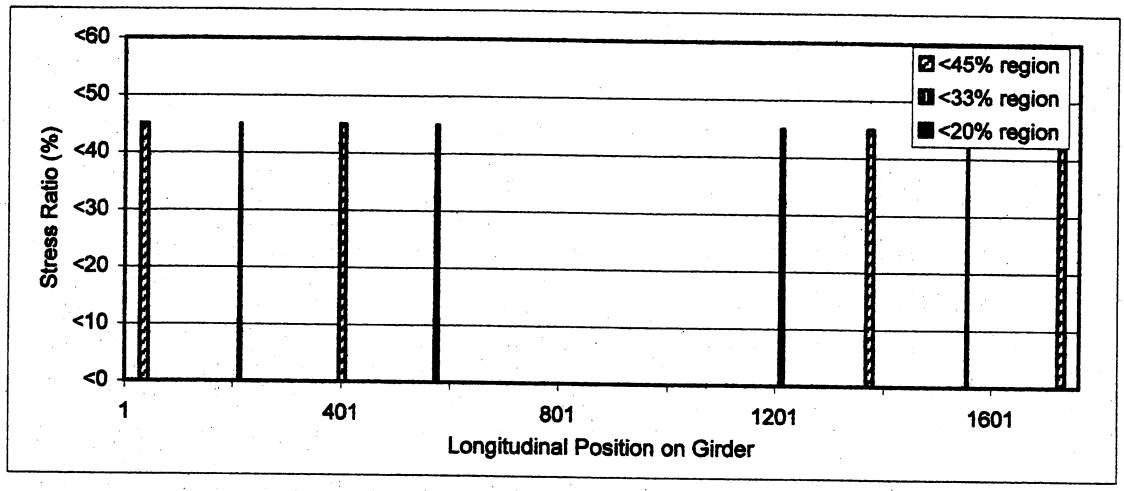

(a)

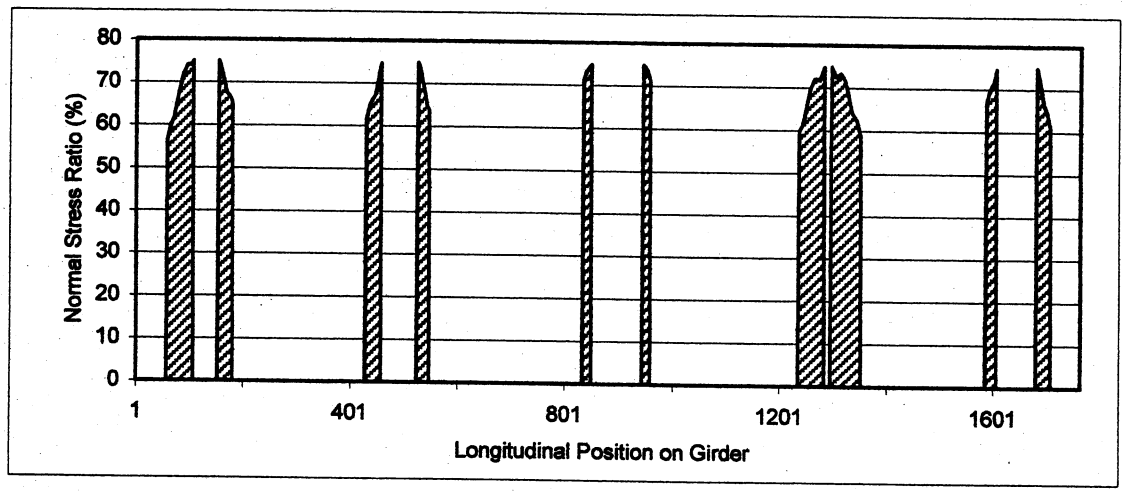

(b)

Figure 141: Regions of low stresses for Br.538b (a-Approach III, b-Approach IV)

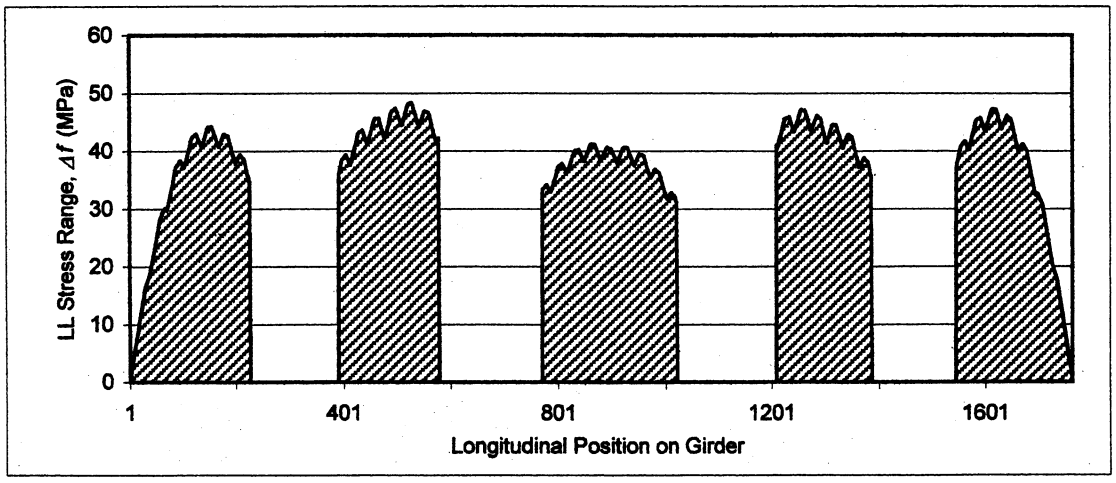

(a)

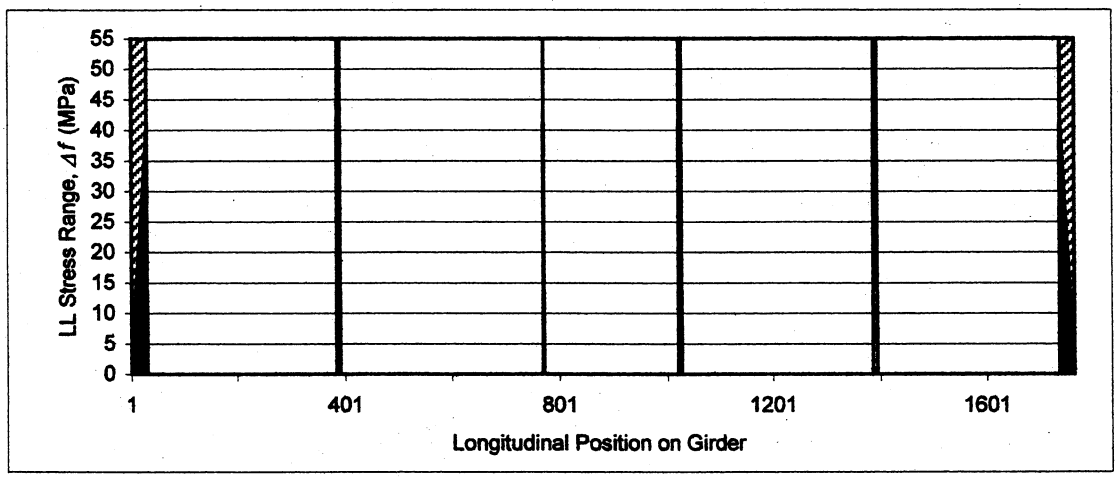

(b)

Figure 142: Br.538b (a-Live load fatigue stress range, b-Low stress regions according to Approach V)

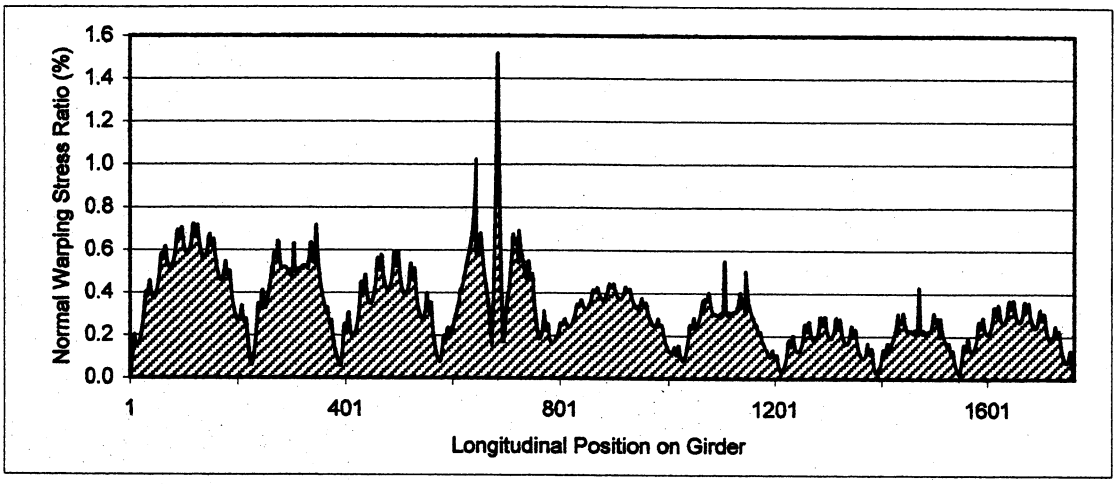

(a)

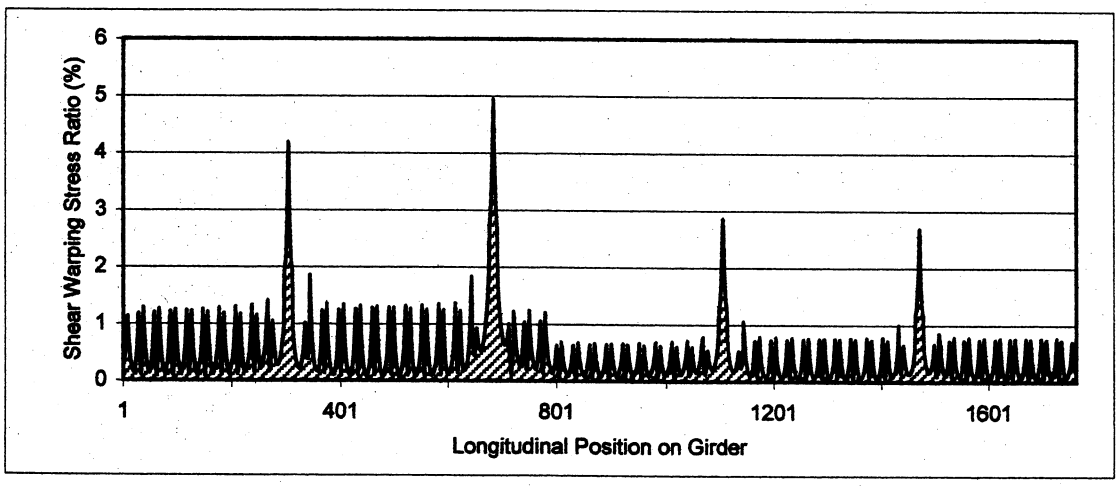

(b)

Figure 143: Warping stress ratios for Br.538b
a) σ_ω / σ_T, b) τ_ω / τ_T)

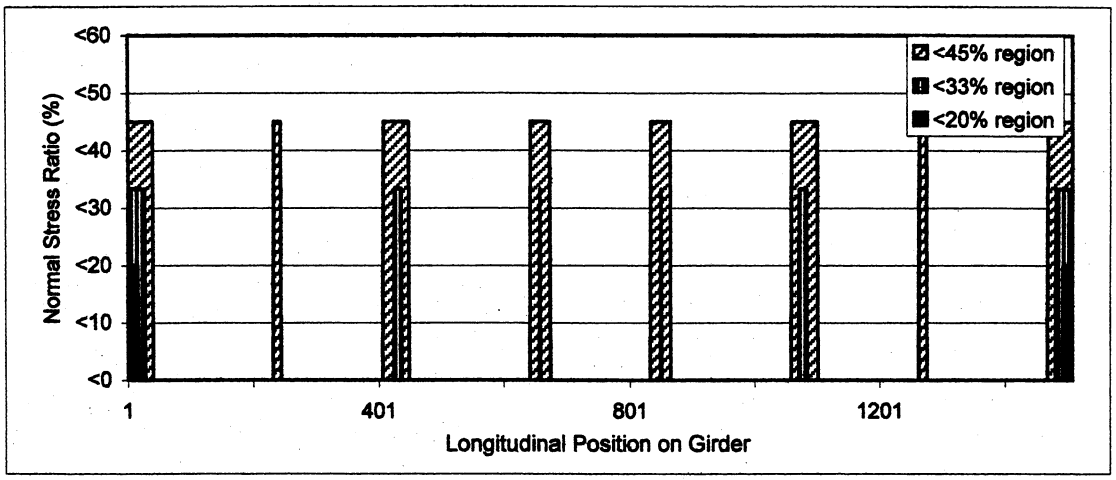

(a)

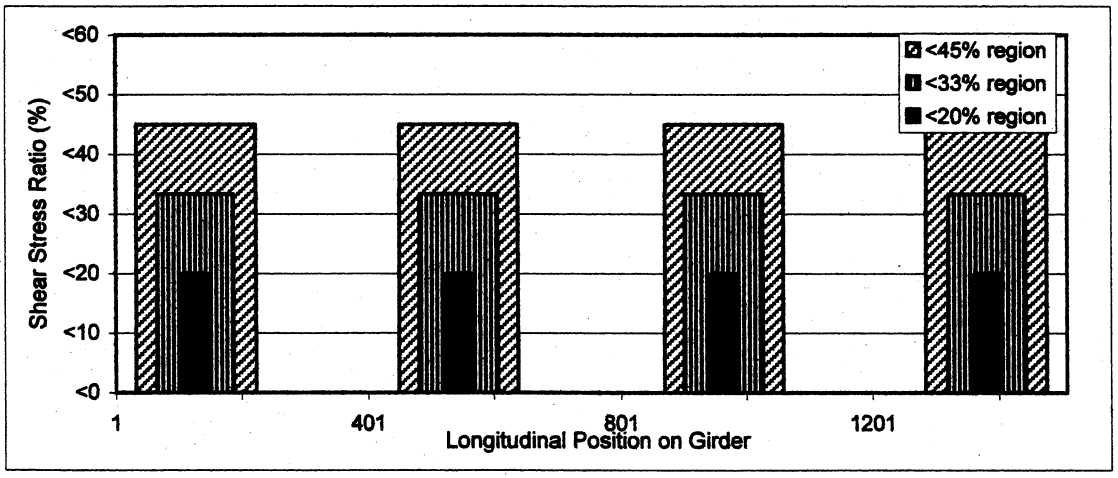

(b)

Figure 144: Regions of low stresses for Br.538c (a-Approach I, b-Approach II)

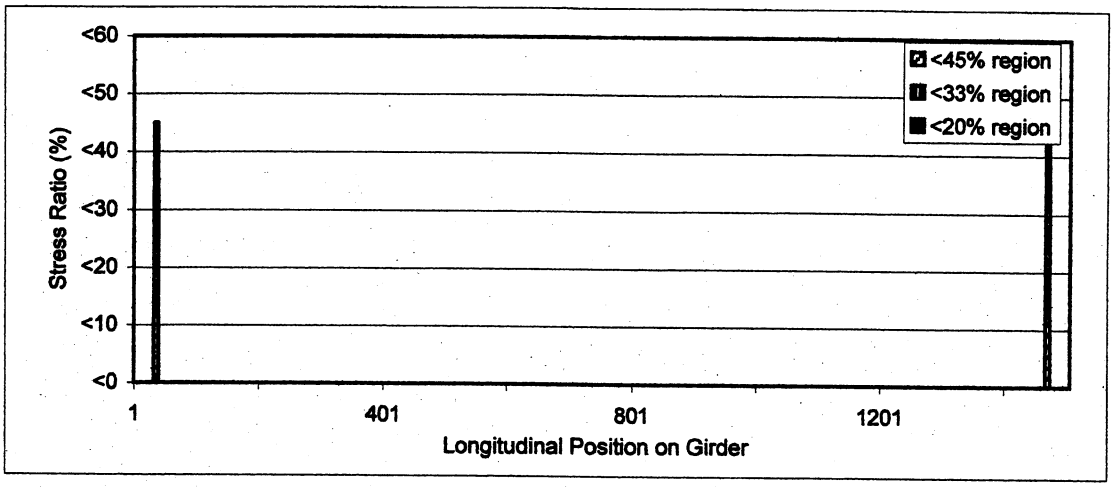

(a)

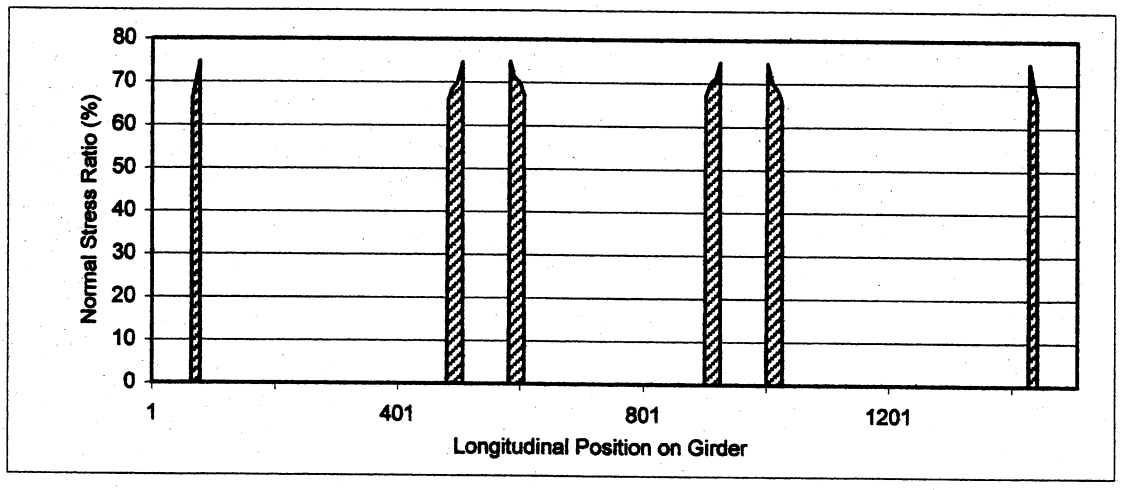

(b)

Figure 145: Regions of low stresses for Br.538c (a-Approach III, b-Approach IV)

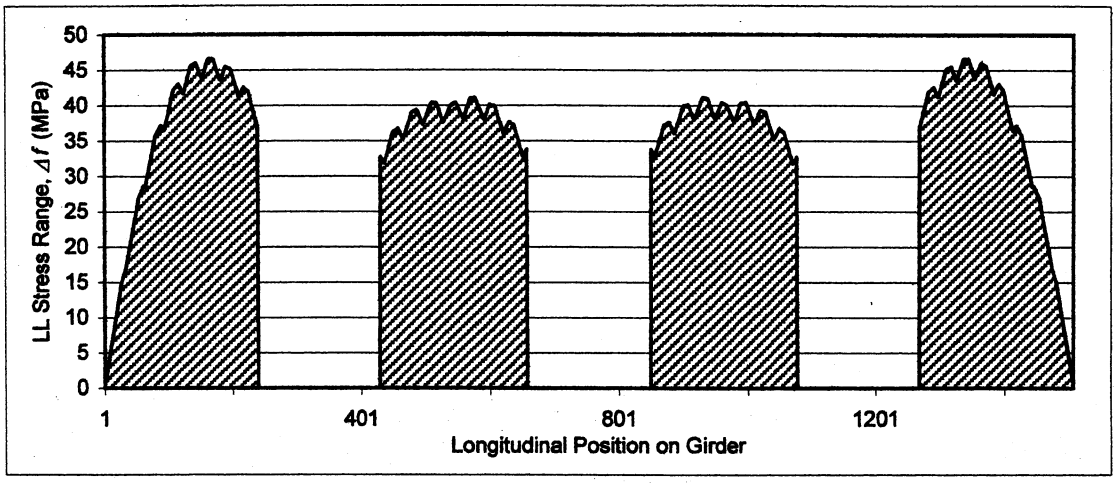

(a)

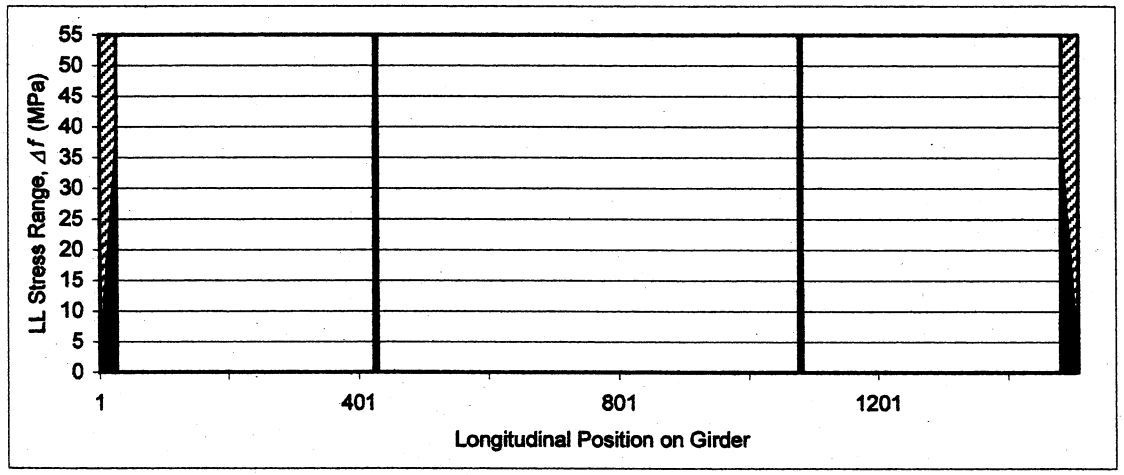

(b)

Figure 146: Br.538c (a-Live load fatigue stress range, b-Low stress regions according to Approach V)

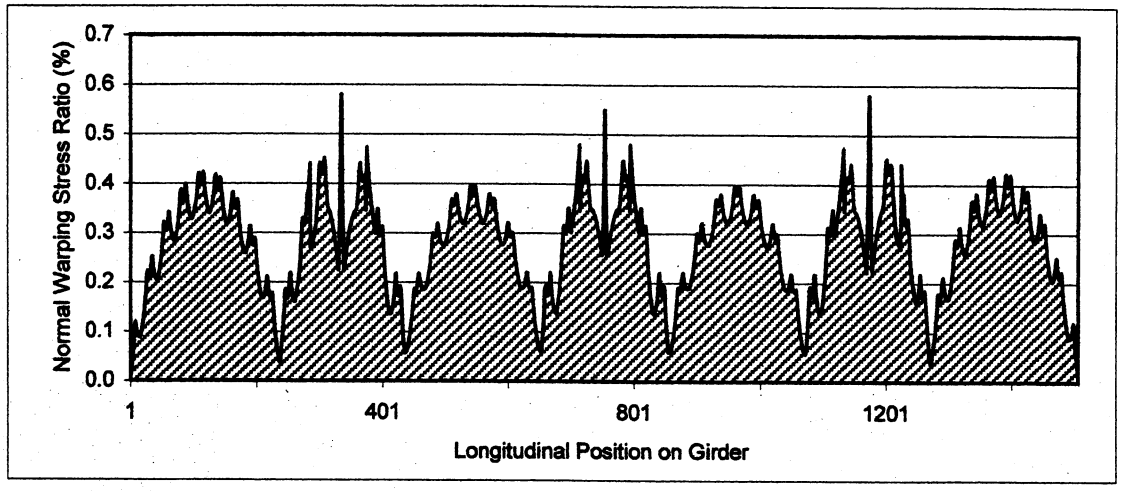

(a)

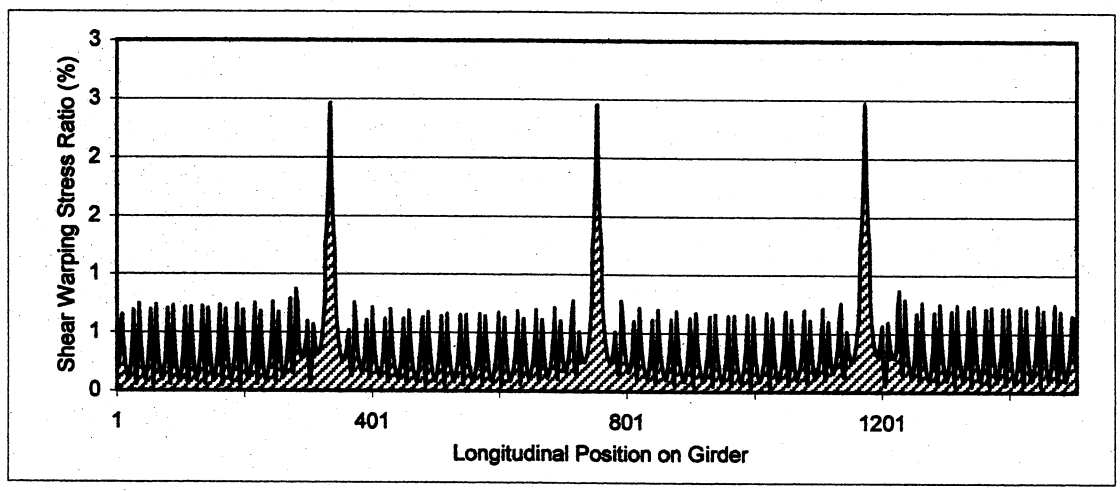

(b)

Figure 147: Warping stress ratios for Br.538c
a) σ_ω / σ_T, b) τ_ω / τ_T)

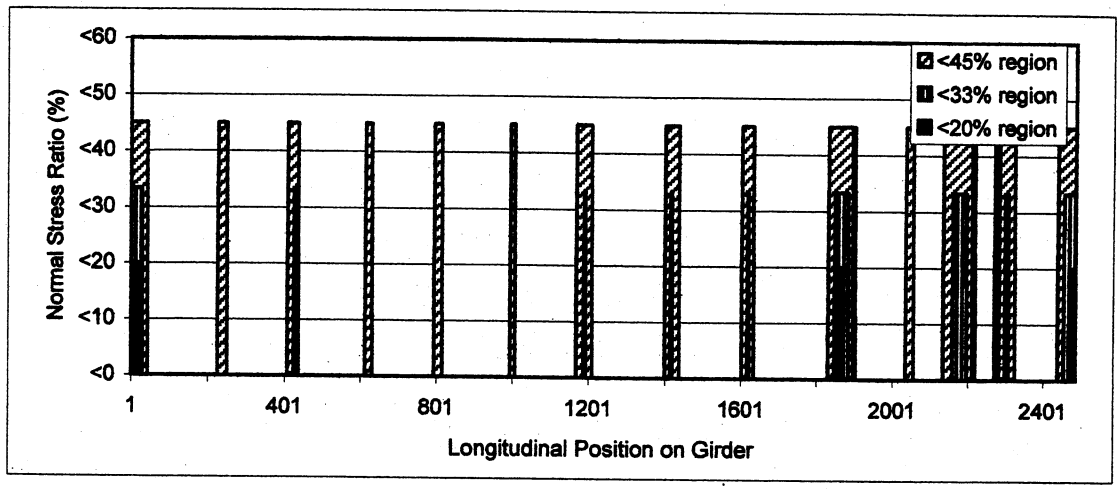

(a)

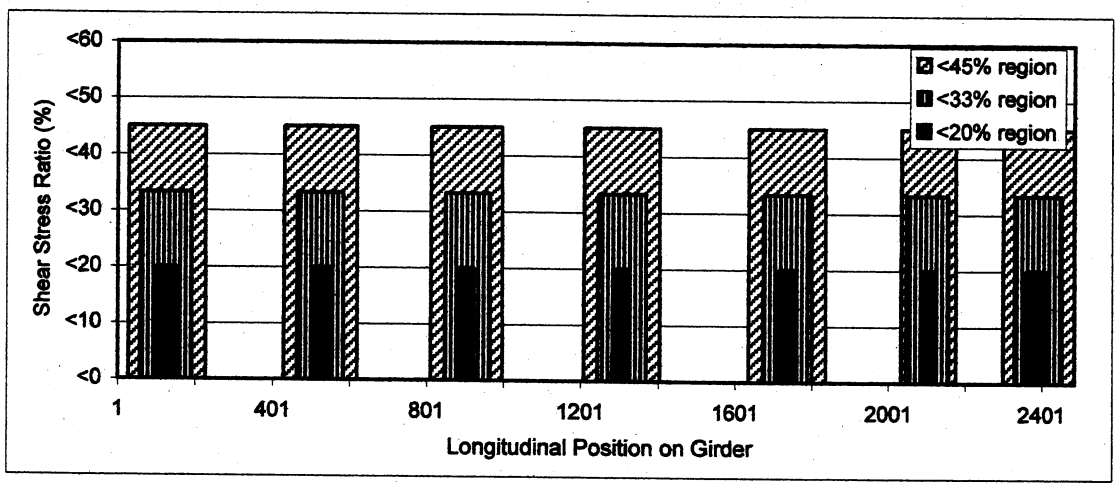

(b)

Figure 148: Regions of low stresses for Br.538d (a-Approach I, b-Approach II)

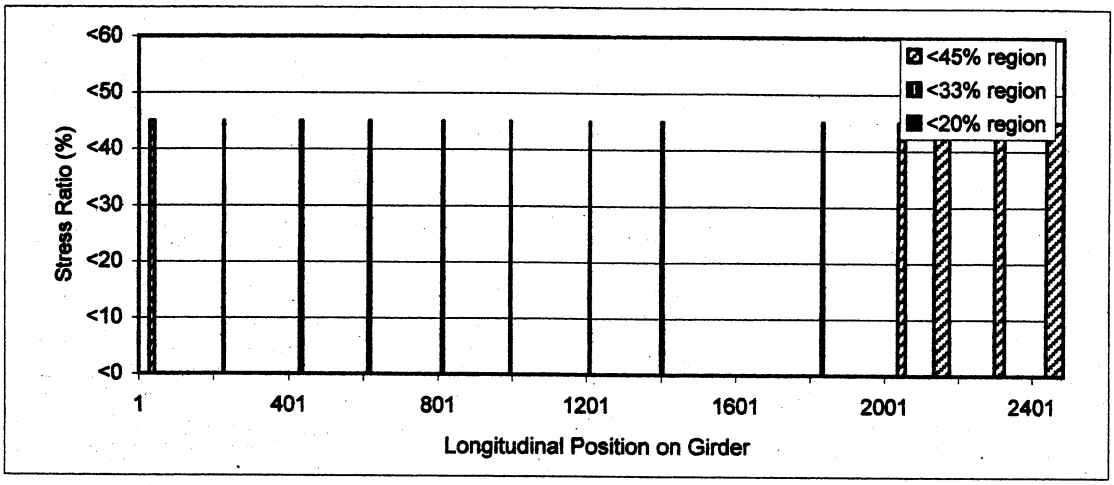

(a)

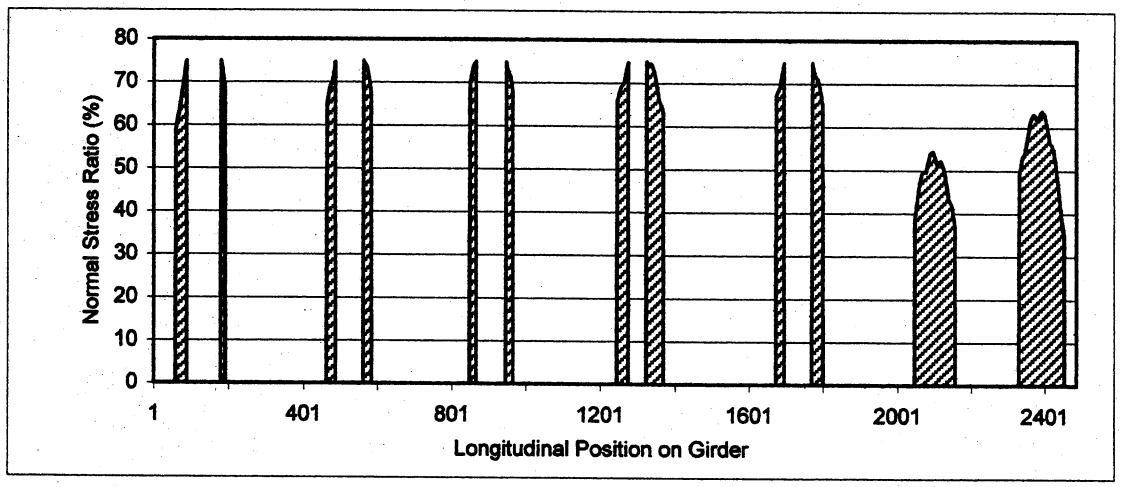

(b)

Figure 149: Regions of low stresses for Br.538d (a-Approach III, b-Approach IV)

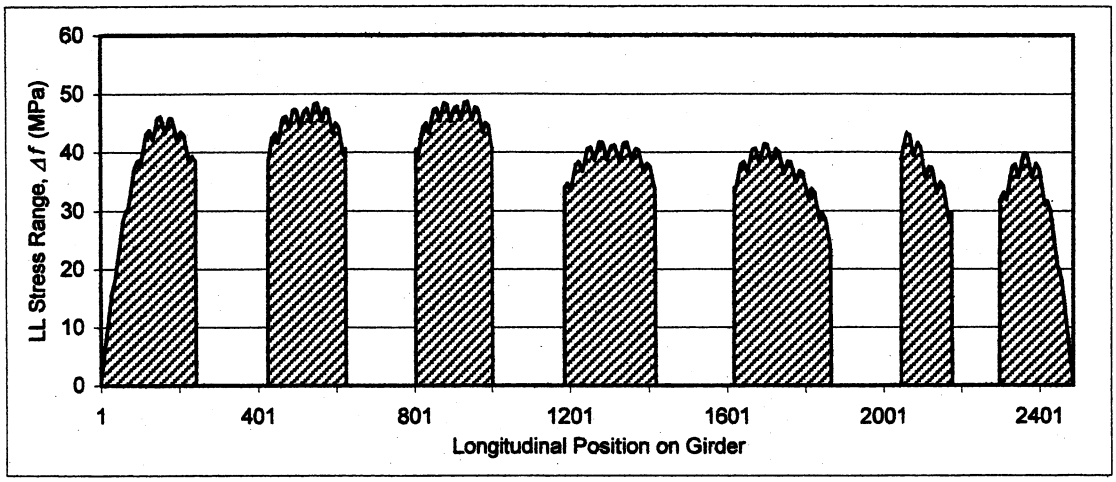

(a)

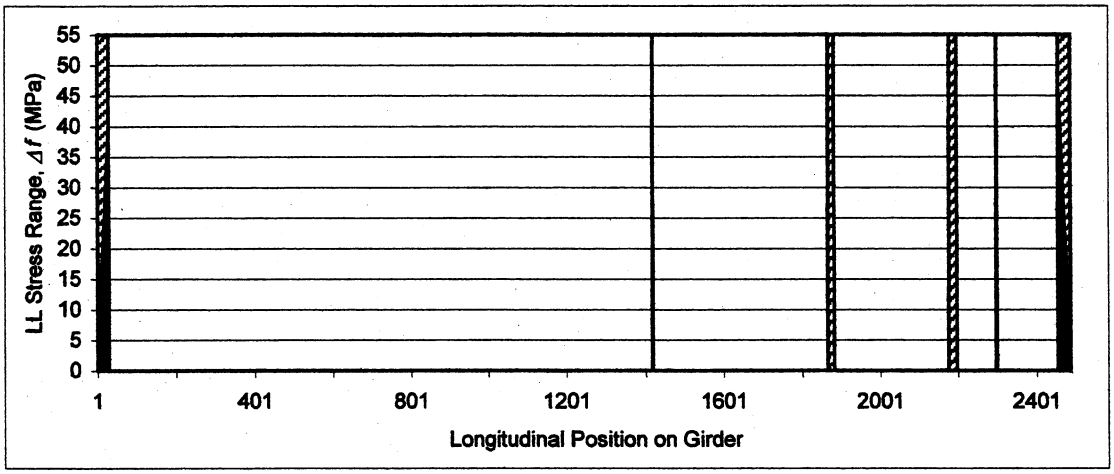

(b)

Figure 150: Br.538d (a-Live load fatigue stress range, b-Low stress regions according to Approach V)

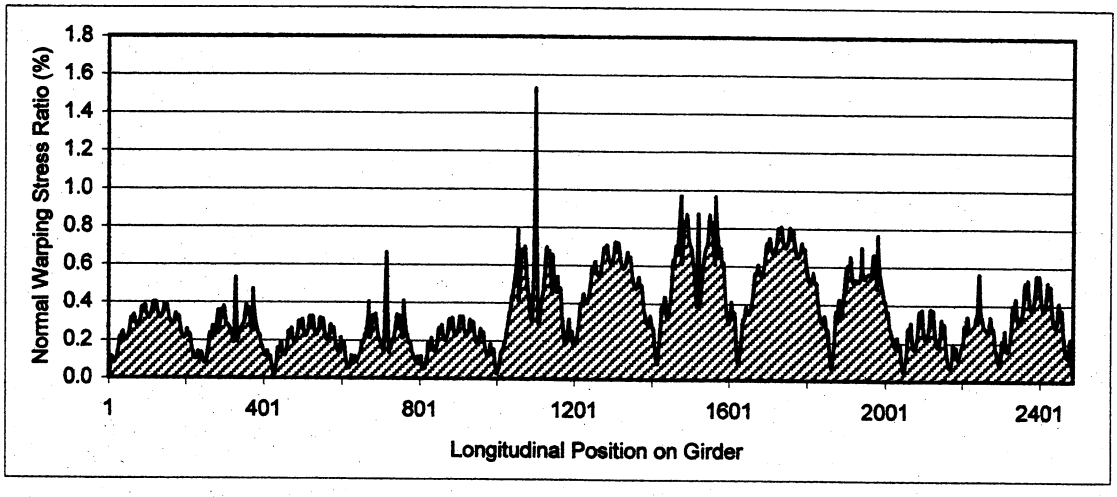

(a)

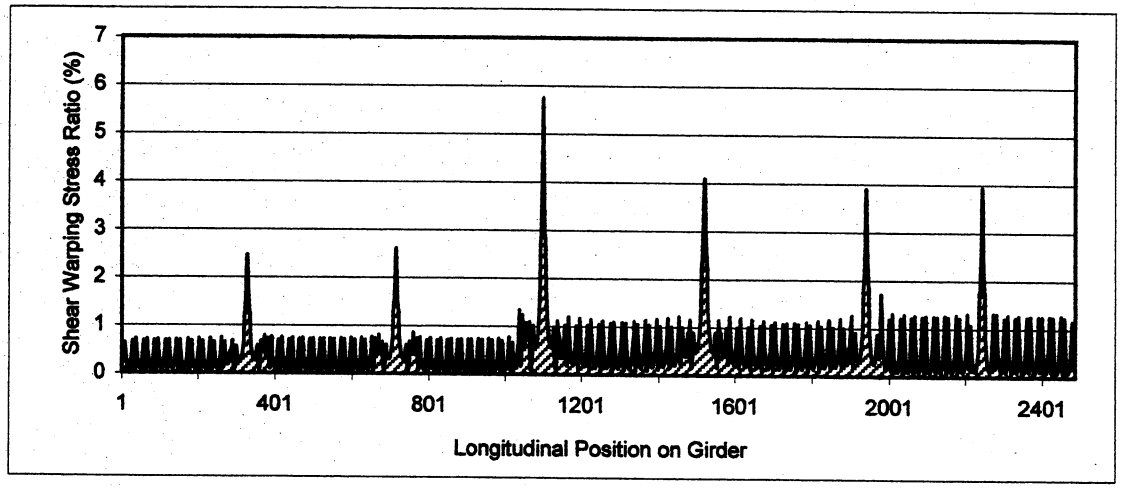

(b)

Figure 151: Warping stress ratios for Br.538d
a) σ_ω / σ_T, b) τ_ω / τ_T)

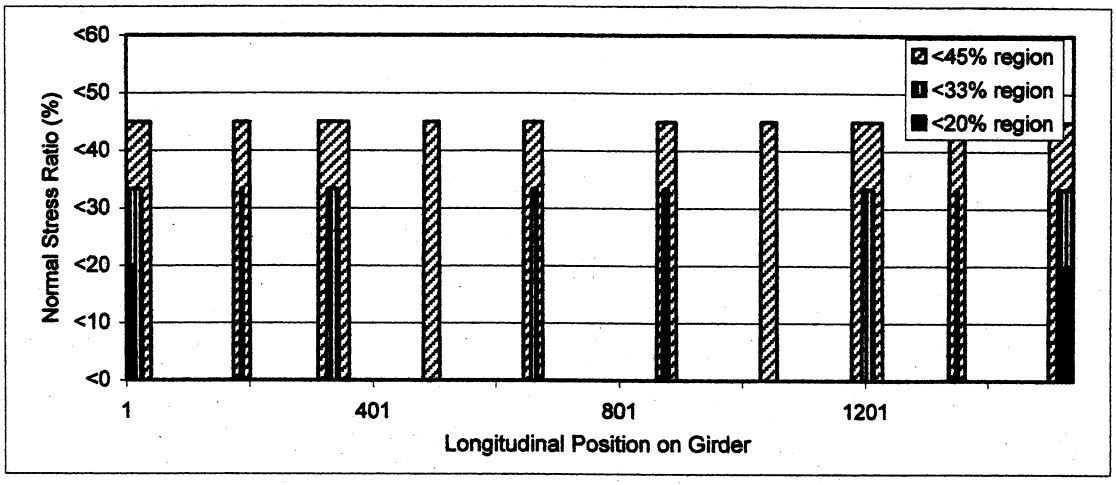

(a)

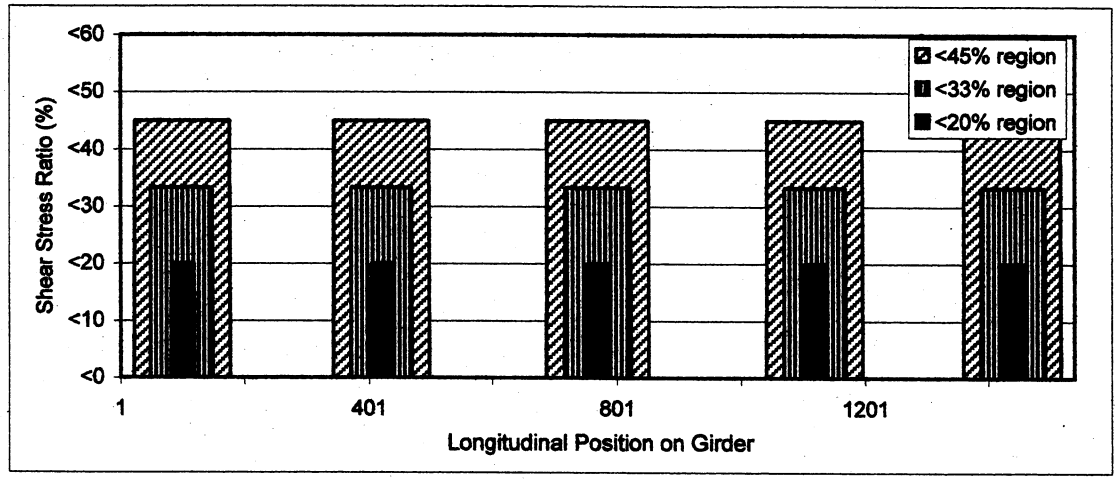

(b)

Figure 152: Regions of low stresses for Br.539 (a-Approach I, b-Approach II)

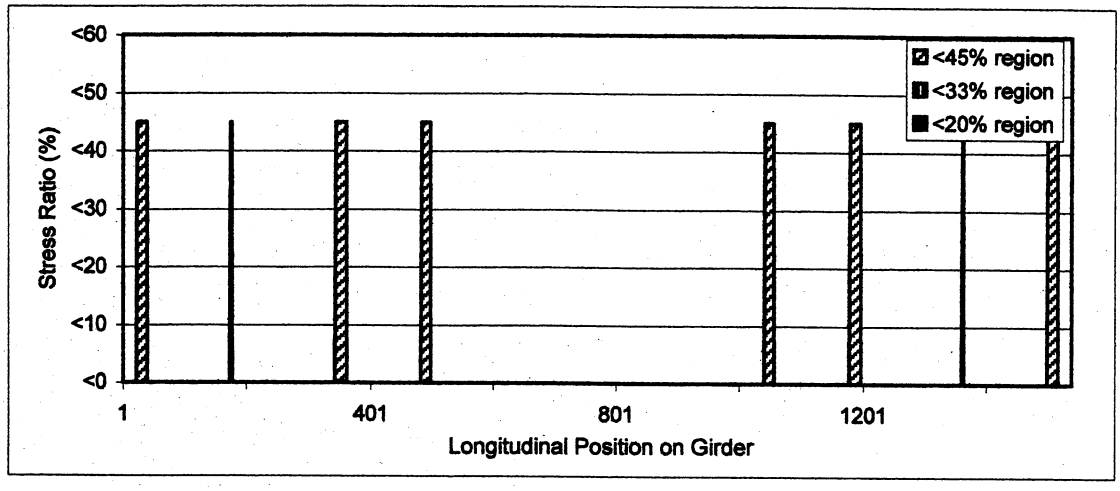

(a)

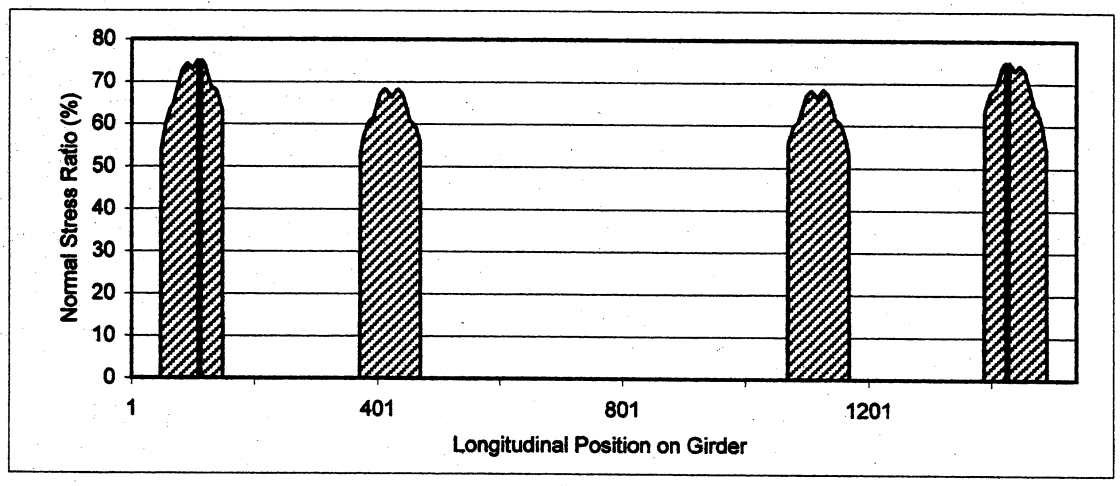

(b)

Figure 153: Regions of low stresses for Br.539 (a-Approach III, b-Approach IV)

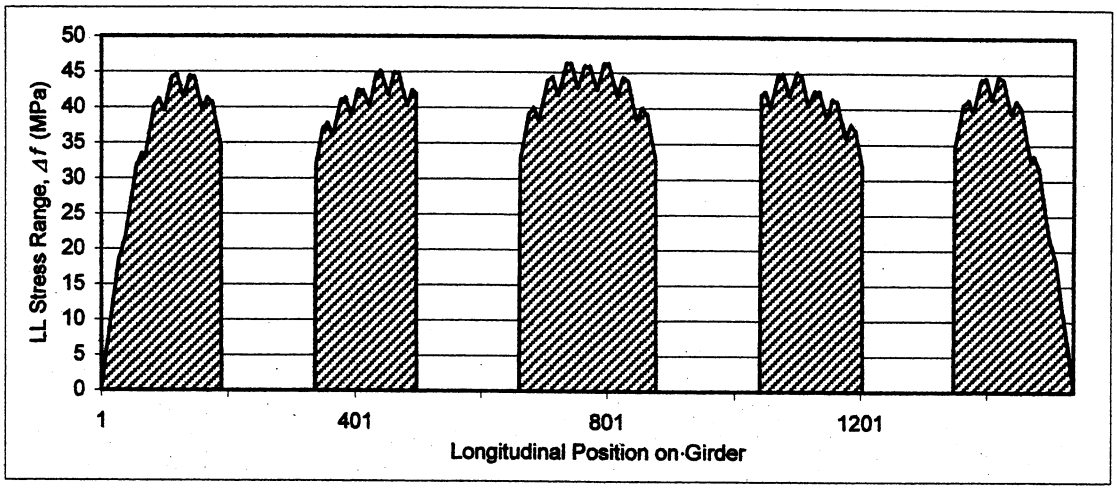

(a)

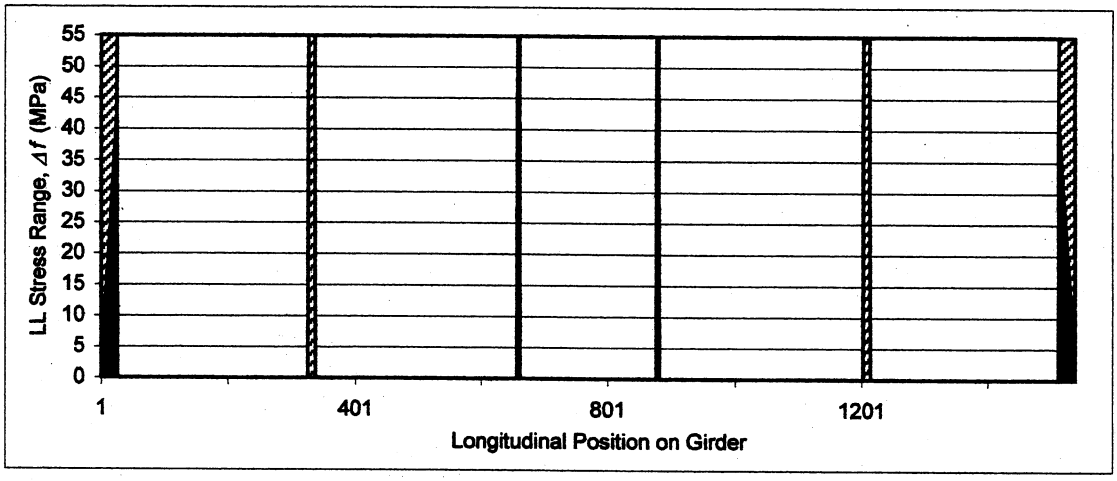

(b)

Figure 154: Br.539 (a-Live load fatigue stress range, b-Low stress regions according to Approach V)

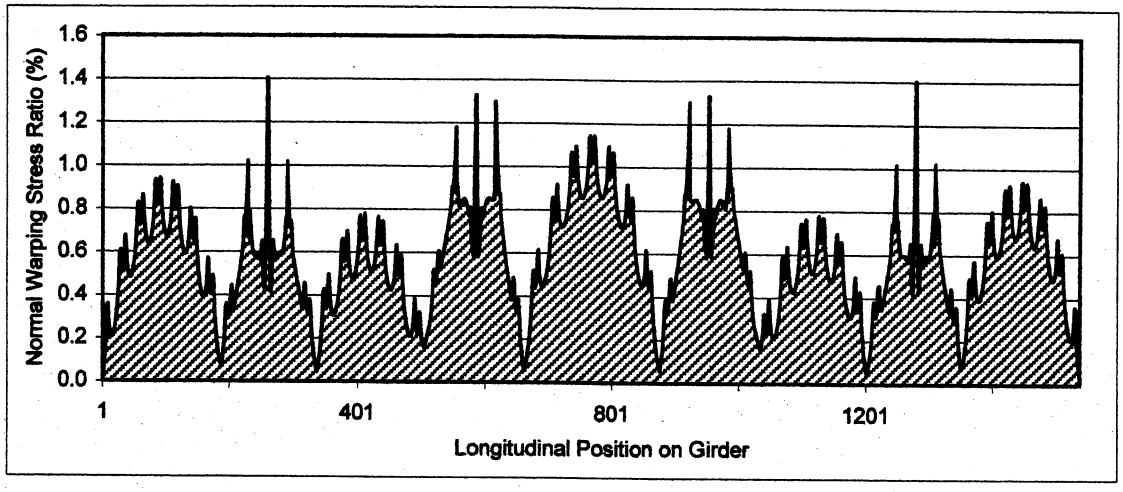

(a)

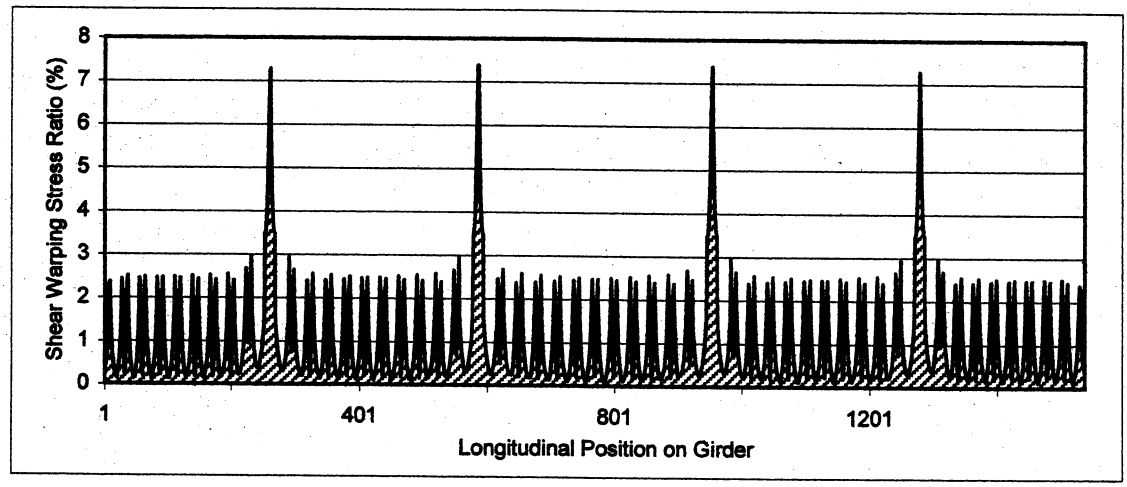

(b)

Figure 155: Warping stress ratios for Br.539
a) σ_ω / σ_T, b) τ_ω / τ_T)

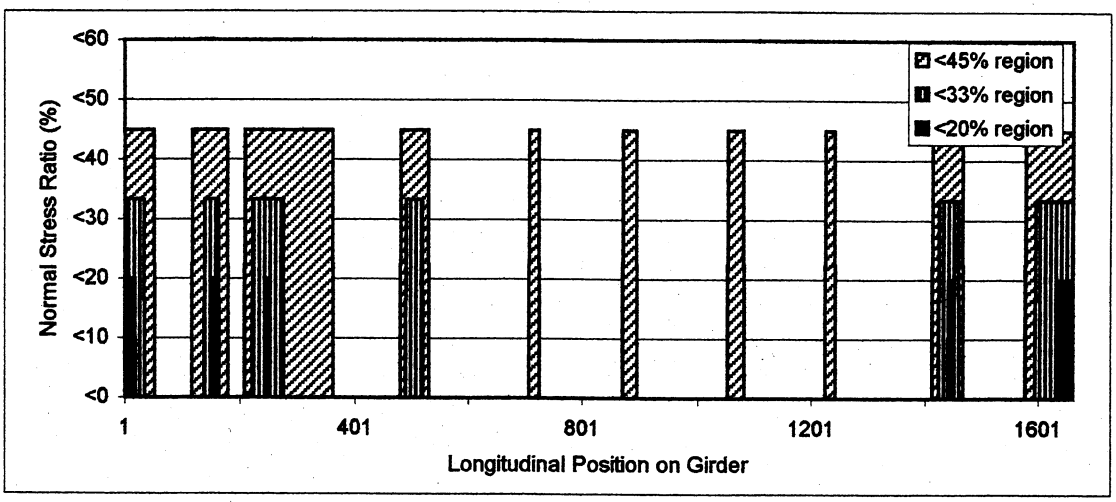

(a)

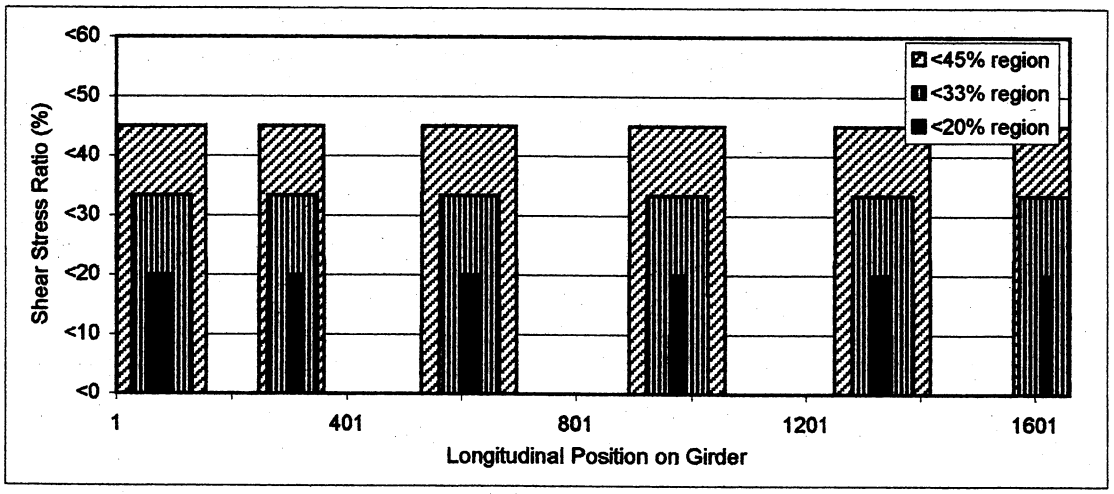

(b)

Figure 156: Regions of low stresses for Br.540 (a-Approach I, b-Approach II)

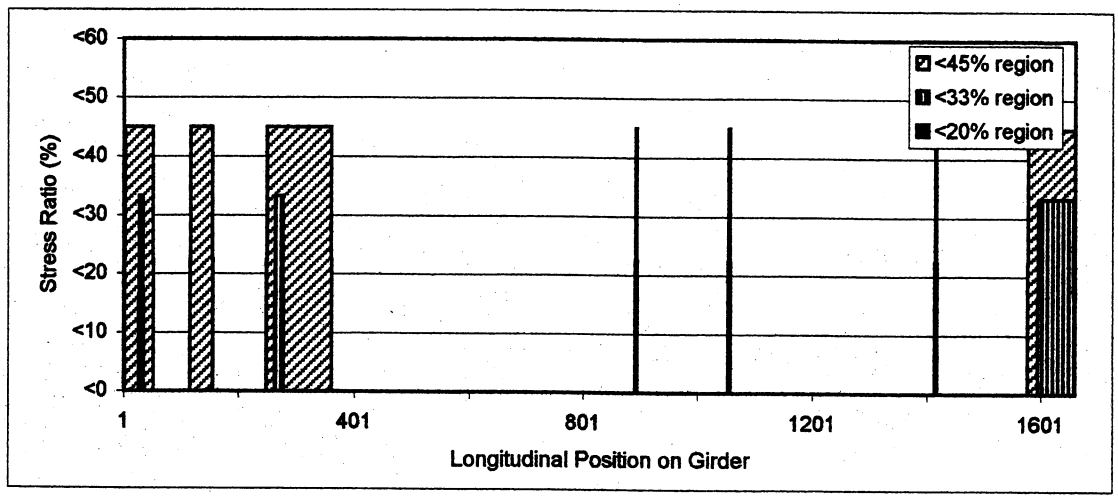

(a)

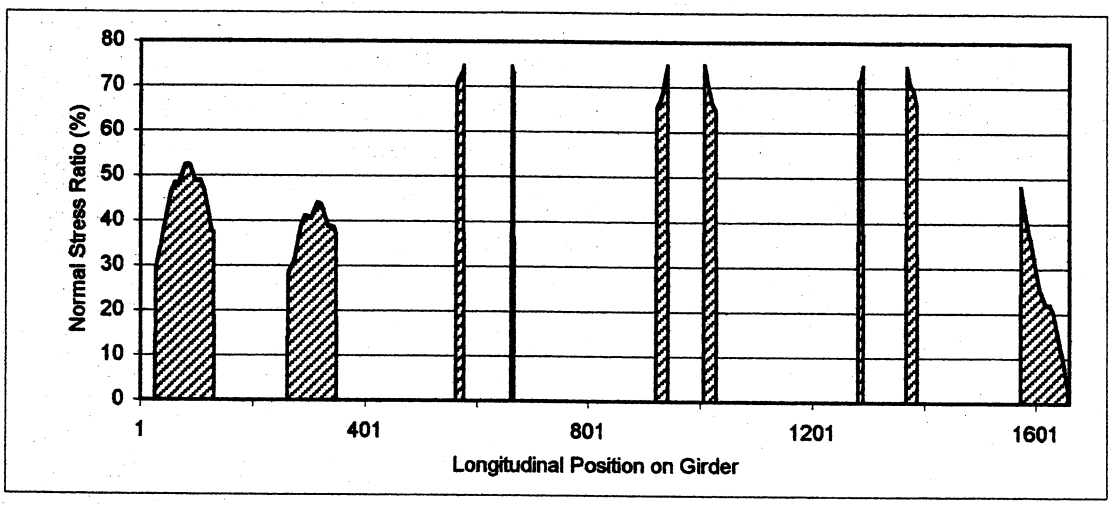

(b)

Figure 157: Regions of low stresses for Br.540 (a-Approach III, b-Approach IV)

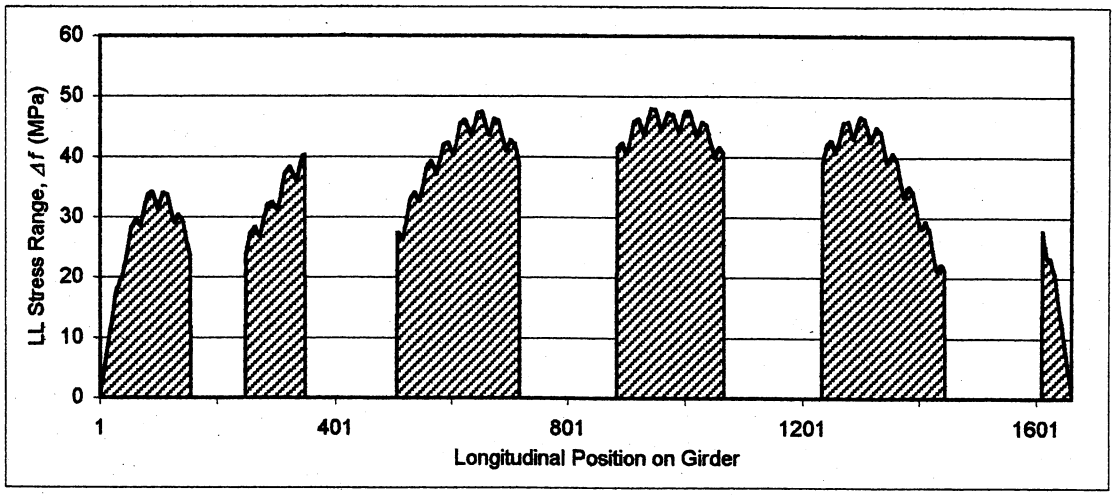

(a)

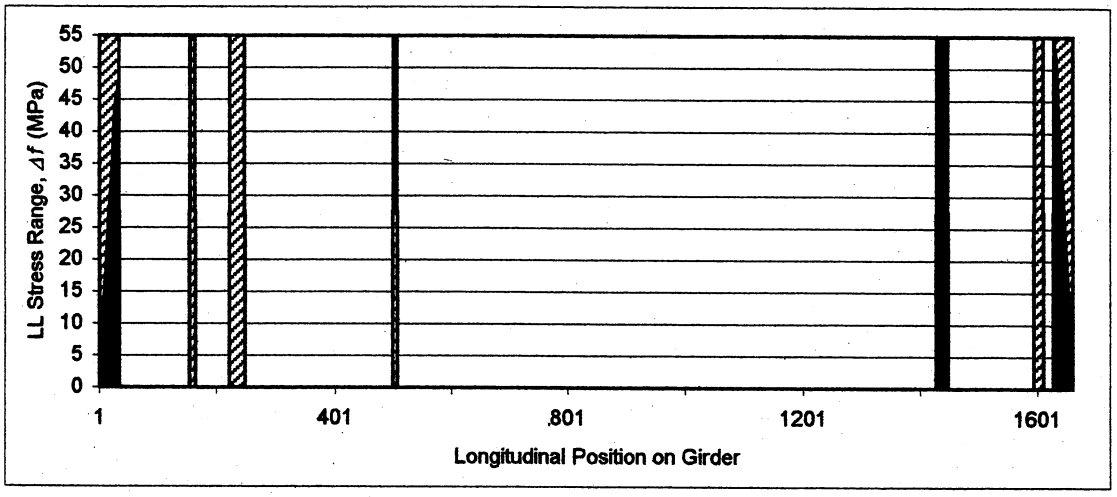

(b)

Figure 158: Br.540 (a-Live load fatigue stress range, b-Low stress regions according to Approach V)

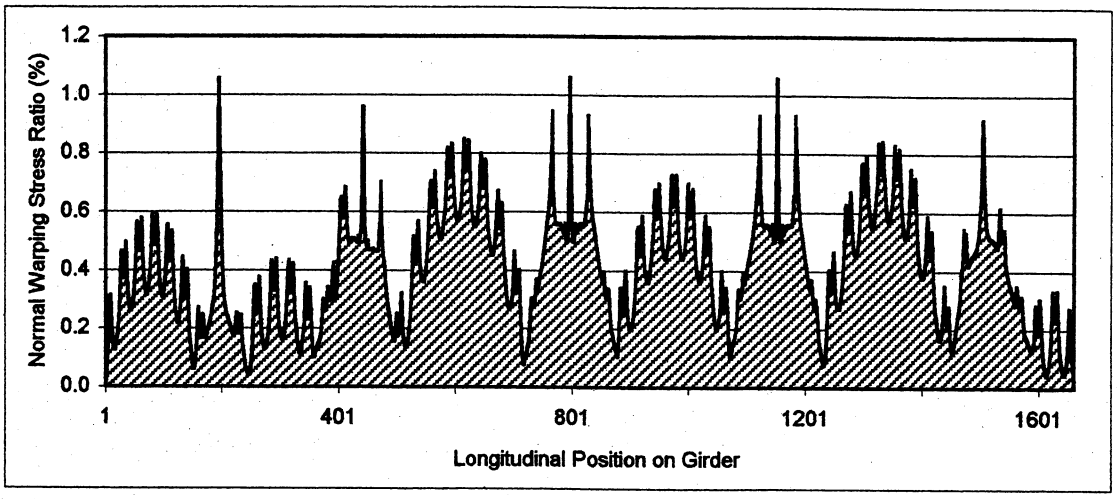

(a)

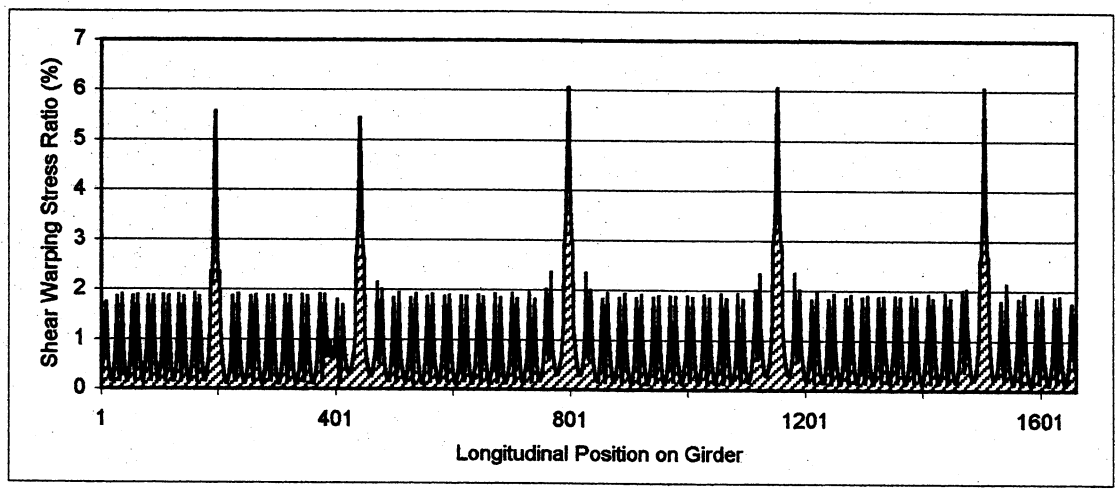

(b)

Figure 159: Warping stress ratios for Br.540
a) σ_ω / σ_T, b) τ_ω / τ_T)

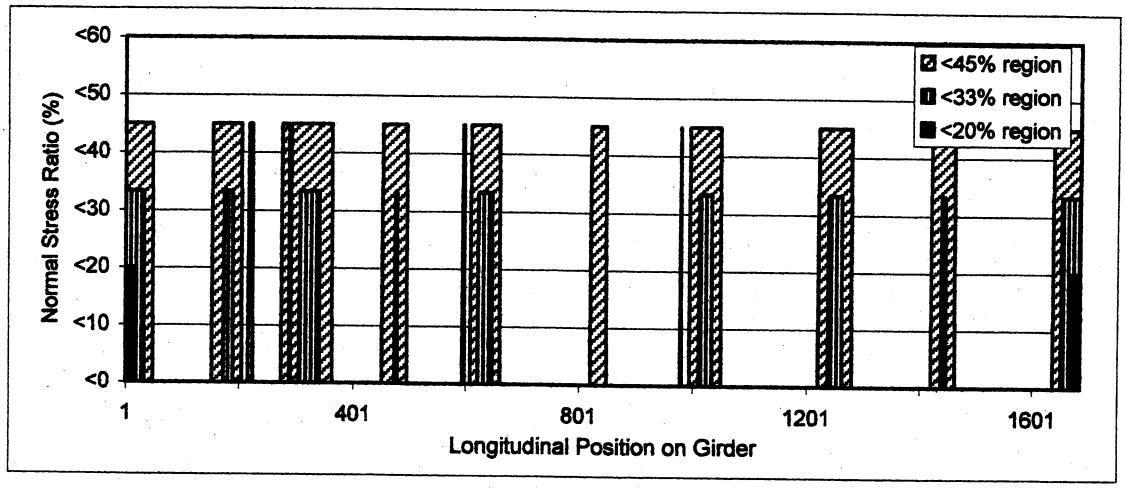

(a)

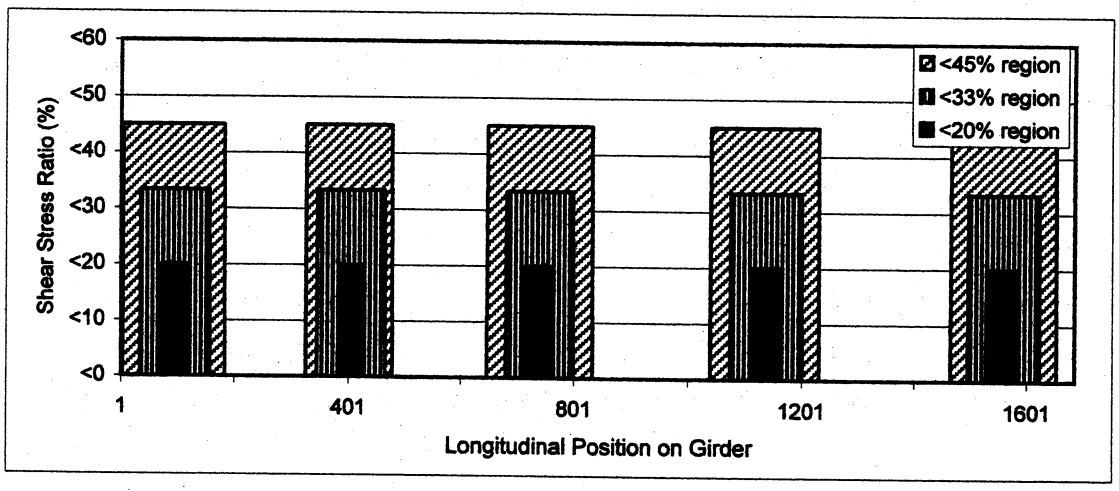

(b)

Figure 160: Regions of low stresses for Br.541a (a-Approach I, b-Approach II)

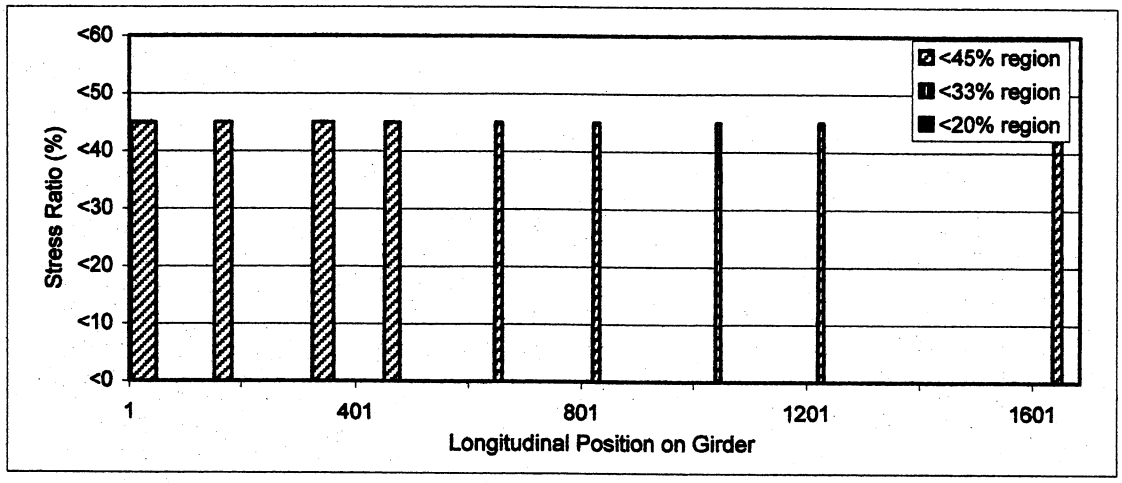

(a)

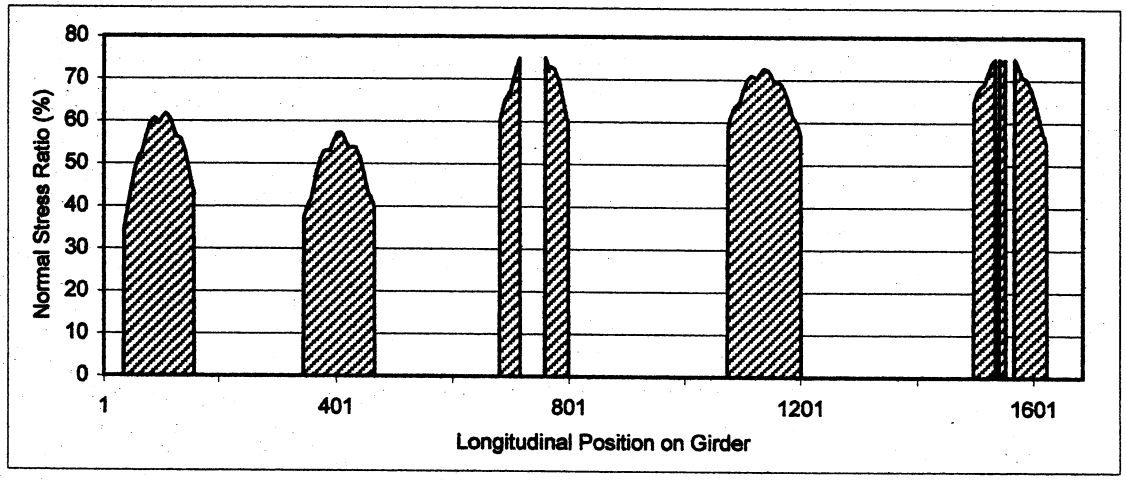

(b)

Figure 161: Regions of low stresses for Br.541a (a-Approach III, b-Approach IV)

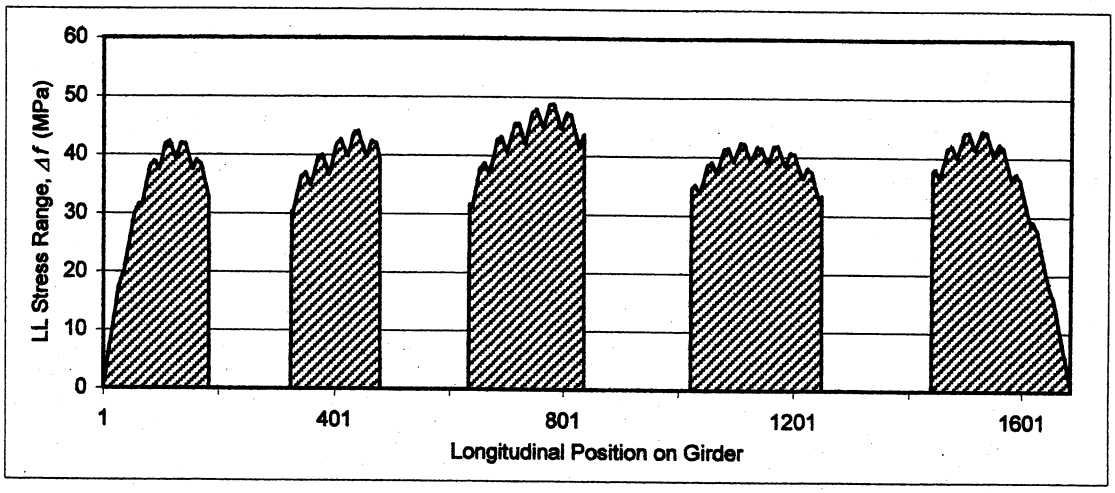

(a)

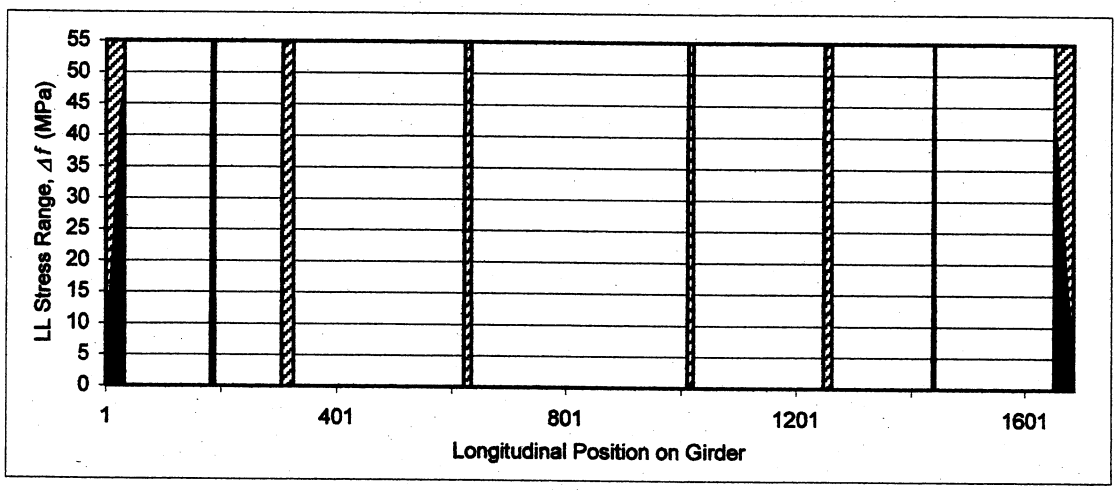

(b)

Figure 162: Br.541a (a-Live load fatigue stress range, b-Low stress regions according to Approach V)

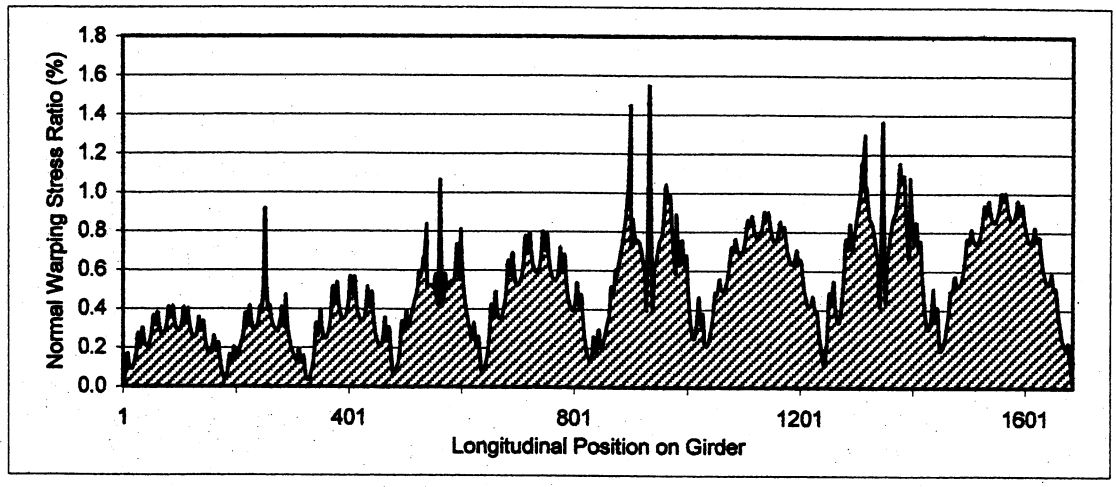

(a)

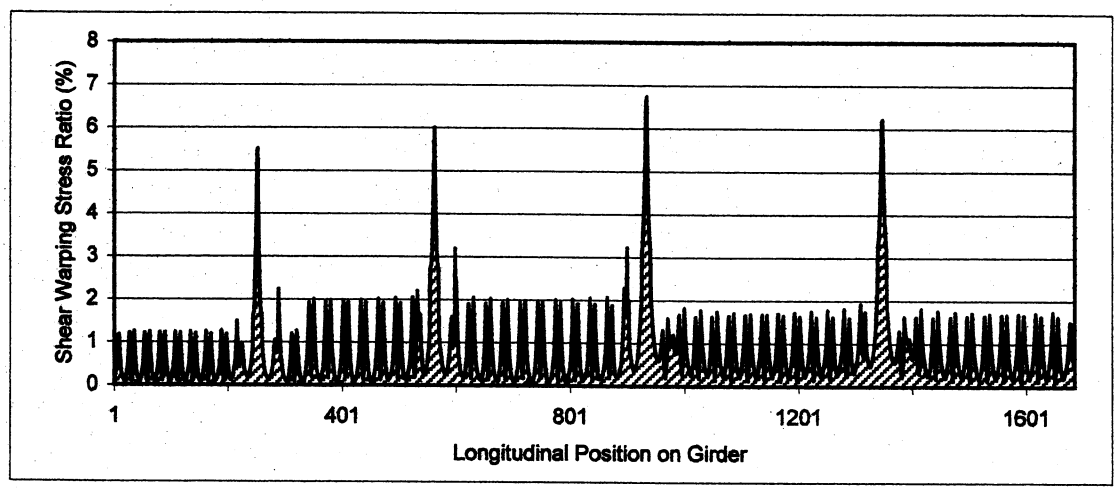

(b)

Figure 163: Warping stress ratios for Br.541a
a) σ_ω / σ_T, b) τ_ω / τ_T)

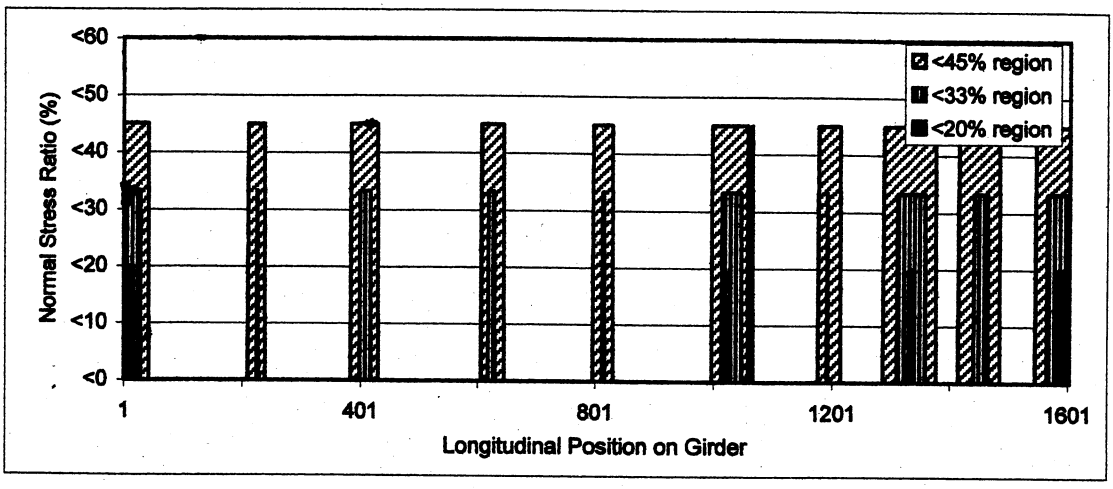

(a)

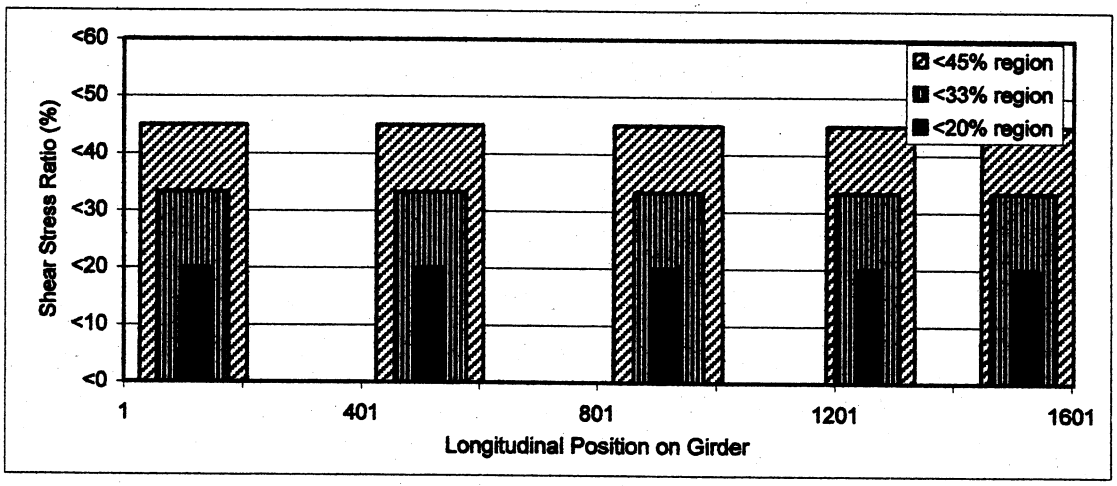

(b)

Figure 164: Regions of low stresses for Br.541b (a-Approach I, b-Approach II)

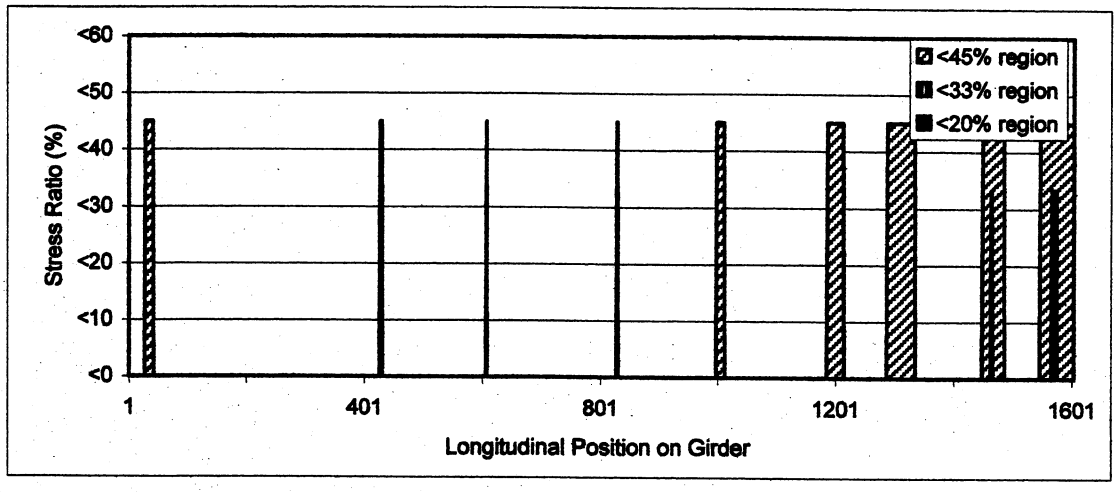

(a)

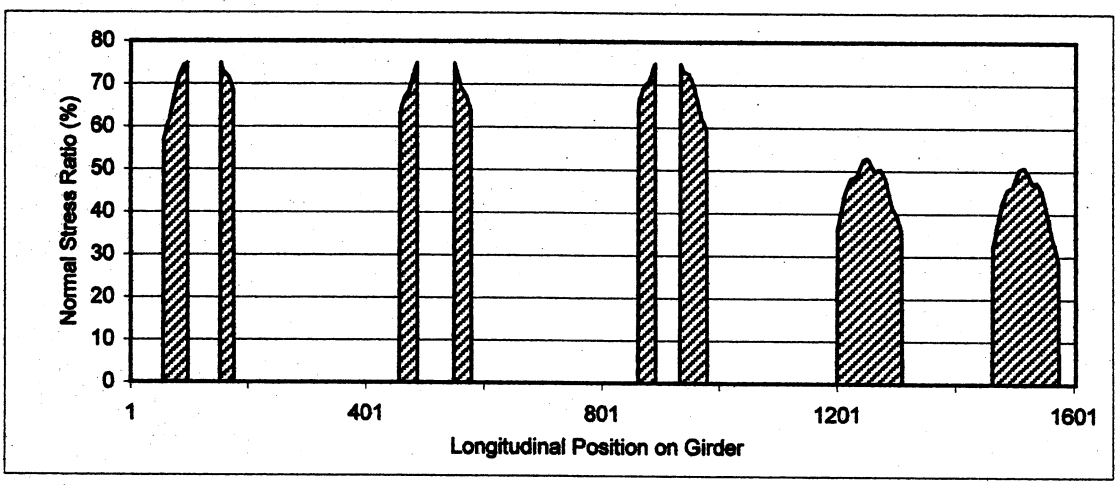

(b)

Figure 165: Regions of low stresses for Br.541b (a-Approach III, b-Approach IV)

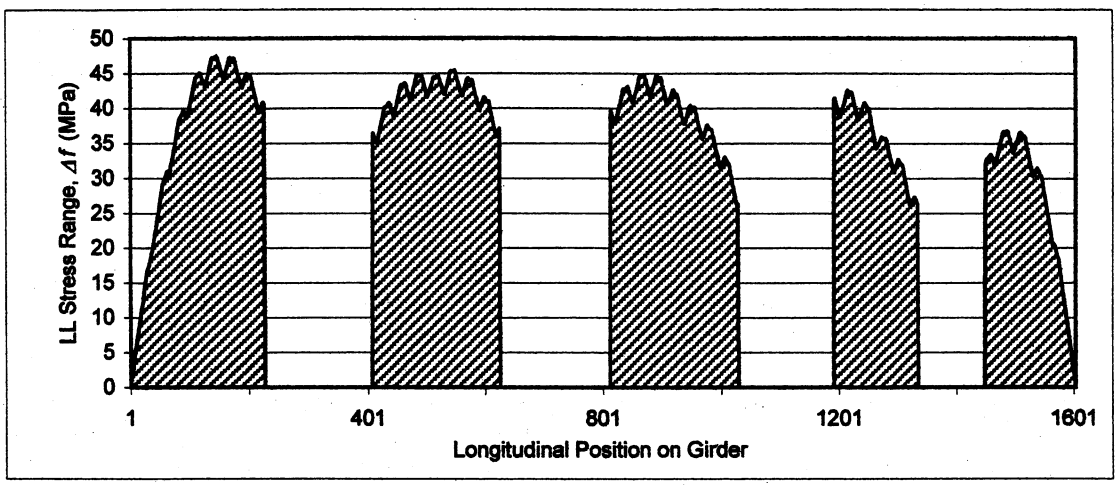

(a)

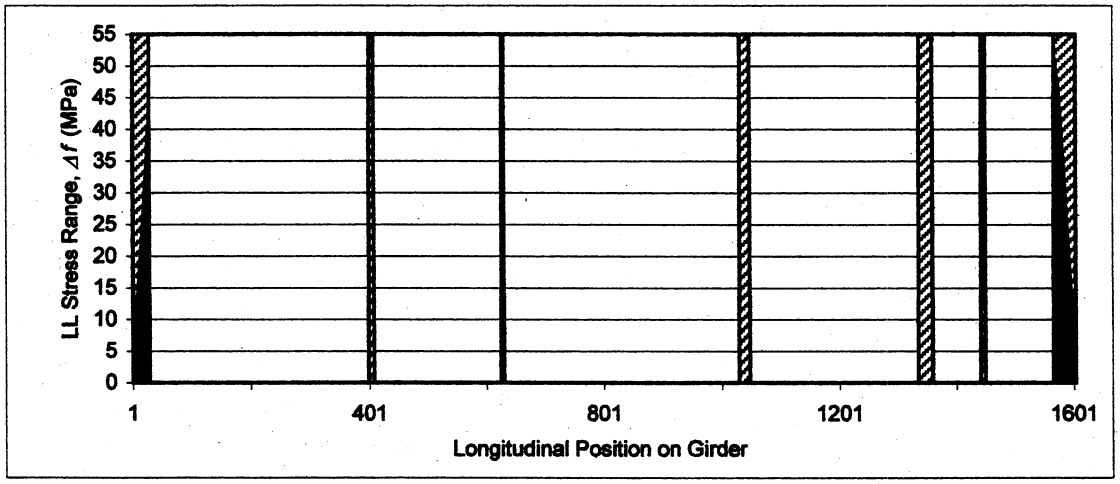

(b)

Figure 166: Br.541b (a-Live load fatigue stress range, b-Low stress regions according to Approach V)

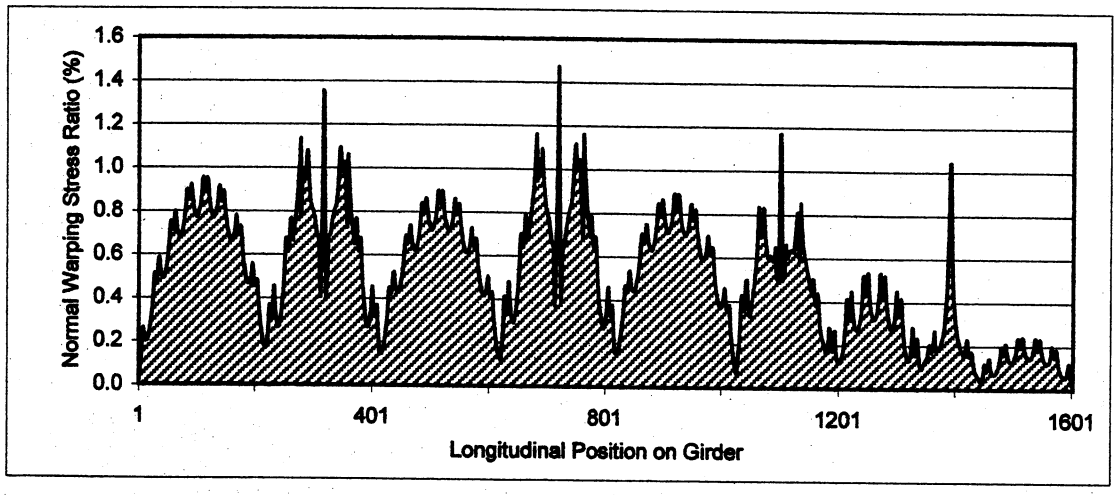

(a)

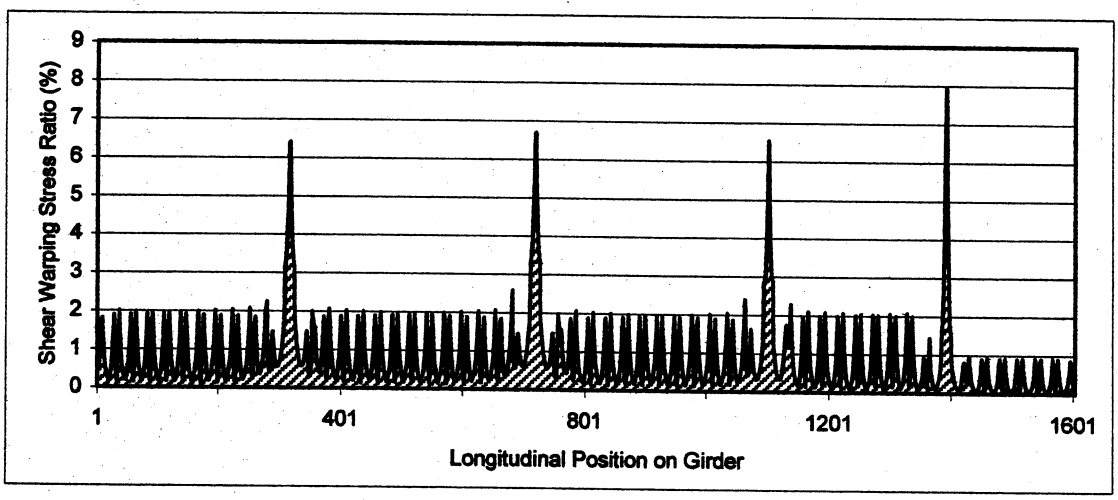

(b)

Figure 167: Warping stress ratios for Br.541b
a) σ_ω / σ_T, b) τ_ω / τ_T)

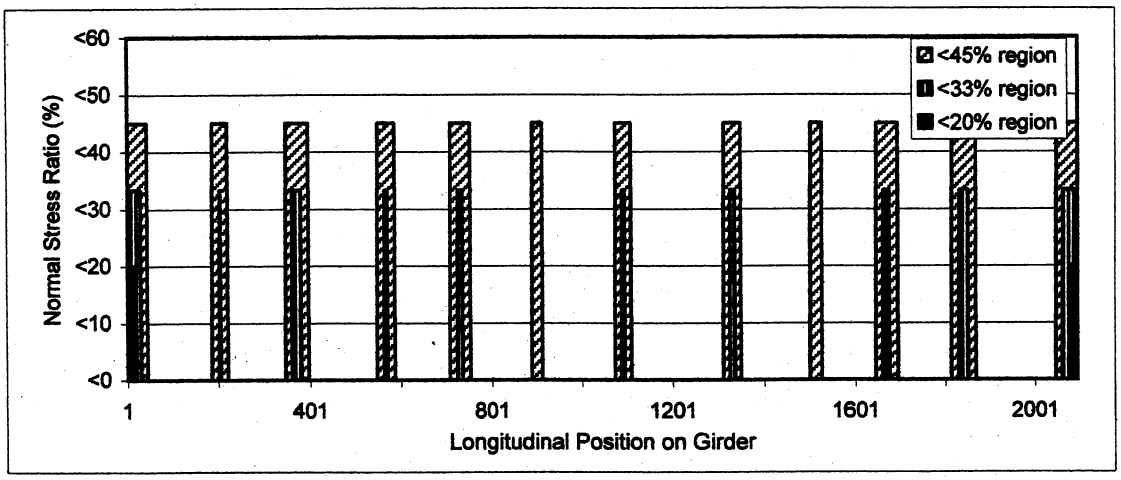

(a)

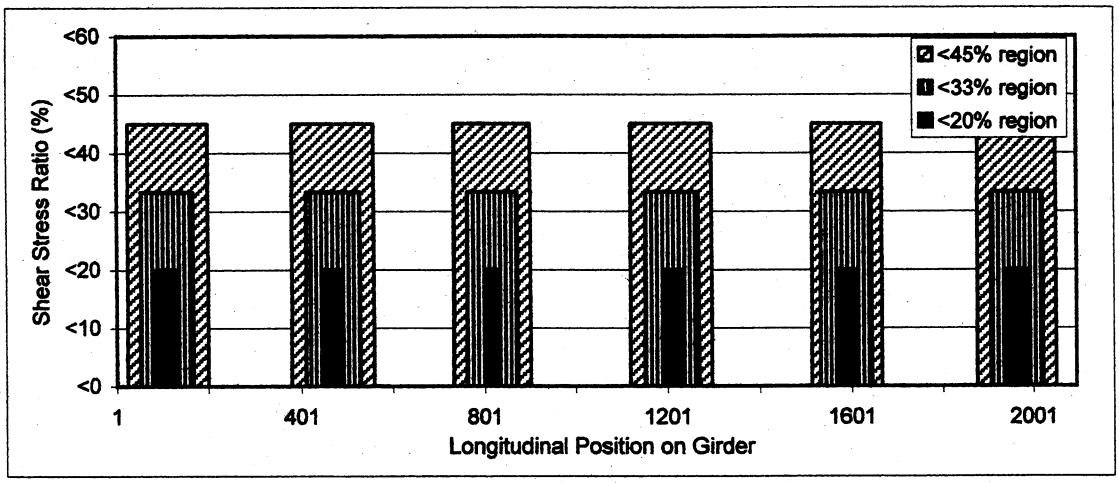

(b)

Figure 168: Regions of low stresses for Br.542a (a-Approach I, b-Approach II)

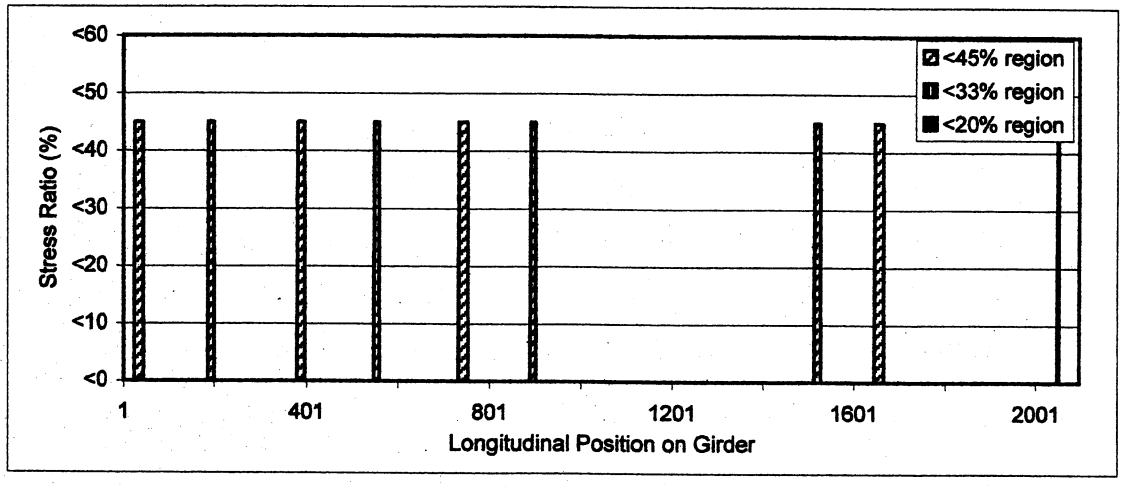

(a)

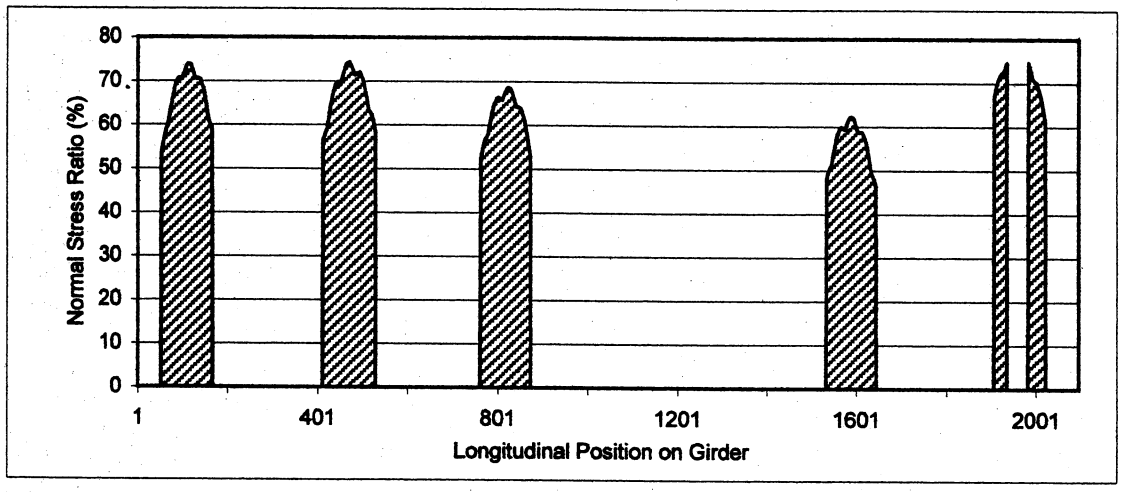

(b)

Figure 169: Regions of low stresses for Br.542a (a-Approach III, b-Approach IV)

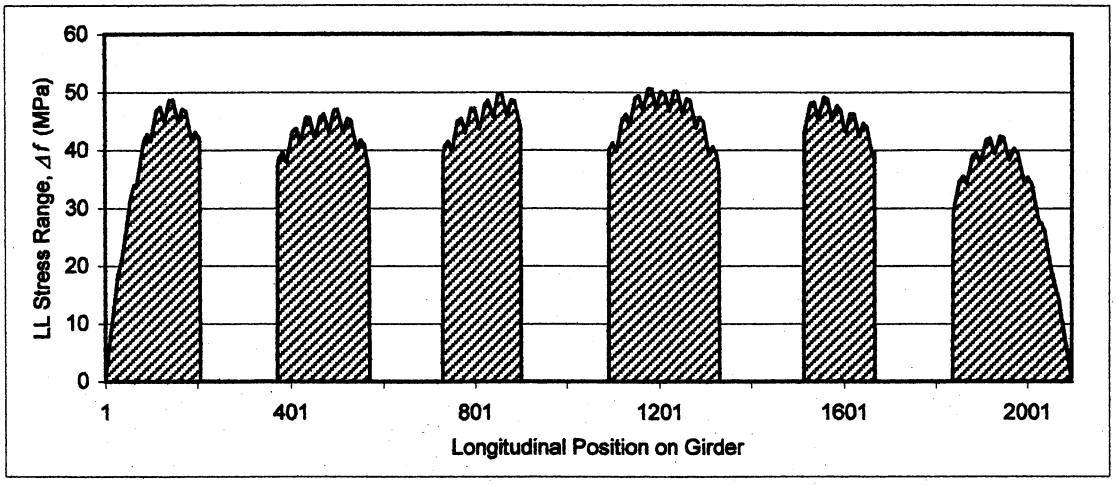

(a)

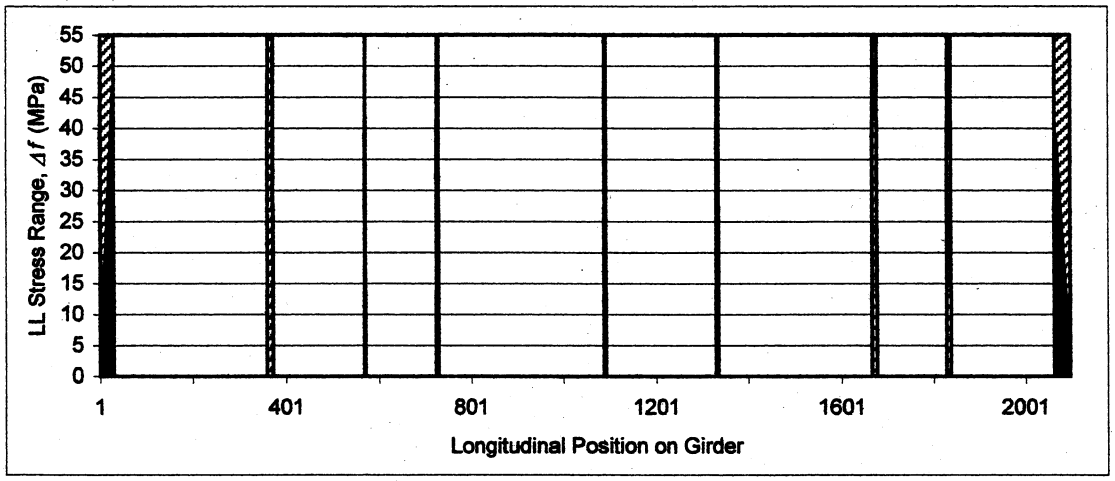

(b)

Figure 170: Br.542a (a-Live load fatigue stress range, b-Low stress regions according to Approach V)

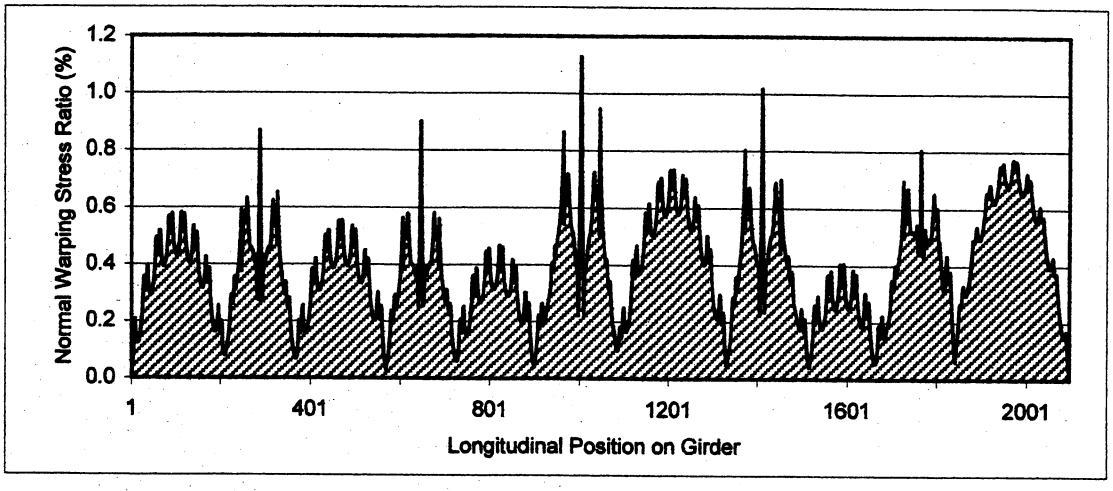

(a)

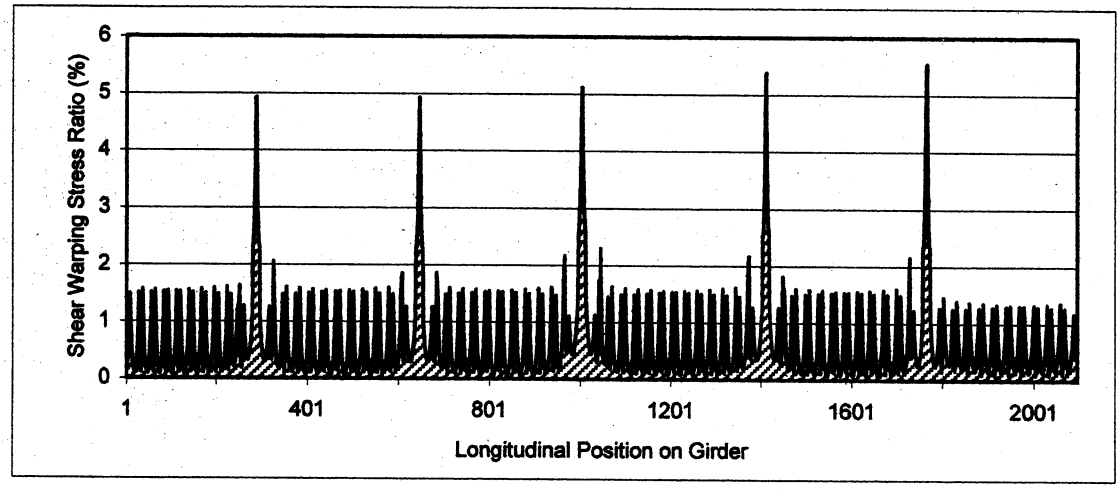

(b)

Figure 171: Warping stress ratios for Br.542a
a) σ_ω / σ_T, b) τ_ω / τ_T)

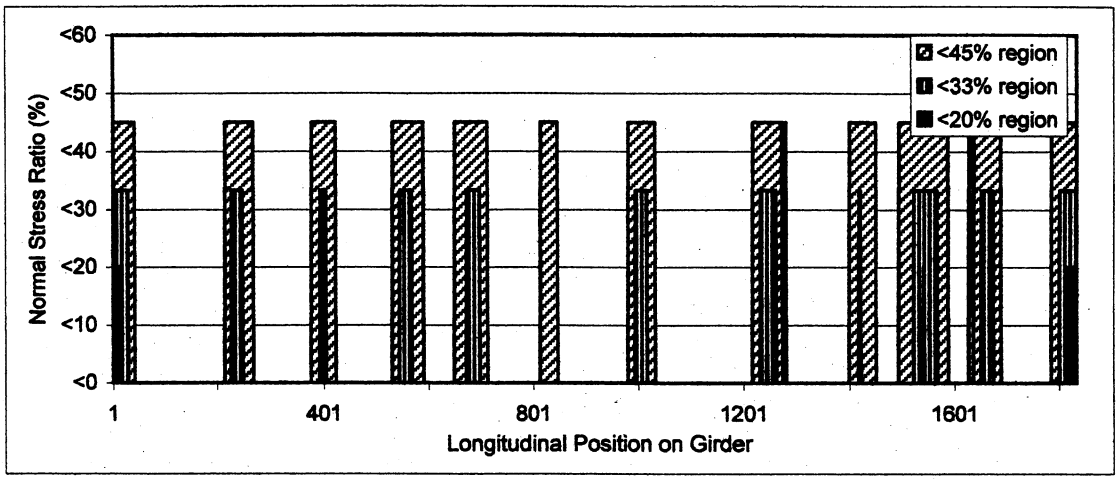

(a)

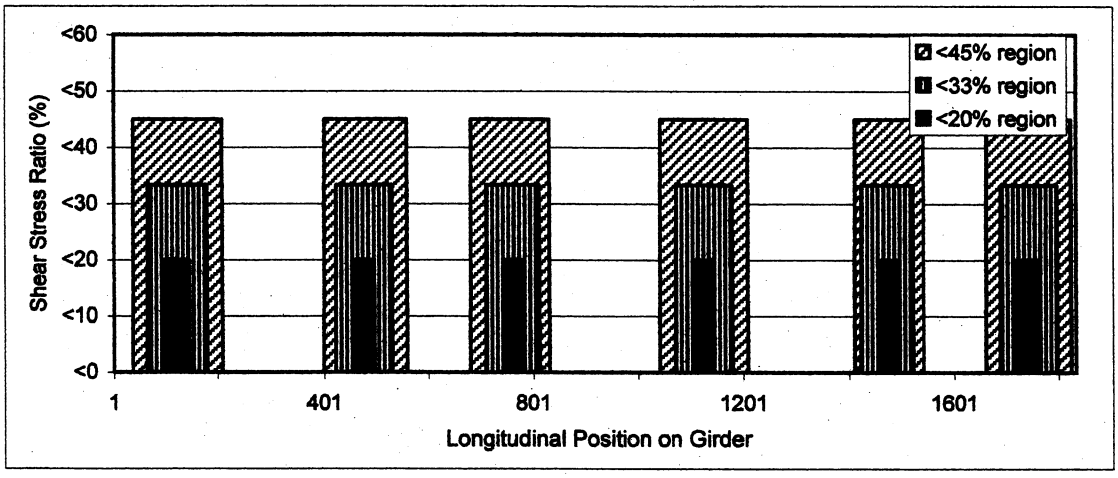

(b)

Figure 172: Regions of low stresses for Br.542b (a-Approach I, b-Approach II)

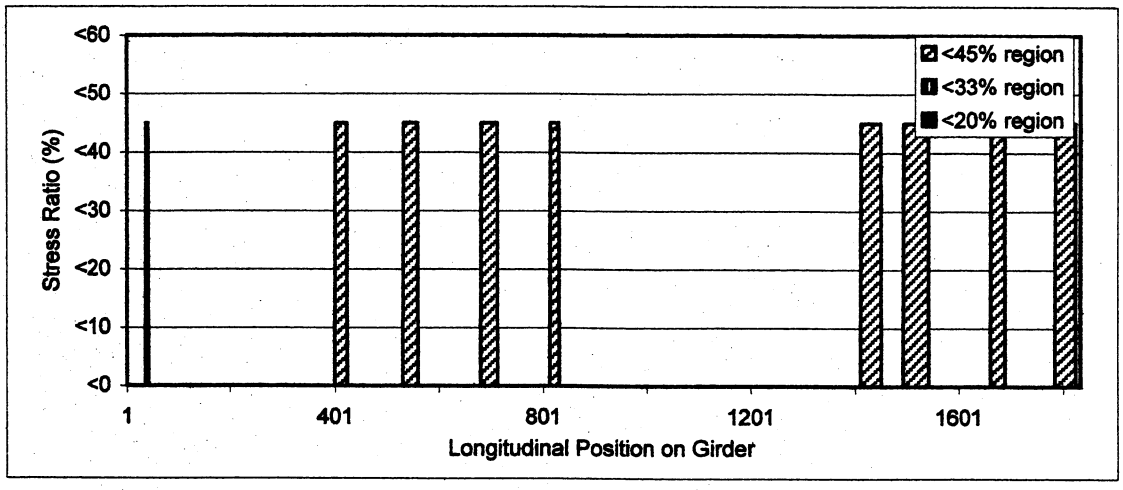

(a)

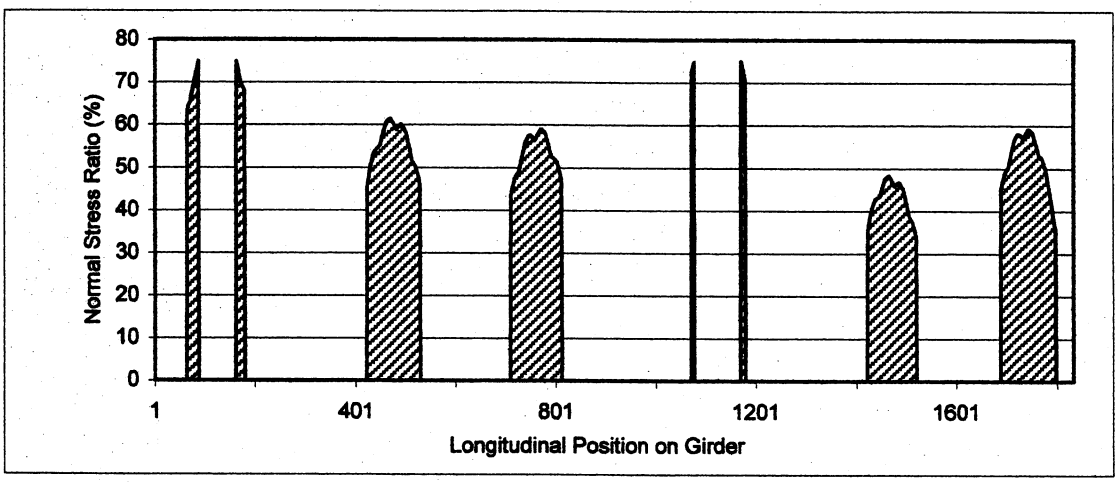

(b)

Figure 173: Regions of low stresses for Br.542b (a-Approach III, b-Approach IV)

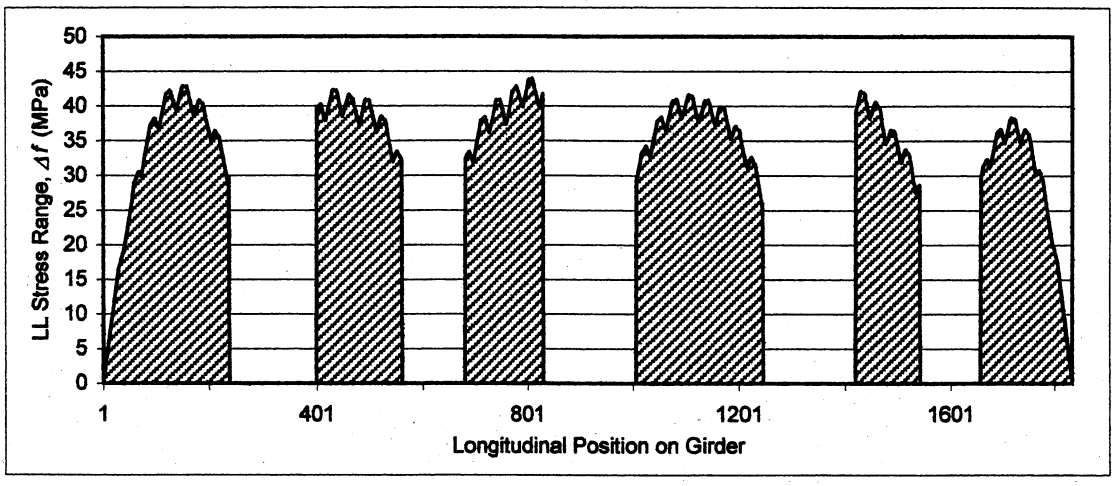

(a)

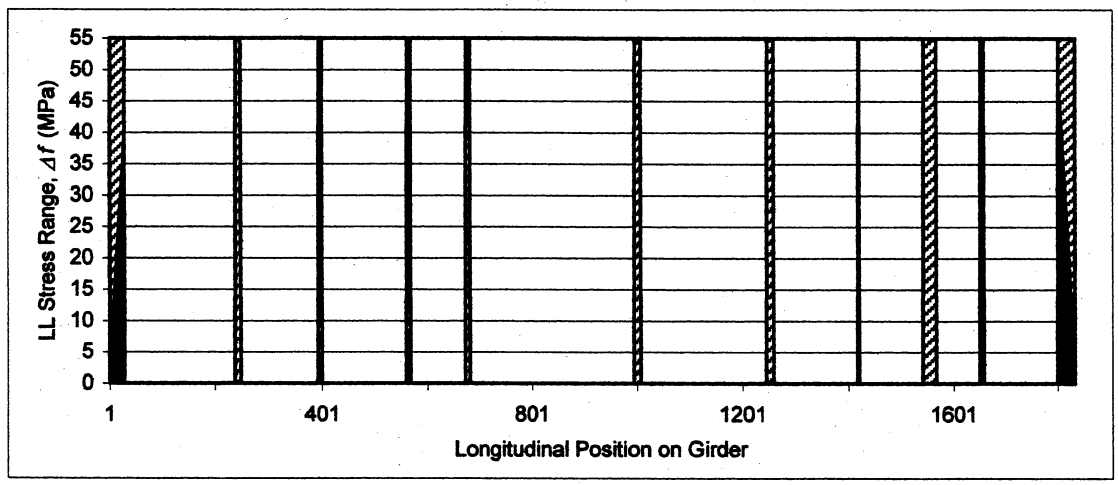

(b)

Figure 174: Br.542b (a-Live load fatigue stress range, b-Low stress regions according to Approach V)

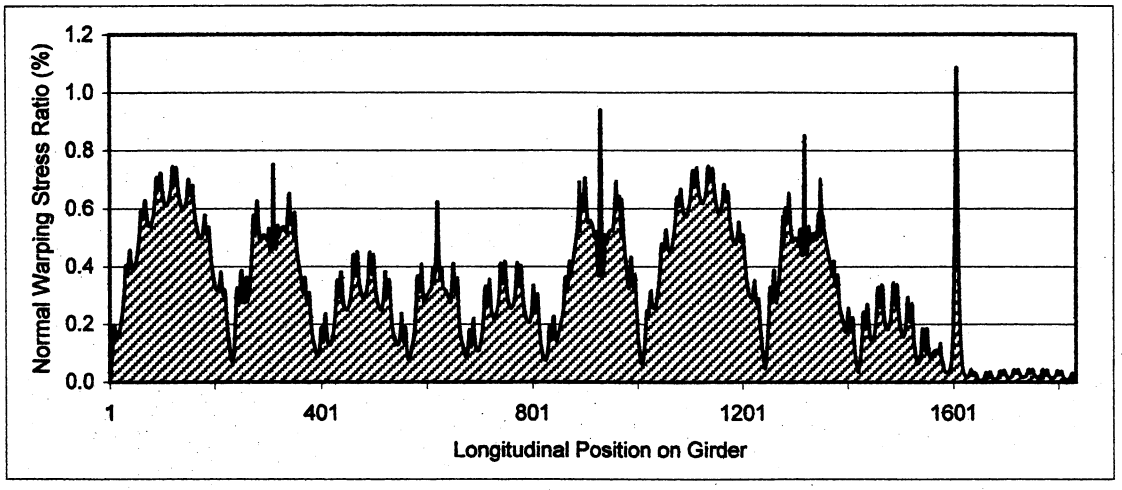

(a)

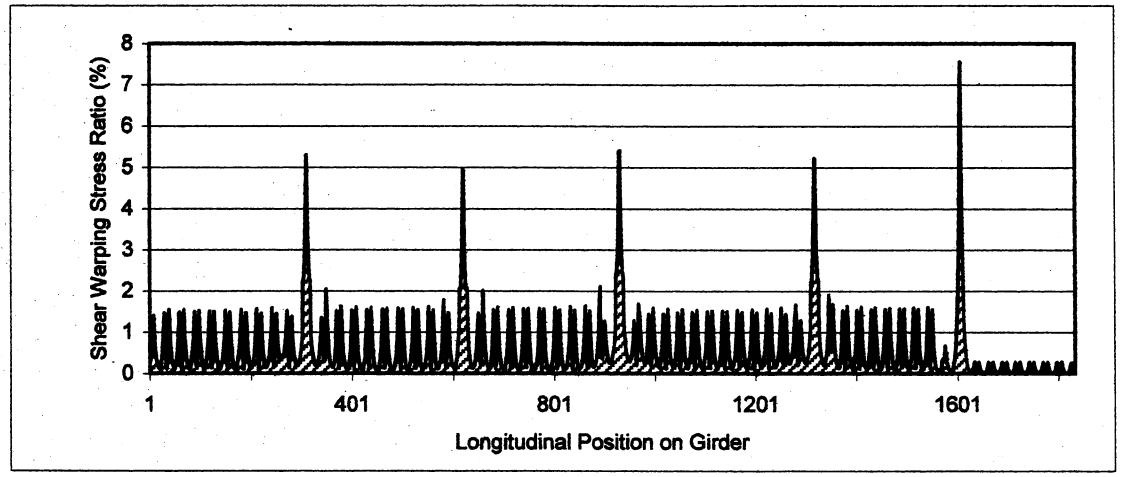

(b)

Figure 175: Warping stress ratios for Br.542b
a) σ_ω / σ_T, b) τ_ω / τ_T)